Fe65-Amyloid Precursor Protein Signalling and Alzheimer's Disease

Dunbar, Charlotte Emily

Awarding institution:
King's College London

Fe65-Amyloid Precursor Protein Signalling and Alzheimer's Disease

Charlotte Emily Dunbar BSc (Hons)

Thesis submitted in fulfilment of the degree of Doctor of Philosophy

Department of Basic and Clinical Neuroscience
King's College London
Institute of Psychiatry, Psychology and Neuroscience

June, 2016

DECLARATION

I hereby declare that, with the exception of the western blots of Fzd1 siRNA tests and the GSK3β and tau ELISAs shown in Chapter 4 and the co-immunoprecipitations, GST pull-downs and neurite outgrowth studies in Chapter 5, all of the work presented in this thesis is my own. Gábor Mórotz ran the Fzd1 siRNA test and associated western blots. Lizzie Glennon ran the GSK3β and tau ELISAs and performed the initial analyses and I ran the statistical analyses on the ELISA data. Hei Nga Maggie Cheung performed the co-immunoprecipitations and GST pull-downs of Fe65 and ARF6 and the neurite outgrowth studies.

Charlotte Dunbar

June 2016

ACKNOWLEDGEMENTS

I would first like to thank my supervisor Chris Miller for his support, advice and endless supply of funny stories. I would also like to thank my second supervisor Wendy Noble and my personal tutor Deepak Srivastava for their help and encouragement throughout my PhD. A special thanks goes to Lizzie Glennon for being my absolute rock, helping with the neuron prep, performing the GSK3β and tau ELISAs and putting up with me for 4 years. Thank you also to Gábor Mórotz for testing the Fzd1 siRNAs and teaching me the ropes when I first started and thank you to the rest of the Miller group. Finally, a big thank you to my Dad for all the hours spent proof-reading and to the rest of my family and friends for their continued encouragement and support. This work was funded by Alzheimer's Research UK.

ABSTRACT

Deposition of Aβ in amyloid plaques and accumulation of hyperphosphorylated tau in neurofibrillary tangles are hallmark pathologies of Alzheimer's disease. Changes in APP processing alter Aβ generation and are likely to affect APP function, which may also contribute to Alzheimer's disease. APP binds to adaptor protein Fe65 and one proposed function of this complex is to signal to the nucleus to regulate gene transcription. However, the mechanisms that regulate APP-Fe65 binding and the genes regulated by this pathway are poorly understood. Phosphorylation is a common mechanism for regulating protein-protein interactions and Fe65 is phosphorylated by several kinases, including ERK1/2. The first hypothesis investigated in this thesis is that BDNF signalling, which leads to ERK1/2 activation, stimulates Fe65 phosphorylation to regulate its binding to APP. BDNF was found to induce ERK1/2-dependent phosphorylation of Fe65 and, in a variety of assays including the use of phosphomutants, BDNF-induced phosphorylation of Fe65 was shown to inhibit the binding of Fe65 to APP. Unpublished next generation sequencing of Fe65 knockout mouse brains suggested that Fe65 may affect the wnt signalling pathway, which regulates GSK3β activity. GSK3β is a kinase involved in the hyperphosphorylation of tau in Alzheimer's disease. The second hypothesis tested in this thesis is that Fe65 regulates genes that are linked to GSK3β activity and tau phosphorylation. RT-qPCR carried out on Fe65 knockout mouse brains and siRNA-treated rat cortical neurons found that expression of wnt receptor Fzd-1 was affected by loss of Fe65. Additionally, loss of Fe65 decreased both GSK3β activity and tau phosphorylation. These results show that Fe65 is involved with APP to function in a key process that can be regulated by BDNF, a treatment previously shown to be neuroprotective in Alzheimer's disease models. Furthermore, they reaffirm the link between APP and Fe65 and link Fe65 to tau phosphorylation, which may be the first step in understanding the relationship between the two hallmark pathologies of Alzheimer's disease.

Publications in refereed journals arising from work undertaken in this PhD:

Cheung, H.N.M., Dunbar, C., Mórotz, G.M., Cheng, W.H., Chan, H.Y.E., Miller, C.C.J., Lau, K.-F., 2014. FE65 Interacts with ADP-Ribosylation Factor 6 to Promote Neurite Outgrowth. The FASEB Journal 28, 337–349.

TABLE OF CONTENTS

DECLARATION **1**

ACKNOWLEDGEMENTS **2**

ABSTRACT **3**

TABLE OF CONTENTS **4**

TABLE OF FIGURES **8**

TABLE OF TABLES **10**

ABBREVIATIONS **11**

CHAPTER 1: INTRODUCTION **15**

1.1 ALZHEIMER'S DISEASE **16**

1.1.1 PREVALENCE AND BURDEN OF ALZHEIMER'S DISEASE 16

1.1.2 CELLULAR PATHOLOGY OF AD 16

1.1.3 GENETICS OF AD 18

1.1.4 THE AMYLOID CASCADE HYPOTHESIS 20

1.2 THE AMYLOID PRECURSOR PROTEIN **22**

1.2.1 APP PROTEOLYTIC PROCESSING 24

1.2.2 APP SECRETASES 26

1.2.3 APP FUNCTIONS 26

1.2.4 APP INTERACTING PROTEINS 28

1.3 FE65 ..... **29**

1.3.1 FE65 BINDING PROTEINS 31

1.3.2 FE65 FUNCTIONS 33

1.3.3 OTHER FUNCTIONS OF FE65 37

1.3.4 FE65 AND APP PROCESSING 38

1.4 SIGNALLING PATHWAYS IN ALZHEIMER'S DISEASE **39**

1.4.1 BDNF SIGNALLING 39

1.4.2 WNT SIGNALLING 42

1.5 HYPOTHESES AND AIMS **44**

CHAPTER 2: MATERIALS AND METHODS **45**

2.1 MATERIALS **46**

2.1.1 ANTIBODIES 46

2.1.2 Enzyme-linked immunosorbent assays (ELISA) 47
2.1.3 Plasmid vectors 48
2.2 General biochemical reagents 48
2.2.1 General tissue culture reagents 48
2.2.2 Mammalian cell culture and transfection 49
2.2.3 Cell treatments 49
2.2.4 Duolink proximity ligation assay (PLA) 50
2.2.5 Quantitative real-time PCR (RT-qPCR) 50
2.3 Methods 50
2.3.1 General microbiology methods 50
2.3.2 Mammalian cell culture and transfection 51
2.3.3 Cell treatments 53
2.3.4 Determination of protein concentration (Bio-Rad protein assay) 54
2.3.5 SDS-PAGE and western blotting 55
2.3.6 Co-immunoprecipitation 57
2.3.7 GST fusion protein pull-down assay 57
2.3.8 ELISA 59
2.3.9 Immunofluorescence 60
2.3.10 Duolink PLA 60
2.3.11 Fe65KO transgenic mice 63
2.3.12 RNA isolation, reverse transcription and SYBR Green RT-qPCR 64

CHAPTER 3: BDNF INDUCES ERK1/2 PHOSPHORYLATION OF FE65 TO REGULATE ITS BINDING TO APP 69

3.1 Introduction 70
3.2 Results 72
3.2.1 Commercial antibodies detect Fe65 on western blots 72
3.2.2 Detection of the APP-Fe65 interaction 74
3.2.3 BDNF activates ERK1/2 and induces Fe65 phosphorylation in CHO cells expressing TrkB 81
3.2.4 BDNF activates ERK1/2 and induces Fe65 phosphorylation in rat cortical neurons 84
3.2.5 BDNF treatment shows no significant effect on APP-Fe65 binding in co-immunoprecipitation and GST-APP$_C$ pull-down assays from CHO-TrkB cells 86
3.2.6 BDNF treatment reduces binding between endogenous APP and Fe65 in proximity ligation assays in both CHO-TrkB cells and rat cortical neurons 90
3.2.7 The Fe65 phospho-mimicking mutant has reduced binding to APP in GST-APP$_C$ pull-down assays 93

3.3 DISCUSSION 97
3.3.1 LIMITATIONS 103

CHAPTER 4: FE65 INDEPENDENTLY REGULATES FRIZZLED-1 EXPRESSION, GSK3B ACTIVITY AND TAU PHOSPHORYLATION 104

4.1 INTRODUCTION 105
4.2 RESULTS 107
4.2.1 ESTABLISHING ANIMAL AND CELLULAR MODELS IN WHICH FE65 AND APP EXPRESSION ARE REDUCED 107
4.2.2 OPTIMISATION OF RT-QPCR FOR ANALYSIS OF GENE EXPRESSION 112
4.2.3 LOSS OF FE65 REDUCES FZD1 MRNA LEVELS BUT DOES NOT AFFECT WNT3A, GSK3A, GSK3B, LRP6, APP OR TAU LEVELS IN FE65KO BRAINS 116
4.2.4 LOSS OF FE65 DOES NOT ALTER EXPRESSION OF GSK3A, GSK3B, LRP6, APP OR TAU PROTEIN LEVELS IN FE65KO MOUSE BRAINS AND ANTIBODIES THAT DETECT FZD1 OR WNT3A PROTEINS COULD NOT BE IDENTIFIED 119
4.2.5 LOSS OF FE65 DOES NOT ALTER FZD1 OR APP MRNA LEVELS IN FE65 SIRNA TREATED RAT CORTICAL NEURONS AND LOSS OF APP DOES NOT AFFECT FZD1 OR FE65 MRNA LEVELS IN APP SIRNA TREATED RAT CORTICAL NEURONS 123
4.2.6 LOSS OF FE65 REDUCES TAU SER^{202} PHOSPHORYLATION BUT DOES NOT ALTER GSK3B SER^{9} PHOSPHORYLATION IN FE65KO BRAINS 125
4.2.7 LOSS OF FE65 REDUCES TAU PHOSPHORYLATION AND GSK3B ACTIVITY IN RAT CORTICAL NEURONS 127
4.3 DISCUSSION 129
4.3.1 LIMITATIONS 134

CHAPTER 5: FE65 INTERACTS WITH ARF6 TO REGULATE NEURITE OUTGROWTH 135

5.1 INTRODUCTION 136
5.2 RESULTS 137
5.2.1 FE65 INTERACTS WITH ARF6 IN CHO CELLS AND RAT BRAIN LYSATE 137
5.2.2 ARF6 BINDS TO THE PTB1 DOMAIN OF FE65 139
5.2.3 ARF6 IS LOCALISED TO PERINUCLEAR REGIONS AND COLOCALISES WITH FE65 IN GROWTH CONES OF RAT CORTICAL NEURONS 141
5.2.4 FE65 AND ARF6 ENHANCE NEURITE OUTGROWTH 143
5.3 DISCUSSION 145

CHAPTER 6: SUMMARY AND FUTURE DIRECTIONS 147

6.1 SUMMARY 148
6.2 FUTURE DIRECTIONS 150

CHAPTER 7: REFERENCES 152

APPENDIX A: FE65 INTERACTS WITH ADP-RIBOSYLATION FACTOR 6 TO PROMOTE NEURITE OUTGROWTH 187

TABLE OF FIGURES

Figure 1.1: The hallmark pathologies of AD **17**
Figure 1.2: The amyloid cascade hypothesis **22**
Figure 1.3: The structure of the APP isoforms **23**
Figure 1.4: APP processing occurs via two mutually exclusive pathways **25**
Figure 1.5 The structure of the Fe65 proteins **31**
Figure 3.1: Commercial antibodies detects Fe65 on western blots **73**
Figure 3.2: The APP-Fe65 interaction can be detected by co-immunoprecipitation involving Fe65, but not APP C-terminal antibodies **76**
Figure 3.3: The APP-Fe65 interaction can be detected by GST pull-down assays involving the APP cytoplasmic domain **78**
Figure 3.4: Interaction of endogenous APP and Fe65 can be detected by proximity ligation assays **80**
Figure 3.5: BDNF activates ERK1/2 and induces Fe65 phosphorylation in CHO cells expressing TrkB **83**
Figure 3.6: BDNF activates ERK1/2 and induces Fe65 phosphorylation in rat cortical neurons **85**
Figure 3.7: BDNF treatment has no effect on APP-Fe65 binding in co-immunoprecipitation assays from CHO-TrkB cells **88**
Figure 3.8: BDNF treatment has no effect on APP-Fe65 binding in GST-APP_C pull-down assays from CHO-TrkB cells **89**
Figure 3.9: BDNF treatment of CHO-TrkB cells reduces binding between endogenous APP and Fe65 **91**
Figure 3.10: BDNF inhibits binding between endogenous APP and Fe65 in primary cortical neurons **92**
Figure 3.11: The Fe65 phosphorylation mutants do not show changed binding to APP in co-immunoprecipitation assays **95**
Figure 3.12: The Fe65 phospho-mimicking mutant has reduced binding to the cytoplasmic tail of APP **96**
Figure 4.1: Characterisation of Fe65KO mice **108**
Figure 4.2: Fe65 siRNAs abolish Fe65 expression and APP siRNAs abolish APP expression in rat cortical neurons **111**
Figure 4.3: High quality RNA was isolated from WT and Fe65KO mouse brain samples **113**
Figure 4.4: GAPDH and ATP5B are appropriate reference genes for normalisation in RT-qPCR analyses in WT and Fe65KO mice brains **114**
Figure 4.5: Loss of Fe65 reduces Fzd1 mRNA expression in Fe65KO brains but does not affect GSK3α, GSK3β, LRP6, wnt3a, APP or tau mRNA levels in Fe65KO mouse brains **117**
Figure 4.6: Loss of Fe65 does not alter expression of GSK3α, GSK3β, LRP6, APP or tau protein levels in Fe65KO mouse brains **120**
Figure 4.7: Antibodies that detect Fzd1 and Wnt3a proteins on western blot could not be identified **122**

Figure 4.8: Loss of Fe65 does not alter Fzd1 or APP mRNA levels in Fe65 siRNA treated rat cortical neurons and loss of APP does not affect Fzd1 or Fe65 mRNA levels in APP siRNA treated rat cortical neurons **124**
Figure 4.9: Loss of Fe65 reduces tau phosphorylation but has no effect on GSK3β phosphorylation in Fe65KO brains **126**
Figure 4.10: Loss of Fe65 reduces tau phosphorylation and GSK3β activity in Fe65 siRNA treated rat cortical neurons **128**
Figure 5.1: Fe65 interacts with ARF6 in CHO cells and rat brain lysates **138**
Figure 5.2: ARF6 binds to the PTB1 domain of Fe65 **140**
Figure 5.3: ARF6 is present in perinuclear regions and colocalises with Fe65 in the growth cones of developing neurites **142**
Figure 5.4: Fe65 and ARF6 enhance neurite outgrowth **144**

TABLE OF TABLES

Table 1.1: Proteins reported to interact with the Fe65 PTB2 domain **32**
Table 1.2: Proteins reported to interact with the Fe65 PTB1 domain **32**
Table 1.3: Proteins reported to interact with the Fe65 WW domain **33**
Table 1.4: Genes reported to be positively regulated by APP-Fe65 signalling **35**
Table 2.1: Primary antibodies used in these studies **46**
Table 2.2: Mammalian and bacterial expression plasmids used in these studies **48**
Table 2.3: Growth media and transfection reagents for cell lines **49**
Table 2.4: siRNA sequences used to achieve Fe65 and APP knockdown in rat cortical neurons **50**
Table 2.5: Polyacrylamide gel recipes for SDS-PAGE **55**
Table 2.6: Primer sequences used for PCR genotyping of Fe65KO mice **63**
Table 2.7: Fe65KO mouse PCR genotyping program **64**
Table 2.8: RT-qPCR amplification program **66**
Table 2.9: GeNorm reference gene primer details. Specific primer sequences were not disclosed by PrimerDesign **66**
Table 2.10: Primer sequences used for RT-qPCR on Fe65KO mouse brain samples **67**
Table 2.11: Primer sequences used for RT-qPCR on siRNA treated rat cortical neurons **67**

ABBREVIATIONS

Amino acids: single letter code and abbreviations

Single letter code	Abbreviation	Amino Acid
A	Ala	Alanine
C	Cys	Cysteine
D	Asp	Aspartic acid
E	Glu	Glutamic acid
F	Phe	Phenylalanine
G	Gly	Glycine
H	His	Histidine
I	Ile	Isoleucine
K	Lys	Lysine
L	Leu	Leucine
M	Met	Methionine
N	Asn	Asparagine
P	Pro	Proline
Q	Gln	Glutamine
R	Arg	Arginine
S	Ser	Serine
T	Thr	Threonine
V	Val	Valine
W	Trp	Tryptophan
X	Xxx	Any amino acid
Y	Tyr	Tyrosine

Other abbreviations

AD	Alzheimer's disease
ADAM	A disintegrin and metalloproteinase
AICD	APP intracellular domain
ANOVA	Analysis of variance
Aph-1	Anterior pharynx-defective phenotype-1
APLP	Amyloid precursor-like protein
apoE	Apolipoprotein E
ApoER2	ApoE receptor 2
APP	Amyloid precursor protein
APS	Ammonium persulfate
ARF6	ADP-ribosylation factor 6
ATM	Ataxia telangiectasia mutated
ATR	Ataxia-telangiectasia- and Rad3-related
Aβ	Amyloid-β
BACE1	β-amyloid cleaving enzyme 1
BDNF	Brain-derived neurotrophic factor
c-Abl	c-Abl tyrosine kinase
CAT	Chloramphenicol acetyltransferase
cdk5	Cyclin-dependent kinase 5
CHO	Chinese hamster ovary
CHO-TrkB	CHO cells stably transfected with TrkB
Dab1	Disabled-1
DIV	Days *in vitro*
DMEM	Dulbecco's modified Eagle medium
DMSO	Dimethyl sulfoxide
DNA	Deoxyribonucleic acid
DNase	Deoxyribonuclease
E. coli	*Escherichia coli*
ECL	Enhanced chemiluminescence
EDTA	Etylenediamintetraacetic acid
EGTA	Ethylene glycol-bis(β-aminoethylether)-N,N,N',N'-tetraacetic acid
ELISA	Enzyme-linked immunosorbent assay
ERK	Extracellular regulated kinase
ERα	Estrogen receptor α
FBS	Fetal bovine serum

Fe65KO	Fe65 knockout
Fe65L	Fe65-like
Fzd1	Frizzled 1
GRB2	Growth factor receptor-bound protein 2
GSK3α/β	Glycogen synthase kinase 3α/β
GST	Glutathione-*S*-transferase
HBSS	Hank's balanced salt solution
HEK	Human embryo kidney
IPTG	Isopropyl β-D-1-thiogalactopyranoside
JIP1	c-jun N-terminal kinase-interacting protein 1
JNK	c-jun N-terminal kinase
KPI	Kunitz protease inhibitor
LB	Luria-Bertani
LB-amp	Luria-Bertani broth containing 100 µg/ml ampicillin
LRP	Low-density lipoprotein receptor-related protein
LTP	Long-term potentiation
MAP	Mitogen-activated protein
MEK	MAP kinase kinase
Mena	Mammalian enabled
Mint	munc-18 interacting
mRNA	Messenger RNA
NFT	Neurofibrillary tangles
NGF	Nerve growth factor
NMDA	N-methyl-D-aspartate
OD	Optical density
PBS	Phosphate buffered saline
PCR	Polymerase chain reaction
PEN-2	PS enhancer 2
PFA	Paraformaldehyde
PLA	Proximity ligation assay
PS	Presenillin
PTB	Phosphotyrosine binding
RIPA	Radio-immunoprecipitation assay
RNA	Ribonucleic acid
RT-qPCR	Quantitative real-time PCR
sAPPα/β	Secreted APPα/β
S.D.	Standard deviation
SDS	Sodium dodecyl sulphate

SDS-PAGE	SDS-polyacrylamide gel electrophoresis
SGK1	Serum- and glucocorticoid-induced kinase 1
SH2	Src-homology-2
siRNA	Small interfering RNA
TAE	Tris-Acetate-EDTA
TBS	Tris buffered saline
TCF/LEF	T-cell factor/lymphoid enhancer factor
TEMED	Tetramethylethylenediamine
Tris	Tris(hydroxymethyl)aminomethane
Triton-PBS	0.1 % (v/v) Triton X-100 in PBS
TrkB	Tyrosine receptor kinase B
UPS	Ubiquitin-proteasome system
WT	Wild-type

CHAPTER 1: INTRODUCTION

1.1 Alzheimer's disease

1.1.1 Prevalence and burden of Alzheimer's disease

Alzheimer's disease (AD) is the most common cause of dementia. It is a progressive neurodegenerative disorder that affects over 850,000 people in the UK and 44 million sufferers worldwide (http://www.alzheimersresearchuk.org/). Due to a lack of effective treatments or cures, most patients live with AD for a number of years. During this time, disease symptoms become increasingly severe and more debilitating. This creates a huge burden on the carers and families and costs the UK alone £23 billion per year. The prevalence of AD is increasing and it is estimated that worldwide, 115.4 million people will be living with the disease by 2050 (World Health Organization, 2012). These alarming figures make it clear that finding a treatment for AD is of vital importance.

There are several subclasses of AD that are categorised by age of onset, progression rate of disease and whether there is an underlying genetic cause. Over 90 % of AD cases are sporadic, late-onset disease occurring in those aged 65 and over (http://www.alzheimersresearchuk.org/). Unlike the rare, familial forms of disease, sporadic AD is not linked to a particular genetic mutation and does not show a predictable pattern of inheritance. Patients with AD usually present a syndrome of clinical symptoms. These can include problems with learning, remembering information, language usage, understanding complex tasks, visuospatial difficulties and personality changes. AD can be difficult to diagnose because there are several forms of dementia with overlapping symptoms. Also, some people develop mixed dementia, where more than one form of dementia is responsible for their cognitive decline (Jellinger and Attems, 2010). As many of the dementia diseases display similar biochemical abnormalities within the brain, studying AD may help to shed light on causes and treatments of other neurodegenerative diseases.

1.1.2 Cellular pathology of AD

AD was originally described in 1906 by Dr Alois Alzheimer as a range of symptoms observed in a 51 year-old patient. These symptoms included personality changes, memory loss and disorientation. Post-mortem investigation of the cortical tissue revealed atrophy and abnormal 'minute miliary foci' and 'tangles of fibrils' (Stelzmann et al., 1995). The examination of brain samples from other AD patients over the last century has revealed that two hallmark pathologies – extracellular neuritic plaques and intracellular neurofibrillary tangles – are present in AD (see Figure 1.1).

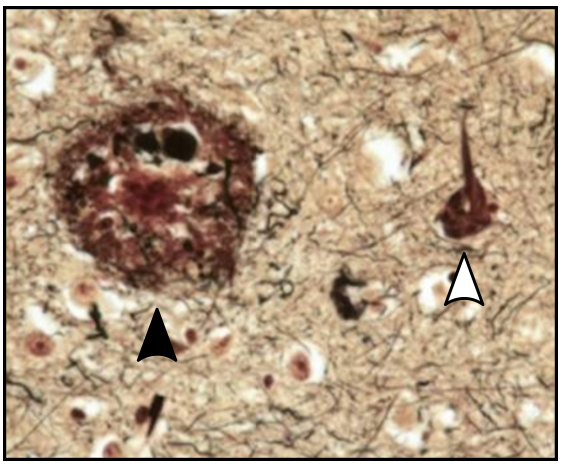

Figure 1.1: The hallmark pathologies of AD. *Silver stain of brain tissue showing (black arrowhead) a neuritic plaque and (white arrowhead) a neurofibrillary tangle. (Image from Serrano-Pozo et al., 2011).*

1.1.2.1 Neuritic plaques

Neuritic plaques contain a core that mainly consists of aggregated amyloid-β (Aβ). Aβ exists mainly as a 40-42 amino acid peptide that is derived from the amyloid precursor protein (APP) by proteolytic cleavage (Zhang et al., 2011). $A\beta_{40/42}$ peptides are produced by the same pathway but the longer peptide is more prone to aggregation and is believed to be the first form of Aβ deposited in plaques (Gravina et al., 1995; Jarrett et al., 1993; Roher et al., 1993). The neuritic plaques are heterogeneous and contain other proteins including acetylcholinesterase, apolipoproteins, growth factors and their receptors (Armstrong et al. 2008). Neuritic plaques are usually surrounded by degenerating neurites and can also contain processes from microglia, the immune cells of the brain (Dickson, 1997; Meyer-Luehmann et al., 2008; Pike et al., 1995). Neuritic abnormalities and microglial recruitment occur shortly after plaque formation, suggesting these are responses to either the plaques themselves or toxic molecules released by plaques (Meyer-Luehmann et al., 2008). In AD brains, neuritic plaques are found in the hippocampus and cortex, areas most vulnerable to disease. However, they are not exclusive to AD and can develop during normal ageing, although they are far fewer in number in these cases (Herrup, 2015; Morris et al., 1996; Snowdon et al., 1997).

1.1.2.2 Neurofibrillary tangles

The other pathology of AD is the presence of intraneuronal neurofibrillary tangles (NFTs) comprising the microtubule-associated protein tau. There are six different tau isoforms in the human brain that are derived from alternative splicing of exons. The isoforms contain either three or four C-terminal microtubule-binding domains and none,

one or two N-terminal inserts (Noble et al., 2013; Wang and Mandelkow, 2015). Tau is predominantly expressed in neurons and is involved in regulating microtubule stabilisation and cytoskeletal dynamics and may play a role in regulating axonal transport (Elie et al., 2015; Wang and Mandelkow, 2015). Tau is a phosphoprotein that contains 85 potential phosphorylation sites (Noble et al., 2013; Wang and Mandelkow, 2015). Regulation of tau phosphorylation is performed by many kinases and phosphatases and is important because tau is hyperphosphorylated in NFTs (Noble et al., 2013; Šimić et al., 2016). A number of serine/threonine and tyrosine kinases have been implicated in the hyperphosphorylation of tau in AD; particularly cyclin-dependent kinase 5 (cdk5)/p35 and glycogen synthase kinase 3 (GSK3; Hooper et al., 2008; Noble et al., 2013; Su and Tsai, 2011).

Although both neuritic plaques and NFTs are hallmark pathologies of AD, the severity of tau pathology correlates best with disease progression and spread along vulnerable brain regions (Braak and Braak, 1991; Wilcock and Esiri, 1982). NFTs are found in a number of neurodegenerative disorders that display tau pathology termed tauopathies (Šimić et al., 2016; Spillantini and Goedert, 2013; Wang and Mandelkow, 2015). Aggregated tau may cause cellular dysfunction by loss of normal function or by gain of toxic function of insoluble tau oligomers. Indeed, tau appears to facilitate Aβ neurotoxicity (Ittner and Götz, 2011). However, NFTs may not be neurotoxic themselves as they can be present in cells for many years without causing cell death (Spillantini and Goedert, 2013; Wang and Mandelkow, 2015).

How these two pathologies begin and escalate has been a key focus of AD research, with the rationale that the cause of disease should provide a target for therapeutic development. The majority of drug development has focussed on combating neuritic plaques, however all clinical trials to date on therapeutics intended to clear neuritic plaques from the brain have failed to ameliorate disease symptoms, even when plaque load has been successfully reduced (Doody et al., 2014; Herrup, 2015; Holmes et al., 2008; Salloway et al., 2014). Along with evidence that both neuritic plaques and NFTs can be found in individuals without AD (Herrup, 2015; Lee et al., 2001; Morris et al., 1996; Snowdon et al., 1997; Wang and Mandelkow, 2015), these failures imply that AD is more complex than originally thought.

1.1.3 Genetics of AD

Although the vast majority of AD cases are sporadic, research into the genetic causes of familial AD has helped to identify genes involved in the disease. Autosomal dominant mutations that cause early-onset, familial AD are found in one of three

genes: *APP*, *PS1* (encoding presenilin 1; PS1) or *PS2* (encoding presenilin 2; PS2). Mutations in *MAPT*, the gene encoding tau, do not cause AD but cause some forms of another inherited tauopathy called frontotemporal lobar degeneration with tau pathology (Goedert et al., 2012).

1.1.3.1 APP

The first genetic link discovered in AD was that patients with Down's Syndrome (trisomy of chromosome 21) over the age of forty develop typical AD pathology. The *APP* gene is located on chromosome 21, so these patients carry three copies of *APP*, suggesting that an excess of APP protein can cause disease (St George-Hyslop et al., 1987; Wisniewski et al., 1985). Indeed, duplication of the *APP* gene has since been found to cause familial AD (Rovelet-Lecrux et al., 2006; Sleegers et al., 2006). A number of autosomal dominant mutations of APP have also been shown to cause familial AD. These pathogenic mutations occur close to the Aβ domain of APP and act to enhance or alter Aβ production (www.alzforum.org; Schellenberg & Montine 2012; Tanzi 2012). In particular, some mutations increase total Aβ production, some mutations increase the relative levels of the more pathogenic $A\beta_{42}$ peptide and some mutations make Aβ more prone to aggregation or more "amyloidogenic". Interestingly, one APP mutation has been identified that protects against AD and this inhibits the production of Aβ (Jonsson et al., 2012).

1.1.3.2 PS1 and PS2

Mutations in *PS1* and *PS2* are the most common cause of familial AD. The presenilins form part of the γ-secretase complex that is involved in the proteolytic cleavage of APP to produce Aβ (De Strooper et al., 2010). Familial AD-linked *PS1/2* mutations are loss-of-function mutations that alter the production of Aβ from APP by influencing the specificity of γ-secretase cleavage. *PS1/2* mutations enhance generation of the more pathogenic $A\beta_{42}$ peptide over the less pathogenic $A\beta_{40}$ peptide (De Strooper and Annaert, 2010; Duff et al., 1996; Fernandez et al., 2014; Scheuner et al., 1996).

1.1.3.3 MAPT

The *MAPT* gene encodes tau and resides on chromosome 17. To date, no mutations in *MAPT* have been found that cause familial AD. Instead they lead to the development of some forms of frontotemporal lobar degeneration with tau pathology (Lee et al., 2001; Šimić et al., 2016; Spillantini and Goedert, 2013). *MAPT* mutations either alter the ability of tau to bind to microtubules or alter the ratio of tau isoforms via alternative splicing changes (Spillantini and Goedert, 2013). Both types of mutations enhance tau aggregation into intracellular NFTs.

1.1.3.4 Risk factor genes

A number of other genes are now known to increase the risk of developing AD. The ε4 allele of the *APOE* gene, encoding apolipoprotein E (apoE), is the strongest risk factor discovered to date for late-onset, sporadic AD. There are three *APOE* alleles: ε2, ε3 and ε4. Individuals carrying one copy of the *APOE-ε4* allele have a 3-fold increased risk, while people carrying two copies have a greater than 10-fold increased risk of developing sporadic AD (Corder et al., 1993; Genin et al., 2011; Kim et al., 2009; Verghese et al., 2011). In contrast, the ε2 allele of *APOE* is neuroprotective and carriers of this allele have a lower risk of AD (Corder et al., 1994; Hu et al., 2015). The exact mechanism of apoE pathogenicity is unknown but it may be involved in Aβ aggregation, clearance of Aβ, or tau phosphorylation (Castellano et al., 2011; Kim et al., 2009).

In addition to *APOE*, recent genome-wide association studies have identified over twenty other genes that are associated with AD (Bertram et al., 2010; Harold et al., 2009; Hollingworth et al., 2011; Karch et al., 2014; Lambert, 2013; Naj et al., 2011; Seshadri et al., 2010). These can be broadly grouped into genes involved in lipid metabolism, protein trafficking and inflammation (Karch and Goate, 2015; Schellenberg and Montine, 2012). Although the effect of these genes on the risk of developing AD is much lower than *APOE*, they may help to elucidate further pathways involved in disease.

1.1.4 The amyloid cascade hypothesis

As described above, the pathology of AD involves extracellular accumulation of Aβ in neuritic plaques and intracellular accumulation of tau in NFTs. Mutations in *APP* and *PS1/2* alter APP processing to enhance Aβ production. These pathogenic mutations cause familial AD, which displays both neuritic plaques and NFTs. Mutations in *MAPT* cause related dementias, but do not initiate amyloid pathology. This evidence suggests that mismetabolism of APP can affect tau phosphorylation and supports the amyloid cascade hypothesis, which is the most widely accepted hypothesis for AD development and progression. The amyloid cascade hypothesis describes two key events that lead to the two hallmark pathologies of disease; 1) the altered processing of APP, leading to Aβ plaque formation and 2) the hyperphosphorylation of tau, leading to NFT development (see Figure 1.2). The hypothesis proposes that changes in APP metabolism occur prior to the hyperphosphorylation and aggregation of tau. In support of this hypothesis, familial AD cases are associated with mutations in the *APP* gene or *PS1/2* genes (see section 1.1.3). These mutations fall into 3 classes; enhanced APP production, enhanced amyloidogenic processing or enhanced $A\beta_{42}$ generation

(Schellenberg and Montine, 2012; Scheuner et al., 1996; Tanzi, 2012). In contrast, mutations in the gene encoding tau have not yet been linked to AD, but instead cause frontotemporal lobar degeneration and increase the risk of developing other tauopathies that have NFT pathology without neuritic plaque development (Goedert et al. 2012; Spillantini & Goedert 2013; Wang & Mandelkow 2015).

Recently, soluble Aβ oligomers, rather than insoluble Aβ aggregates have been proposed as an alternative or complementary route to synapse loss and cell death from APP mismetabolism (Benilova et al., 2012). Monomeric Aβ can aggregate into soluble oligomers of varying molecular size that cause neurotoxicity (Sakono and Zako, 2010). However, there is some dispute over the physiological relevance of these findings, due to the high concentrations of Aβ required to induce cell death (Benilova et al., 2012; Hardy, 2009).

The causative link between Aβ generation, or even general altered APP processing and tau hyperphosphorylation is still unknown. Indeed, most APP animal models do not develop tau pathology, requiring mutations of both *APP* (or APP processing-linked) and *MAPT* genes to fully model disease (Elder et al., 2010; Richardson and Burns, 2002). The hypothesis also does not explain how Aβ aggregates can be found in healthy individuals without tau pathology and why Aβ fails to correlate well with disease severity (Herrup, 2015; Morris et al., 1996; Snowdon et al., 1997).

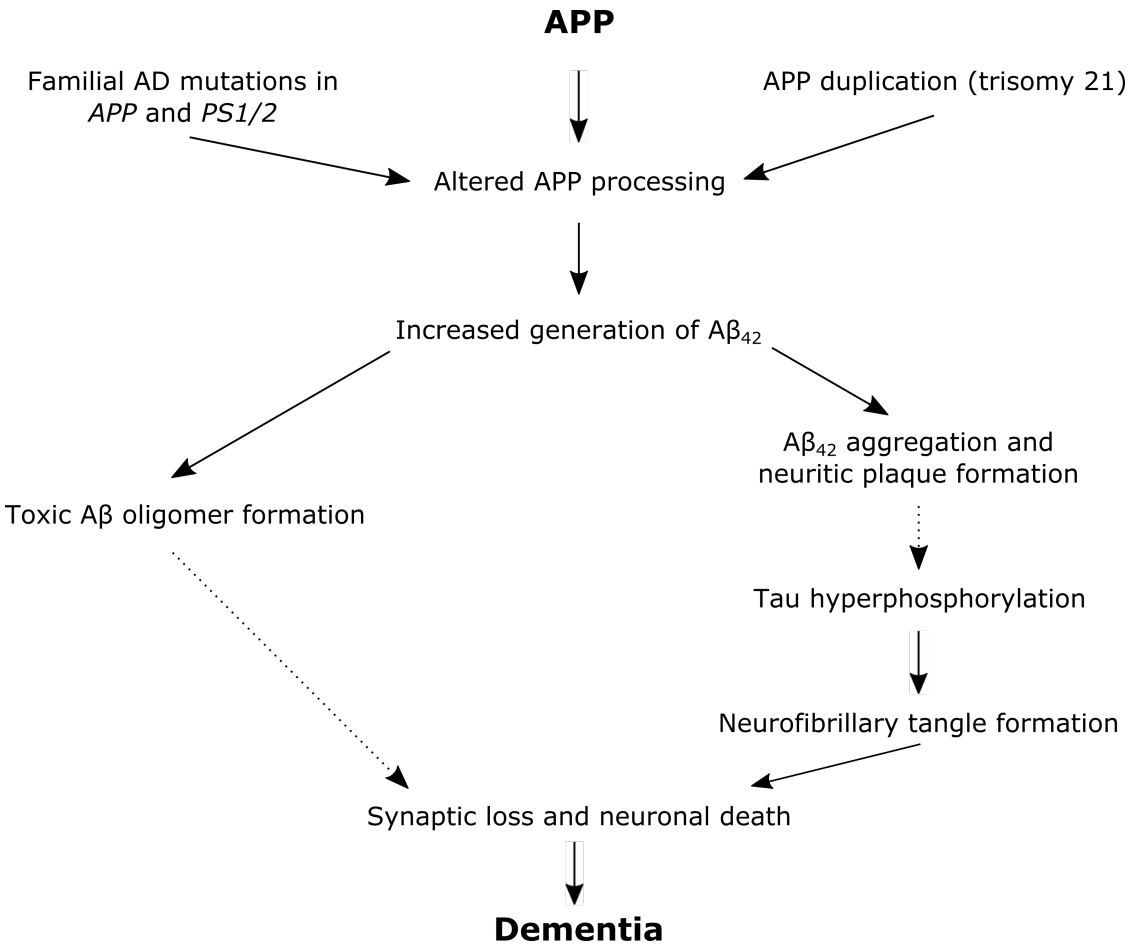

Figure 1.2: The amyloid cascade hypothesis. *A diagram to show the outline of the amyloid cascade hypothesis.*

1.2 The amyloid precursor protein

APP belongs to a small family of proteins comprising APP and amyloid precursor-like protein 1 and 2 (APLP1 and APLP2). These three proteins are very similar in structure and have overlapping expression patterns (Sprecher et al., 1993; Wasco et al., 1993, 1992). The APP genes are highly conserved in mammals and APP-family knockout mouse models suggest some level of functional redundancy between APP and APLP1/2 (Eggert et al., 2004; Heber et al., 2000; Herms et al., 2004; Müller and Zheng, 2012; Slunt et al., 1994).

APP is a type-1 transmembrane protein containing an N-terminal signal sequence (17 residues), a large extracellular domain that is stabilised by disulfide bonds and is glycosylated, a transmembrane domain (23 residues) and a small intracellular domain (47 residues; Dyrks et al., 1988; Kang et al., 1987; Oltersdorf et al., 1989). The Aβ encoding sequence is located in the extracellular and transmembrane domains (Dyrks et al. 1988; see Figure 1.3). The *APP* gene is located on chromosome 21 at position

21q21.3 (Goldgaber et al., 1987; Kang et al., 1987; Robakis et al., 1987; Tanzi et al., 1987) and undergoes alternative splicing of exons to generate a number of different isoforms. Three major isoforms of APP are produced, which contain 695, 751 or 770 amino acids. The two longer isoforms contain a Kunitz protease inhibitor (KPI) domain that is capable of inhibiting serine proteases such as trypsin (Petersen et al., 1994; Tanzi et al., 1988) and may play a role in blood coagulation and wound repair (Schmaier et al., 1993; Smith et al., 1990). APP_{770} also contains an Ox2 domain (see Figure 1.3), which may be involved in cell-surface binding (Dawkins and Small, 2014), although very little is known about the function of this domain. APP_{695} is the main APP isoform expressed in brain tissue, while APP_{751} and APP_{770} are expressed ubiquitously throughout many cell types (Kitaguchi et al., 1988; Oltersdorf et al., 1989; Ponte et al., 1988; Tanzi et al., 1988; Zhang et al., 2011).

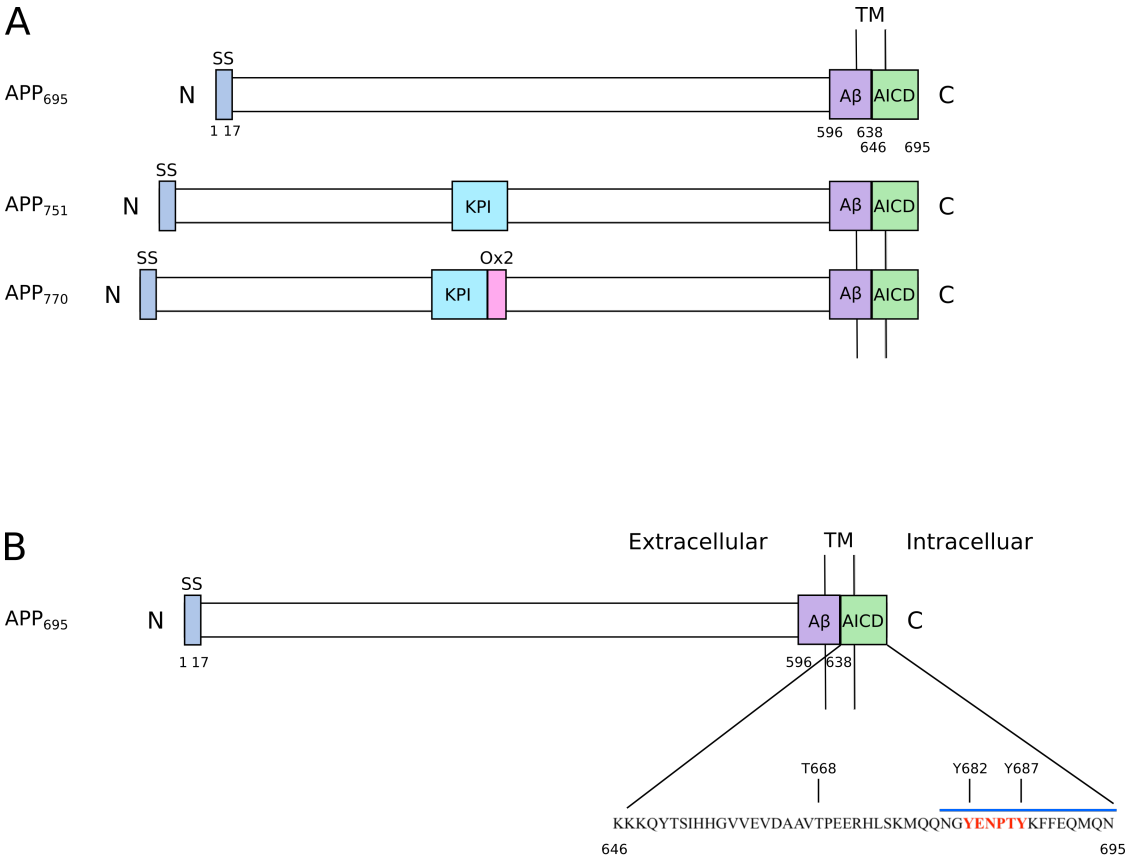

Figure 1.3: The structure of the APP isoforms. *A) The labelled domains of the APP isoforms are the signal sequence (SS), Kunitz protease inhibitor (KPI), Ox2, amyloid-β (Aβ) and the APP intracellular domain (AICD). TM indicates the transmembrane region of the APP proteins B) APP_{695} domain details including the sequence of the AICD, the YENPTY binding domain that interacts with Fe65 (red) and the epitope to which CT-17 (the C-terminal APP antibody used in this thesis) was raised against (blue line;* Cousins et al., 2009*). Also indicated are the phosphorylation sites of APP (Thr^{668}, Tyr^{682} and Tyr^{687}).*

APP is most abundantly expressed in the brain, heart and spleen, although it is also found in other peripheral tissues (Kitaguchi et al., 1988; Tanzi et al., 1988, 1987). Within the brain, APP is particularly localised to the cerebral cortex and hippocampus, areas that are affected in AD (Arai et al., 1991; Bahmanyar et al., 1987). The subcellular localisation of APP is linked to both its complex processing pathways and its proposed functions. APP is found in the endoplasmic reticulum and Golgi apparatus, which is where it is synthesised and post-translationally modified (Haass et al., 1992; Marquez-Sterling et al., 1997). It is also localised to the plasma membrane and to secretory vesicles and endosomes that transport APP to and from the cell surface (Schubert et al., 1991; Sisodia, 1992; van der Kant and Goldstein, 2015). APP is transported through axons by fast, anterograde transport in a kinesin-1-dependent manner and in developing axons, it is thought to play a role in cell motility (Cheung et al., 2014; Fu and Holzbaur, 2013; Koo et al., 1990; Marquez-Sterling et al., 1997; Moya et al., 1994; Stokin et al., 2005; Vagnoni et al., 2012). APP is also found in vesicles in the presynaptic terminals of many synapses, where it may function in synapse development and synaptic transmission (Lee et al., 2010; Priller et al., 2006; Schubert et al., 1991; Tyan et al., 2012; van der Kant and Goldstein, 2015; Weyer et al., 2011).

1.2.1 APP proteolytic processing

APP can be proteolytically processed via two mutually exclusive pathways (Figure 1.4). These pathways consist of a sequence of cleavage events by a combination of three enzymes or enzyme complexes that are termed secretases. α-secretase cleavage occurs within the extracellular Aβ domain of APP (Lys^{16} of the Aβ sequence), precluding the generation of the Aβ peptide (Anderson et al., 1991; Esch et al., 1990; Sisodia, 1992; Sisodia et al., 1990; Wang et al., 1991). Alternatively, APP can be processed by β-secretase. β-secretase cleaves full-length APP at two sites; between Met^{596} and Asp^{597} or between Tyr^{606} and Glu^{607}, which are both at the N-terminus of the Aβ encoding sequence (APP_{695} numbering; Deng et al., 2013; Seubert et al., 1993; Shoji et al., 1992; Sinha et al., 1999). Once α- or β-secretase cleavage has occurred, the remaining membrane-tethered C-terminal APP fragment is sequentially cleaved by γ-secretase at the C-terminus of the Aβ sequence (Haass et al. 2012; Figure 1.4). The APP processing pathway that involves cleavage of APP by α- and γ-secretase is the non-amyloidogenic pathway and it precludes Aβ generation. The amyloidogenic APP processing pathway involves β- and γ-secretase cleavage of APP and releases the Aβ peptide. A recent study reported a new processing event driven by η-secretase cleavage of APP between Asn^{504} and Met^{505} followed by α- or β-secretase cleavage, however this has not yet been replicated (Willem et al., 2015).

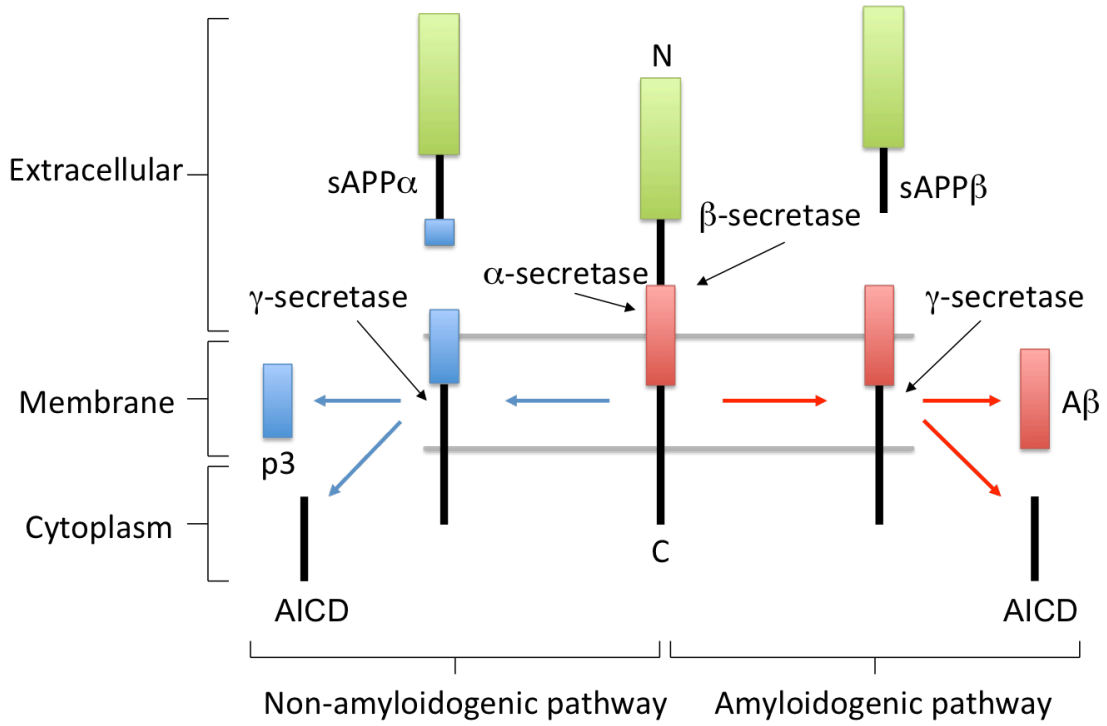

Figure 1.4: APP processing occurs via two mutually exclusive pathways. *APP processing via the non-amyloidogenic pathway creates three peptides; secreted APPα (sAPPα), p3 and APP intracellular domain (AICD). The amyloidogenic pathway generates secreted APPβ (sAPPβ), the amyloidogenic fragment amyloid-β (Aβ), which is involved in amyloid plaques and AICD.*

The majority of APP is metabolised via the non-amyloidogenic pathway. This produces a soluble extracellular N-terminal fragment (sAPPα), a C-terminal APP intracellular domain (AICD) and a small peptide termed p3. Processing by the amyloidogenic pathway produces a soluble N-terminal domain (sAPPβ), AICD and Aβ (Haass et al., 2012). The low sequence specificity of γ-secretase accounts for the creation of varying lengths of Aβ peptide (Zhang et al., 2011). These cleavage events may also occur in different cellular compartments (Hartmann et al., 1997). sAPPβ and Aβ fragments are then secreted from the cell (Chow et al., 2010; Haass et al., 2012). The processing pathways are differentially localised within the cell, suggesting that APP trafficking to and from the cell surface may play a vital role in determining the balance of α- and β-processing of APP (Haass et al., 2012). This may also explain why AICD from the amyloidogenic pathway is reported to regulate gene transcription, while AICD generated from the non-amyloidogenic pathway is not (Belyaev et al., 2010; Goodger et al., 2009).

1.2.2 APP secretases

Because of their influence on the fate of APP, much research has been carried out to identify the secretase enzymes responsible for the cleavage of APP. β-secretase has been identified as β-amyloid cleaving enzyme 1 (BACE1). BACE1 is a type-1 membrane-spanning aspartyl protease that is active in the low pH environment of the endosomal/lysosomal system and Golgi, where it cleaves APP (Shoji et al., 1992; Sinha et al., 1999; Vassar et al., 1999; Yan et al., 1999). γ-secretase is a multiprotein complex consisting of aspartic proteases PS1/2, PS enhancer 2 (PEN-2), nicastrin and anterior pharynx-defective phenotype-1 (Aph-1). PEN-2, nicastrin and Aph1 are believed to be chaperone proteins or involved in targeting the γ-secretase complex to its substrates (Strooper et al. 2012). α-secretase has still not been fully identified but it has recently been reported to be a metalloprotease of the a disintegrin and metalloproteinase (ADAM) family. ADAM9, ADAM10 and ADAM17 are all capable of α-secretase cleavage of APP and there appears to be some functional redundancy among these proteins (Kuhn et al., 2010; Vingtdeux and Marambaud, 2012). In addition, a BACE1 homologue, BACE2, may also cleave APP at the α-secretase site, although BACE2 is only expressed at very low levels in neurons (Basi et al., 2003; Bennett et al., 2000; Yan et al., 2001).

1.2.3 APP functions

The precise function of APP is unknown. APP, APLP1 and APLP2 knockout mice are viable and display only minor phenotypes of reduced body weight and locomotor deficits (Heber et al., 2000; Shariati and De Strooper, 2013). APP/APLP1 double knockout mice are also viable but double knockout of either APP or APLP1 with APLP2 causes death shortly after birth. Despite this, these double knockouts show no obvious histopathological abnormalities (Heber et al., 2000; Shariati and De Strooper, 2013).

While the APP knockout mice are viable, they show neuronal abnormalities such as reduced synaptic density, increased neurite branching and an increase in defective synapses (Li et al., 2010; Wang, 2005). This suggests that APP plays a role in neurite outgrowth and synapse formation, which is supported by evidence that loss of APP reduces neurite length while exogenous APP and AICD augments neurite growth (Allinquant et al., 1995; Koo et al., 1993; Milward et al., 1992; Qiu et al., 1995; Zhou et al., 2012). In addition to this, sAPPα acts as a trophic support molecule for elongating processes (Milward et al., 1992; Ohsawa et al., 1999; Tyan et al., 2012; Young-Pearse et al., 2008). APP also enhances cell surface expression of a receptor for nerve growth factor (NGF), another trophic support factor for developing neurites (Matrone et al., 2011; Milward et al., 1992; Patapoutian and Reichardt, 2001; Wallace et al., 1997) and

finally, APP is involved in the regulation of actin cytoskeleton dynamics in growth cones via its interaction with Fe65 (Cheung et al., 2014; Sabo et al., 2003). In contrast, others report that loss of APP enhances outgrowth (Young-Pearse et al., 2008) and inhibits cell proliferation and neurogenesis (Ghosal et al., 2010; Ma et al., 2008). These conflicting data suggest that both too much and too little APP can be detrimental to normal neuronal development.

APP also appears to play an important role in calcium signalling during synaptic transmission (Gautam et al., 2015; Leissring et al., 2002; Wang, 2005). Both APP overexpressing and knockout mice show enhanced susceptibility to seizures in response to stress (Koike et al., 2012; Vogt et al., 2011), and have a large proportion of non-functioning synapses (Wang, 2005). This may be due to impaired APP-mediated calcium signalling at synapses or the misregulation of cell surface receptors. APP interacts with N-methyl-D-aspartate (NMDA) glutamate receptors and increases their cell surface expression (Cousins et al., 2009), which enhances calcium signalling and synaptic transmission (Carroll and Zukin, 2002; Lau and Zukin, 2007). In contrast to full-length APP, Aβ has the opposite effect on NMDA receptors and instead promotes receptor endocytosis (Snyder et al., 2005).

Another key function of APP is its role in the regulation of gene expression. It carries out this role in conjunction with its binding partner Fe65 (Borg et al., 1996; Bressler et al., 1996; Cao and Südhof, 2004, 2001; Fiore et al., 1995; McLoughlin and Miller, 1996; Trommsdorff et al., 1998; Zambrano et al., 1997). Although there is strong evidence that APP and Fe65 are involved in modulating gene transcription, the genes that are affected by this signalling pathway are not consistently reported (Belyaev et al., 2009; Grimm et al., 2015; Kim et al., 2003; Lau et al., 2008; Pardossi-Piquard et al., 2005; Perkinton et al., 2004; Ryan and Pimplikar, 2005; von Rotz et al., 2004; Xu et al., 2011). The regulation of gene transcription by APP and Fe65 is discussed in more detail in section 1.3.2.

APP has also been implicated in intracellular axonal transport via kinesin-1 (van der Kant and Goldstein, 2015), although others have disputed this finding (Brunholz et al., 2012). There is also evidence linking APP with metal homeostasis (Ayton et al., 2013). In addition, the longer, KPI domain-containing isoforms may also function in regulating blood clotting and wound repair (Dawkins and Small, 2014).

1.2.4 APP interacting proteins

A large number of proteins have been shown to bind to APP (van der Kant and Goldstein, 2015; Van Gassen et al., 2000). The best-characterised APP interacting proteins are those that bind to the ^{682}YENPTY^{687} motif in the intracellular domain of APP. These proteins interact with APP via phosphotyrosine binding (PTB) domains or src-homology-2 (SH2) domains and include Fe65 family proteins, disabled-1 (Dab1), X11 family proteins, c-jun N-terminal kinase (JNK) interacting protein (JIP1), ShcA/C and growth factor receptor-bound protein 2 (GRB2; van der Kant & Goldstein 2015).

The Fe65 protein family comprises Fe65, Fe65-like 1 and Fe65-like 2 (Fe65L1 and Fe65L2). They are all adaptor or scaffolding proteins that contain a number of protein-protein interaction domains, through which, they mediate the assembly of protein complexes. The best-studied family member is Fe65, which is the topic of this thesis and its structure, function and binding to APP are discussed in more detail in section 1.3.

Dab1 is another adaptor protein that interacts with APP via its YENPTY domain (Homayouni et al., 1999; Howell et al., 1999), outcompeting Fe65 for binding (Kwon et al., 2010). Both APP and Dab1 are involved in cell migration (Young-Pearse et al., 2007), possibly by pathways that involve apoE receptors. Interactions between APP and apoE receptors are thought to play a role in modulating lipoprotein metabolism (Hoe and Rebeck, 2008). Fe65 may also be involved in this pathway as it can bind to apoE receptor 2 (ApoEr2) and low-density lipoprotein receptor-related protein (LRP) 1 (Hoe et al., 2006; Kinoshita et al., 2001; Pietrzik et al., 2004; Trommsdorff et al., 1998).

The X11 or munc-18 interacting (Mint) family proteins comprise three adaptor proteins (X11α, X11β and X11γ) that contain a PTB domain that interacts with the YENPTY domain of APP. X11α and X11β are neuron-specific isoforms, while X11γ is ubiquitously expressed (Rogelj et al., 2006). The X11s may facilitate an interaction between APP and the γ-secretase complex to regulate APP processing (Lau et al., 2000a; Mueller et al., 2000). X11β and Fe65 compete for YENPTY binding, with APP preferentially interacting with Fe65 (Lau et al., 2000b). The X11s may also function in APP trafficking via binding to calsyntenin-1 (also known as alcadein α1), a kinesin-1 light chain ligand (Araki et al., 2003). X11β may act as a Golgi coat protein to load APP onto calsyntenin-1-containing vesicles for axonal transport on kinesin-1 motors (Vagnoni et al., 2012).

JIP1 is also thought to be involved in APP transport as it interacts with both APP and kinesin-1 light chain (Fu and Holzbaur, 2013; Matsuda et al., 2001; Muresan and Muresan, 2005; Scheinfeld et al., 2002), although there is conflicting evidence regarding this (Vagnoni et al., 2013). JIP1-dependent transport may facilitate the role of APP in neuronal outgrowth by delivering APP to neurite terminals (Muresan and Muresan, 2005). JIP1 may also enhance the phosphorylation of APP at Thr^{668} by JNK (Inomata et al., 2003; Kimberly et al., 2005). This has been shown to impact other protein interactions with APP, including weakening the APP-Fe65 complex (Ando et al., 2001; Barbagallo et al., 2010; Nakaya and Suzuki, 2006) and enhancing APP-JIP1 binding (Muresan and Muresan, 2005).

ShcA, ShcC and GRB2 adaptor proteins are all capable of interacting with APP via binding to the YENPTY domain of APP (Russo et al., 2005, 2002; Zhou et al., 2004). ShcA-GRB2-APP complexes are reported to be upregulated in AD and may be involved in enhancing extracellular regulated kinase (ERK) 1/2 signalling (Nizzari et al., 2007; Russo et al., 2002; Venezia et al., 2006), although the physiological relevance of this function is unclear. There is also evidence that these adaptor proteins may be involved in regulating APP processing (Nizzari et al., 2007; Xie et al., 2007).

Phosphorylation of specific APP residues regulates these protein-protein interactions. Both X11s and Fe65 bind to unphosphorylated YENPTY domains while Shc proteins have phosphorylation-dependent binding (Borg et al., 1996). Phosphorylation of Tyr^{682} (**Y**ENPTY) on APP facilitates ShcA/C binding by inhibiting the interaction between APP and Fe65 (Tarr et al., 2002a, 2002b) and reducing JIP1 binding (Tamayev et al., 2009). In contrast, phosphorylation of Tyr^{687} (YENPT**Y**) does not alter APP interactions but instead regulates endocytosis and processing of APP (Rebelo et al., 2007; Takahashi et al., 2008). Despite being upstream of the YENPTY motif of APP, phosphorylation at Thr^{668} also inhibits APP-Fe65 binding (Ando et al., 2001; Barbagallo et al., 2010; Nakaya and Suzuki, 2006), although this is not consistently reported (Chang et al., 2006; see Figure 1.3B).

1.3 Fe65

Fe65 is a member of a small family of adaptor proteins comprising Fe65, Fe65L1 and Fe65L2. All three proteins contain an N-terminal WW domain and two C-terminal PTB domains (see Figure 1.5; Bork & Sudol 1994; Bork & Margolis 1995). Through these three domains, the Fe65s can bind to other proteins and act as scaffolds for the formation of larger complexes (see section 1.3.1). WW domains recognise proline-rich

ligands containing a conserved sequence of PPXY or PPLP, while the PTB domains bind to proteins containing phosphotyrosine motifs. The Fe65s show at least some level of functional redundancy (Chow et al., 2015a; McLoughlin and Miller, 2008; Minopoli et al., 2012). For example, all members of the Fe65 family can interact with APP family members via their second C-terminal PTB domain (PTB2; Bressler et al., 1996; Duilio et al., 1998; Guénette et al., 1996; Li et al., 2008; Mcloughlin et al., 1999). While Fe65 family members share structural and functional similarities, they differ in their patterns of protein expression. Fe65 is most highly expressed in neurons with the Fe65L1/2 proteins showing a more widespread, peripheral localisation (Bressler et al., 1996; Duilio et al., 1991).

Fe65 knockout (Fe65KO) and Fe65L1 knockout mice are viable and show no obvious phenotype (Guénette et al., 2006). Fe65/Fe65L1 double knockout mice occur at a lower than predicted frequency, are smaller and often display bilateral circling (Guénette et al., 2006). Fe65 has been better characterised than Fe65L1 or Fe65L2. The *Fe65* gene is located on chromosome 11 at position 11q15 (Bressler et al., 1996). It undergoes alternative splicing to create two Fe65 isoforms that vary in length by 2 residues, located within the PTB1 domain. The longer of these two isoforms is exclusively expressed in neurons and is the most abundant form found in the brain, while the shorter isoform is expressed in non-neuronal cells and is found in both brain and peripheral tissues (Duilio et al., 1991; Hu et al., 1998, 1999). An N-terminally truncated 60 kDa isoform of Fe65 is also expressed in cells and is generated by proteolytic cleavage (Cool et al., 2010; Domingues et al., 2011; Guénette et al., 2006; Hu et al., 2005; McLoughlin and Miller, 2008).

Fe65 mRNA is predominantly expressed in the brain, particularly in the hippocampus, cerebellum and cortex (Bressler et al., 1996; Kesavapany et al., 2002; Simeone et al., 1994). Fe65 is primarily expressed in neurons but it has also been detected in some astrocytes within the hippocampus (Kesavapany et al., 2002). There is limited evidence regarding expression changes of Fe65 in AD brain tissue, but a small-scale study of post-mortem brain samples found an increase of Fe65 in late stage AD. The same study found a co-localisation of Fe65 with neurofibrillary tangles but not amyloid plaques (Delatour et al., 2001). The subcellular localisation of Fe65 within neurons is diffuse, with a high proportion of protein found in the cytoplasm. It co-localises with APP at plasma membranes (Cao and Südhof, 2001; Lau et al., 2000b; Minopoli et al., 2001; Sabo et al., 1999) and is also concentrated in growth cones of developing neurons (Cheung et al., 2014). Some Fe65 is also found in the nucleus, the majority of

which is phosphorylated (Lau et al., 2000b; Minopoli et al., 2001; Zambrano et al., 1998).

Fe65 is a phosphoprotein and is phosphorylated on Ser^{175}, Ser^{228}, Ser^{287}, Ser^{347}, Ser^{459}, Ser^{517}, Tyr^{547}, Ser^{566}, Ser^{610}, Ser^{699} and Thr^{709}. The kinases that phosphorylate these sites are ERK1/2 (Ser^{175}, Ser^{287}, Ser^{347} and Thr^{709}), ataxia telangiectasia mutated (ATM) and ataxia-telangiectasia- and Rad3-related (ATR) protein kinases (Ser^{228}), serum- and glucocorticoid-induced kinase 1 (SGK1; Ser^{566} and Ser^{610}) and c-Abl tyrosine kinase (c-Abl; Tyr^{547}; Chow et al., 2015b; Franz-Wachtel et al., 2012; Jowsey and Blain, 2015; Lau et al., 2008; Lee et al., 2008; Perkinton et al., 2004; Standen et al., 2003). These post-translational modifications can alter the binding affinity of Fe65 to its interacting partners (see section 1.3.2).

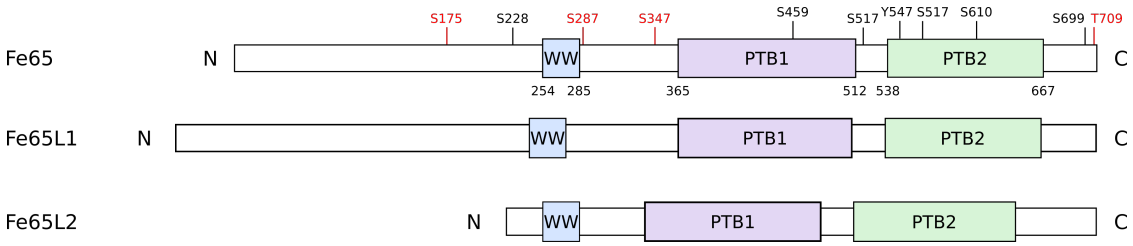

Figure 1.5 The structure of the Fe65 proteins. *The protein-protein interaction domains of the Fe65s are the WW domain and phosphotyrosine binding domains 1 and 2 (PTB1 and PTB2). Also indicated are the phosphorylation sites of Fe65 (Ser^{228}, Ser^{459}, Ser^{517}, Tyr^{547}, Ser^{566}, Ser^{610} and Ser^{699}) and the four ERK1/2 phosphorylation sites of Fe65 (Ser^{175}, Ser^{287}, Ser^{347} and Thr^{709}) that are investigated in this thesis are shown in red.*

1.3.1 Fe65 binding proteins

As stated above, Fe65 contains three protein-protein interaction domains, the N-terminal WW domain and two C-terminal PTB domains. Through these, Fe65 binds to a number of other proteins and facilitates the assembly of multi-protein complexes (Chow et al., 2015a). APP binds to PTB2 and is the best-characterised Fe65 binding protein, but two other proteins have also been reported to bind at this site (see Table 1.1). The best-studied ligands that bind to Fe65 PTB1 are histone acetyltransferase Tip60, LRP1 and transcription factor CP2/LSF/LBP1, although a number of different proteins can interact with PTB1 (see Table 1.2). The third interaction motif of Fe65 is the WW domain, which binds to proline-rich ligands (Salah et al., 2012). Several Fe65 WW domain-interacting proteins have been described (see Table 1.3), of which, mammalian enabled (Mena) and c-Abl are the best characterised.

Fe65 has also been reported to interact with other proteins including Bloom syndrome protein, calsyntenin-1, Dab1, Megalin, Notch, protein phosphatase 1γ, Rac1, sarcoplasmic/ER Ca^{2+} ATPase 2 and synaptic vesicle glycoprotein 2A (Alvira-Botero et al., 2010; Araki et al., 2004; Chow et al., 2015a; Kim et al., 2012; Kwon et al., 2010; Nensa et al., 2014; Rebelo et al., 2013; Schrötter et al., 2013; Wang et al., 2011). The precise interaction domains of Fe65 to which they bind are unknown and they may interact indirectly through multiprotein complexes.

Table 1.1: Proteins reported to interact with the Fe65 PTB2 domain

PTB2 ligand	**Reference(s)**
APP	(Borg et al., 1996; Bressler et al., 1996; Fiore et al., 1995; McLoughlin and Miller, 1996; Zambrano et al., 1997)
Dexras1	(Lau et al., 2008)
Estrogen receptor α (ERα)	(Bao et al., 2007; Sun et al., 2014)

Table 1.2: Proteins reported to interact with the Fe65 PTB1 domain.

PTB1 ligand	**Reference(s)**
ADP-ribosylation factor 6 (ARF6)	(Cheung et al., 2014)
ApoEr2	(Hoe et al., 2006)
CP2/LSF/LBP1	(Kim et al., 2003; Zambrano et al., 1998)
LRP1	(Kinoshita et al., 2001; Pietrzik et al., 2004; Trommsdorff et al., 1998)
Tau	(Barbato et al., 2005)
Teashirt	(Kajiwara et al., 2009)
Tip60	(Cao and Südhof, 2001; Stante et al., 2009)
Very low density lipoprotein receptor	(Dumanis et al., 2012)

Table 1.3: Proteins reported to interact with the Fe65 WW domain.

WW ligand	Reference(s)
c-Abl	(Perkinton et al., 2004; Zambrano et al., 2001)
GSK3β	(Lee et al., 2008b)
Huntingtin	(Chow et al., 2012)
Mena	(Ermekova et al., 1997; Sabo et al., 2001)
Neuronal precursor cell expressed developmentally downregulated 4-2	(Telese et al., 2005)
P2X receptor $P2X_2$ subunit	(Masin et al., 2006)
Nucleosome assembly factor SET	(Telese et al., 2005)

1.3.2 Fe65 functions

A heavily researched role of Fe65 is in the regulation of gene transcription. It carries out this role in a complex with AICD after γ-secretase cleavage of APP. AICD was originally thought to be able to regulate gene transcription alone, in a similar manner to Notch. Like APP, Notch is a type-1 transmembrane protein that undergoes proteolytic cleavage by γ-secretase to produce an intracellular domain. Once released, the Notch intracellular domain translocates to the nucleus where it binds to transcription factors and regulates the expression of Notch responsive genes (Kopan and Ilagan, 2009). Many studies have shown that after γ-secretase cleavage, AICD also translocates to the nucleus, where it is involved in regulating gene transcription (Alves da Costa et al., 2006; Belyaev et al., 2009; Cao and Südhof, 2004, 2001; Kajiwara et al., 2009; Kim et al., 2003; Lau et al., 2008; Li et al., 2010; Ma et al., 2008; McLoughlin and Miller, 2008; Müller et al., 2007; Nakaya and Suzuki, 2006; Pardossi-Piquard et al., 2005; Perkinton et al., 2004; Robinson et al., 2014; Schrötter et al., 2013; von Rotz et al., 2004; Xu et al., 2011). In contrast to the Notch intracellular domain however, AICD is relatively small (~50 residues). While AICD has been shown to interact directly with Mediator, an RNA polymerase II subunit (Xu et al., 2011), it may require its interaction with Fe65 to facilitate the recruitment of other nuclear proteins to create a complex that can regulate gene transcription of target genes. Fe65 may also be required for the nuclear translocation of AICD (Cao and Südhof, 2001; Kinoshita et al., 2002). Contrary to this however, some studies report that APP-Fe65 nuclear signalling is not involved in gene transcription (Hébert et al., 2006; Waldron et al., 2008)

The route of AICD-Fe65 nuclear signalling is unclear. γ-secretase cleavage of APP could release AICD-bound Fe65 from the transmembrane fragment of APP, allowing nuclear translocation of the AICD-Fe65 complex. Alternatively, Fe65 could dissociate from full-length APP, perhaps triggered by phosphorylation events that weaken the

interaction between the two proteins (Ando et al., 2001; Barbagallo et al., 2010; Chow et al., 2015b; Nakaya and Suzuki, 2006; Zhou et al., 2009). This would allow Fe65 to translocate to the nucleus alone, where it could bind to nuclear AICD fragments. The translocation of Fe65 is not AICD-dependent (Kim et al., 2003) and while several studies report that nuclear trafficking of AICD requires Fe65 (Cao and Südhof, 2001; Kinoshita et al., 2002), this does not always appear to be the case (Nakaya and Suzuki, 2006).

While AICD is produced from both proteolytic processing pathways of APP, there is evidence that only β-secretase processed AICD is transcriptionally active (Belyaev et al., 2010; Waldron et al., 2008). This is perhaps due to the location of the protein fragment after β-secretase processing in the endosomal/lysosomal system, rather than α-secretase processing at the cell surface. The shift in equilibrium in APP processing seen in AD means that there is likely to be more transcriptionally active AICD present in cells, along with an increase in Fe65 (Delatour et al., 2001; Zhang et al., 2011).

Two extracellular proteins have been reported to regulate gene transcription via APP-Fe65 nuclear signalling. TAG1 binds to APP and enhances γ-secretase-mediated release of AICD and promotes gene transcription (Ma et al., 2008). F-spondin is a secreted signalling molecule that also binds to the extracellular domain of APP. In contrast to TAG1, F-spondin inhibits AICD-Fe65 signalling by preventing β-secretase-mediated processing of APP, which may reduce the amount of transcriptionally active AICD available (Belyaev et al., 2010; Ho and Südhof, 2004).

A number of genes have been proposed to be regulated by APP-Fe65 signalling (see Table 1.4) and some of these genes are linked to AD pathogenesis. Most of this work has focussed on genes regulated by AICD, while the role of Fe65 has been less well studied. This may be due to the well-established link between APP and AD.

Table 1.4: Genes reported to be positively regulated by APP-Fe65 signalling.

Gene(s)	Reference(s)
GSK3β	(Kim et al., 2003; Lau et al., 2008; Perkinton et al., 2004)
APP	(von Rotz et al., 2004)
Neprilysin	(Belyaev et al., 2009; Grimm et al., 2015; Pardossi-Piquard et al., 2005; Xu et al., 2011)
KAI1	(Baek et al., 2002; Bao et al., 2007; Ryan and Pimplikar, 2005)
p53	(Alves da Costa et al., 2006)
Microtubule associated monooxygenase, calponin and LIM domain containing 2, Fibronectin 1	(Müller et al., 2007; Xu et al., 2011)
BACE1, Tip60	(von Rotz et al., 2004)
Insulin like growth factor binding protein 3, Solute carrier family 7 member 5, Actin α2, Transgelin, Tropomyosin 1, RAB3B	(Müller et al., 2007)
Transthyretin, Klotho	(Li et al., 2010)
BLM, Minichromosome maintenance complex component 3	(Schrötter et al., 2013)
Caspase 4, apoptosis-related cysteine peptidase	(Kajiwara et al., 2009)
Aquaporin	(Xu et al., 2011)

Exactly how the APP-Fe65 complex regulates gene transcription has not been fully elucidated and the mechanism of action may differ between target genes. The best-studied mechanism of gene regulation by APP-Fe65 is of neprilysin, a protein involved in the degradation of Aβ (Saido and Leissring, 2012). AICD binds directly to both promoter regions of the *neprilysin* gene and recruits Fe65, Tip60 and Mediator. This complex acts as a transcriptional activator and enhances neprilysin expression in an APP-dependent manner (Belyaev et al., 2009; Grimm et al., 2015; Pardossi-Piquard et al., 2005; Xu et al., 2011). However, high-throughput methods of quantifying gene expression changes failed to detect changes to neprilysin expression (Giliberto et al., 2008; Müller et al., 2007), and others report a similar lack of neprilysin expression level changes in transfected cells (Hébert et al., 2006; Waldron et al., 2008).

The APP-Fe65-Tip60 complex also regulates the expression of the tetraspanin KAI1. In this system, a repressor complex binding to the *KAI1* promoter region normally inhibits KAI1 expression. When this repressor is replaced by the APP-Fe65-Tip60 complex, RNA polymerase II is recruited and gene expression increases (Baek et al., 2002; Ryan and Pimplikar, 2005). Expression of KAI1 also requires an interaction between the APP-Fe65-Tip60 complex and SET (Telese et al., 2005). Oestrogens negatively regulate this complex by enhancing ERα recruitment. ERα displaces Tip60 from the APP-Fe65-Tip60 complex and prevents KAI1 expression (Bao et al., 2007). As with neprilysin expression however, there are also reports to the contrary, which do not show an increase in KAI1 expression in response to overexpression of AICD or AICD and Fe65 (Giliberto et al., 2008; Hébert et al., 2006; Müller et al., 2007; Waldron et al., 2008).

APP-Fe65 nuclear signalling does not only enhance gene transcription but can reduce expression of target genes as well. The expression of stathmin 1, F-actin capping protein and thymidylate synthase is inhibited by the APP-Fe65 complex (Bruni et al., 2002; Müller et al., 2013). For these genes, the APP-Fe65 complex may be acting as a repressor, rather than an activator. The inhibition of thymidylate synthase involves the Fe65-CP2/LSF/LBP1 interaction (Bruni et al., 2002). Interestingly, stathmin 1 and F-actin capping protein are involved in regulating cytoskeleton dynamics, a process that both APP and Fe65 have also been implicated in regulating (Müller et al., 2013; Sabo et al., 2003, 2001).

Phosphorylation of both APP and Fe65 can regulate their interaction. Phosphorylation of Thr^{668} and Tyr^{682} on APP inhibits its binding to Fe65 (Ando et al., 2001; Barbagallo et al., 2010; Nakaya and Suzuki, 2006; Zhou et al., 2009), as does phosphorylation of Fe65 at Ser^{610} (Chow et al., 2015b). As Fe65 binds to both full-length APP and AICD and these interactions have different consequences, it is unclear what effect destabilising the interaction may have on APP-Fe65-mediated gene transcription. Reducing the interaction between full-length APP and Fe65 may enhance Fe65 nuclear translocation, but reducing the interaction between Fe65 and AICD in the nucleus may reduce transcription of target genes.

The APP-Fe65 complex is not solely modulated by phosphorylation events. A number of other Fe65 binding partners have been identified as regulators of Fe65-mediated gene transcription. These include Dexras1, calsyntenin-1, Tip60, ERα, the intracellular domain of LRP1 and Teashirt (Araki et al., 2004; Bao et al., 2007; Kajiwara et al., 2009; Kinoshita et al., 2003; Lau et al., 2008). The ways in which these proteins modulate

Fe65 function varies from preventing Fe65-protein interactions, such as LRP1 competing with APP for Fe65 binding and sequestering Tip60 (Kinoshita et al., 2001; Mulvihill et al., 2011), to activating other pathways that inhibit gene transcription, such as Teashirt, which increases histone deacetylase activity to act in opposition to Tip60 (Kajiwara et al., 2009).

1.3.3 Other functions of Fe65

A number of other functions have been ascribed to Fe65. Another nuclear function of Fe65 is regulating the repair of deoxyribonucleic acid (DNA) damage. Cells derived from Fe65KO mice are more sensitive to DNA damage, suggesting that Fe65 may also be involved in DNA repair pathways (Minopoli et al., 2007). Fe65 is required for effective DNA repair and binds to chromatin to facilitate the recruitment of Tip60 and other repair proteins to DNA damage sites (Minopoli et al., 2007; Stante et al., 2009). In this role, Fe65 inhibits cell death (Nakaya et al., 2008), however, other studies suggest that overexpression of Fe65 enhances apoptosis (Vázquez et al., 2009).

Other functions of Fe65 relate to cell motility in neuronal development and neurite outgrowth. While Fe65KO mice have no anatomical abnormalities (Guénette et al., 2006; Wang et al., 2004, 2009), they show enhanced neurogenesis (Ma et al., 2008), suggesting a role for Fe65 in the regulation of developing neurons. Simultaneous knockout of Fe65 and Fe65L1 results in neuronal migration defects similar to those seen in APP family knockout mouse models (Guénette et al., 2006; Herms et al., 2004). As with APP mouse models, this suggests that there is functional redundancy between the Fe65 family proteins. Fe65KO mice show impairments in hippocampal-dependent learning and long-term potentiation (LTP) indicating that while Fe65 may not play an essential role in brain development, it is required for normal hippocampal learning and memory (Guénette et al., 2006; Wang et al., 2004, 2009).

Another function of Fe65 is the regulation of protein degradation via the ubiquitin-proteasome system (UPS). Fe65 stabilises the intracellular domain of APP (Huysseune et al., 2007; Pietrzik et al., 2004; Waldron et al., 2008; Walsh et al., 2003), although this may only be the case for exogenous AICD (Kimberly et al., 2001; Nakaya and Suzuki, 2006). Fe65 also protects full-length APP, apoptotic factor p53 and mutant huntingtin from UPS-mediated degradation. Decreasing the degradation of proteins contributes to their accumulation in cells. Considering the functions of these proteins, this may be one mechanism by which Fe65 enhances gene transcription, apoptosis and mutant huntingtin aggregation (Chow et al., 2015b, 2012; Nakaya et al., 2008).

Evidence that Fe65 positively regulates cell motility and neurite outgrowth in cellular models corroborates a role for Fe65 in neuronal development. Overexpression of Fe65 and APP increases the rate of cell migration (Sabo et al., 2001) and Fe65 interacts with Mena, ARF6 and Rac1, proteins involved in regulating actin cytoskeleton dynamics (Cheung et al., 2014; Ermekova et al., 1997; Sabo et al., 2001; Wang et al., 2011). In addition to this, Fe65, APP and Rac1 co-localise in extending lamellipodia (Sabo et al., 2001; Wang et al., 2011) and Fe65 stimulates Rac1 activation via small GTPase ARF6, to augment neurite outgrowth (Cheung et al., 2014; see Chapter 5).

1.3.3.1 ARF6

ARF6 is a member of the Ras superfamily of small GTPases. These GTPases are members of signalling cascades and cycle between inactive GDP bound and active GTP bound conformational states. GTPase activating proteins (GAPs) accelerate the hydrolysis of bound GTP to GDP, inactivating the GTPase, while guanine nucleotide releasing proteins (GNRPs) promote dissociation of GDP, allowing uptake of GTP and activation of the GTPase (Cherfils and Zeghouf, 2013). ARF6 KO mice are embryonic lethal, indicating that, while ARF6 belongs to a large family of similar proteins, there is not enough redundancy between protein functions to rescue the loss of ARF6. Conditional ARF6 KO mice have deficient myelination of neurons, which has been linked to ARF6-dependent impairments of the migration of cells responsible for axon myelination (Akiyama and Kanaho, 2015). In addition, ARF6 has been linked to many functions including cytoskeletal organisation and membrane trafficking in endocytosis and exocytosis (Akiyama and Kanaho, 2015; Cheung et al., 2014; Gillingham and Munro, 2007). Chapter 5 describes novel work to which I contributed which showed that Fe65 binds to ARF6 to stimulate neurite outgrowth. This work has now been published and the paper is presented in the Appendix.

1.3.4 Fe65 and APP processing

The effects of Fe65 on APP processing and Aβ production have been studied by several groups but the results are conflicting. In cultured cells, Fe65 overexpression increases APP cell surface presentation (Hoe et al., 2006; Sabo et al., 1999) and several studies report increases in sAPPα secretion (Dumanis et al., 2012; Hoe et al., 2006; Pietrzik et al., 2004; Suh et al., 2011). Conversely, some report that APP processing is decreased by Fe65 overexpression (Ando et al., 2001; Kwon et al., 2010). The effect of Fe65 on Aβ production is also unclear. While most studies show that Fe65 decreases amyloidogenic processing of APP (Ando et al., 2001; Hoe et al., 2006; Kwon et al., 2010; Wiley et al., 2007; Xie et al., 2007), increased Aβ production has also been detected in response to exogenous Fe65 expression (Sabo et al., 1999).

This may be due to cell-specific responses as these studies were carried out in a variety of cell types.

Mice overexpressing APP and Fe65 show reduced levels of APP processing and Aβ production (Santiard-Baron et al., 2005). Fe65 overexpression also reduces the amount of APP Thr^{668} phosphorylation (Santiard-Baron et al., 2005), which is consistent with a reduction of APP processing (Ando et al., 2001; Lee et al., 2003; Liu et al., 2003). However, Fe65KO mouse models can also have decreased Aβ secretion (Guénette et al., 2006; Suh et al., 2011; Wang et al., 2004), suggesting that the role of Fe65 in APP processing is not simple. One possible reason for this is that Fe65 may have a dominant negative impact on APP and its interacting partners. This may explain why both loss and gain of Fe65 appears to decrease Aβ production (Pietrzik et al., 2004).

Mice overexpressing Fe65 and AICD develop AD-like tau pathology (Ghosal et al., 2009), potentially linking an alteration in APP processing (which, in these mice, is mimicked by elevated AICD production) to the development of tau hyperphosphorylation and aggregation into NFTs. These mice also show enhanced levels of GSK3β activity (Ryan and Pimplikar, 2005).

To summarise, the precise roles of Fe65 on APP processing, Aβ production and tau phosphorylation are not properly understood and some of the data are conflicting. Further work is needed to determine what role, if any, Fe65 may have in AD.

1.4 Signalling pathways in Alzheimer's disease

Along with APP-Fe65 signalling, disruption of other signalling pathways has been linked to AD. These include JNK stress-activated signalling (Yarza et al., 2016), signalling via inflammatory factors (McCaulley and Grush, 2015) and insulin signalling (Ferreira et al., 2014; Liu et al., 2011). Two signalling pathways relevant to this thesis are the brain-derived neurotrophic factor (BDNF) and wnt pathways described below.

1.4.1 BDNF signalling

BDNF is an extracellular growth factor that is expressed highly in the brain, and interestingly, in areas that are affected by neuron loss in AD (Hofer et al., 1990; Murer et al., 1999; Murray et al., 1994; Phillips et al., 1990). BDNF is secreted from excitatory neurons and binds to membrane-bound tyrosine receptor kinase B (TrkB), which is presented on the cell surface of both excitatory and inhibitory neurons (Arancibia et al.,

2008; Huang and Reichardt, 2001). This activates TrkB and initiates downstream signalling to the ERK, phosphoinositide 3-kinase/Akt and phospholipase C pathways (Kaplan and Miller, 2000; Numakawa et al., 2010; Figure 1.6). BDNF-mediated signal transduction is important for neuron survival, differentiation and LTP (Alderson et al., 1990; Arancibia et al., 2008; Bonni et al., 1999; Ghosh et al., 1994; Kang and Schuman, 1995; Knüsel et al., 1992; Korte et al., 1995; Lindholm et al., 1996; Patterson et al., 1996).

One of the intracellular cascade pathways that BDNF-TrkB activation initiates is the ERK1/2 mitogen-activated protein (MAP) kinase cascade (Yang et al., 2013). This involves activation of the small GTPase Ras and sequential activation of kinases RAF, MAP kinase kinase (MEK) and ERK. ERK can then phosphorylate various proteins including the activation of transcription factors (Seger and Krebs, 1995). The MAP kinase cascade is a global signalling pathway that has been linked to many cellular processes (Yang et al., 2013).

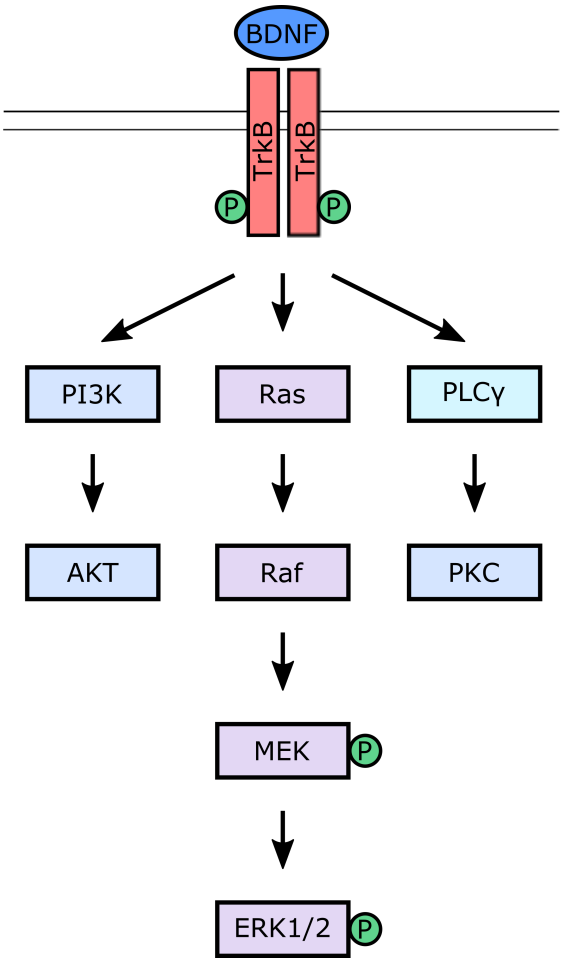

Figure 1.6: The BDNF signalling pathways. *BDNF binds to receptor TrkB and activates several intracellular pathways: PI3K, the ERK MAP kinase cascade and PLCγ.*

A number of lines of evidence link BDNF signalling with AD. BDNF knockout mice have reduced hippocampal synaptic transmission and synaptic density, increased cell death and impaired LTP, while mice overexpressing BDNF have increased LTP (Barco et al., 2005; Lindholm et al., 1996; Patterson et al., 1996). The phenotypes of BDNF-deficient mice can be rescued by exogenous application of BDNF (Lindholm et al., 1996; Patterson et al., 1996). Addition of BDNF also restores synaptic density and hippocampal-dependent memory deficits in AD mouse models (Blurton-Jones et al., 2009; Nagahara et al., 2009). These findings are consistent with data from cellular models showing that BDNF increases synaptic density and protects against cell death (Alderson et al., 1990; Blurton-Jones et al., 2009; Ghosh et al., 1994; Knüsel et al., 1992; Lindholm et al., 1996; Nagahara et al., 2009).

Expression of both BDNF and TrkB is reduced in disease-vulnerable areas in AD (Conner et al., 1997; Durany et al., 2000; Ferrer et al., 1999; Murer et al., 1999; Narisawa-Saito et al., 1996; Phillips et al., 1991; Pláteník et al., 2014). In addition to this, BDNF can be detected in neuritic plaques, particularly in the dystrophic neurites surrounding the Aβ core. This indicates either a possible protective response by the brain or sequestration of BDNF by neuritic plaques (Ferrer et al., 1999; Murer et al., 1999). Indeed, BDNF protects neurons from Aβ-induced toxicity (Arancibia et al., 2008; Nagahara et al., 2009), although it has no effect on plaque development or clearance. This may be due to a lack of TrkB expression in some neurons (Ferrer et al., 1999; Murer et al., 1999). Both the decrease of BDNF seen in AD and apparent sequestering of the limited neurotrophin to neuritic plaques may contribute to neuronal degradation via withdrawal of the cell-survival function of BDNF. Recently BDNF has been identified as a target of the wnt signalling pathway via β-catenin and T-cell factor/lymphoid enhancer factor (TCF/LEF)-mediated gene transcription (Fragoso et al., 2011; Seitz et al., 2010; Yi et al., 2012). There is evidence that β-catenin nuclear signalling may be impaired in AD (Zhang et al. 1998; Nishimura et al. 1999), so disruption of the wnt signalling pathway may contribute to decreased levels of BDNF expression in AD (Conner et al., 1997; Durany et al., 2000; Ferrer et al., 1999; Murer et al., 1999; Narisawa-Saito et al., 1996; Phillips et al., 1991; Pláteník et al., 2014).

BDNF also shows neuroprotective effects against neuron death induced by entorhinal cortex damage. BDNF treatment increases cell survival and partially restores LTP and learning deficits in both mice and non-human primates with entorhinal cortical lesions (Ando et al., 2002; Nagahara et al., 2009). These findings are promising as they suggest that BDNF treatment may be effective even after synapse loss and neuronal death, which is currently the only stage at which AD can be diagnosed. Finally, BDNF

expression is increased in response to physical exercise and enhances learning ability (Adlard and Cotman, 2004; Adlard et al., 2004), which is consistent with physical exercise being a neuroprotective environmental factor for AD (Adlard et al., 2005).

Fe65 has been identified as a substrate for ERK1/2, which phosphorylates Fe65 on at least 4 residues (Standen et al., 2003). However, the biological effect of Fe65 phosphorylation at these sites and how ERKs might be activated to phosphorylate Fe65 are unknown. Phosphorylation of both APP and Fe65 at other sites influence the APP-Fe65 interaction and this may impact the ability of the complex to regulate gene transcription (Ando et al., 2001; Barbagallo et al., 2010; Chow et al., 2015b; Nakaya and Suzuki, 2006; Zhou et al., 2009). Whether BDNF induces the phosphorylation of Fe65 via the MAP kinase cascade, and what effect this has on the APP-Fe65 interaction has not yet been studied, but it may provide insight into an intracellular mechanism for the neuroprotective action of BDNF.

1.4.2 Wnt signalling

Wnts are a large family of secreted glycoproteins that act in an autocrine and paracrine fashion (Clevers and Nusse, 2012). They bind to specific cell surface receptors called Frizzled (Fzd) that are coupled to LRP5/6 co-receptors. Receptor-ligand binding activates the intracellular domains of the receptors and initiates either the canonical or non-canonical wnt signalling pathway (MacDonald et al., 2009). There are 19 wnt ligands and 10 Fzd receptors and the specific combination of wnt ligand and Fzd receptor may determine which pathway is activated, although the relationships between them have not all been comprehensively described (Clevers and Nusse, 2012; Niehrs, 2012). The canonical pathway leads to changes in gene transcription. The non-canonical planar cell polarity pathway regulates the cytoskeleton and the non-canonical Ca^{2+} pathway regulates Ca^{2+} homeostasis (Niehrs, 2012).

In the canonical pathway, in the absence of wnt signal, GSK3 is present in a multimeric protein complex termed the ‘destruction complex’ also containing Axin, casein kinase I and adenomatous polyposis coli (Kimelman and Xu, 2006). The destruction complex is constitutively active and leads to phosphorylation of the nuclear signalling molecule β-catenin. This phosphorylation targets β-catenin for degradation by the UPS (Clevers and Nusse, 2012; Kimelman and Xu, 2006). Wnt-Fzd binding activates the cytoplasmic protein, dishevelled, which causes dissociation of the destruction complex. This allows β-catenin to translocate and accumulate in the nucleus where it binds to TCF/LEF transcription factors and activates transcription of a large number of target genes (Behrens et al., 1996; http://web.stanford.edu/group/nusselab/cgi-bin/wnt/target_genes;

Schuijers et al., 2014; Figure 1.). The canonical wnt pathway regulates a variety of functions including development, LTP, synapse formation, neurogenesis and cell adhesion (Inestrosa and Varela-Nallar, 2014; Logan and Nusse, 2004; Purro et al., 2014).

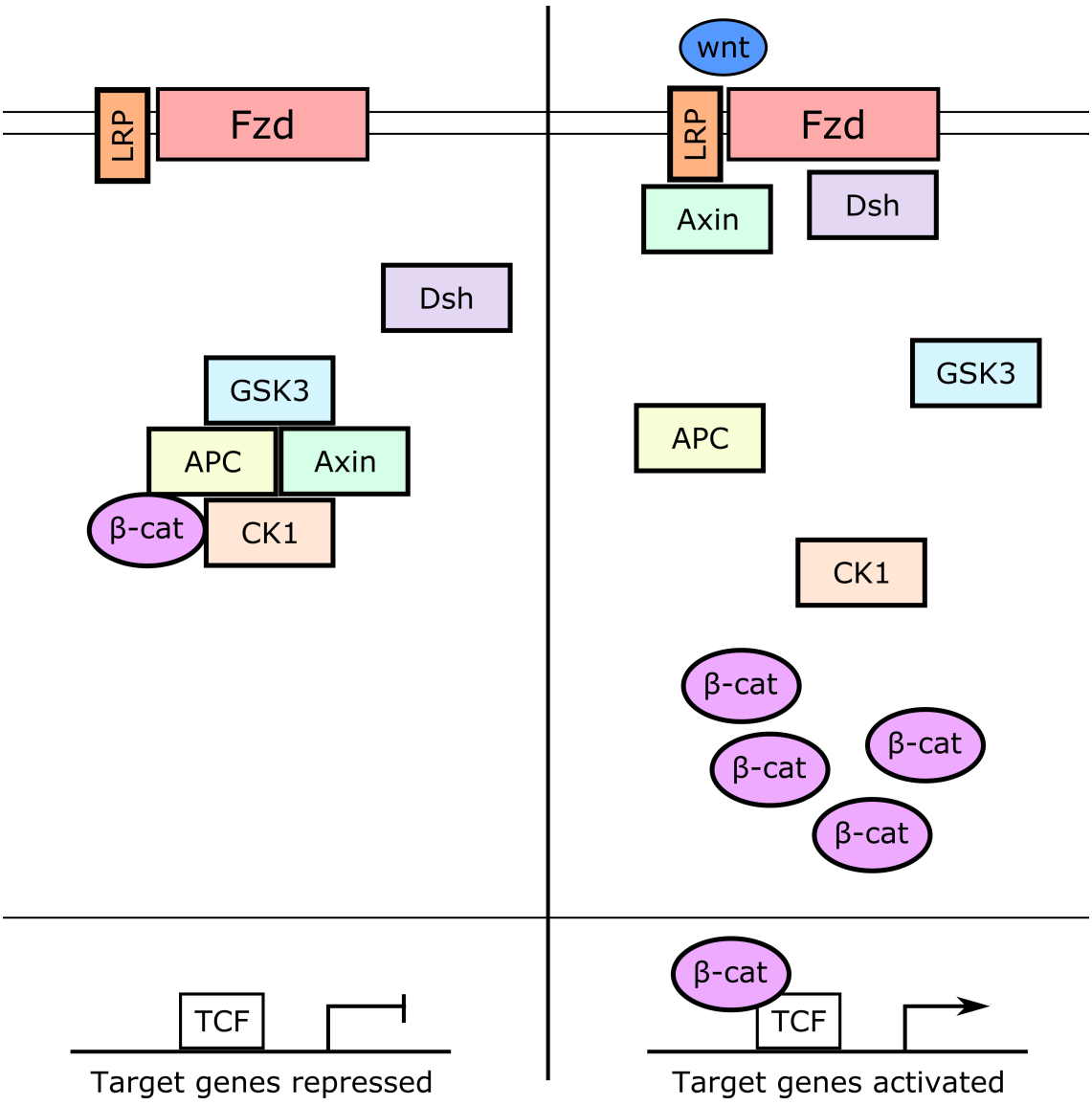

Figure 1.7: The wnt signalling pathway. *In the absence of wnt signal, GSK3, Axin, casein kinase I (CK1) and adenomatous polyposis coli (APC) are present in the constitutively active destruction complex, which targets β-catenin (β-cat) for degradation. Wnt-Fzd binding activates dishevelled (dsh), resulting in dissociation of the destruction complex, which allows β-catenin to translocate and accumulate in the nucleus where it is involved with the transcription factor TCF in activating gene transcription.*

The canonical wnt pathway is of particular interest in the field of AD as it regulates the activity of GSK3, one of the kinases involved in the phosphorylation of tau (Hernández et al., 2010; Hooper et al., 2008). It forms the basis of the GSK3 hypothesis of AD which proposes that GSK3 hyperactivity is responsible for tau hyperphosphorylation (Hooper et al. 2008). Unlike other pathways of GSK3 regulation, the wnt signalling pathway does not appear to inactivate the two GSK3 isoforms (GSK3α and GSK3β) via $Ser^{21/9}$ phosphorylation (on GSK3α and GSK3β respectively; Ding et al., 2000). Two mechanisms of GSK3 inactivation that have been proposed are LRP-mediated inhibition of the GSK3 active site and endocytosis of LRP-GSK3 complexes into vesicles (Metcalfe and Bienz, 2011).

In addition to GSK3 inactivation, β-catenin has been shown to be neuroprotective against Aβ toxicity (Alvarez et al., 2004; Chacón et al., 2008; De Ferrari et al., 2003). There is also evidence that wnt signalling is impaired in AD. β-catenin degradation is increased in familial AD cases caused by *PS1* mutations (Zhang et al., 1998) and its nuclear translocation is also disrupted (Nishimura et al., 1999). Reductions of β-catenin in AD may limit the ability of cells to resist Aβ neurotoxicity (He and Shen, 2009). This may be catalysed by a concomitant Aβ-induced rise in expression of Dikkopf-1, a negative regulator of the wnt signalling pathway (Caricasole et al., 2004; Killick et al., 2014; Purro et al., 2012).

1.5 Hypotheses and aims

Abnormal metabolism of APP is strongly linked to the pathogenesis of AD but much of the research supporting this link is focused on Aβ and not on APP function. There is evidence that the APP-Fe65 complex signals to the nucleus to regulate gene transcription and this provides a complementary route in which defects in APP metabolism might contribute to AD. However, the mechanisms that regulate binding of Fe65 to APP and the genes that are regulated by this signalling pathway are unclear. Phosphorylation is a common mechanism for regulating protein-protein interactions and ERK1/2 has recently been shown to phosphorylate Fe65.

The studies presented in this thesis address two related hypotheses:
1. That BDNF signalling, which leads to activation of ERK1/2 in neurons, stimulates Fe65 phosphorylation to regulate its binding to APP
2. That Fe65 regulates genes that are linked to GSK3α/β activity and tau phosphorylation.

The aims of this thesis were to begin to test these hypotheses.

CHAPTER 2: MATERIALS AND METHODS

2.1 Materials

Unless otherwise stated, all chemicals and reagents were purchased from Sigma-Aldrich (Dorset, UK). Solutions and buffers were prepared using ultrapure H_2O from a Milli-Q purification system (Merck Millipore; Watford, UK). When required, sterilisation was carried out using a 0.2 µm pore Nalgene filter (ThermoFisher Scientific; Loughborough, UK) or by autoclaving at 121 °C and 101 kPa for 20 min.

2.1.1 Antibodies

Primary antibodies were obtained from Abcam (Cambridge, UK), BD Biosciences (Oxford, UK), Cell Signaling (Leiden, The Netherlands), DAKO (Cambridge, UK), Millipore, R&D Systems (Abingdon, UK), Santa Cruz (Heidelberg, Germany), Sigma-Aldrich or made in house and are detailed in Table 2.1.

Table 2.1: Primary antibodies used in these studies.

Antigen	Species	Manufacturer	Dilution
APP (CT-17)	Rabbit	In house (Cousins et al., 2009)	1:5000 (WB) 1:400 (PLA)
ARF6	Rat	In house (Cheung et al., 2014)	1:1000 (WB) 1:500 (IF)
Fe65 (2877)	Rabbit	Cell Signaling Technology	1:1000 (WB)
Fe65 (4H324)	Mouse	Abcam	1:5000 (WB exogenous) 1:1000 (WB endogenous) 1:400 (PLA)
Fe65 (sc-19751)	Goat	Santa Cruz Biotechnology	1:200 (IP) 1:1000 (WB)
Fe65 (C60)	Rabbit	In house (Lau et al., 2000b)	1:1000 (WB)
ERK1/2 (M12320)	Mouse	BD Biosciences	1:1000 (WB)
Phospho-ERK1/2 (Thr^{202}/Tyr^{20}, Thr^{185}/Tyr^{187}; 9102)	Rabbit	Cell Signaling Technology	1:1000 (WB)
Fzd1 (AF1120)	Rabbit	R&D Systems	1:500 (WB)

Table continued overleaf

Table 2.1: Primary antibodies used in these studies (continued).

Antigen	Species	Manufacturer	Dilution
Fzd1 (sc-30428)	Goat	Santa Cruz Biotechnology	1:500 (WB)
Pan Fzd (sc-9169)	Rabbit	Santa Cruz Biotechnology	1:500 (WB)
GAPDH (14C10)	Rabbit	Cell Signaling Technology	1:20000 (WB)
GSK3α (9338)	Rabbit	Cell Signaling Technology	1:1000 (WB)
GSK3β (610201)	Mouse	BD Biosciences	1:1000 (WB)
Phospho-GSK3β (Ser^{9}; 9336	Rabbit	Cell Signaling Technology	1:1000 (WB)
LRP6 (C5C7)	Rabbit	Cell Signaling Technology	1:1000 (WB)
Myc (9B11)	Mouse	Cell Signaling Technology	1:2000 (WB)
Tau (A0024)	Rabbit	DAKO	1:10000 (WB)
Phospho-Tau (Ser^{202}; CP13)	Mouse	Gift from Peter Davies (Albert Einstein College of Medicine, USA)	1:400 (WB)
α-Tubulin (T6199)	Mouse	Sigma-Aldrich	1:20000 (WB)
Wnt3a (2391)	Rabbit	Cell Signaling Technology	1:750 (WB)

WB = western blot, PLA = proximity ligation assay, IP = co-immunoprecipitation

Secondary antibodies used in western blotting were polyclonal goat anti-mouse, polyclonal goat anti-rabbit or polyclonal rabbit anti-goat immunoglobulins conjugated to horseradish peroxidase. Secondary antibodies were obtained from DAKO and used at a dilution of 1:8000.

2.1.2 Enzyme-linked immunosorbent assays (ELISA)

Total tau and Ser^{199} phosphorylated tau ELISA kits were purchased from ThermoFisher Scientific. The Phospho/Total GSK3β ELISA kit was purchased from Meso Scale Diagnostics (Maryland, USA) and measured both total GSK3β and GSK3β phosphorylated at Ser^{9}.

2.1.3 Plasmid vectors

Table 2.2: Mammalian and bacterial expression plasmids used in these studies.

Construct	Vector	Reference
APP	pCI-neo	(Mcloughlin et al., 1999)
Fe65	pCI-neo	(Lau et al., 2000b)
Fe65-myc	pCI-neo	(Lau et al., 2000b)
$Fe65_{QuadA}^{*}$	pCI-neo	(Standen et al., 2003)
$Fe65_{QuadE}^{*}$	pCI-neo	(Standen et al., 2003)
ARF6-myc	pCI-neo	(Cheung et al., 2014)
Chloramphenicol acetyltransferase (CAT)	pCI-neo	(Lau et al., 2002)
Glutathione-*S*-transferase (GST)	pGEX-5X-1	(Standen et al., 2001) G.E. Healthcare (Buckinghamshire, UK)
$GST\text{-}APP_C$	pGEX-5X-1	(Standen et al., 2001)
GST-ARF6	pCI-neo	(Cheung et al., 2014)
GST-Fe65WW	pCI-neo	(Cheung et al., 2014)
GST-Fe65PTB1	pCI-neo	(Cheung et al., 2014)
GST-Fe65PTB2	pCI-neo	(Cheung et al., 2014)
Fe65ΔPTB1	pCMV	(Cao and Südhof, 2001)
Fe65ΔPTB2	pCMV	(Cao and Südhof, 2001)

$^{*}Fe65_{QuadA}$ and $Fe65_{QuadE}$ phosphorylation mutants contain mutations at Ser^{175}, Ser^{287}, Ser^{347} and Thr^{709} to alanine and glutamic acid respectively.

2.2 General biochemical reagents

Luria-Bertani (LB) agar and LB broth were obtained from Life Technologies Ltd (Paisley, UK). The HiSpeed plasmid purification midi kit, RNeasy mini kit and RNase-free DNase I set were obtained from Qiagen (Manchester, UK). The protein assay kit was obtained from Bio-Rad (Hertfordshire, UK). REDExtract-N-Amp™ tissue polymerase chain reaction (PCR) kit was purchased from Sigma-Aldrich.

2.2.1 General tissue culture reagents

Fetal Bovine Serum (FBS), L-glutamine (200 mM) and trypsin-etylenediamintetraacetic acid (EDTA) solution (0.05 % (v/v)/0.02 % (v/v) in phosphate buffered saline; PBS) were supplied by G.E. Healthcare. Opti-MEM reduced serum medium, Ham's F12 medium, Dulbecco's modified Eagle medium (DMEM), DMEM/Ham's F12 medium,

Hank's balanced salt solution without Ca^{2+} and Mg^{2+} (HBSS (-/-)), HBSS with Ca^{2+} and Mg^{2+} (HBSS (+/+)), Neurobasal media, B-27 supplement, AlbuMAX-I, penicillin/streptomycin (100x), Lipofectamine and Lipofectamine 2000 were supplied by Life Technologies Ltd. Blasticidin (powder, prepared to a stock solution of 1500 µg/ml in DMEM/Ham's F12 medium) was obtained from Santa Cruz and Zeocin (100 mg/ml) was from Invivogen (Toulouse, France). Deoxyribonuclease (DNase) I, soybean trypsin inhibitor, Trypan blue (0.4 %) and plasticware were from Sigma-Aldrich.

2.2.2 Mammalian cell culture and transfection

Table 2.3: Growth media and transfection reagents for cell lines.

Cell Line	Growth medium	Transfection reagent	Manufacturer
Chinese hamster ovary cells (CHO)	Ham's F12 4.5 g/L glucose 2 mM L-glutamine 0 % (v/v) FBS	Lipofectamine 2000	Life Technologies Ltd
		FuGene 6	Roche
CHO cells stably transfected with TrkB (CHO-TrkB)	DMEM 4.5 g/L glucose 2 mM L-glutamine 10 % (v/v) FBS 5 µg/ml Blasticidin 200 µg/ml Zeocin	Lipofectamine 2000	Life Technologies Ltd
Human embryo kidney (HEK) 293 cells	DMEM 4.5 g/L glucose 2 mM L-glutamine 10 % (v/v) FBS	Lipofectamine	Life Technologies Ltd

2.2.3 Cell treatments

BDNF was from PeproTech (London, UK), K252a was from Sigma-Aldrich, U0126 was from Millipore. Accell small interfering RNAs (siRNAs) specific to APP (#13 and #16), Fe65 (#14), Fzd1 (pool) and non-targeting control (#1) siRNAs were purchased from Dharmacon (Buckinghamshire, UK).

Table 2.4: siRNA sequences used to achieve Fe65 and APP knockdown in rat cortical neurons.

siRNA	Target Sequence
Fe65 #14	GUGGCAGUCAACAAUUGUA
APP #13	GCACUAACUUGCACGACUA
APP #16	CGGUGAAGACAAAGUCGUA
Fzd1 (pool)	GCGUUAUUAUUAUUAUUGU UUAUGAUGCUCUACUUCUU GCAGUGUGUUCAAUGUAAA CUUUUACCCUUCUAUGAGA
Non-targeting control	UGGUUUACAUGUCGACUAA

2.2.4 Duolink proximity ligation assay (PLA)

The Duolink PLA kits used were *In Situ* detection reagents (orange), *In Situ* wash buffers (fluorescence) and *In Situ* PLA probe kits for rabbit PLUS and mouse MINUS PLA probes. All Duolink PLA kits were obtained from Sigma-Aldrich.

2.2.5 Quantitative real-time PCR (RT-qPCR)

The kits and plasticware used in the RT-qPCR studies were purchased from PrimerDesign (Southampton, UK) and include nanoScript2 reverse transcription kit, PrecisionPLUS mastermix with inert blue dye, GeNorm reference gene analysis kit and custom primers (detailed in 2.3.12.4).

2.3 Methods

2.3.1 General microbiology methods

2.3.1.1 Storage and growth of E. coli for DNA purification

Escherichia coli (*E. coli*) transformed with plasmids of interest were stored at -80°C in sterile 25 % (v/v) glycerol solution in LB broth (20 g/L, autoclaved) containing 100 µg/ml filter-sterilised ampicillin (LB-amp) for selection of the plasmid vector. For bacterial growth, *E. coli* containing the plasmid of interest were grown on LB agar (32 g/L, autoclaved) plates containing 100 µg/ml filter-sterilised ampicillin for selection of the plasmid vector. Selection plates were incubated at 37 °C for 16 h. Single bacterial colonies picked from these selection plates were used to inoculate 5 ml aliquots of LB-amp. These starter cultures were incubated at 37 °C for 8 h in a shaking

incubator at 220 rpm before being used to inoculate 100 ml LB-amp cultures that were incubated for a further 16 h at 220 rpm.

2.3.1.2 Plasmid DNA purification

Plasmid DNA was purified from bacterial cultures using a HiSpeed plasmid purification midi kit (Qiagen) as per the manufacturer's instructions. The concentration of plasmid DNA was quantified by measuring absorbance at 260 nm using a NanoDrop 1000 spectrophotometer (ThermoFisher Scientific) and the 260/280 nm absorbance ratio was used to determine DNA purity; pure DNA has a ratio of 1.8. Plasmid DNA was stored at -20 °C until required.

2.3.1.3 Agarose gel electrophoresis

To prepare agarose gels, 1-1.5 % (w/v) agarose (Ultra pure, electrophoresis grade; Life Technologies Ltd) was heated in 1x Tris-Acetate-EDTA (TAE) buffer containing 40 mM Tris(hydroxymethyl)aminomethane (Tris), 0.11 % (v/v) acetic acid and 1 mM EDTA, buffered to pH 8.0 with NaOH. This solution was poured into a gel bed containing a 15-well comb and ethidium bromide was added to a working concentration of 300 ng/ml before the gel set. The set gel was then moved to an electrophoresis tank and submerged in 1x TAE buffer. Ribonucleic acid (RNA) or PCR samples were diluted with loading buffer containing 0.04 % (w/v) Bromophenol blue and 6.6 % (w/v) sucrose, loaded into the wells and run at 100-150 V. DNA and RNA in agarose gels were visualised under ultraviolet light using a GelDoc-It™ Imaging system (Ultra-Violet Products; Cambridge, UK).

2.3.2 Mammalian cell culture and transfection

2.3.2.1 Passaging, freezing and defrosting cells

Cell cultures were grown in the appropriate growth medium (see Table 2.3) in a humidified incubator at 37 °C with 5 % CO_2. Cells were passaged when they reached approximately 80 % confluency. To passage, cells were washed twice with PBS containing 0.01 M phosphate buffer, 0.0027 M potassium chloride and 0.137 M sodium chloride, pH 7.4 and incubated with enough trypsin-EDTA solution to cover the base of the culture vessel for 5-10 min until the cells had detached from the culture vessel. The cell suspension was triturated using a 5 ml pipette to achieve a single-cell suspension before 4-7.5 ml of the appropriate growth medium was added to inactivate the trypsin treatment (4 ml for 25 cm^2 flasks, 7.5 ml for 75 cm^2 and 175 cm^2 flasks). The cell suspension was further diluted and distributed to sterile culture vessels as required.

For cryopreservation, cells were grown and passaged as normal but instead of further dilution, cells were pelleted by centrifugation at 1000 *g* for 5 min and resuspended in 7 ml freeze medium containing 70 % (v/v) growth medium, 20 % (v/v) FBS and 10 % (v/v) dimethyl sulfoxide (DMSO). Cells were immediately divided into 1 ml aliquots in cryovials, placed into a polystyrene box and incubated at -80 °C to freeze gradually. After 24 h, frozen cells were moved to liquid nitrogen for long-term storage.

To defrost, cells were thawed rapidly in a 37 °C water bath and diluted in 10 ml of the appropriate growth medium (see Table 2.3). The cell suspension was spun at 1000 *g* for 3 min and freeze medium was replaced with 5 ml of fresh growth medium. Defrosted cells were initially plated in a 25 cm^2 flask and incubated in a humidified incubator at 37 °C with 5 % CO_2 for 24 h before being passaged and moved to a larger culture vessel as appropriate.

2.3.2.2 Transient transfection of cell lines

2.3.2.2.1 Lipofectamine 2000

CHO-TrkB cells were plated in 6-well and 12-well plates to achieve approximately 80 % confluence before being transfected with Lipofectamine 2000 as per the manufacturer's instructions. For each well of a 6-well plate, 1 µg total DNA and 2.5 µl Lipofectamine 2000 transfection reagent were diluted in 100 µl Opti-MEM and 0.5 µg total DNA and 1.25 µl Lipofectamine 2000 were diluted in 100 µl Opti-MEM per well for 12-well plates. For CHO-TrkB cells, antibiotic-containing medium was aspirated from cells and replaced with antibiotic-free medium prior to transfection. After the DNA-transfection reagent complexes were distributed onto cells, plates were incubated in a humidified incubator at 37 °C with 5 % CO_2 for a further 24 h before being harvested for analysis.

2.3.2.2.2 Lipofectamine

CHO cells were transfected in 6-well plates plated to achieve approximately 80 % confluence using Lipofectamine as per the manufacturer's instructions. For each well, 2 µg total DNA and 4 µl Lipofectamine transfection reagent were diluted in 266 µl Opti-MEM. Cells were incubated in a humidified incubator at 37 °C with 5 % CO_2 for a further 24 h before being harvested for analysis.

2.3.2.2.3 FuGene 6

CHO cells used in the experiments described in Chapter 5 were transfected with FuGene 6 as per the manufacturer's instructions. Cells were incubated in a humidified incubator at 37 °C with 5 % CO_2 for a further 24 h before being harvested for analysis.

2.3.2.3 Rat primary cortical neuron cell culture

All work involving animals was conducted in accordance with the UK Animals (Scientific Procedures) Act 1986. Cortices were harvested from the brains of embryonic day 18 Sprague-Dawley rat pups (Charles River Laboratories; Kent, UK). Cortices were pooled and washed with HBSS (-/-) and incubated in 70 µl 2.5 % trypsin-EDTA in 5 ml HBSS (-/-) at 37 °C for 30 min. An equal volume of filter-sterilised DNase I solution containing 10 µg/ml DNase I in HBSS (+/+) was added to achieve a final concentration of 5 µg/ml before media was aspirated. To dissociate cells, 1 ml triturating solution containing 1 % (w/v) AlbuMAX^{TM} I, 0.5 mg/ml soybean trypsin inhibitor and 10 µg/ml filter-sterilised DNase I in HBSS (+/+) was added. The solution was triturated with flame-polished glass Pasteur pipettes until a single-cell suspension was achieved. The dissociated cells were diluted with phenol red-free Neurobasal medium supplemented with 2 % (v/v) B27 supplement, 2 mM L-glutamine, 100 IU/ml penicillin and 100 µg/ml streptomycin to a volume of 1 ml per pup dissected. Cells were strained through a 70 µm cell strainer before being counted using a haemocytometer. To ensure that only live cells were counted, a small sample was diluted 1:10 in Trypan Blue prior to counting.

For biochemical studies, neurons were plated at 8.0 x 10^5 cells per well in 12-well plates coated with 0.01 % (w/v) poly-D-lysine. For immunofluorescence and PLAs, neurons were plated at 2.5 x 10^4 cells per well in 12-well plates containing 18 mm coverslips (Marienfield; Lauda-Königshofen, Germany) coated with 0.01 % (w/v) poly-D-lysine. Cells were maintained in a humidified incubator at 37 °C with 5 % CO_2 in Neurobasal medium supplemented with 2 % (v/v) B27 supplement, 2 mM L-glutamine, 100 IU/ml penicillin and 100 µg/ml streptomycin.

2.3.3 Cell treatments

2.3.3.1 BDNF, K252a and U0126 cell treatments

Cells were treated with 25 ng/ml BDNF prepared as a 25 µg/ml stock solution in filter-sterilised PBS containing 0.5 % bovine serum albumin for 15 or 30 min. K252a was prepared as a 200 µM stock in DMSO and applied at 200 nM 10 min prior to BDNF treatment. U0126 was prepared as a 20 mM stock in DMSO and applied at 20 µM 15 min prior to BDNF treatment. Neurons were treated with BDNF on the third day of *in vitro* culture (days *in vitro* 3; DIV3). CHO and CHO-TrkB cells were transiently transfected with Fe65 24 h prior to BDNF treatment (as described in section 2.3.2.2). During treatments, cells were incubated in a humidified incubator at 37 °C with 5 % CO_2. Following incubation, cells were washed twice with PBS and lysed for sodium dodecyl sulphate (SDS) polyacrylamide gel electrophoresis (SDS-PAGE) and western

blotting. Cells were grown in 12-well plates and lysed in 75 µl sample buffer containing 50 mM Tris-HCl pH 6.8, 2 % (w/v) SDS, 0.1 % (w/v) bromophenol blue, 20 % (v/v) glycerol. 5 % (v/v) β-mercaptoethanol and complete EDTA-free protease inhibitor cocktail (Roche, West Sussex, UK). Samples were heated for 5 min at 95 °C and frozen at -20 °C until required. For co-immunoprecipitation and GST pull-down assays, cells were grown in 6-well plates and lysed in 500 µl lysis buffer containing 50 mM Tris-citrate, 150 mM NaCl, 1 % (v/v) Triton X-100, 5 mM ethylene glycol-bis(β-aminoethylether)-N,N,N',N'-tetraacetic acid (EGTA), 5 mM EDTA, complete EDTA-free protease inhibitor cocktail. For Duolink PLA studies, cells were washed and fixed as described in section 2.3.9.

2.3.3.2 siRNA treatment

Accell siRNAs were reconstituted in siRNA resuspension buffer containing 60 mM KCl, 6 mM HEPES pH 7.5 and 200 mM $MgCl_2$ to a concentration of 100 µM as per the manufacturer's instructions and stored at -20 °C until required. DIV3 cortical neurons were treated with 1 µM siRNA as per the manufacturer's protocol. Briefly, resuspended siRNA was added to the cells at a final concentration of 1 µM and cells were incubated for a further 4 days in a humidified incubator at 37 °C with 5 % CO_2. For APP siRNAs, where two individual siRNAs were combined, a 50:50 ratio of each siRNA was used to create a total concentration of 1 µM (see Table 2.4).

To harvest for SDS-PAGE and western blotting, cells were washed twice with PBS and scraped into 50 µl lysis buffer (see section 2.3.3.1). Total protein concentration was measured by Bio-Rad protein assay (described in section 2.3.4) and samples were diluted as appropriate to ensure equal protein loading for SDS-PAGE and western blotting.

To harvest for RT-qPCR, cells were washed twice with PBS and scraped into 350 µl buffer RLT containing 1 % (v/v) β-mercaptoethanol (from Qiagen RNeasy mini kit). The cell lysates were homogenised using a rotor-stator homogeniser (Ultra Turrax T8; IKA, Germany) for 3 x 10 s bursts on ice and samples were stored at -80 °C until the rest of the RNeasy kit protocol was performed (described in section 2.3.12.1).

2.3.4 Determination of protein concentration (Bio-Rad protein assay)

Protein concentrations were quantified using a Bio-Rad protein assay kit (Hertfordshire, UK), which is based on the Bradford method of quantifying protein concentration (Bradford, 1976). The assay was performed as per the manufacturer's instructions. Samples were run in triplicate on a 96-well plate alongside a freshly prepared bovine

serum albumin protein standard curve. Absorbance for each sample was measured at 595 nm on a Victor^3 Multilabel Counter spectrophotometer (PerkinElmer; Coventry, UK).

2.3.5 SDS-PAGE and western blotting

Prior to SDS-PAGE, samples were heated in sample buffer (described in 2.3.3.1) for 5 min at 100 °C. For SDS-PAGE, samples were separated on 8 or 10 % (v/v) polyacrylamide gels (see Table 2.5) in running buffer containing 25 mM Tris, 192 mM glycine, 0.1 % (w/v) SDS for 1.5–5 h at 100 V. Samples were run alongside Precision Plus Protein™ Dual Xtra Standards (Bio-Rad) as markers for protein molecular masses.

Table 2.5: Polyacrylamide gel recipes for SDS-PAGE.

Gel	Component	Concentration
8 % Resolving gel	Tris-HCL pH 8.8	372 mM
	30 % (w/v) acrylamide/methylene bisacrylamide (37.5:1 ratio; acrylamide 30 %)	8 % (v/v)
	SDS	0.1 % (w/v)
	Ammonium persulfate (APS)	0.1 % (w/v)
	Tetramethylethylenediamine (TEMED)	0.1 % (v/v)
10 % Resolving gel	Tris-HCL pH 8.8	372 mM
	Acrylamide 30 %	10 % (v/v)
	SDS	0.1 % (w/v)
	APS	0.1 % (w/v)
	TEMED	0.1 % (v/v)
5.6 % Stacking gel	Tris-HCL pH 6.8	117 mM
	Acrylamide 30 %	5.6 % (v/v)
	SDS	0.1 % (w/v)
	APS	0.1 % (w/v)
	TEMED	0.1 % (v/v)

After separation by SDS-PAGE, proteins were transferred to Protran nitrocellulose membrane (0.45 µm pore; G.E. Healthcare) using a Bio-Rad Transblot system. Membranes were then incubated in blocking solution containing 5 % (w/v) skimmed

milk powder, 0.1 % (v/v) Tween 20 in Tris-buffered saline containing 20 mM Tris; 137 mM NaCl; buffered with HCl to pH 7.6 (TBS) for 1 h before being incubated for 16 h with primary antibody diluted appropriately with blocking solution (see Table 2.1). Blots were then washed for 10 min in 0.01 % (v/v) Tween 20 in TBS three times and incubated with the relevant horseradish peroxidase-coupled secondary antibody at a dilution of 1:8000 in blocking solution for 1 h. Western blots were then developed using an enhanced chemiluminescence system (ECL) comprising ECL Western Blotting Detection Reagents and Amersham Hyperfilm ECL (G.E. Healthcare). Hyperfilm was fixed and developed using a Konica Minolta SRX-101A Developer (Banbury, UK).

2.3.5.1 Densitometry and statistical analysis of western blots

Quantification of protein levels detected by SDS-PAGE and western blotting was carried out by densitometry. Developed ECL hyperfilms were digitalised using an Epson Perfection V700 Photo flatbed scanner (Hertfordshire, UK). ImageJ was used to measure the optical density (OD) of each protein band and the background density, which was subtracted from every sample value. Loading controls were run when possible to be used to account for inaccuracies when loading the samples into the gel. ODs for each sample were normalised to the expression level of the loading control for that particular sample. All OD values were then normalised to the mean OD of the control sample group. Statistical analyses were performed using Mann-Witney tests using Excel (Microsoft Corporation) and Prism 6 (GraphPad Software Inc.) and for all statistical tests, $p < 0.05$ was considered statistically significant. Where appropriate, bar charts were plotted using mean values and standard deviation (S.D.) was shown with error bars.

For co-immunoprecipitation and GST pull-down assays where a loading control could not be used, an input sample was run alongside precipitated or pulled-down (output) samples. The input samples measure relative amounts of the proteins of interest present in each reaction so can be used to account for variation in protein levels between samples. For these experiments, ODs of each output sample were normalised to the level of protein expression detected in the input of each sample. For GST pull-down assays, these values were then further normalised to the mean of the control group. For co-immunoprecipitations, the amount of protein co-immunoprecipitated was also normalised to the amount of 'bait' protein immunoprecipitated as variation in available 'bait' could also influence the amount of protein that could be co-immunoprecipitated from samples. As with GST pull-down analyses, treatment values were further normalised to the mean of the control group. Statistical analyses were performed Excel and Prism 6 and for all statistical tests, $p < 0.05$ was considered

statistically significant. BDNF treated samples were compared using Wilcoxon signed-rank tests and Fe65 phosphorylation mutants were compared using Kruskal-Wallis tests followed by Dunn's multiple comparisons tests using $Fe65_{WT}$ as the control group for pairwise comparison. Where appropriate, bar charts were plotted using mean values and S.D. was shown with error bars.

2.3.6 Co-immunoprecipitation

Co-immunoprecipitation assays were performed at 4 °C or on ice to minimise protein degradation. For experiments described in Chapter 3, cells were washed with ice-cold PBS and scraped into lysis buffer (see section 2.3.3.1). The samples were sonicated with 5 pulses at 40 % cycle duty using a Vibra-Cell™ (Sonics & Materials, Inc., Connecticut, USA), before 10 % of the sample was heated in sample buffer (see section 2.3.3.1) for 5 min at 95 °C and then stored at -20 °C. The rest of the sample was centrifuged at 13,000 *g* for 20 min at 4 °C to pellet cellular debris. The total protein concentration of the supernatant was measured via Bio-Rad protein assay (described in section 2.3.4) and the samples were diluted to 1 µg/µl with autoclaved water. Typically, 300-500 µg total protein was used per immunoprecipitation and samples were rotated for 16 h at 4 °C with 1.5-2.5 µg of the appropriate antibody (see Table 2.1). Following washing, the samples were then rotated with 30 µl Protein G Sepharose Fast Flow beads (50 % (v/v) slurry in 0.1 % (v/v) Triton X-100 in PBS; Triton-PBS) for 2 h at 4 °C to allow antibody binding. The beads were then pelleted by centrifugation at 3,000 *g* for 5 s at 4 °C and were washed four times with 1 ml Triton-PBS to remove unbound protein. The beads were heated in 50 µl sample buffer for 5 min at 95 °C to elute the sepharose bead-bound proteins and the sample was moved to a fresh eppendorf tube and stored at -20 °C until analysis via SDS-PAGE and western blotting was carried out. For experiments described in Chapter 5, CHO cells were transfected with the appropriate GST construct, lysed and treated as above with the exception that the samples were not sonicated prior to centrifugation and the antibody was captured by incubating with protein A-Agarose beads (Sigma) for 2 hr at 4 °C.

2.3.7 GST fusion protein pull-down assay

2.3.7.1 GST fusion-protein bead preparation

E. coli transformed with plasmids containing either GST or GST-APP_C were grown on LB agar selection plates containing 100 µg/ml ampicillin and used to make starter cultures (described in section 2.3.1.1). Working cultures of 200 ml LB-amp were inoculated with 2 ml of the starter cultures and incubated at 220 rpm, 37 °C until the optical density measured at 600 nm reached approximately 0.8 (0.6-1.0), indicating that mid-log phase growth had been achieved. Optical density was measured using an

Ultospec 3000 UV/visible spectrophotometer (G.E. Healthcare). Isopropyl β-D-1-thiogalactopyranoside (IPTG) was made up to a stock of 1M and added to cultures to a final concentration of 0.4 mM to induce recombinant protein expression. Bacterial cultures were incubated for a further 2 h at 220 rpm at 37 °C. The bacteria were cooled for 10 min on ice before being pelleted via centrifugation at 3,000 *g* for 10 min at 4 °C. The pellet was resuspended in 10 ml radio-immunoprecipitation assay (RIPA) buffer containing 0.1 % (w/v) SDS, 0.1 % (v/v) Triton X-100 and 1 % (w/v) sodium deoxycholate in TBS and incubated for 30 min on ice. Samples were sonicated on ice for 15 s at full power, 50 % cycle duty, then cellular debris was pelleted by centrifugation at 8,000 *g* for 10 min at 4 °C. The supernatant was incubated on a rotator for 90 min at 4 °C with 750 µl of a 50 % (v/v) slurry of glutathione sepharose™ 4B beads in PBS (G.E. Healthcare) to allow protein adherence before the beads were pelleted by centrifugation at 3,000 *g* for 1 min at 4 °C. The beads were washed three times in 1 ml Triton-PBS to remove unbound protein. The beads were finally resuspended in 750 µl Triton-PBS to create a 50 % (v/v) slurry.

To check that GST and GST-APP_C had coupled to the glutathione sepharose™ 4B beads, 2 µl beads were heated in 20 µl SDS-PAGE sample buffer (described in section 2.3.3.1) for 5 min at 95 °C and the protein eluate was run on a 10 % polyacrylamide gel for 1 h at 100 V (described in section 2.3.5). The polyacrylamide gel was fixed for 1 h in fixing buffer containing 50 % (v/v) methanol and 10 % (v/v) glacial acetic acid and stained for 2 h in 50 % (v/v) methanol, 1 % (v/v) glacial acetic acid and 0.1 % (v/v) Coomassie Brilliant Blue. It was then destained for 3 h in destaining solution containing 40 % methanol and 10 % (v/v) glacial acetic acid to remove background staining. Protein bands were imaged using an Epson Perfection V700 Photo flatbed scanner.

2.3.7.2 GST fusion-protein pull-down assay

GST pull-down assays were performed at 4 °C or on ice to minimise protein degradation. For experiments described in Chapter 3, CHO-TrkB cells were transfected as appropriate (described in section 2.3.2.2) and treated with BDNF as appropriate (described in section 2.3.3.1) before cells were washed with ice-cold PBS and scraped into lysis buffer (see section 2.3.3.1). The samples were sonicated on ice with 5 pulses at 40% cycle duty before 10 % of the sample was collected as the input sample and heated in SDS-PAGE sample buffer (see section 2.3.3.1) for 5 min at 95 °C before being stored at -20 °C. The rest of the sample was centrifuged at 13,000 *g* for 20 min at 4 °C to pellet cellular debris. The total protein concentration of the supernatant was calculated via Bio-Rad protein assay (described in section 2.3.4) and the samples were diluted to 1 µg/µl. Typically, 300-500 µg total protein was used per GST pull-down.

Samples were incubated with 30 µl of either GST coupled glutathione sepharose™ 4B beads or GST-APP_C coupled glutathione sepharose™ 4B beads on a rotator for 2 h at 4 °C. The beads were then pelleted by centrifugation at 3,000 *g* for 15 s at 4 °C. The beads were washed four times with 1 ml Triton-PBS and the retained protein eluted from the beads into 50 µl sample buffer. The protein solution was heated for 5 min at 95 °C and frozen at -20 °C until required. For experiments described in Chapter 5, CHO cells were transfected with the appropriate GST construct, lysed and treated as above with the exception that the samples were not sonicated prior to centrifugation and they were incubated with unconjugated glutathione sepharose™ 4B beads for 1 hr.

2.3.8 ELISA

2.3.8.1 Total tau and phosphorylated tau ELISA

Total tau levels were measured using the ThermoFisher Scientific tau (total) ELISA kit and tau phosphorylated at Ser^{199} was measured using the ThermoFisher Scientific tau (pS199) ELISA kit. ELISAs were performed on DIV3 rat cortical neurons treated with siRNAs (described in section 2.3.3.2). To perform the ELISAs, cells were washed twice with PBS and incubated in 100 µl ELISA cell extraction buffer containing 10 mM Tris, pH 7.4, 100 mM NaCl, 1 mM EDTA, 1 mM EGTA, 1 mM sodium fluoride, 20 mM sodium pyrophosphate, 2 mM sodium orthovanadate, 1 % (v/v) Triton X-100, 10 % (v/v) glycerol, 0.1 % (w/v) SDS, 0.5 % (w/v) sodium deoxycholate, 1 mM phenylmethylsulfonyl fluoride and complete EDTA-free protease inhibitor cocktail for 30 min at 40 °C. Following incubation, the samples were spun at 13,000 *g* for 10 min at 4 °C and supernatants were collected and diluted 1:500 prior to application to the ELISA plate. The kits were used as per the manufacturer's instructions and the provided tau standard curves were run alongside samples. The ELISA plates were read at 450 nm on a $Victor^3$ Multilabel Counter spectrophotometer.

2.3.8.2 Total GSK3β and phosphorylated GSK3β ELISA

Both total GSK3β and GSK3β phosphorylated at Ser^9 were measured using the Meso Scale Diagnostics phospho/total GSK-3β whole cell lysate ELISA kit. ELISAs were performed on DIV3 rat cortical neurons treated with siRNAs (described in section 2.3.3.2). Cells were washed twice with PBS and incubated in 100 µl ELISA cell extraction buffer (described in 2.3.8.1) for 30 min at 40 °C. The samples were spun at 13,000 *g* for 10 min at 4 °C. Cell lysates were then diluted 1:50 prior to application to the ELISA plate. The kits were used as per the manufacturer's instructions and no standards were supplied for standard curves so relative OD values were compared. The ELISA plate was read at 450 nm on a $Victor^3$ Multilabel Counter spectrophotometer.

2.3.8.3 Statistical analysis of ELISA data

Relative tau phosphorylation was analysed using Excel by calculating phosphorylated tau as a proportion of total (including phosphorylated) tau levels. These values were then normalised to the control mean. In a similar manner, relative GSK3β phosphorylation was analysed by calculating phosphorylated GSK3β as a proportion of total (including phosphorylated) GSK3β. Again, these values were then normalised to the control mean before statistical analyses were carried out. Statistical analyses were carried out using Mann-Witney tests. All statistical analyses were performed using Excel and Prism 6 and for all statistical tests $p < 0.05$ was considered statistically significant. Where appropriate, bar charts were plotted using mean values and S.D. was shown with error bars.

2.3.9 Immunofluorescence

Rat cortical neurons were plated out as described in section 2.3.2.3 and grown to DIV3 in a humidified incubator at 37 °C with 5 % CO_2. Following the incubation period, media was aspirated from cells, which were then washed with PBS. Cells were fixed in 4 % (w/v) PFA in PBS for 15 min before being washed twice with PBS. Coverslips were washed once with quenching solution containing 50 mM NH_4Cl and then incubated in quenching solution for 15 min. Cells were then washed again with PBS and permeabilised by incubation in 0.2 % (v/v) Triton X-100 in PBS for 3 min. After 3 further washes with PBS cells were blocked in 5 % FBS in PBS for 30 min before being incubated with the appropriate primary antibodies for 1 hr. Coverslips were washed three times with 5 % FBS and incubated in the appropriate secondary antibody for 45 min. Again, coverslips were washed three times with 5 % FBS followed by incubation with 0.1 µg/ml DAPI stain for 15 min. Finally, cells were washed five times in PBS to remove all excess stain and mounted onto glass coverslips using Fluorecent Mounting Medium (DAKO). Images were captured using a Leica DM5000B microscope with 63x HCX PL Fluotar phase objective (Milton Keynes, UK). For intensity correlation analysis, images were analysed using ImageJ with the Intensity Correlation Analysis plugin (described in Cheung et al., 2014). Statistical analysis was carried out using one-sample t-tests using Excel and Prism 6.

2.3.10 Duolink PLA

In situ PLAs were used to monitor the APP-Fe65 interaction (Söderberg et al., 2006; Weibrecht et al., 2010). Cells were fixed using paraformaldehyde (PFA) cross-linking and probed with primary antibodies followed by secondary antibodies coupled to specific oligonucleotides. If the antigens are situated close enough (within 30 nm), these oligonucleotides hybridize and initiate rolling-circle amplification of fluorescent

oligonucleotides. These fluorescent signals can then be detected and used to quantify the interaction between the two labelled proteins of interest (Figure 2.1).

For PLAs, CHO-TrkB cells were plated out to achieve ~5 % confluence in 12-well plates containing 18 mm diameter glass coverslips (Marienfield) and grown for 48 h in a humidified incubator at 37 °C with 5 % CO_2. Following the incubation period, media was aspirated from cells, which were then washed with PBS. Cells were fixed in 4 % (w/v) PFA in PBS for 15 min before being washed twice with PBS. Coverslips were washed once with quenching solution containing 50 mM NH_4Cl and then incubated in quenching solution for 15 min. Cells were then washed again with PBS and permeabilised by incubation in 0.2 % (v/v) Triton X-100 in PBS for 3 min. After 3 further washes with PBS, PLAs were performed as per the Duolink In Situ PLA protocol using the Duolink In Situ range of: detection reagents (orange), wash buffers (fluorescence) and PLA probe kits. All incubation steps were carried out in a humidity chamber pre-heated to 37 °C. Briefly, coverslips were incubated in Duolink blocking solution at 37 °C for 30 min. Coverslips were then incubated in primary antibodies (see Table 2.1) diluted 1:400 in Duolink antibody diluent for 1 h at 37 °C and washed three times in 5 ml PBS for 5 min. The coverslips were then incubated in Rabbit PLUS and mouse MINUS Duolink PLA probes used at a dilution of 1:5 in Duolink blocking solution at 37 °C for 1 h. Following this incubation period, the coverslips were washed twice in 5 ml Duolink wash buffer A containing 10 mM Tris, 150 mM NaCl and 0.05 % (v/v) Tween 20 for 5 min then incubated in 40 µl Duolink ligase solution containing 1 U ligase at 37°C for 30 min. Coverslips were washed twice in 5 ml Duolink wash buffer A for 2 min and incubated in 40 µl Duolink amplification solution containing 0.5 U polymerase at 37 °C for 100 min. From this stage on, foil was used to protect the photosensitive reaction from light at all steps. Coverslips were washed in 0.5 µg/ml DAPI in Duolink wash buffer B containing 200 mM Tris and 100 mM NaCl for 10 min, followed by a further wash in 5 ml Duolink wash buffer B for 10 min and 5 ml Duolink wash buffer B diluted 1:100 with autoclaved H_2O for 1 min. Finally, coverslips were mounted onto microscope slides using fluorescence mounting medium (DAKO) and stored at 4 °C until required.

For PLA analyses, images were captured using a Leica DM5000B microscope with 63x HCX PL Fluotar phase objective. For CHO-TrkB cells, a single image could not capture all the in-focus PLA signals (seen as fluorescent dots) so a z-stack of 6-12 images per cell was compiled as necessary and analysed using ImageJ with the ‘Extended Depth of Field’ plug-in (Forster et al., 2004). For primary cortical neurons, depth of field was

not an issue so a single image was taken. The number of fluorescent dots present in each cell was counted using the 'Analyze Particles' function of ImageJ.

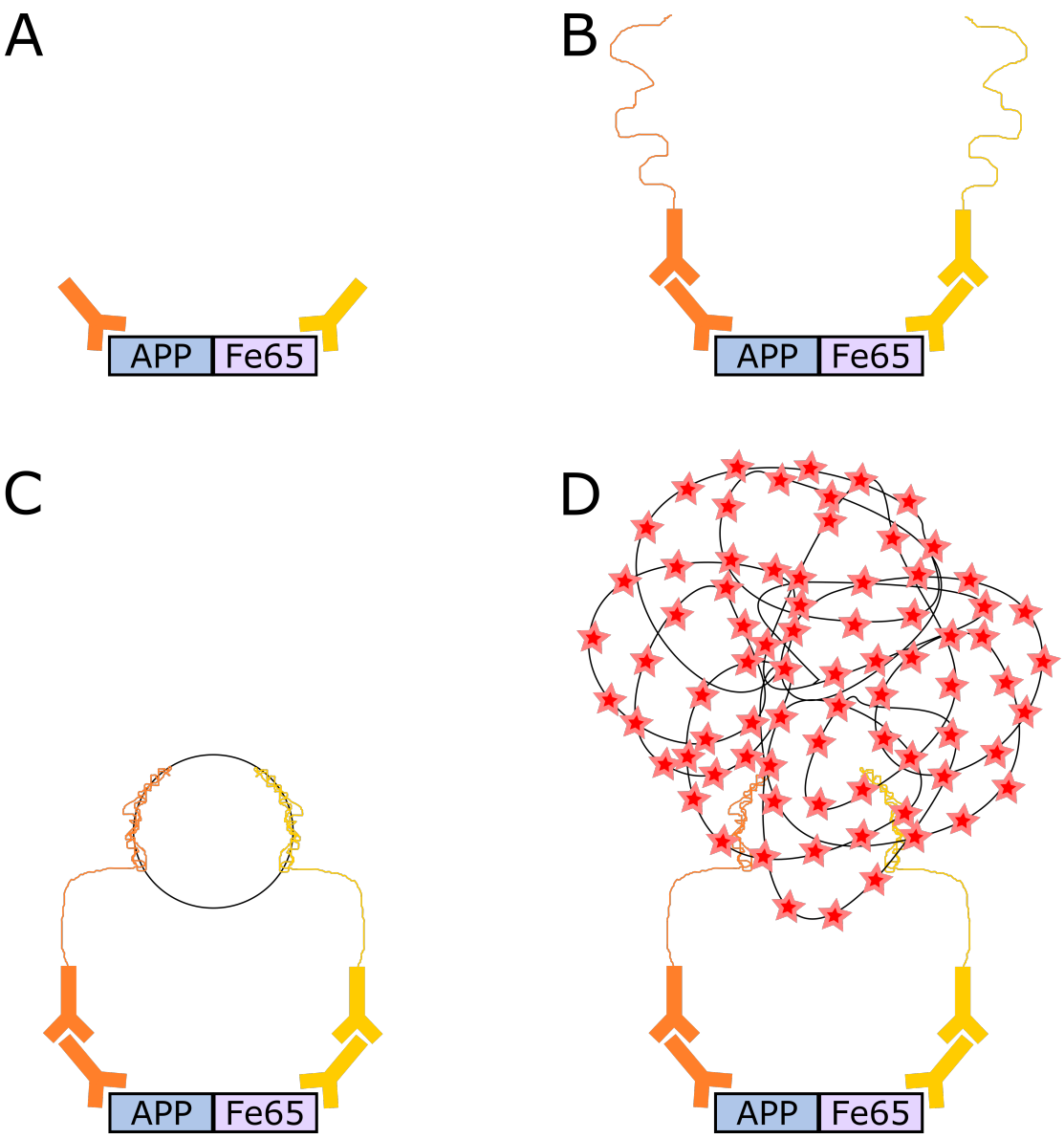

Figure 2.1: A diagram to show the Duolink PLA process. *A) Primary antibodies are used to label the proteins of interest in fixed, permeabilised cells. B) Proprietary secondary antibodies that are conjugated to complementary oligonucleotides bind to the primary antibodies. C) If the PLA probes bind to antibodies within 30 nm of each other, they hybridise during the ligation step. D) The hybridised oligonucleotides act as primers for rolling-circle amplification of fluorescent oligonucleotides that can be visualised as a single red dot under a fluorescent microscope.*

2.3.10.1 Statistical analysis of PLA data

Raw data of individual experiments were checked for normality using the Kolmogorov-Smirnov test and equal variance was determined using F tests. For BDNF

experiments, data were normalised to the untreated control sample and the normalised data for BDNF treated cells from three independent experiments were pooled and compared using Mann-Witney tests. Data from control experiments were analysed using one-way ANOVA followed by Dunnett's multiple comparisons test using APP+Fe65+PLA probes as the control group for pairwise comparison. All statistical analyses were performed using Excel and Prism 6 and for all statistical tests, $p < 0.05$ was considered statistically significant.

2.3.10.2 Neurite length measurements

Rat cortical neurons were grown to DIV2 before being transfected with EGFP alongside the appropriate constructs. Neurons were immunostained (see section 2.3.9) to verify that both constructs had been transfected successfully before being chosen for analysis. The longest neurite of each cell examined was measured 24 hr after transfection. The length was determined as the distance from the tip of the growth cone to the cell body and was quantified using ImageJ using the NeuronJ plug-in (Cheung et al., 2014). Data were analysed using one-way ANOVA followed by Bonferroni *post hoc* test. All statistical analyses were performed using Excel and Prism 6 and for all statistical tests, $p < 0.05$ was considered statistically significant.

2.3.11 Fe65KO transgenic mice

2.3.11.1 PCR genotyping of Fe65 knockout mice

Fe65KO mice were as originally described (Guénette et al., 2006) and maintained on a C57BL/6 genetic background. To identify transgenic littermates, DNA from ear or tail tissue was extracted using REDExtract-N-Amp™ tissue PCR kit as per the manufacturer's instructions. For PCR, 4 µl of the extracted DNA sample was added to 10 µl REDExtract-N-Amp™ PCR reaction mix and 4 pmol of the appropriate primers (see Table 2.6) in a final volume of 20 µl. Together these primers detect both wild-type (WT) and the targeted mutant Fe65 alleles. The PCR was run in a G-Storm thermocycler (Somerset, UK; see Table 2.7). To visualise PCR genotyping results, 10 µl of the reaction was run on a 1.5 % (w/v) agarose gel for 20 min (see section 2.3.1.3).

Table 2.6: Primer sequences used for PCR genotyping of Fe65KO mice.

Primer	Sequence
Neo5	5'-GAGAACCTGGGTGCAATCCATC-3'
WTR3	5'-AATGTTGGACTGAGGGTATAGGCT-3'
Fe65	5'-GTCTTCTCCTCCAGGGCTACCTGAG-3'

Table 2.7: Fe65KO mouse PCR genotyping program.

Step	Cycles	Time (min)	Temperature (°C)
Initial denaturation	1	5	95
Denaturation, annealing and elongation	30	1 1 1	95 62 72
Extension/Elongation	1	5	72
Cooling		hold	4

2.3.11.2 Tissue harvesting from Fe65KO mice

Brains were harvested from Day 0 male mouse pups. The brain hemispheres were separated via a sagittal cut and each hemisphere was snap-frozen in liquid nitrogen separately for later processing. PCR genotyping was carried out on tail tissue from carcasses to identify WT and Fe65KO pups (described in section 2.3.11.1). One hemisphere of each brain sample was homogenised in 200 µl extra strong lysis buffer containing 10 mM Tris-HCl, pH 7.5, 75 mM NaCl, 0.5% (w/v) SDS, 20 mM sodim deoxycholate, 1 % (v/v) Triton X-100, 1 mM sodium pyrophosphate, 2 mM sodium orthovanadate, 1.25 mM sodium fluoride, 10 mM EDTA and complete EDTA-free protease inhibitor cocktail per 10 mg brain and processed for SDS-PAGE and western blotting to analyse protein expression (as described in section 2.3.5).

2.3.12 RNA isolation, reverse transcription and SYBR Green RT-qPCR

2.3.12.1 RNA isolation

The remaining mice brain hemispheres (described in section 2.3.11.2) were processed using the RNeasy mini kit (Qiagen) used in conjunction with the suggested on-column DNase treatment using the RNase-free DNase I set (Qiagen). Brain samples were homogenised in 350 µl Buffer RLT containing 1 % (v/v) β-mercaptoethanol per 10 mg of tissue using a rotor-stator homogeniser (Ultra Turrax T8). All tissue was kept on ice to minimise protein and messenger RNA (mRNA) degradation and samples were stored in aliquots at -80 °C until required. Following homogenisation, the RNeasy mini kit was used as per the manufacturer's instructions. RNA was eluted off the column by incubation in 50 µl ribonuclease-free water. The eluted RNA was then re-applied to the column, incubated and spun as before to ensure maximum yield. The concentration of RNA yield was determined by measuring its absorbance at 260 nm using a NanoDrop 1000 spectrophotometer. The 260/280 ratio was used to determine RNA purity; pure RNA has a ratio of 2.0. To assess RNA quality and check for genomic DNA

contamination and RNA degradation, 0.1-0.2 µg RNA was run on a 1 % (w/v) agarose gel (see section 2.3.1.3). RNA samples were stored at -80 °C until required to preserve RNA quality.

2.3.12.2 Reverse transcription

RNA was reverse transcribed to cDNA using the nanoScript2 reverse transcription kit (PrimerDesign) as per the manufacturer's instructions using the supplied oligo-dT primers to enhance primer annealing to the 3' polyA tail of mRNA. Incubation steps were performed using a G-storm thermocycler. cDNA samples were stored at -20 °C until required (for a maximum of 12 months). Reverse transcription-null controls were run alongside reverse transcription reactions and these contained all the same reagents and samples as full reactions with the exception of the reverse transcriptase enzyme.

2.3.12.3 GeNorm reference gene analysis

The GeNorm reference gene analysis kit (PrimerDesign) was used to identify appropriate reference genes to use for relative quantification of mRNA expression. For GeNorm analysis, 12 reference genes were analysed (see Table 2.9). Reference gene RT-qPCR was carried out in duplicate on 4 WT and 4 Fe65KO mouse brain samples. To reduce inter-run variability, all samples for each gene were run on the same plate. SYBR Green RT-qPCR was carried out using PrecisionPLUS mastermix (PrimerDesign) containing inert blue dye as per the manufacturer's instructions. Each 20 µl reaction contained 300 nM primer mix, 1 x PrecisionPLUS mastermix and 25 ng cDNA. SYBR Green RT-qPCR was performed using an ABI 7900HT Fast Real-Time PCR system (ThermoFisher Scientific) using 384-well BrightWhite RT-qPCR plates (PrimerDesgin) and adhesive optical seals. The amplification protocol used is described in Table 2.8. Results were collected and analysed using SDS 2.3 (ABI) and Prism 6 and GeNorm analysis was carried out using qbase+ 3.0 software (Biogazelle; Zwijnaarde, Belgium; Vandesompele et al. 2002).

2.3.12.4 SYBR green RT-qPCR

For relative quantification of mRNA expression of seven genes of interest, mouse brain samples and cell lysates of siRNA treated rat cortical neurons were analysed via SYBR Green RT-qPCR as described in section 2.3.12.3. RT-qPCR was carried out using technical triplicates alongside no-template controls and reverse transcription-null controls (described in section 2.3.12.2). Custom primers for mouse genes (see Table 2.10) and rat genes of interest (see Table 2.11) were purchased from PrimerDesign

and were guaranteed to have greater than 90 % efficiency to be suitable for relative quantification analysis using the $2^{-\Delta\Delta Ct}$ method (Livak and Schmittgen, 2001).

Table 2.8: RT-qPCR amplification program.

Step	Cycles	Time (sec)	Temperature (°C)
Enzyme activation	1	120	95
Denaturation	40	15	95
Data collection		60	60
Dissociation curve	1	15	95
		15	60
		15	95

Table 2.9: GeNorm reference gene primer details. Specific primer sequences were not disclosed by PrimerDesign.

Gene	Anchor Nucleotide	Context Length Sequence (bp)
18S	134	99
ACTB	597	94
ATP5B	1115	142
B2M	202	159
CANX	2827	127
CYC1	514	203
EIF4A2	876	215
GAPDH	793	180
RPL13A	691	180
SDHA	2018	181
UBC	2225	178

Table 2.10: Primer sequences used for RT-qPCR on Fe65KO mouse brain samples.

Gene	Forward primer (5'-3')	Reverse primer (5'-3')
APP	TGGCGGTGAAGACAAAGTAGT	CCATCCTCCACATCCTCATCAT
Fzd1	CCCGCCCATTCCAGATCC	ATCTCAAATAAGCAGCATCAGGAA
GSK3α	CCCCCAGGCTACCACTCC	AGGGAAGGGAAGACGAGAGA
GSK3β	CACCATCCTTATCCCTCCACAT	CCACGGTCTCCAGCATTAGTA
LRP6	TGGACTGACTGGAATACACACT	ATGGGAGAGAAGATGTTAGAATGAAT
MAPT (3R)	TGTGGAGGTAATCTGTGAACTTC	AGGCTATGGATCTGAGGTCAAT
Wnt3	GGCGAGATTCTGTGTCCAAG	CGGGGCTCTGTCCTACTTC

Table 2.11: Primer sequences used for RT-qPCR on siRNA treated rat cortical neurons.

Gene	Forward primer (5'-3')	Reverse primer (5'-3')
APP	CTGAGGATGACGAGGATGTG	TGTGGTAGTGGTGGCAATG
Fe65 (APBB1)	CTCTCCTACCACAAAAACAATCTACA	TGACGATGGGCTGGGCAT
Fzd1	CCCGCCCATTCCAGATCC	ATCTCAAATAAGCAGCATCAGGAA

2.3.12.5 Analysis of RT-qPCR data

RT-qPCR results were analysed using SDS 2.3, Excel and Prism 6. First the dissociation curve raw data were analysed using SDS 2.3 to check that no primer dimers were formed during the PCR experiment for any of the primers used. Technical replicates differing by >0.5 Ct (number of cycles taken for SYBR Green fluorescence to reach a threshold level) were excluded from analyses and biological replicates were excluded if they did not have ≥2 replicate data points. Relative quantification was calculated using the $2^{-\Delta\Delta Ct}$ method (Livak and Schmittgen, 2001) using *GAPDH/ATP5B* as reference genes. Specifically, the following equation was used:

$$\Delta\Delta Ct = (Ct_{GOI} - Ct_{REF})_{mouse\ x} - (Ct_{GOI} - Ct_{REF})_{mouse\ WT}$$

Where Ct_{GOI} = Ct for gene of interest, Ct_{REF} = average Ct of reference genes, mouse x is any biological sample and mouse WT is the mean change in expression of the gene of interest normalised to the reference genes in the WT mouse brain samples.

Statistical analyses were performed using Mann-Whitney tests on $2^{-\Delta Ct}$ values (Livak and Schmittgen, 2001) as appropriate. Bar charts were plotted with $2^{-\Delta\Delta Ct}$ values normalised to the mean of the control group and S.D. was shown with error bars. All statistical analyses were performed using Excel and Prism 6 and for all statistical tests, $p < 0.05$ was considered statistically significant.

CHAPTER 3: BDNF INDUCES ERK1/2 PHOSPHORYLATION OF FE65 TO REGULATE ITS BINDING TO APP

3.1 Introduction

Fe65 is of interest to the field of AD research because it is a major binding partner of APP. This interaction occurs between the second PTB domain of Fe65 and the YENPTY motif on the intracellular domain of APP. The APP-Fe65 complex has been implicated in several cellular processes, including cell motility, apoptosis and gene transcription (see section 1.3.2). Binding between APP and Fe65 is regulated by phosphorylation of both proteins at specific sites. Phosphorylation of APP at Tyr^{682} and Thr^{668} inhibits the interaction between APP and Fe65 (Ando et al., 2001; Barbagallo et al., 2010; Nakaya and Suzuki, 2006; Tarr et al., 2002a, 2002b). In addition, phosphorylation of Fe65 on Ser^{610} by SGK1 can also impair APP-Fe65 binding and inhibits amyloidogenic processing of APP (Chow et al., 2015b; Lee et al., 2008a). Fe65 is also phosphorylated on Tyr^{547} within its second PTB domain, although this does not impact the APP-Fe65 interaction but instead stimulates APP-Fe65 mediated transcription (Perkinton et al., 2004). Finally, Fe65 is phosphorylated on N-terminally located Ser^{228} by ATM/ATR protein kinases (Jowsey and Blain, 2015). In contrast to Tyr^{547} phosphorylation, Ser^{228} phosphorylation inhibits APP-Fe65 mediated transcription, but has no effect on the ability of Fe65 to bind to APP (Jowsey and Blain, 2015).

Fe65 is also phosphorylated at Ser^{175}, Ser^{287}, Ser^{347} and Thr^{709} by ERK1/2 (Standen et al. 2003; Figure 1.3.1), however, the functional effects of this phosphorylation on APP-Fe65 binding have not yet been investigated. In addition, the regulatory mechanisms that control phosphorylation of these sites by ERK1/2 is also unknown. One well characterised mechanism of ERK1/2 activation within the nervous system involves stimulation of TrkB signalling by BDNF (Yang et al., 2013). Interestingly, BDNF has been proposed as a potential therapy for AD as it can restore synaptic defects in animal models of disease and ameliorate cognitive impairments, but the precise mechanisms underlying these effects are not clear (Blurton-Jones et al., 2009; Nagahara et al., 2013, 2009).

In this chapter, the effect of BDNF on phosphorylation of Fe65 by ERK1/2 was studied. The consequences of this BDNF-mediated Fe65 phosphorylation on the interaction between APP and Fe65 were also explored. Finally, Fe65 phosphorylation mutants were utilised to investigate how phosphorylation of Fe65 at ERK1/2-specific sites regulates its binding to APP. For experiments investigating the binding of Fe65 to APP, assays were required that can reliably quantify subtle changes in binding between the two proteins. Whilst immunoprecipitation and pull-down assays have been used

previously to detect the APP-Fe65 interaction, they have been used mainly to detect whether or not binding occurs, rather than for measuring quantitative changes in binding. Therefore, the first stage of these experiments was to establish several complementary assays that are able to detect the APP-Fe65 interaction quantitatively and to optimise them for the proteins of interest. The second stage of this investigation was to use these assays to determine how phosphorylation of Fe65 affects its binding to APP.

3.2 Results

3.2.1 Commercial antibodies detect Fe65 on western blots

As a number of experiments in this investigation relied on detection of Fe65 by western blotting, an appropriate Fe65 antibody needed to be identified. Homemade antibodies have previously been generated that recognise Fe65 (Kesavapany et al., 2002), but these were damaged in a freezer defrost accident. Commercial Fe65 antibodies sc-19751 (Santa Cruz), 4H324 (Abcam), 2877 (Cell Signaling Technology) and a homemade Fe65 antibody, C60 (Lau et al., 2000b), were used to probe western blots of cell lysates from CHO cells transiently transfected with either chloramphenicol acetyltransferase (CAT) from *E. coli* as a control vector (Ctrl) or Fe65 plasmid vector (described in Table 2.2). Fe65 was strongly detected by both 4H324 and 2877 antibodies at both concentrations tested. The western blots probed with C60 showed a specific band detected at the correct molecular weight for Fe65, however, the large amount of non-specific staining also seen suggested that the concentrations tested for this antibody were too high. Finally, the sc-19751 antibody only detected a very weak Fe65 signal at the concentrations tested (Figure 3.1). For all further western blots, 4H324 was used to detect Fe65 unless otherwise specified.

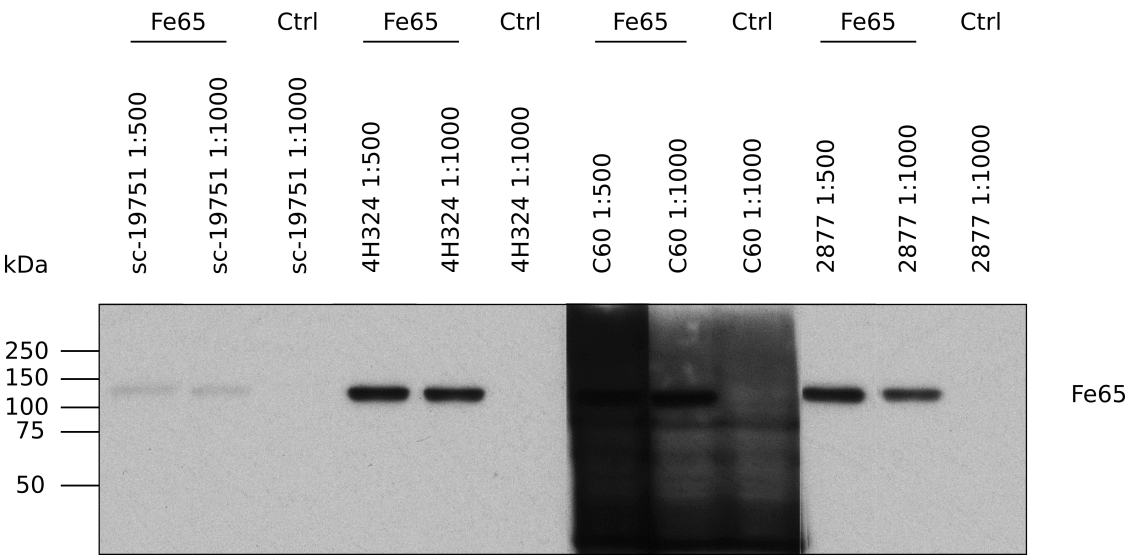

Figure 3.1: Commercial antibodies detects Fe65 on western blots.

CHO cells transiently transfected with CAT (Ctrl) or Fe65 plasmid vectors were lysed 24 hr post-transfection and western blotted for Fe65. The four antibodies tested were sc-19751 (Santa Cruz), 4H324 (Abcam), C60 (Homemade) and 2877 (Cell Signaling Technology). Each antibody was tested at a dilution of 1:500 and 1:1000 in 5 % BSA for Fe65 transfected cells and 1:1000 in 5 % BSA for control transfected cells. Molecular mass markers are shown.

3.2.2 Detection of the APP-Fe65 interaction

The studies described below were aimed at determining how BDNF and phosphorylation of Fe65 on the ERK1/2-responsive sites (Ser^{175}, Ser^{287}, Ser^{347} and $Thr^{709)}$ affected its binding to APP. Reliable assays to detect and quantify the APP-Fe65 interaction firstly needed to be established. In addition, while many studies have demonstrated the interaction between transfected APP and Fe65 (for example, Borg et al., 1996; Bressler et al., 1996; Lau et al., 2008), detecting an interaction between endogenous APP and Fe65 has proved more difficult. To resolve this, proximity ligation assays (PLAs) were also established to study this interaction in untransfected cells (Söderberg et al., 2006).

3.2.2.1 The APP-Fe65 interaction can be detected by co-immunoprecipitation involving Fe65, but not APP C-terminal immunoprecipitating antibodies

To work up reliable immunoprecipitation assays to detect and quantify binding of transfected APP and Fe65, HEK293 and CHO cells were transiently transfected with CAT (Ctrl), APP, myc epitope-tagged Fe65 (Fe65-myc), APP+Fe65-myc, wild-type Fe65 ($Fe65_{WT}$) or APP+$Fe65_{WT}$ plasmid vectors (described in Table 2.2). Immunoprecipitations were then performed with three different antibodies. 9B11, an antibody that detects the myc-tag, Fe65 antibody sc-19751 and C-terminal APP antibody CT-17. Western blots of total cell lysate inputs revealed that all cells were appropriately transfected. Extended exposures of these input blots with the APP and Fe65 antibodies enabled detection of endogenous proteins in non-transfected cells (not shown for all blots; Figure 3.2). Western blots of the immunoprecipitates revealed an interaction between APP and Fe65 in APP+Fe65 co-transfected cells following immunoprecipitation with 9B11 or the Fe65 antibody (Figure 3.2A, B). The absence of signal in control, APP or Fe65 only transfected cell immunoprecipitates in these experiments demonstrates the specificity of the assays. However, while the APP antibody immunoprecipitated APP, no bound Fe65 could be detected (Figure 3.2C). The signal for Fe65 pulled down in APP+Fe65-myc co-transfected cells is relatively weaker than the signal for Fe65 pulled down in singly, Fe65-myc transfected cells (Figure 3.2A). This could be due to pipetting error resulting in fewer beads being added to the sample or issues with eluting the protein from the beads after co-immunoprecipitation. For all co-immunoprecipitation assays, the APP signal is normalised to the amount of Fe65 precipitated to ensure that any fluctuations in signal between groups is accounted for.

Immunoprecipitation assays involving pull-down of Fe65 via the myc tag, or by using an Fe65 antibody detected binding of APP in transfected cells (Figure 3.2A, B). However, immunoprecipitation assays using antibody CT-17 pulled down APP, but not any bound Fe65 (Figure 3.2C). CT-17 was generated by immunisation of rabbits with a peptide comprising the 17 C-terminal amino acids of APP (see Figure 1.3B). This contains the C-terminal YENPTY motif, which is also the binding site of Fe65. One possible explanation for CT-17 failing to co-immunoprecipitate APP-bound Fe65 is that CT-17 cannot recognise APP-Fe65 complexes because Fe65 blocks access to the CT-17 epitope, resulting in only unbound APP being precipitated. Due to the success of sc-19751 in detecting the APP-Fe65 interaction without the use of an epitope tag, future co-immunoprecipitations were performed using this Fe65 antibody.

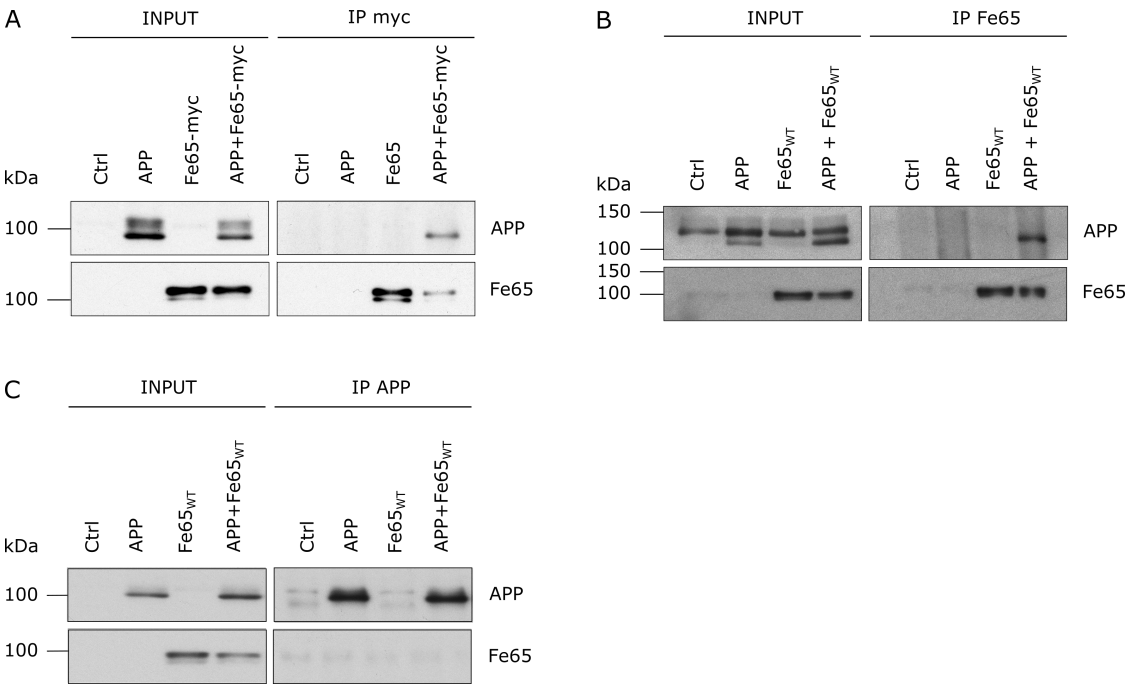

Figure 3.2: The APP-Fe65 interaction can be detected by co-immunoprecipitation involving Fe65, but not APP C-terminal antibodies.

A) HEK293 cells were transiently transfected with CAT (Ctrl), APP, Fe65-myc or APP+Fe65-myc plasmid vectors as indicated. Fe65-myc was immunoprecipitated using antibody 9B11 that recognises the myc tag. B), C) CHO cells were transiently transfected with CAT control vector (Ctrl), APP, $Fe65_{WT}$ or APP+$Fe65_{WT}$ as indicated. B) $Fe65_{WT}$ was immunoprecipitated using Fe65 antibody sc-19751. C) APP was immunoprecipitated using CT-17, a C-terminal APP antibody. Input samples and immunoprecipitates were analysed by western blotting. Fe65 was detected using 4H324 antibody and APP using CT-17. Molecular mass markers are shown.

3.2.2.2 The APP-Fe65 interaction can be detected by GST pull-down assays involving the APP cytoplasmic domain

To work up methods for detecting the APP-Fe65 interaction by GST-APP_C pull-down assays, a construct of APP that contains only the 46 C-terminal residues (including the YENPTY motif) fused to Glutathione S-Transferase (GST) was expressed in *E. coli* (vector described in Table 2.2) and recombinant GST-APP_C was then used to isolate Fe65 from transfected cells (Standen et al. 2001). GST and GST-APP_C fusion protein expression was induced with IPTG and *E. coli* lysates were analysed by coomassie blue staining of SDS-PAGE gels. Expression of both constructs was enhanced by IPTG induction of *E. coli* as seen by the appearance of 26 kDa GST and 30 kDa GST-APP_C species (Figure 3.3A). Proteins were then purified on glutathione sepharose 4B beads. Protein samples eluted from GST and GST-APP_C beads were also analysed by coomassie staining of SDS-PAGE gels, which verified correct expression of the two recombinant proteins (Figure 3.3A).

Pull-down experiments with GST and GST-APP_C beads were then performed from cell lysates of CHO cells stably expressing TrkB (CHO-TrkB) transiently transfected with CAT (Ctrl) or $Fe65_{WT}$ plasmid vectors (described in Table 2.2). Input, GST and GST-APP_C pull-downs were separated by SDS-PAGE and analysed by western blotting. Fe65 was detected in input samples of cells transfected with $Fe65_{WT}$ but not control vector (Figure 3.3B). GST-APP_C pulled-down Fe65 in cells transfected with $Fe65_{WT}$ but not control cells, while GST alone did not pull-down Fe65 from either cell lysate (Figure 3.3B). These experiments demonstrate the specificity of the GST-APP_C pull-down assay but show that it is only capable of detecting interactions between GST-APP_C and transfected, not endogenous Fe65.

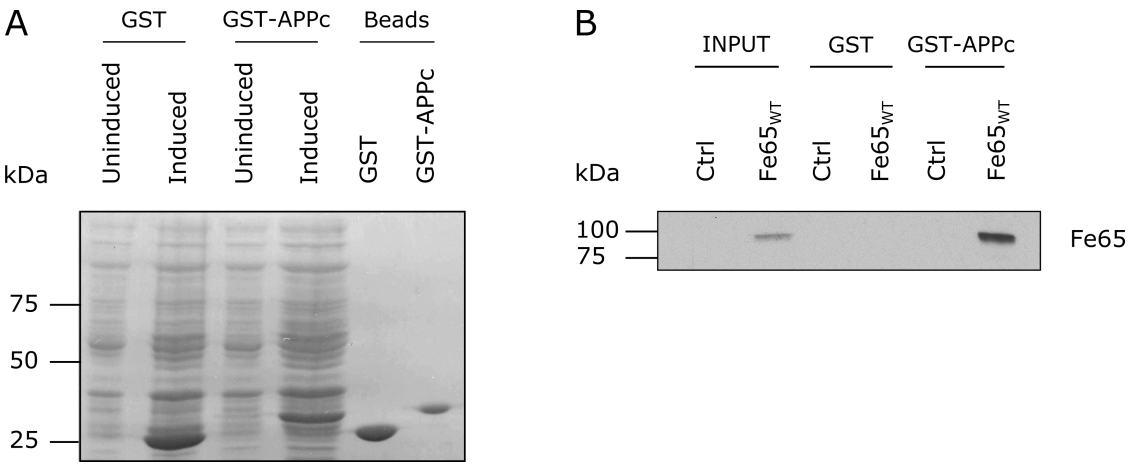

Figure 3.3: The APP-Fe65 interaction can be detected by GST pull-down assays involving the APP cytoplasmic domain.

A) *E. coli* transformed with either GST or GST-APP_C expressing plasmids were induced to express protein with 0.4 mM IPTG treatment. Total lysates from uninduced and IPTG-induced *E. coli* were analysed by coomassie staining of SDS-PAGE gels. GST and GST-APP_C recombinant proteins were purified using glutathione sepharose 4B beads and also analysed by coomassie blue staining of SDS-PAGE gels (Beads). B) CHO-TrkB cells were transiently transfected with CAT control vector (Ctrl) or $Fe65_{WT}$ as indicated. $Fe65_{WT}$ was pulled-down from cell lysates by glutathione sepharose 4B beads coupled with either GST or GST-APP_C and analysed by western blotting. Fe65 was detected with 4H324. Molecular mass markers are shown.

3.2.2.3 Interaction of endogenous APP and Fe65 can be detected by proximity ligation assays

The assays described above detect binding of exogenous Fe65 to APP. To detect binding of endogenous Fe65 to APP *in situ* within cells, PLAs for APP and Fe65 were established. CHO-TrkB cells were fixed and permeabilised before being probed with APP and Fe65 primary antibodies. PLA probes were used instead of fluorescently labelled secondary antibodies to detect interactions between the two labelled proteins. PLA probes are antibodies coupled to complementary oligonucleotides (one for each of the two primary antibodies) that, when situated within approximately 30 nm of each other, hybridise and serve as primers for rolling-circle amplification of fluorescent oligonucleotides. The resulting fluorescent signals appear as distinct dots that correspond to interacting protein pairs. The numbers of these fluorescent dots were then quantified via fluorescence microscopy and used as a measure of the strength of the protein-protein interaction between APP and Fe65 (Söderberg et al., 2006). PLAs are now being used in an increasing number of studies to quantify protein-protein interactions (Weibrecht et al., 2010).

For these studies, Fe65 was labelled with mouse antibody 4H324 and APP with rabbit antibody CT-17. Control experiments in CHO-TrkB cells were performed to demonstrate the specificity of the assays. These involved primary antibodies and no PLA conjugates (Primary), no primary antibodies and both PLA conjugates (PLA), APP antibody CT-17 and both PLA conjugates (APP+PLA), Fe65 antibody 4H324 and both PLA conjugates (Fe65+PLA) and finally, Fe56 and APP antibodies with both PLA conjugates (Primary+PLA). Stained cells were imaged in z-stacks and the 'Extended Depth of Field' plugin of Image J was used for focus stacking. The 'Analyze Particles' plugin of Image J was used to quantify PLA signal dots. None or very few signals were detected in control experiments involving primary antibodies only, only one primary antibody or PLA probes only. However, robust signals were obtained when both primary antibodies and PLA probes were present (Figure 3.4). These results verify that PLAs can be used to reliably detect and quantify the endogenous APP-Fe65 interaction.

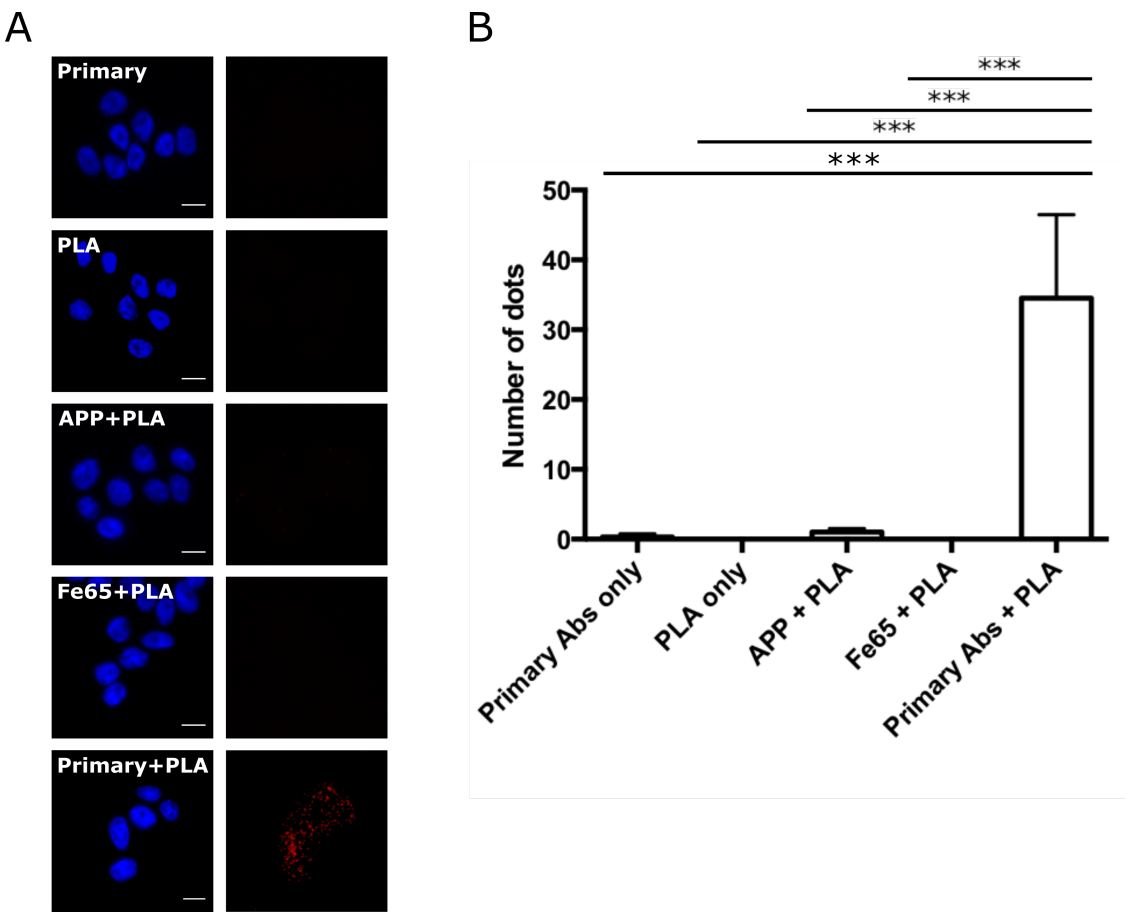

Figure 3.4: Interaction of endogenous APP and Fe65 can be detected by proximity ligation assays.

CHO-TrkB cells were fixed, permeabilised and labelled with APP and Fe65 primary antibodies (Primary), mouse plus and rabbit minus Duolink PLA probes (PLA), APP and both PLA probes (APP+PLA), Fe65 and both PLA probes (Fe65+PLA) or both primary antibodies and both PLA probes (Primary+PLA). A) Photos were acquired on a fluorescence microscope and z-stack images compiled with the 'Extended Depth of Field' plugin of Image J. APP was labelled using CT-17 and Fe65 was labelled using 4H324 primary antibodies. Scale bar = 10 µM. B) Bar chart shows the mean number of dots observed in each cell for each treatment group. Dots were recorded from images using the 'Analyze Particles' plugin of Image J. A minimum of 8 cells were analysed per treatment for control experiments. Statistical analysis was performed using one-way ANOVA followed by Dunnett's multiple comparisons test (error bars show S.D., *** = $p < 0.001$, n = 8).

3.2.3 BDNF activates ERK1/2 and induces Fe65 phosphorylation in CHO cells expressing TrkB

CHO cells are a common cell line for biochemical studies as they are easily maintained and can be transfected with a high level of efficiency. However, they are not a neuronal cell line and so are unlikely to express TrkB and respond to BDNF treatment. CHO-TrkB cells that stably express the BDNF receptor were therefore used (kind gift from Professor Pat Doherty; originally from Life Technologies). As the aim of this investigation was to measure the effect of BDNF signalling on Fe65 phosphorylation, the ability of CHO cells and CHO-TrkB cells to respond to BDNF treatment was first determined. Lysates from CHO cells treated with either vehicle (Ctrl) or BDNF (25 ng/ml for 15 min) were analysed by SDS-PAGE and western blotting. On SDS-PAGE, Fe65 migrates as three major species and these are known to be due to differential phosphorylation states. The fastest migrating species represents non- or low-phosphorylated Fe65 while the slower migrating species represent phosphorylated Fe65 (Standen et al., 2003; Zambrano et al., 1998). The migration patterns of Fe65 and the levels of total ERK1/2 and ERK1/2 phosphorylated on its dual Thr/Tyr regulatory sites were monitored in cells treated with BDNF. Phosphorylation of ERK1/2 by MEK on these regulatory sites is required for activity, so the strength of phosphorylated ERK1/2 (pERK) signals represents the level of active ERK1/2. BDNF had no effect on Fe65 phosphorylation as measured by band migration (Figure 3.5A). Similarly pERK and total ERK levels were also unaffected, demonstrating that the MAP kinase cascade was not activated by BDNF treatment in CHO cells (Figure 3.5A). These results are consistent with the absence of TrkB expression in this cell line.

To determine whether CHO-TrkB cells respond to BDNF, cells were treated with either vehicle (Ctrl) or BDNF (25 ng/ml for 15 min). To confirm specificity of the BDNF treatment, some cells were also pre-treated with K252a, a potent inhibitor of TrkB (Knüsel and Hefti, 1992), or U0126, to prevent ERK activation. K252a inhibits TrkB signal transduction by preventing autophosphorylation of the receptor in response to ligand binding, while U0126 disrupts ERK1/2 signalling by inhibiting MEK, the upstream activator of ERK1/2 (Favata et al., 1998; Knüsel and Hefti, 1992; Ohmichi et al., 1992). As before, Fe65 migration, pERK and total ERK levels were monitored by western blotting. In CHO-TrkB cells, BDNF treatment caused an increase in the relative amounts of the slowest migrating Fe65 species and a reduction in the amount of the fastest migrating Fe65 species (Figure 3.5B). This change in Fe65 migration pattern on SDS-PAGE is consistent with BDNF treatment inducing Fe65 phosphorylation. Cells treated with BDNF also had higher levels of pERK but unaltered levels of total ERK (Figure 3.5B), indicating that the MAP kinase cascade was activated in these cells. As

expected, the effect of BDNF on Fe65 and pERK was abolished in cells pre-treated with K252a or U0126 (Figure 3.5B), indicating that BDNF-induced phosphorylation of Fe65 is TrkB- and ERK1/2-dependent. As CHO-TrkB cells responded to BDNF, this cell line was considered to be appropriate for further studies.

To complement the above studies, phosphorylation mutants of Fe65 involving the ERK1/2 sites were studied. Fe65 contains four ERK1/2-responsive phosphorylation sites; Ser^{175}, Ser^{287}, Ser^{347} and Thr^{709} (Standen et al. 2003; see Figure 1.5). Two Fe65 phosphomutants were used to investigate how BDNF and ERK1/2 affected Fe65. $Fe65_{QA}$ is a phospho-precluding mutant that contains substitution mutations to alanine at each of the four ERK-responsive sites to prevent phosphorylation. $Fe65_{QE}$ contains substitutions of these phosphorylation sites to glutamic acid, which has been shown to mimic the effect of constitutive phosphorylation in many studies (for example, Ackerley et al. 2003; Vagnoni et al. 2011). These mutants have been described previously (Standen et al., 2003). Lysates from cells transiently transfected with $Fe65_{WT}$, $Fe65_{QA}$ or $Fe65_{QE}$ were analysed by western blotting to confirm that the Fe65 phosphorylation mutants show distinct migration patterns. In accordance with previous reports (Standen et al., 2003; Zambrano et al., 1998), $Fe65_{QA}$ displayed an altered pattern of migration on SDS-PAGE with an increase in the amount of the faster migrating, non-phosphorylated species. Conversely, $Fe65_{QE}$ displayed increased amounts of the slower migrating species (Figure 3.5C). These data also demonstrate that the Fe65 antibody 4H324 can detect $Fe65_{WT}$ and both Fe65 phosphorylation mutants on western blots.

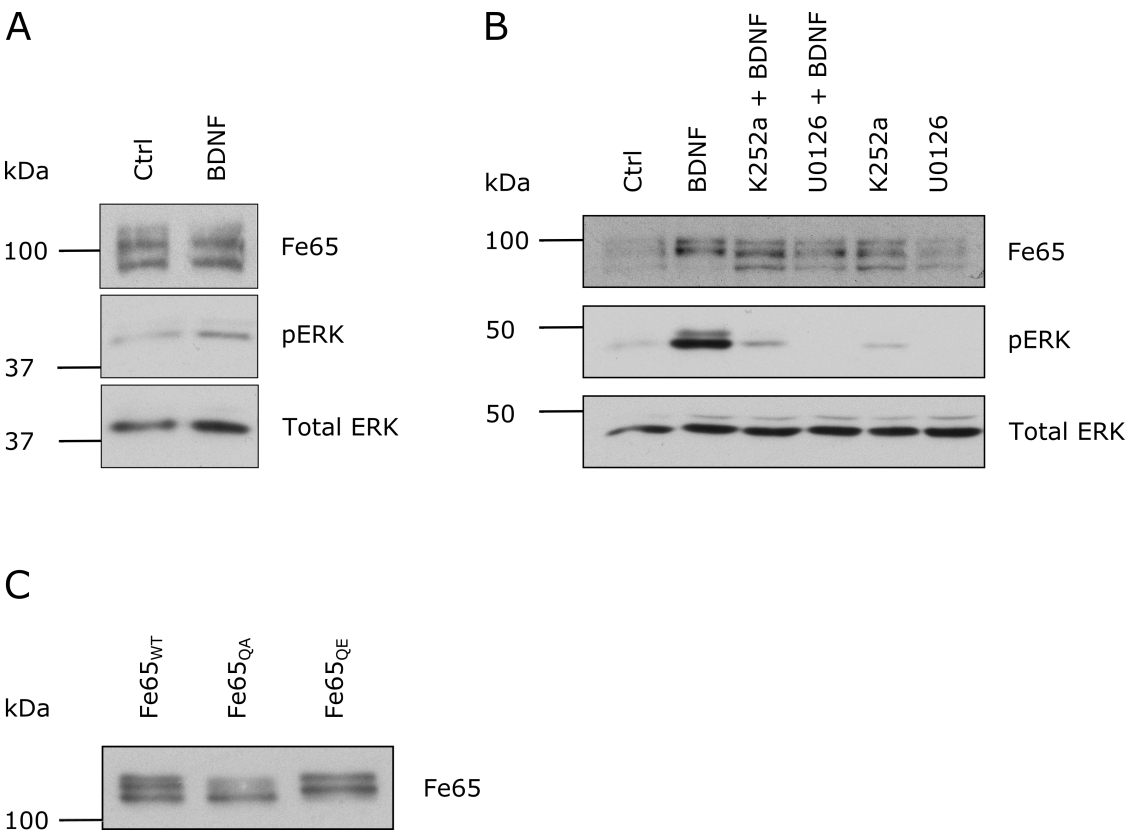

Figure 3.5: BDNF activates ERK1/2 and induces Fe65 phosphorylation in CHO cells expressing TrkB.

A) CHO cells were treated with vehicle (Ctrl) or BDNF (25 ng/ml) for 15 min as indicated. Lysates were probed for Fe65, pERK and total ERK by western blotting. B) CHO-TrkB cells were treated with vehicle (Ctrl), BDNF (25 ng/ml) for 15 min, K252a (200 nM) or U0126 (20 µM) as indicated. Where appropriate, K252a and U0126 treatments were administered 10 min and 15 min prior to BDNF respectively. Samples were then analysed by SDS-PAGE and western blotting for Fe65, pERK and total ERK. C) Lysates from CHO-TrkB cells transfected with $Fe65_{WT}$, $Fe65_{QA}$ or $Fe65_{QE}$ (phosphomutants containing mutations of ERK-phosphorylated residues Ser^{175}, Ser^{287}, Ser^{347} and Thr^{709}) were probed on western blots for Fe65. Fe65 was detected with 4H324, pERK was detected with 9102 and total ERK was detected with M12320 for all treatment groups. Molecular mass markers are shown.

3.2.4 BDNF activates ERK1/2 and induces Fe65 phosphorylation in rat cortical neurons

While CHO-TrkB cells are useful for biochemical studies, they are not neuronal cells and do not naturally respond to BDNF. To confirm that BDNF is also capable of inducing Fe65 phosphorylation in neurons, rat primary cortical neurons were treated with either vehicle (Ctrl) or BDNF (25 ng/ml for 15 min) and samples were analysed by SDS-PAGE and western blotting for Fe65, pERK and total ERK. Treatment of cells with BDNF induced an increase in the relative levels of the slower migrating, phosphorylated Fe65 species and a decrease in the faster migrating, non-phosphorylated Fe65 species. Consistent with the findings from CHO-TrkB cells, these changes were at least partially prevented by pre-treatment with the TrkB signalling inhibitor K252a or the MEK inhibitor U0126 (Figure 3.6). These results show that BDNF induces endogenous Fe65 phosphorylation in cortical neurons by activating the endogenous ERK1/2 MAP kinase signal transduction pathway.

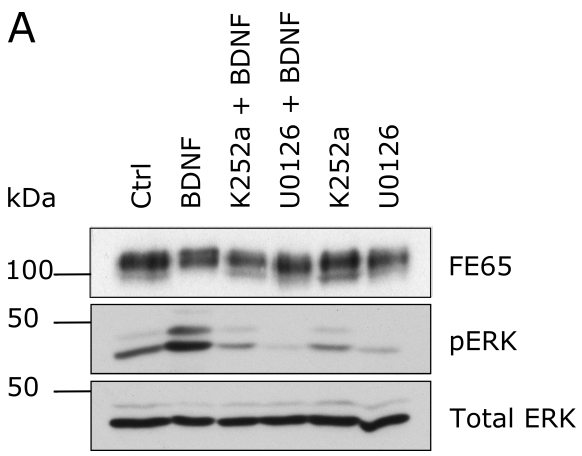

Figure 3.6: BDNF activates ERK1/2 and induces Fe65 phosphorylation in rat cortical neurons.

A) DIV 5 rat cortical neurons were treated with either vehicle (Ctrl), BDNF (25 ng/ml) for 15 min, K252a (200 nM) or U0126 (20 μM) as indicated. Where appropriate, K252a and U0126 treatments were administered 10 min and 15 min prior to BDNF respectively. The western blot migration pattern of Fe65 was monitored in cell lysates from each treatment group. Fe65 was detected with 4H324, pERK was detected with 9102 and total ERK was detected using M12320 for all treatment groups. Molecular mass markers are shown.

3.2.5 BDNF treatment shows no significant effect on APP-Fe65 binding in co-immunoprecipitation and GST-APP$_C$ pull-down assays from CHO-TrkB cells

The results in sections 3.2.3 and 3.2.4 show that BDNF induces phosphorylation of Fe65 via ERK1/2. Four different Fe65 ERK1/2 phosphorylation sites have been identified (Ser^{175}, Ser^{287}, Ser^{347} and Thr^{709}; Standen et al. 2003), but the functional consequences of this phosphorylation is unknown. As APP is well characterised as a binding partner of Fe65 (Borg et al., 1996; Bressler et al., 1996; Fiore et al., 1995; McLoughlin and Miller, 1996), one possibility is that BDNF-induced phosphorylation of Fe65 via ERK1/2 affects its binding to APP. Phosphorylation is a common mechanism for regulating protein-protein interactions and phosphorylation of Fe65 on another site (Ser^{610}) has been shown to alter its binding to APP (Chow et al., 2015b).

To investigate whether BDNF influences the interaction between APP and Fe65, biochemical studies were performed using CHO-TrkB cells. Co-immunoprecipitation assays were carried out on cells transfected with either CAT (Ctrl), or APP+Fe65 plasmid vectors (described in Table 2.2) and treated with vehicle or BDNF (25 ng/ml for 30 minutes). While 15 min treatment with BDNF consistently activated ERK1/2 and induced phosphorylation of Fe65 (see Figure 3.5 and 3.6), optimisation experiments indicated that 30 min BDNF treatment was required to detect robust changes to the APP-Fe65 interaction (data not shown), so for all further experiments discussed, BDNF was applied to cells for 30 min.

Fe65 was immunoprecipitated with antibody sc-19751 and SDS-PAGE and western blotting was used to detect the amount of co-immunoprecipitated APP. Probing of total cell lysates for APP, Fe65 and pERK demonstrated that the cells were appropriately transfected and that BDNF treatment activated ERK1/2 (Figure 3.7A). Analyses of the immunoprecipitates showed that BDNF treatment had no significant effect on the interaction between APP and Fe65 (Figure 3.7B), although there is a non-significant trend towards a decrease in binding after BDNF treatment.

The migratory shift in Fe65 described in sections 3.2.3 and 3.2.4 cannot be observed in western blots of co-immunoprecipitation samples and GST pull-down samples. This is because the gels were not run to separate the individual species of Fe65 to facilitate densitometry analysis of protein pull down. Instead, to confirm that BDNF treatment was successful, western blots were also probed for pERK as an indicator of BDNF-induced activation of the ERK MAPK cascade (as also seen in Figure 3.5 and Figure 3.6).

To complement these studies, GST-APP_C pull-down assays were performed from CAT control vector (Ctrl) or Fe65 transfected CHO-TrkB cells treated with either vehicle or BDNF (25 ng/ml for 30 minutes). The recombinant GST-APP_C used in these assays is not phosphorylated (protein phosphorylation does not occur in standard *E. coli* strains), so any BDNF-induced changes to binding of Fe65 to APP in these pull-down assays cannot be attributed to altered phosphorylation of APP. As such, any changes are more likely to be due to changes in Fe65 phosphorylation. Western blots of inputs demonstrated that the cells were transfected with Fe65 and that BDNF induced activation of ERK1/2 (Figure 3.8A). Consistent with co-immunoprecipitation findings, BDNF treatment showed a non-significant trend towards a reduction in the amount of Fe65 pulled-down by GST-APP_C (Figure 3.8B).

These studies show that treatment of CHO-TrkB cells with BDNF induces phosphorylation of Fe65 and, although findings did not reach a level of significance, they show a consistent trend towards BDNF reducing binding between APP and Fe65. This occurs in both co-immunoprecipitation and GST-APP_C pull-down assays. The finding that BDNF reduces binding of Fe65 to APP in the GST-APP_C pull-down assays eliminates the possibility that this effect is due to BDNF acting on APP, for example by altering APP phosphorylation.

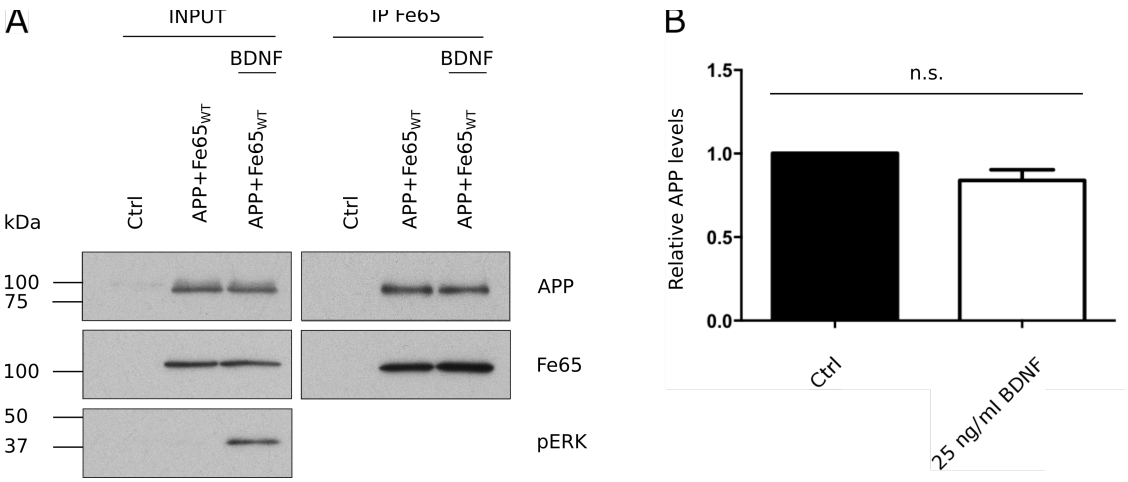

Figure 3.7: BDNF treatment has no effect on APP-Fe65 binding in co-immunoprecipitation assays from CHO-TrkB cells.

A) CHO-TrkB cells were transiently transfected with CAT (Ctrl) or APP+Fe65$_{WT}$ plasmid vectors and treated with vehicle or BDNF (25 ng/ml) for 30 min as indicated. Fe65 was immunoprecipitated using sc-19751 and bound APP was analysed by western blotting. Fe65 was detected using 4H324, APP using CT-17 and pERK using 9102. Molecular mass markers are shown. B) Bar chart shows relative APP levels bound to Fe65 in the immunoprecipitates. Signals on western blots were quantified by densitometry and bound APP signals were normalised to immunoprecipitated Fe65 signals. Data from BDNF treated cells were then normalised to vehicle treated controls and statistical analysis was carried out using Wilcoxon-signed ranks test (error bars show S.D., n.s. = $p > 0.05$, n = 3).

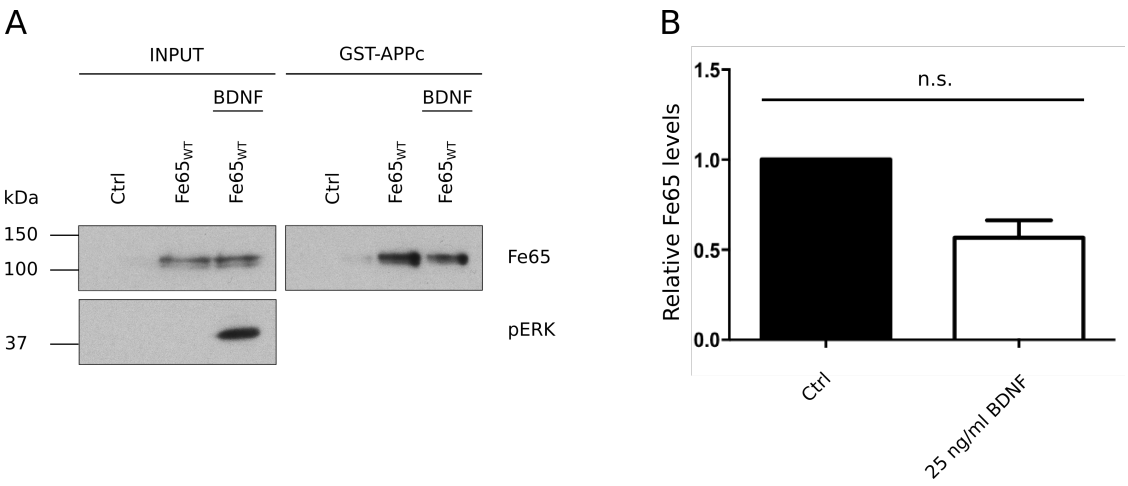

Figure 3.8: BDNF treatment has no effect on APP-Fe65 binding in GST-APP$_C$ pull-down assays from CHO-TrkB cells.

A) CHO-TrkB cells were transiently transfected with CAT control vector (Ctrl) or Fe65$_{WT}$ and treated with either vehicle or BDNF (25 ng/ml) for 30 min as indicated. Fe65 was pulled down with GST-APP$_C$-conjugated glutathione sepharose 4B beads and bound Fe65 was analysed by western blotting. Fe65 was detected using 4H324 and pERK was detected by 9102. Molecular mass markers are shown. B) Bar chart shows relative Fe65 levels bound to GST-APP$_C$. Signals on western blots were quantified by densitometry and data from BDNF treated cells were normalised to vehicle treated controls. Statistical analysis was carried out using Wilcoxon-signed ranks test (error bars show S.D., n.s. = $p > 0.05$, n = 3).

3.2.6 BDNF treatment reduces binding between endogenous APP and Fe65 in proximity ligation assays in both CHO-TrkB cells and rat cortical neurons

The above studies show that BDNF reduces the interaction between exogenous APP and Fe65. To determine whether BDNF has a similar effect on endogenous APP and Fe65, PLAs were used. CHO-TrkB cells were treated with either vehicle or BDNF (25 ng/ml for 30 minutes) and PLAs were performed using primary antibodies to detect APP (CT-17) and Fe65 (4H324). BDNF treatment significantly reduced the number of PLA signals detected in cells compared to vehicle treatment (Figure 3.9). PLAs were then performed in rat cortical neurons treated with either vehicle or BDNF (25 ng/ml for 30 minutes). Again, BDNF treatment significantly reduced the number of PLA signals (Figure 3.10). These experiments complement the results from the co-immunoprecipitation and GST-APP_C pull-down assays, showing that treatment with BDNF reduces binding of APP and Fe65. Importantly, these PLAs demonstrate that this is the case for endogenous APP and Fe65 and, more specifically, endogenous proteins in cortical neurons.

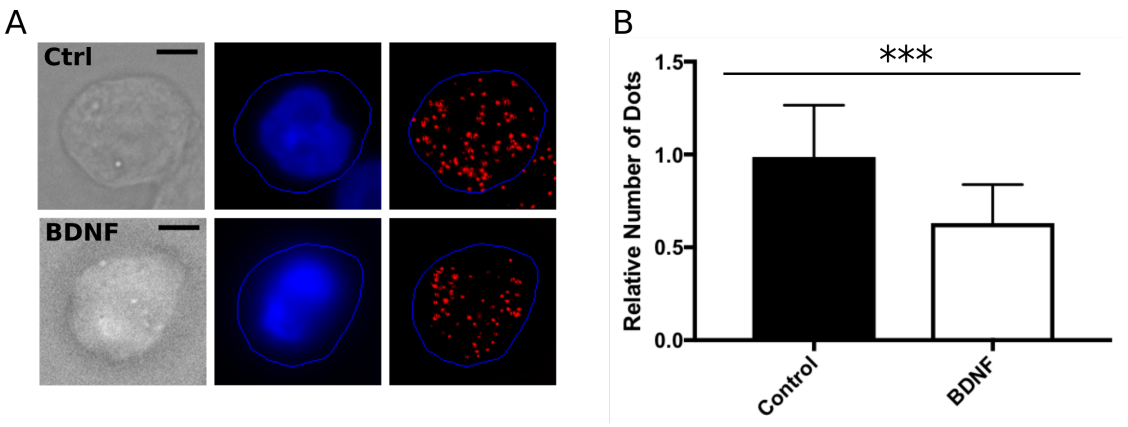

Figure 3.9: BDNF treatment of CHO-TrkB cells reduces binding between endogenous APP and Fe65.

A) CHO-TrkB cells were fixed, permeabilised and labelled with APP and Fe65 primary antibodies and PLAs carried out. Microscopy images were acquired and z-stack images compiled with the 'Extended Depth of Field' plugin of Image J. The number of dots observed in each cell was recorded from images using the 'Analyze Particles' plugin of Image J. APP was labelled using CT-17 and Fe65 was labelled using 4H324 primary antibodies. Scale bar = 10 μM. B) Bar chart shows relative number of PLA signals (dots) counted per cell. Data were normalised to vehicle treated controls and statistical analysis was carried out using a Mann-Witney test (error bars show S.D., *** = $p < 0.0001$, n = 107).

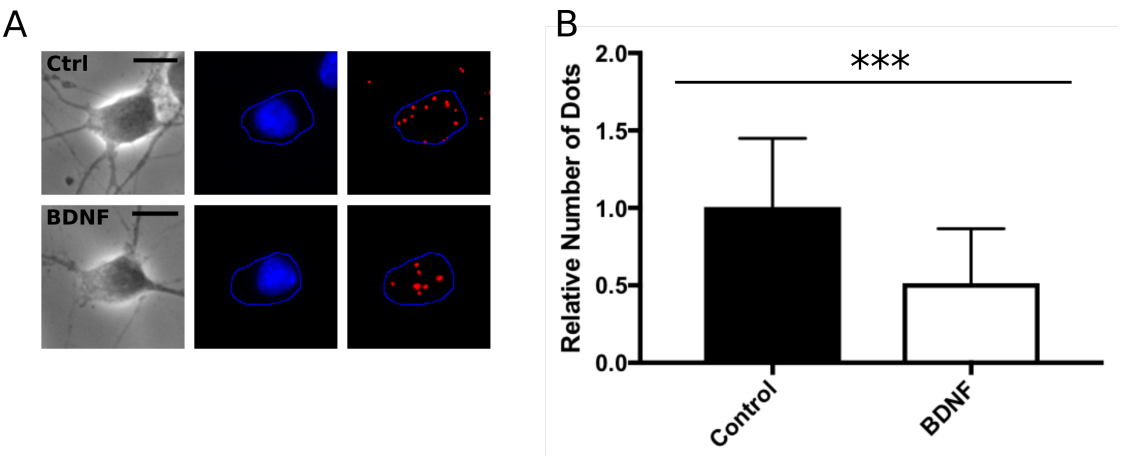

Figure 3.10: BDNF inhibits binding between endogenous APP and Fe65 in primary cortical neurons.

A) DIV 3 rat cortical neurons were fixed, permeabilised and labelled with APP and Fe65 primary antibodies and PLAs carried out. Microscopy images were acquired and z-stack images compiled with the 'Extended Depth of Field' plugin of Image J. The number of dots observed in each cell was recorded from images using the 'Analyze Particles' plugin of Image J. APP was labelled using CT-17 and Fe65 was labelled using 4H324 primary antibodies. Scale bar = 10 μM. B) Bar chart shows relative number of PLA signals (dots) counted per cell. Data were normalised to vehicle treated controls and statistical analysis was carried out using a Mann-Witney test (error bars show S.D., *** = $p < 0.0001$, n = 164).

3.2.7 The Fe65 phospho-mimicking mutant has reduced binding to APP in GST-APP$_C$ pull-down assays

The results in sections 3.2.3-3.2.6 show that BDNF treatment induces phosphorylation of Fe65 via ERK1/2 and that BDNF treatment reduces the interaction between APP and Fe65. This was shown in both CHO-TrkB cells and cortical neurons using three different techniques. Together, these results indicate that BDNF induces phosphorylation of Fe65 by ERK1/2 and affects its binding to APP. However, they do not eliminate the possibility that BDNF alters the APP-Fe65 interaction via other routes. For example, BDNF may induce phosphorylation of other proteins that bind to APP such as the X11s and this may indirectly influence APP binding to Fe65. In addition, they do not definitively demonstrate that phosphorylation of Fe65 on its four ERK1/2 sites alters its binding to APP.

To investigate whether the effects of BDNF treatment on the APP-Fe65 interaction are indeed due to phosphorylation at one or more of the four identified ERK1/2 phosphorylation sites of Fe65 (Ser^{175}, Ser^{287}, Ser^{347} and Thr^{709}), the ability of Fe65 phospho-mimicking and phospho-precluding mutants to bind to APP was studied. Co-immunoprecipitation assays were carried out on CHO-TrkB cells transfected with either CAT control vector (Ctrl), APP+Fe65$_{WT}$, APP+Fe65$_{QA}$ or APP+Fe65$_{QE}$. Fe65 was immunoprecipitated with antibody sc-19751 and SDS-PAGE and western blotting was used to detect the amount of co-immunoprecipitated APP. Input samples probed for APP and Fe65 demonstrated that the cells were transfected as required (Figure 3.11A). Analyses of the immunoprecipitates found that the Fe65 phospho-mimicking mutant (Fe65$_{QE}$) showed a non-significant trend towards impaired binding to APP compared to Fe65$_{WT}$. Interestingly the phospho-precluding mutant (Fe65$_{QA}$) showed a non-significant trend towards increased binding to APP compared to Fe65$_{WT}$ (Figure 3.11B).

To complement these studies, GST-APP$_C$ pull-down assays were also performed on CHO-TrkB cells transfected with CAT control vector (Ctrl), Fe65$_{WT}$, Fe65$_{QA}$ or Fe65$_{QE}$. Western blots of inputs confirmed that the cells were appropriately transfected with Fe65 constructs (Figure 3.12A). Consistent with the non-significant trend seen in co-immunoprecipitation assays, Fe65$_{QE}$ showed reduced binding to GST-APP$_C$ compared to Fe65$_{WT}$ and this change was significantly different as detected by GST pull-down. As with the co-immunoprecipitation results, GST-APP$_C$ pull-down assays did not show a significant change in binding between Fe65$_{QA}$ and GST-APP$_C$ compared to Fe65$_{WT}$ (Figure 3.12B), although the non-significant trend in GST pull-downs did not match co-immunoprecipitation data.

These studies show that mutation of the four identified ERK1/2 phosphorylation sites of Fe65 to mimic permanent phosphorylation reduces its binding to APP in GST-APP_C pull-down assays. However, mutation of these sites to preclude phosphorylation showed no significant effect on Fe65 binding to APP in either co-immunoprecipitation assays or GST-APP_C pull-down assays. The results in this chapter support the hypothesis that BDNF negatively regulates the APP-Fe65 interaction by inducing ERK1/2-mediated phosphorylation of Fe65.

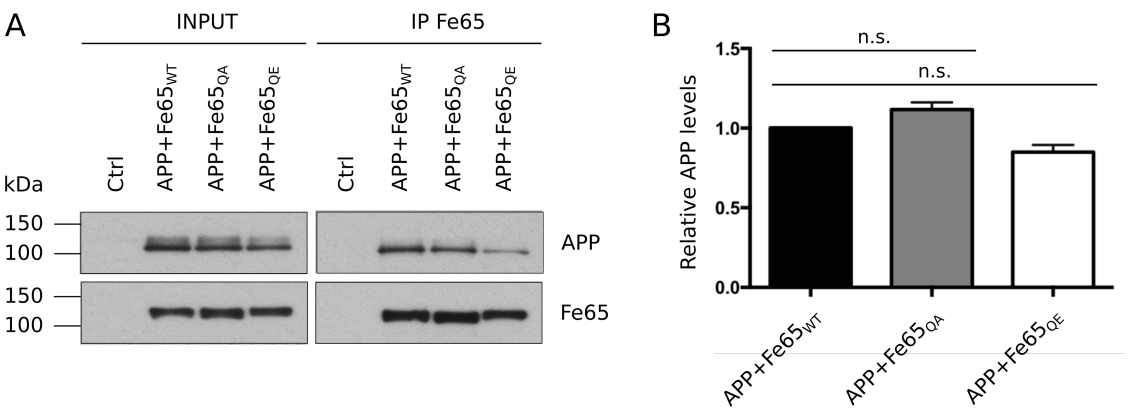

Figure 3.11: The Fe65 phosphorylation mutants do not show changed binding to APP in co-immunoprecipitation assays.

A) CHO-TrkB cells were transiently transfected with control vector (Ctrl), APP+Fe65$_{WT}$ APP+Fe65$_{QA}$ or APP+Fe65$_{QE}$ as indicated. Fe65 was immunoprecipitated using sc-19751 and bound APP was detected on western blots. Fe65 was detected using 4H324 and APP using CT-17. Molecular mass markers are shown. B) Bar chart shows relative APP levels bound to Fe65 in immunoprecipitates. Signals on western blots were quantified by densitometry and bound APP signals were normalised to immunoprecipitated Fe65 signals. Data from BDNF treated cells were then normalised to APP+Fe65$_{WT}$ data and statistical analysis was carried out using Kruskal-Wallis test followed by Dunn's multiple comparisons test (error bars show S.D., n.s. = $p > 0.05$, n = 3).

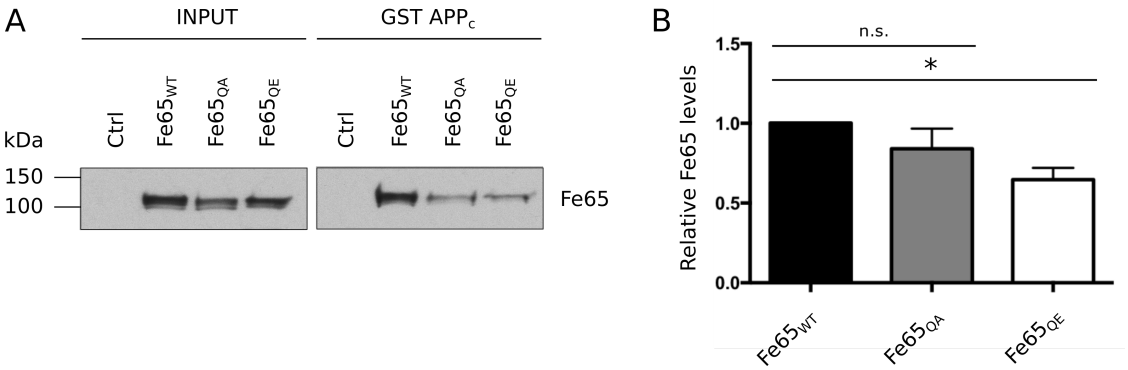

Figure 3.12: The Fe65 phospho-mimicking mutant has reduced binding to the cytoplasmic tail of APP.

A) CHO-TrkB cells were transfected with CAT control vector (Ctrl), Fe65$_{WT}$, Fe65$_{QA}$ or Fe65$_{QE}$ as indicated. Fe65 was pulled-down using GST-APP$_C$ and detected on western blots using 4H324. Molecular mass markers are shown. B) Bar chart shows relative Fe65 levels bound to GST-APP$_C$. Signals on western blots were quantified by densitometry and data were normalised to Fe65$_{WT}$. Statistical analysis was carried out using Kruskal-Wallis test followed by Dunn's multiple comparisons test (error bars show S.D., n.s. = not significant, * = $p < 0.05$, n = 3).

3.3 Discussion

In this chapter, the effect of BDNF on Fe65 phosphorylation and APP-Fe65 binding was investigated. This was achieved by monitoring Fe65 phosphorylation and the APP-Fe65 interaction in response to BDNF treatment in CHO cells stably transfected with TrkB and rat cortical neurons. Fe65 phosphorylation was also investigated using phospho-mimicking and phospho-precluding Fe65 mutants in which, four known Fe65 ERK1/2 phosphorylation sites were mutated to glutamic acid or alanine, respectively.

BDNF treatment stimulated Fe65 phosphorylation in both CHO-TrkB cells and in cortical neurons. Fe65 phosphorylation was measured by a shift in its migration on SDS-PAGE, which has previously been reported to be indicative of Fe65 phosphorylation state (Standen et al., 2003; Zambrano et al., 1997). BDNF-induced phosphorylation of Fe65 was reduced by inhibition of either the TrkB receptor by K252a or the MEK inhibitor U0126, which inhibits ERK1/2. Although TrkB inhibition did not completely abolish ERK1/2 activation, presumably because other signalling molecules can activate the ERK1/2 MAP kinase cascade (Yang et al., 2013), both inhibitors rescued the effect of BDNF on Fe65 phosphorylation as judged by its migration profile on SDS-PAGE. These experiments show that the shift in Fe65 phosphorylation induced by BDNF involves ERK1/2, however they do not identify the specific Fe65 residues that are phosphorylated by BDNF-induced ERK1/2 phosphorylation.

Four ERK1/2 phosphorylation sites have been identified in Fe65 and these were mutated to either alanine ($Fe65_{QA}$) or glutamic acid ($Fe65_{QE}$; Standen et al., 2003). These Fe65 phosphomutants display changes in SDS-PAGE migration profiles that are similar ($Fe65_{QE}$) or opposite ($Fe65_{QA}$) to the migration profiles of BDNF treated cells. As such, these data further support the conclusion that the BDNF-induced Fe65 migration changes are due to ERK1/2 phosphorylation at these sites. While BDNF is known to activate the ERK1/2 MAP kinase cascade (Yang et al., 2013) and Fe65 has been identified as an ERK1/2 substrate (Standen et al., 2003), the link between these pathways had not previously been established. The findings presented here provide this novel connection by demonstrating that BDNF treatment can induce Fe65 phosphorylation in an ERK1/2-dependent manner. More formal demonstration that BDNF-induced ERK1/2 phosphorylation of Fe65 involves the four known ERK1/2 sites (Ser^{175}, Ser^{287}, Ser^{347} and Thr^{709}) could involve mass spectrometry analysis or alternatively, the generation of phospho-specific Fe65 antibodies to these sites.

To gain insight into the function of this BDNF-induced phosphorylation of Fe65, methods were established to measure the APP-Fe65 interaction. After optimisation, co-immunoprecipitations, GST-APP_C pull-down assays and PLAs were all able to detect the interaction between APP and Fe65. Interestingly, in co-immunoprecipitation assays Fe65 antibodies successfully pulled-down APP, but in the reciprocal assay, a C-terminal APP antibody was unable to co-immunoprecipitate Fe65. One possible explanation for this observation is that the C-terminal APP antibody, which recognises the YENPTY Fe65-binding motif of APP, cannot bind to its epitope if Fe65 is bound to APP. Consequently, in co-immunoprecipitation assays, the APP antibody would be precipitating only APP that is not bound to Fe65. Since co-immunoprecipitations are carried out on total cell lysates, the cellular localisation of the proteins should not influence binding of the APP antibody. Similarly, both Fe65 and APP C-terminal antibodies detect proteins by western blotting. It is possible that use of an N-terminal APP antibody to immunoprecipitate APP might be more successful since it would not compete with Fe65 for APP binding. However, this might not be appropriate for detection of the APP-Fe65 interaction because Fe65 interacts with the C-terminus of APP and APP undergoes proteolytic cleavage to shed its N-terminal domain. An APP C-terminal antibody raised to an epitope that does not overlap with the Fe65 binding site would be useful in this context, but none have so far been characterised.

Interestingly, the C-terminal APP antibody was able to detect the APP-Fe65 interaction in intact cells via the PLA technique. Although the reason for this is unclear, the PLA protocol involves paraformaldehyde fixation of cells prior to staining. This is a cross-linking method that can alter protein conformation and antigen availability (Hewitson et al., 2010). A common issue with cross-linked fixation is the masking of antigen sites, however, in this case cross-linking may alter the conformation of APP and/or Fe65 to expose the C-terminal APP antibody epitope and allow protein recognition. While paraformaldehyde cross-linking can modify protein conformation, it fixes proteins in place and would therefore not interfere with detection of the APP-Fe65 interaction in the PLAs, which reveal protein interactions by measuring the proximity of the two proteins of interest.

These three optimised protein interaction assays were used to determine how BDNF treatment affects the APP-Fe65 interaction. BDNF reduced binding of Fe65 to APP in proximity ligation assays, however this reduction failed to reach significance in co-immunoprecipitation assays and GST pull-downs although a consistent trend was seen. The co-immunoprecipitation assays revealed that BDNF induced a 16 % decrease in APP bound to Fe65, while the GST-APP_C pull-down assays and PLAs

produced 43 % and approximately 40-50 % reductions in APP-Fe65 binding respectively (The PLAs showed 37 % and 49 % decreases in CHO-TrkB and cortical neurons respectively). The co-immunoprecipitation assays detected a smaller decrease than the GST-APP_C pull-downs and PLAs, although only PLA studies reached statistical significance. One possibility for the less marked effect of BDNF on APP-Fe65 binding in the co-immunoprecipitation assays is that these involved co-transfection of both APP and Fe65. This may increase the expression of these proteins to such levels that they could not be completely phosphorylated by endogenous levels of ERK1/2. Co-transfection of ERK1/2 as well as APP and Fe65 may induce a decrease in binding similar to that shown by the PLAs. The sample sizes tested in these experiments were small and as such, could not be tested for normality so non-parametric tests had to be used. Larger sample sizes would give more power to these findings and may be able to resolve more subtle changes to APP-Fe65 binding than the studies discussed here.

Overexpression of proteins can cause mislocalisation and accumulation in unusual cellular compartments. As such, the co-immunoprecipitation and GST-APP_C pull-down assays used in this study are not as powerful as assays that detect the binding of endogenous proteins. Because of these limitations, the effect of BDNF on binding of endogenous APP to Fe65 was investigated using PLAs. In these assays, BDNF treatment resulted in a significant decrease in APP-Fe65 binding in both CHO-TrkB cells and rat cortical neurons and the scale of inhibition was similar in both cell types. One limitation of the PLA technique in cortical neurons is that only protein interactions in the cell body were analysed due to the difficulty of properly identifying neurites. To expand this experiment to include APP-Fe65 complexes in axons and dendrites, a counter-stain for a cytoskeletal component could be used.

To determine how phosphorylation of Fe65 at the four known ERK1/2 sites altered its binding to APP, co-immunoprecipitation and GST-APP_C pull-down assays were performed in CHO-TrkB cells transiently transfected with either $Fe65_{WT}$, $Fe65_{QA}$ or $Fe65_{QE}$ (for the GST-APP_C pull-down assays) or co-transfection of APP with either $Fe65_{WT}$, $Fe65_{QA}$ or $Fe65_{QE}$ (for the immunoprecipitation assays). PLAs were not used to study the Fe65 phosphorylation mutants because these assays involve the analysis of individual cells. Transient transfection of cells does not result in uniform overexpression levels and cells expressing high levels of Fe65 are likely to produce higher PLA signals than those expressing low levels of protein. This could confound the interpretation of the effects of the mutants on APP binding. The use of

EGFP-tagged Fe65 constructs would allow normalisation of PLA signals to the level of Fe65 overexpression in individual cells, which would resolve this issue.

The phospho-mimicking $Fe65_{QE}$ mutant showed a significant decrease in APP binding in GST-APP_C pull-down assays and displayed a consistent but non-significant trend towards lower binding to APP than wild-type Fe65 in both co-immunoprecipitation assays. As with the BDNF studies, this effect was more pronounced when measured by GST pull-down assay compared to co-immunoprecipitation (35 % decrease and 15 % decrease in relative protein binding respectively) and only the GST pull-down study reached significance. Interestingly, the phospho-precluding Fe65 mutant did not have a consistent effect on the APP-Fe65 interaction. It displayed non-significant and conflicting changes to binding in co-immunoprecipitation and GST-APP_C pull-down assays. One possible explanation for this is that the phosphorylation mutants have amino acid substitutions at all four ERK1/2-responsive sites, but ERK1/2 may not phosphorylate all of these sites to an equal extent. Indeed, there is evidence that Thr^{709} is more readily phosphorylated by ERK1/2 than the other three residues (Standen et al., 2003). If, in the CHO-TrkB cells used for these assays, the majority of Fe65 remains unphosphorylated at these four ERK1/2-responsive sites, mutation of these sites to alanine would only have a minor effect on its interaction with APP compared to wild-type Fe65. Whatever the precise scenario, the results using these Fe65 phosphorylation mutants complement and extend the data from BDNF treated cells, but again, possibly require larger sample sizes in order to reach statistical significance. They are consistent with BDNF-induced Fe65 phosphorylation by ERK1/2 causing a reduction in APP-Fe65 binding and confirm that this effect is due to phosphorylation of at least one of the four known ERK1/2-responsive sites.

Although none of the ERK1/2-responsive residues are located within the protein interaction domains of Fe65, Ser^{287} is located two residues downstream of the WW domain and Thr^{709} is ten residues downstream of the PTB2 motif (Standen et al. 2003; Figure 1.5). One previously proposed mechanism for the regulation of Fe65 activity is a phosphorylation-induced conformational switch, in which, the N-terminal WW domain of Fe65 interacts with its own C-terminal domain (Cao and Südhof, 2004). As Ser^{287} and Thr^{709} are situated close to the functional domains proposed to be involved in regulating Fe65 conformation, they may play a role in mediating this switch. Alternatively, due to its location, the addition of a phosphate group at Thr^{709} may render the PTB2 domain inaccessible to the binding domain of APP. Further investigation using individual phosphorylation mutants would help identify which phosphorylation sites are crucial to the inhibition of the APP-Fe65 interaction.

The results discussed so far show that BDNF activates ERK1/2 to induce Fe65 phosphorylation to decrease binding between APP and Fe65. They also demonstrate that mutation of ERK1/2 phosphorylation sites on Fe65 to mimic permanent phosphorylation reduces the APP-Fe65 interaction. To show that the inhibitory effect of BDNF on this protein-protein interaction is via phosphorylation of Fe65 at one or more of these four sites, future studies that monitor binding between the Fe65 phospho-precluding mutant ($Fe65_{QA}$) and APP after BDNF treatment could be employed. If BDNF reduces APP-Fe65 binding via Fe65 phosphorylation at ERK1/2-responsive sites, this inhibitory effect should be rescued by the use of the $Fe65_{QA}$ mutant.

BDNF is being investigated as a therapeutic approach for AD. This is because production of BDNF is impaired in AD and restoration of BDNF can improve memory deficits and rescue synapse loss and neuronal death in AD models (Ando et al., 2002; Arancibia et al., 2008; Blurton-Jones et al., 2009; Nagahara et al., 2013, 2009). In addition, BDNF shows neuroprotective effects against Aβ toxicity and reduces amyloidogenic processing of APP (Arancibia et al., 2008; Matrone et al., 2008). The exact molecular pathways involved in these beneficial effects of BDNF are unclear but several studies have shown that ERK1/2 signalling is required for BDNF-mediated neuroprotective effects and dendritic spine growth (Almeida et al., 2005; Alonso et al., 2004; Han and Holtzman, 2000; Nguyen et al., 2009; Sun et al., 2008). The data presented in this chapter extend current knowledge by describing a BDNF-induced signalling pathway that activates ERK1/2 to phosphorylate Fe65 and inhibit APP-Fe65 binding. As APP and Fe65 are thought to be involved in gene transcription, cell motility and APP processing (see sections 1.2.3, 1.3.2 and 1.3.3), part of the protective effect of BDNF may be linked to phosphorylation of Fe65 and its binding to APP.

Although BDNF can protect cells against apoptosis, Aβ toxicity and rescue synapse loss (Ando et al., 2002; Arancibia et al., 2008; Blurton-Jones et al., 2009; Matrone et al., 2008; Nagahara et al., 2013, 2009), there are limitations to its use as a therapeutic molecule. One problem with using BDNF as a therapy for AD is that it does not easily cross the blood-brain barrier. In addition, the expression of the TrkB receptor is highly regulated so infusion of BDNF into the brain is not effective because local sites receive an acute dose of BDNF, which triggers a reduction in TrkB, while distal sites receive much lower doses (Frank et al., 1997). Viral vector delivery of BDNF has shown more promising results in animal models (Kells et al., 2004; Nagahara et al., 2013, 2009) and a synthetic TrkB agonist is able to cross the blood-brain barrier and shows similar efficacy to BDNF treatment (Devi and Ohno, 2012; Hsiao et al., 2014). Enhancing

endogenous BDNF expression is another avenue of BDNF treatment that is being explored and the AD-approved acetylcholinesterase inhibitor donepezil restores BDNF levels in AD patients to expression levels seen in control subjects (Leyhe et al., 2008). Other methods of augmenting endogenous BDNF include enhancing cAMP response element binding protein phosphorylation, which is involved in positively regulating BDNF expression, dietary supplements of zinc and the flavonoid rutin and low-level laser therapy (Caccamo et al., 2010; Corona et al., 2010; Meng et al., 2013; Moghbelinejad et al., 2014).

In summary, this chapter shows that BDNF induces phosphorylation of Fe65 via induction of the ERK1/2 MAP kinase cascade, of which Fe65 is a known substrate. In addition to linking these pathways, the results presented here also show that phosphorylation of Fe65 at ERK1/2-responsive sites negatively impacts on the APP-Fe65 interaction. By being able to influence this interaction with an extracellular signalling molecule, it may be possible to regulate the functions of the APP-Fe65 complex, one of which is mediating gene transcription. APP acts as a membrane-bound tether for Fe65 and prevents its translocation to the nucleus (Cao and Südhof, 2001; Minopoli et al., 2001). The evidence detailed here shows that BDNF inhibits the APP-Fe65 interaction and therefore may increase the amount of Fe65 capable of translocating to the nucleus. This is consistent with evidence that the majority of Fe65 found in the nucleus is phosphorylated (Zambrano et al., 1998). Future analysis of subcellular fractions of BDNF treated cells would help to confirm whether more Fe65 is released for nuclear translocation in response to BDNF. The effect of an increase in available Fe65 on gene transcription would likely vary from gene to gene as previous research has shown that APP and Fe65 do not regulate all target genes by the same mechanism (see section 1.3.2). BDNF activates a variety of intracellular signalling pathways, so data collected from reporter gene assays, which have been used previously to measure changes to the transactivation function of Fe65 (Bao et al., 2007; Belyaev et al., 2009; Bruni et al., 2002; Cao and Südhof, 2004, 2001; Kajiwara et al., 2009; Kim et al., 2003; Kinoshita et al., 2003; Lau et al., 2008; Pardossi-Piquard et al., 2005; Perkinton et al., 2004; Xu et al., 2011; Yang et al., 2006) in response to BDNF treatment would be difficult to attribute solely to Fe65 phosphorylation. The formal identification of Fe65-regulated genes is required to characterise the role of BDNF-induced phosphorylation on any Fe65-mediated gene transcription.

It has been previously established that the APP-Fe65 interaction is involved in the regulation of gene transcription, although the affected genes are not consistently

reported (see section 1.3.2). Chapter 4 of this thesis focuses on monitoring the effect of loss of Fe65 on transcription and the identification of novel genes that are regulated by Fe65.

3.3.1 Limitations of the study

1. Fe65 phosphorylation was assessed by changes in protein migration on SDS-PAGE. For the future, the generation and use of phosphorylation-specific antibodies to the sites under investigation would enhance the study. If these cannot be generated, then changes in phosphorylation could be monitored by mass spectrometry approaches.

2. For both co-immunoprecipitation and GST pull-down assays, protein overexpression was required to detect the interaction between APP and Fe65. As overexpression can alter protein localisation in cellular compartments, this can detect interactions that, while physically compatible, do not occur endogenously. This limitation was addressed by the use of PLAs, which were carried out to measure interactions between endogenous proteins in intact, fixed cells.

3. With the exception of PLAs, sample sizes used for these studies were small and often failed to reach statistical significance although consistent changes in protein interaction were seen. Increased sample sizes may reduce variability and allow detection of more subtle changes via these assays.

CHAPTER 4: FE65 INDEPENDENTLY REGULATES FRIZZLED-1 EXPRESSION, GSK3B ACTIVITY AND TAU PHOSPHORYLATION

4.1 Introduction

The interaction between APP and Fe65 is widely reported to be involved in regulating gene transcription (Alves da Costa et al., 2006; Bao et al., 2007; Belyaev et al., 2009; Bruni et al., 2002; Cao and Südhof, 2004, 2001; Kajiwara et al., 2009; Kim et al., 2003; Lau et al., 2008; Li et al., 2010; Ma et al., 2008; McLoughlin and Miller, 2008; Müller et al., 2007; Nakaya and Suzuki, 2006; Pardossi-Piquard et al., 2005; Perkinton et al., 2004; Robinson et al., 2014; Schrötter et al., 2013; von Rotz et al., 2004; Xu et al., 2011). The target genes for this transactivation complex are unclear as many of these studies utilise reporter gene assays. While these assays demonstrate that APP-Fe65 signalling is capable of stimulating expression, they do not formally identify regulated genes. In fact, Fe65 is capable of translocating to the nucleus alone (Cao and Südhof, 2001; Kim et al., 2003; Kinoshita et al., 2002) and can enhance reporter gene expression without APP overexpression (Cao and Südhof, 2001; Kajiwara et al., 2009; Lau et al., 2008; Perkinton et al., 2004; Yang et al., 2006). Despite this, the majority of research in this nuclear signalling function has focused on the role of APP and/or AICD in the regulation of gene expression, while the role of Fe65 has been less well studied.

Prior to the start of this project, experiments were carried out by colleagues in collaboration with Dr Kwok-Fai Lau (Chinese University of Hong Kong) to try and identify genes regulated by Fe65. This involved Solexa next generation sequencing (NGS) of mRNA transcripts from Fe65KO mice and their non-transgenic littermates. The Fe65KO mice were kindly provided by Professor Suzanne Guénette (Massachusetts General Hospital) and have been previously described (Guénette et al., 2006). For these experiments, pooled mRNAs were prepared from the brains of 5 Fe65KO and 5 WT male mice and reverse transcribed to cDNAs. These samples were then sequenced by Solexa sequencing and biostatistical analyses were carried out by Dr Lau using PANTHER (Protein Analysis Through Evolutionary Relationships; Mi et al. 2016). PANTHER identified several components of the wnt signalling pathway as showing different expression levels between Fe65KO and WT mouse brains. In particular, expression levels of the wnt receptor frizzled-1 (Fzd1), GSK3α and wnt3a were altered. As detailed in section 1.4.2, the wnt signalling pathway is one of the pathways that modulates the activation state of GSK3α and GSK3β, which are kinases that can phosphorylate tau in AD (Clevers and Nusse, 2012; Hernández et al., 2010; Hooper et al., 2008). In addition, wnt signalling regulates the degradation of neuroprotective β-catenin, which has also been previously proposed as a target for therapeutic intervention (Alvarez et al., 2004; Chacón et al., 2008; Clevers and Nusse, 2012; Inestrosa and Varela-Nallar, 2014; Kimelman and Xu, 2006). As such, there is

increasing interest in the role of wnt signalling in AD (Inestrosa and Varela-Nallar, 2014; Purro et al., 2014).

Data generated by high-throughput techniques such as NGS should be validated using low-throughput methods. As such, one aim of the studies described in this chapter was to confirm the effects of Fe65 loss on Fzd1, GSK3α and wnt3a expression in the mouse brains. In addition, the effects of Fe65 loss on a number of related genes were also studied in this mouse model. These genes were LRP6, GSK3β, APP and tau. LRP6 is a co-receptor with Fzd1 for wnt ligands while GSK3β activity is regulated by canonical wnt signalling (Chacón et al., 2008; Clevers and Nusse, 2012). APP and tau were chosen for analysis because of their strong involvement in AD (see section 1.1). Finally, an alternative strategy for studying Fe65 and APP loss was established using Fe65 and APP siRNAs to reduce expression in cultured rat cortical neurons. This was utilised as a complementary system for studying changes in gene expression.

4.2 Results

4.2.1 Establishing animal and cellular models in which Fe65 and APP expression are reduced

4.2.1.1 Fe65KO mice

Fe65KO mice were generated by integration of a lacZ-neo cassette into exon 2 of the Fe65 gene (Guénette et al. 2006; Figure 4.1A). Fe65KO mice were maintained on a C57BL/6 genetic background and heterozygous KO individuals were bred to obtain homozygous Fe65KO pups and WT littermates. Brains were harvested from newborn mice and snap-frozen in liquid nitrogen for future use. Tissue was also harvested for genotypic analysis of the mice via PCR. PCR reactions were run on agarose gels to separate DNA fragments for analysis. The primers used in the PCR reactions generate a smaller PCR fragment when the WT allele is present and a larger PCR product when the modified transgene is present. In heterozygotes, two fragments can be observed on the gel as the samples contain one copy of each allele (Figure 4.1B). This means that the genotype of each sample can be determined by the migration pattern of the PCR signals. A no-template control run alongside samples did not contain any bands, demonstrating that signals detected on the gel were due to amplification of the genomic DNA template (Figure 4.1B). Using this method of genotyping, WT and homozygous Fe65KO brain samples were obtained for further studies.

To confirm that Fe65 protein expression was absent in Fe65KO mice, brain homogenates from 5 WT and 5 Fe65KO brain samples were analysed via SDS-PAGE and western blotting. Blots were probed for Fe65 to measure Fe65 expression and GAPDH as a loading control. As expected, Fe65KO mice displayed a lack of Fe65 protein expression (Figure 4.1C, D).

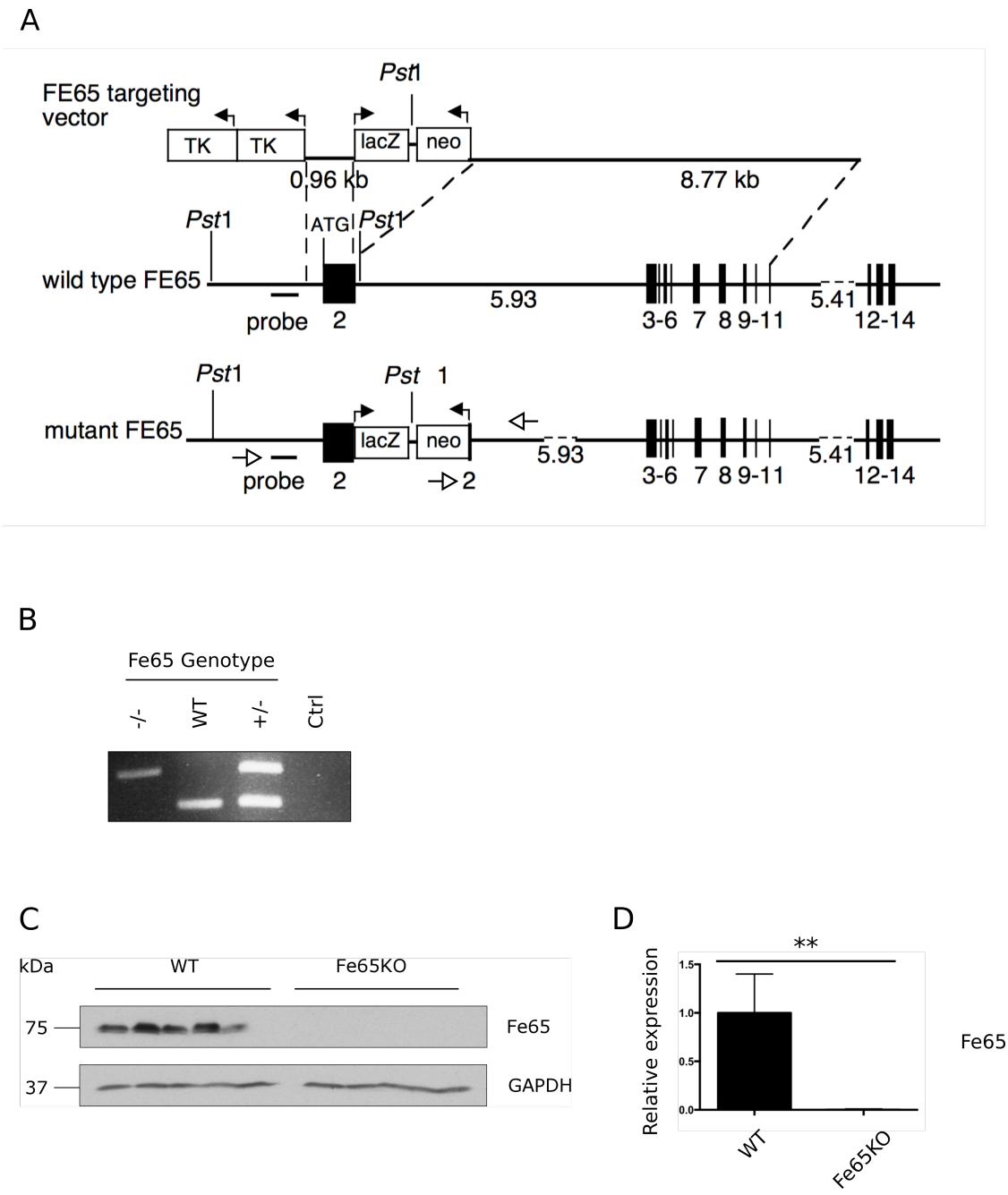

Figure 4.1: Characterisation of Fe65KO mice

A) Schematic showing the strategy for disruption of *Fe65* by insertion of a lacZ-neo cassette into exon 2 (Figure taken from Guénette et al. 2006, not to scale). White arrowheads indicate the location of primers for PCR genotyping. B) PCR genotyping of DNA isolated and amplified from ear tissue of homozygous KO (-/-), wild-type (WT) and heterozygous KO (+/-) mice. Ctrl contains no DNA template. PCR reactions were separated by gel electrophoresis on 1.5% agarose gels containing ethidium bromide. C) Brain homogenates from 5 WT and 5 Fe65KO littermates were analysed by SDS-PAGE and western blotting. Fe65 was detected using sc-19751 and GAPDH (loading control) detected using 14C10. Molecular mass markers are shown. D) Bar chart shows relative Fe65 expression. Signals on western blots were quantified by

densitometry and Fe65KO expression levels were normalised to WT controls. Statistical analysis was carried out using a Mann-Witney test (error bars show S.D., ** = $p < 0.01$, n = 5).

4.2.1.2 Knockdown of Fe65 and APP in cultured rat cortical neurons using siRNAs

Fe65 and APP siRNAs were obtained from Dharmacon. DIV 3 primary cortical neurons were treated with vehicle, non-targeting control siRNA, Fe65 siRNA or APP siRNAs at a concentration of 1 μM for 4 days. Cell lysates were prepared and analysed by SDS-PAGE and western blotting for Fe65, APP and GAPDH as a loading control. Fe65 and APP siRNA treatment markedly reduced Fe65 and APP expression respectively. Control siRNAs had no effect on either Fe65 or APP protein levels, demonstrating the specificity of the treatment (Figure 4.2).

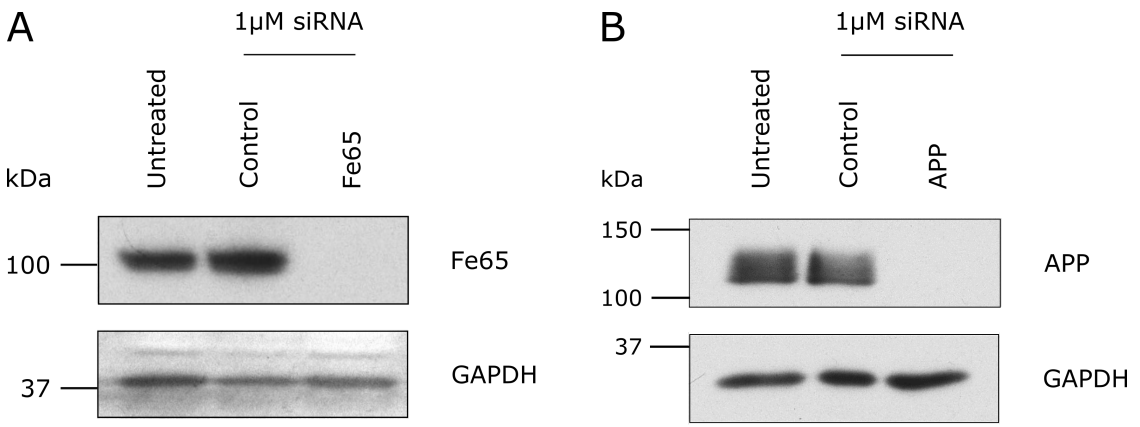

Figure 4.2: Fe65 siRNAs abolish Fe65 expression and APP siRNAs abolish APP expression in rat cortical neurons

DIV 3 rat cortical neurons were treated with vehicle (untreated), control siRNA, A) Fe65 siRNA or B) APP siRNAs at a concentration of 1 μM for 4 days. Cell lysates were analysed by SDS-PAGE and western blotting. Fe65 was probed with 4H324, APP with CT-17 and GAPDH (loading control) using 14C10. Molecular mass markers are shown.

4.2.2 Optimisation of RT-qPCR for analysis of gene expression

The effect of Fe65 on the expression of seven potential target genes was investigated by carrying out RT-qPCR on brain mRNAs from 5 WT and 5 Fe65KO mice. The quality of the RNA isolated from the brain samples was determined by gel electrophoresis and analyses of 28s and 18s ribosomal RNAs. High quality RNA preparations display an approximate 2-fold greater signal of 28s compared to 18s signal. Analyses of the mRNA isolated for these studies revealed that all RNA samples were of high quality (Figure 4.3), so samples were further processed for RT-qPCR experiments.

Relative quantification of mRNA levels by RT-qPCR requires normalisation of data across different treatment groups. As AD is known to affect the expression of a wide variety of genes, a reference gene should only be considered suitable if it shows low variation of expression both between samples within the same treatment group and between treatment groups (Selvey et al., 2001). In addition, more than one reference gene can be used to improve reliability. To address this, GeNorm reference gene analysis was carried out to test which putative reference genes had the most stable gene expression between WT and Fe65KO samples. The mRNA expression of 12 commonly used reference genes (*18S, ATP5B, ACTB, B2M, CANX, CYC1, EIF4A2, GAPDH, RPL13A, SDHA, UBH,* and *YWHAZ*) were measured by RT-qPCR in 4 WT and 4 Fe65KO samples (Figure 4.4A).

GeNorm is an algorithm that can be applied to Ct values of samples from different treatment groups to identify expression stability across groups. It measures the ratio of mRNA expression for each reference gene between treatment groups. The average variation (M) between these ratios for pairs of reference genes is then calculated and higher M values denote higher variation in reference gene expression between treatment groups. The two genes with the lowest M value are the most consistently expressed genes across the treatment groups (Gabrielsson et al., 2005; Vandesompele et al., 2002). *ATP5B* and *GAPDH* were identified by GeNorm analysis as the most stable reference genes for normalisation between WT and Fe65KO samples (Figure 4.4B). Consequently, these two genes were chosen as reference genes for data normalisation in further RT-qPCR experiments.

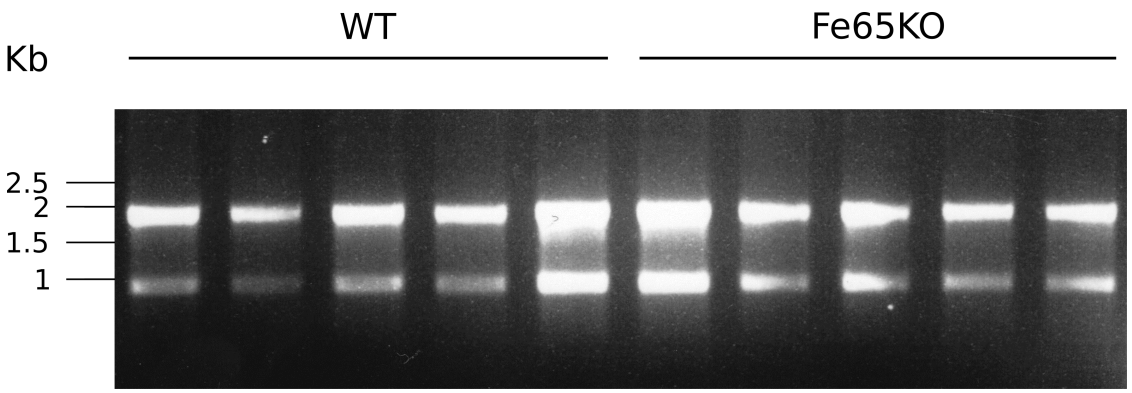

Figure 4.3: High quality RNA was isolated from WT and Fe65KO mouse brain samples

RNA samples isolated from brain homogenates of 5 WT and 5 Fe65KO mice were separated by gel electrophoresis on a 1.5 % agarose gel containing ethidium bromide. 28s (upper) and 18s (lower) species are clearly visible and signal analysis revealed that the 28s subunit was at least 2-fold greater than the 18s subunit. Molecular mass markers are shown.

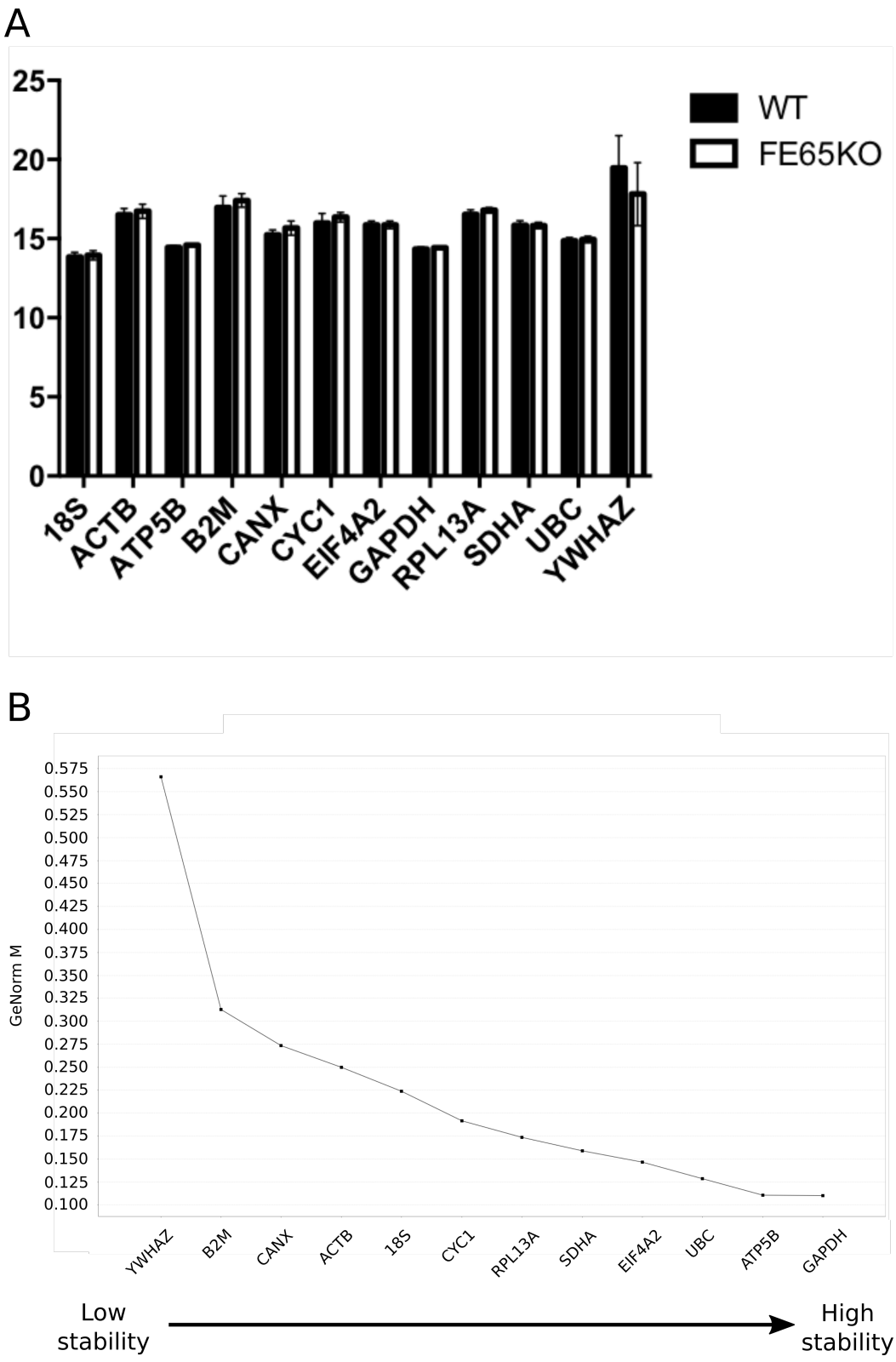

Figure 4.4: GAPDH and ATP5B are appropriate reference genes for normalisation in RT-qPCR analyses in WT and Fe65KO mice brains

A) RT-qPCR was carried out on 4 WT and 4 Fe65KO samples to measure mRNA expression of 12 reference genes. Bar chart shows raw mean Ct values plotted for both samples for each gene (error bars show S.D.). B) GeNorm analysis was carried

out on the Ct values obtained in A) using Biogazelle qbase+ software, which ranks genes in order of expression stability across both samples.

4.2.3 Loss of Fe65 reduces Fzd1 mRNA levels but does not affect wnt3a, GSK3α, GSK3β, LRP6, APP or tau levels in Fe65KO brains

To validate and extend the results of the Solexa sequencing, RT-qPCR was performed to measure differences in mRNA levels between Fe65KO and WT mice brains. As the data generated by Solexa sequencing identified Fzd1, GSK3α and wnt3a as genes that show altered expression in Fe65KO brains, the levels of mRNA for these genes were determined. In addition, the levels of GSK3β, LRP6, APP and tau mRNA were measured by RT-qPCR. These studies were performed on brain samples from 5 WT and 5 Fe65KO newborn male mice so the samples were the same as those used for Solexa sequencing. The levels of Fzd1 mRNA were significantly lower in Fe65KO mouse brain samples compared to WT littermates (Figure 4.5A). However, there were no changes seen in the levels of GSK3α, GSK3β, LRP6, wnt3a, APP or tau mRNA in Fe65KO mouse brains compared to WT littermates (Figure 4.5B-G), although a non-significant trend towards a decrease in mRNA expression was seen for GSK3α and GSK3β and an increase in LRP6. Increasing sample sizes may allow for greater detection power of these studies.

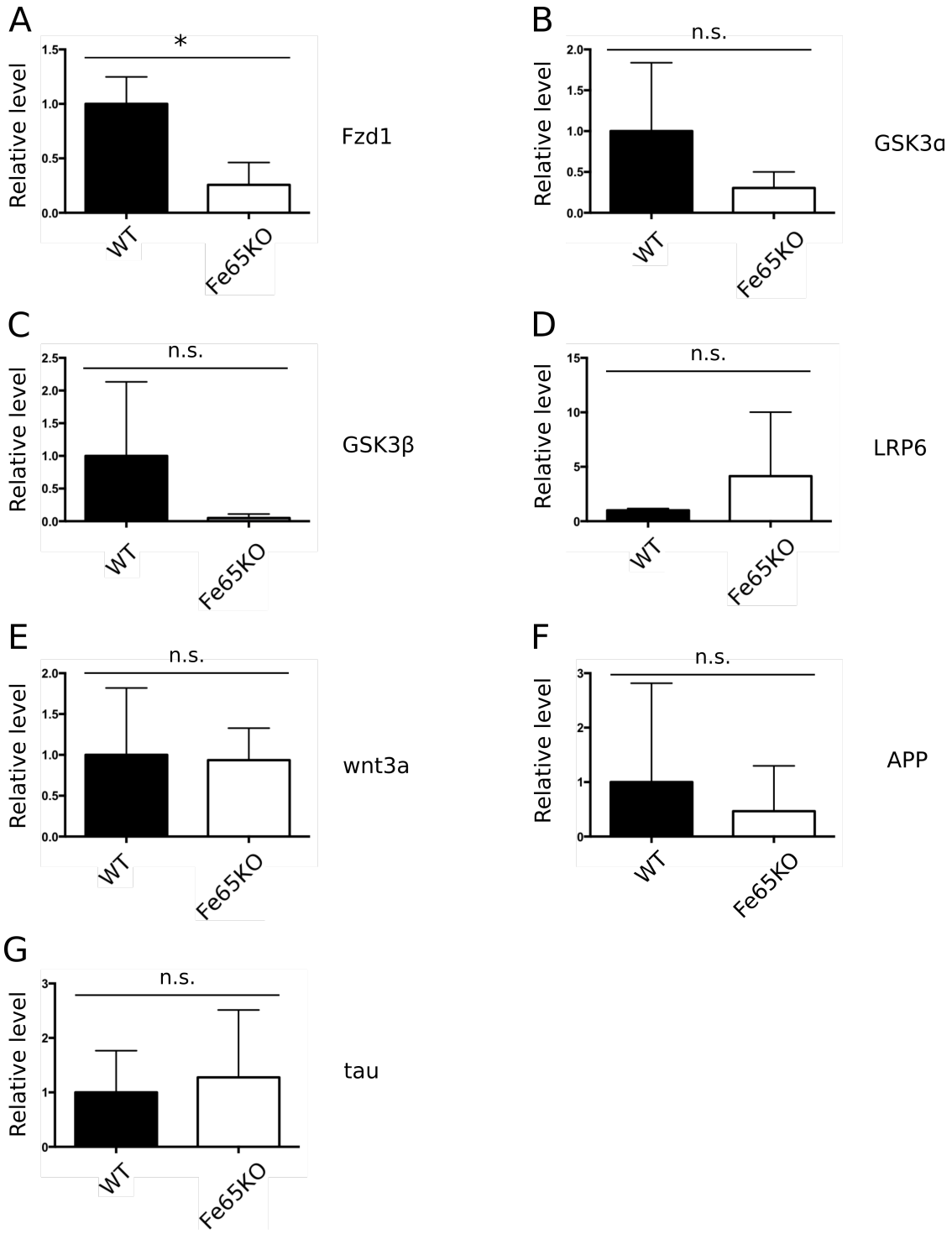

Figure 4.5: Loss of Fe65 reduces Fzd1 mRNA expression in Fe65KO brains but does not affect GSK3α, GSK3β, LRP6, wnt3a, APP or tau mRNA levels in Fe65KO mouse brains

Relative mRNA levels of A) Fzd1, B) GSK3α, C) GSK3β, D) LRP6, E) wnt3a, F) APP and G) tau were measured by RT-qPCR on brain homogenates of 5 WT and 5 Fe65KO littermates. Relative quantification was calculated using the $2^{-\Delta\Delta Ct}$ method (Livak and Schmittgen, 2001) using *GAPDH/ATP5B* as reference genes and samples were further normalised to the WT sample mean. Statistical analyses were performed

using Mann-Witney tests on $2^{-\Delta Ct}$ values (Livak and Schmittgen, 2001), bar charts were plotted using normalised $2^{-\Delta\Delta Ct}$ values (error bars show S.D., * = $p < 0.05$, n.s. = not significant, n = 5).

4.2.4 Loss of Fe65 does not alter expression of GSK3α, GSK3β, LRP6, APP or tau protein levels in Fe65KO mouse brains and antibodies that detect Fzd1 or wnt3a proteins could not be identified

The expression levels of mRNA transcripts do not always correlate with protein levels for the same gene. For example, a particular mRNA, although abundant, may not be translated, or may be translated inefficiently. Additionally, a protein may undergo rapid turnover despite being synthesised efficiently from high levels of mRNA. To address this, the levels of Fzd1, wnt3a, GSK3α, GSK3β, LRP6, APP and tau protein expression were analysed by SDS-PAGE and western blotting in WT and Fe65KO mouse brain samples. Consistent with mRNA RT-qPCR data, there were no significant differences in the levels of GSK3α, GSK3β, LRP6, APP or tau protein between Fe65KO and WT mice (Figure 4.6).

Detection of Fzd1 and wnt3a proved difficult since no antibodies were identified that could convincingly detect these proteins on western blots. Three different Fzd1 antibodies were tested in DIV3 rat cortical neurons treated with vehicle, control siRNA or Fzd1 siRNAs at a concentration of 1 μM for 4 days. These antibodies were sc-30428 (Santa Cruz), AF1120 (R&D Systems) and pan Fzd sc-9169 (Santa Cruz). None of these antibodies specifically detected a species of 71 kDa (the predicted molecular mass of Fzd1) on western blots and there were no differences in labelling between vehicle, control or Fzd1 siRNA treated neurons (Figure 4.7A).

Likewise, probing western blots of WT and Fe65KO brain samples with a wnt3a antibody detected multiple species, which is indicative of non-specific binding (Figure 4.7B). Since no antibodies that could reliably identify Fzd1 or wnt3a protein were identified, this avenue of research was not pursued further.

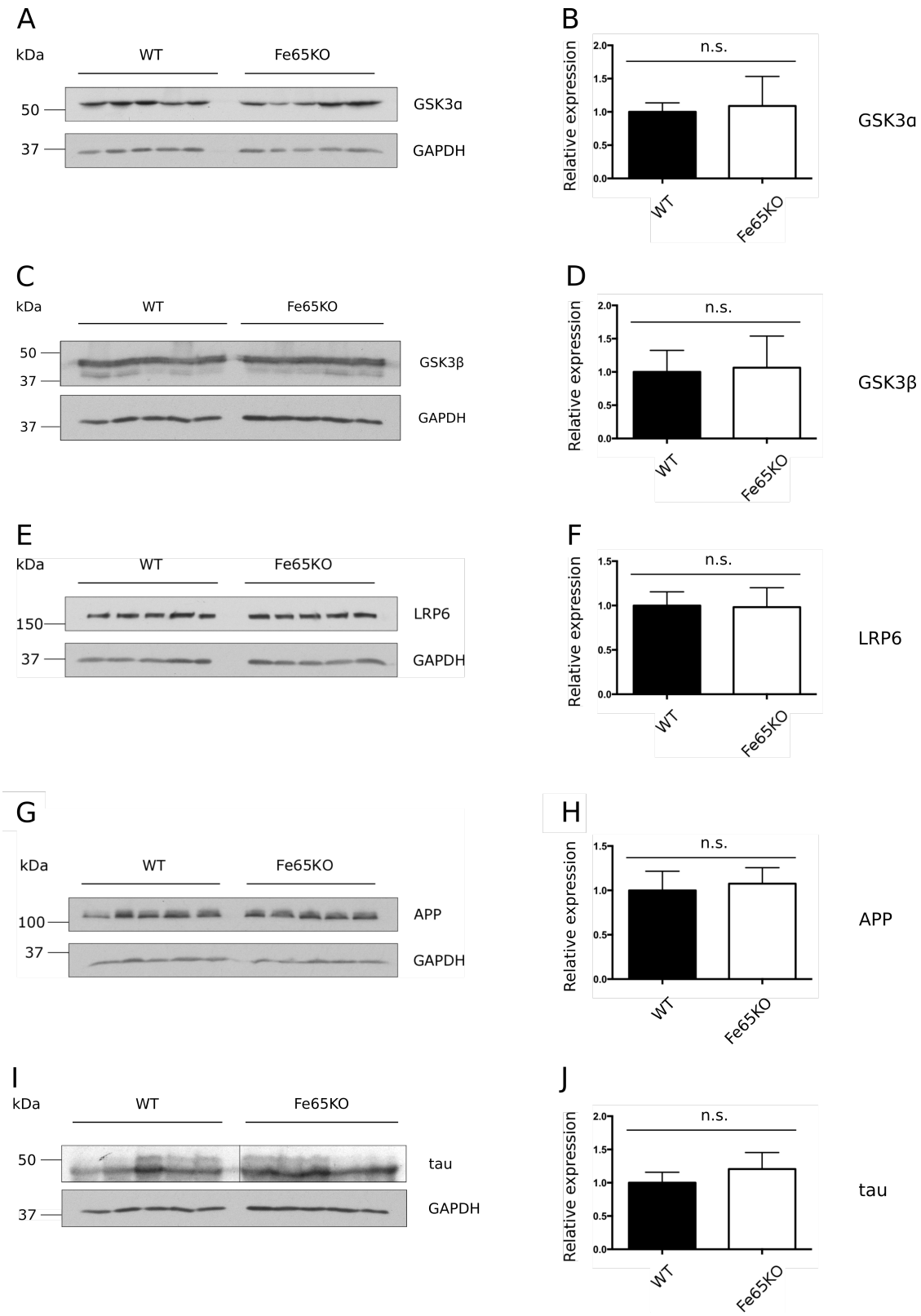

Figure 4.6: Loss of Fe65 does not alter expression of GSK3α, GSK3β, LRP6, APP or tau protein levels in Fe65KO mouse brains

Brain homogenates from 5 WT and 5 Fe65KO mice were analysed by SDS-PAGE and western blotting. A) GSK3α was probed with 9338, C) GSK3β was probed with 610201, E) LRP6 was probed with C47E12, G) APP was probed with CT-17, and I) tau was probed with A0024. For all blots, GAPDH (loading control) was probed with 14C10 and

molecular mass markers are shown. B, D, F, H, J) Bar charts show relative protein expression. Signals on western blots were quantified by densitometry and Fe65KO expression levels were normalised to WT controls. Statistical analyses were carried out using Mann-Witney tests (error bars show S.D., n.s. = not significant, n = 5).

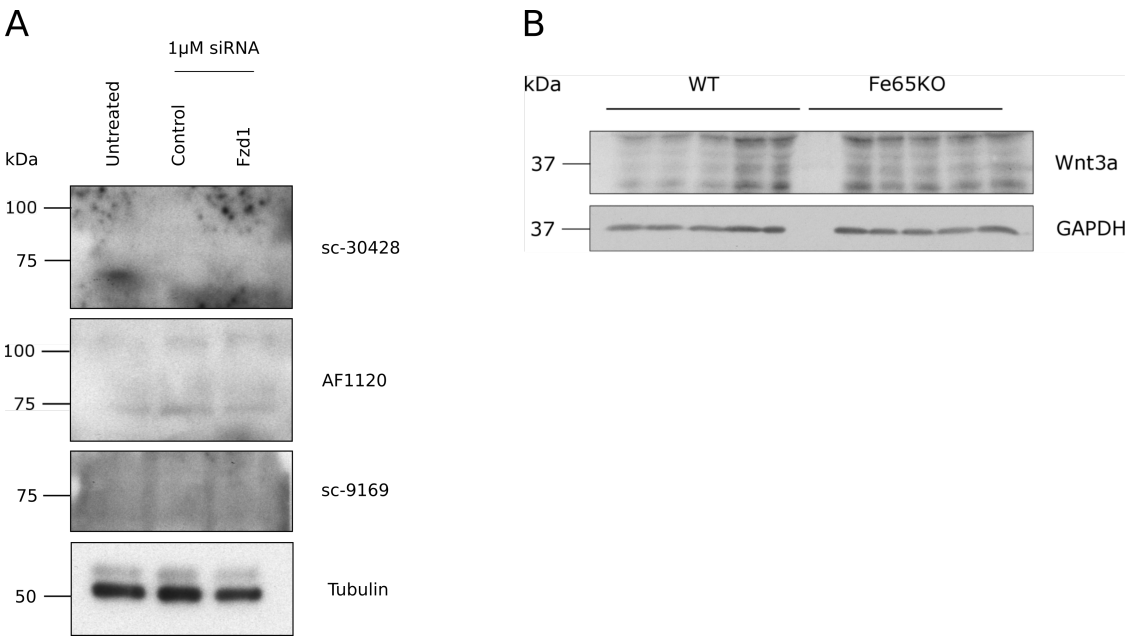

Figure 4.7: Antibodies that detect Fzd1 and Wnt3a proteins on western blot could not be identified

A) DIV 3 rat cortical neurons were treated with vehicle (untreated), control siRNA or Fzd1 siRNAs at a concentration of 1 μM for 4 days. Cell lysates were analysed by SDS-PAGE and western blotting. Fzd1 was probed with sc-30428 (Fzd1 Santa Cruz), AF1120 (Fzd1 R&D) and pan Fzd using sc-9169. Tubulin (loading control) was probed with T6199. Molecular mass markers are shown. B) Brain homogenates from 5 WT and 5 Fe65KO mice were analysed by SDS-PAGE and western blotting. Blots were probed for wnt3a using 2721 and GAPDH (loading control) using 14C10. Molecular mass markers are shown.

4.2.5 Loss of Fe65 does not alter Fzd1 or APP mRNA levels in Fe65 siRNA treated rat cortical neurons and loss of APP does not affect Fzd1 or Fe65 mRNA levels in APP siRNA treated rat cortical neurons

The data presented so far have shown that Fzd1 mRNA expression is impaired in Fe65KO mice. To complement these mouse studies, RT-qPCR analyses were carried out on rat cortical neurons treated with either Fe65 or APP siRNAs. The siRNA treatment achieved highly efficient knockdown of Fe65 or APP expression (Figure 4.2.1.2). As Fzd1 was the only mRNA transcript to show significantly altered expression in Fe65KO mice, these further studies focused on confirming this result in siRNA treated cortical neurons. The effect of APP loss on Fzd1 expression was also investigated because APP and Fe65 are proposed to be involved in the same nuclear signalling pathway. Finally, APP itself has been proposed as a target of APP-Fe65-mediated gene transactivation (von Rotz et al., 2004). If loss of Fe65 altered APP levels, then any effect of Fe65 on Fzd1 expression could occur indirectly and be due to changes in APP expression. To address this, the effect of Fe65 loss on APP expression and the effect of APP loss on Fe65 expression were also monitored.

For these experiments, DIV 3 rat cortical neurons were treated with control siRNAs or Fe65 siRNAs for 4 days. Cell lysates were analysed by RT-qPCR to monitor expression of Fzd1, APP and Fe65. Fzd1 mRNA levels showed a non-significant trend towards a decrease in neurons treated with Fe65 siRNAs (Figure 4.8A), which is consistent with the significant decrease in Fzd1 mRNA detected in Fe65KO mice compared to WT littermates. APP levels were unaffected by Fe65 siRNA treatment (Figure 4.8B). Treatment of cortical neurons with APP siRNAs again had no significant effect on the mRNA levels of either Fzd1 or Fe65 (Figure 4.8C, D), but showed a non-significant trend towards a decrease in mRNA expression.

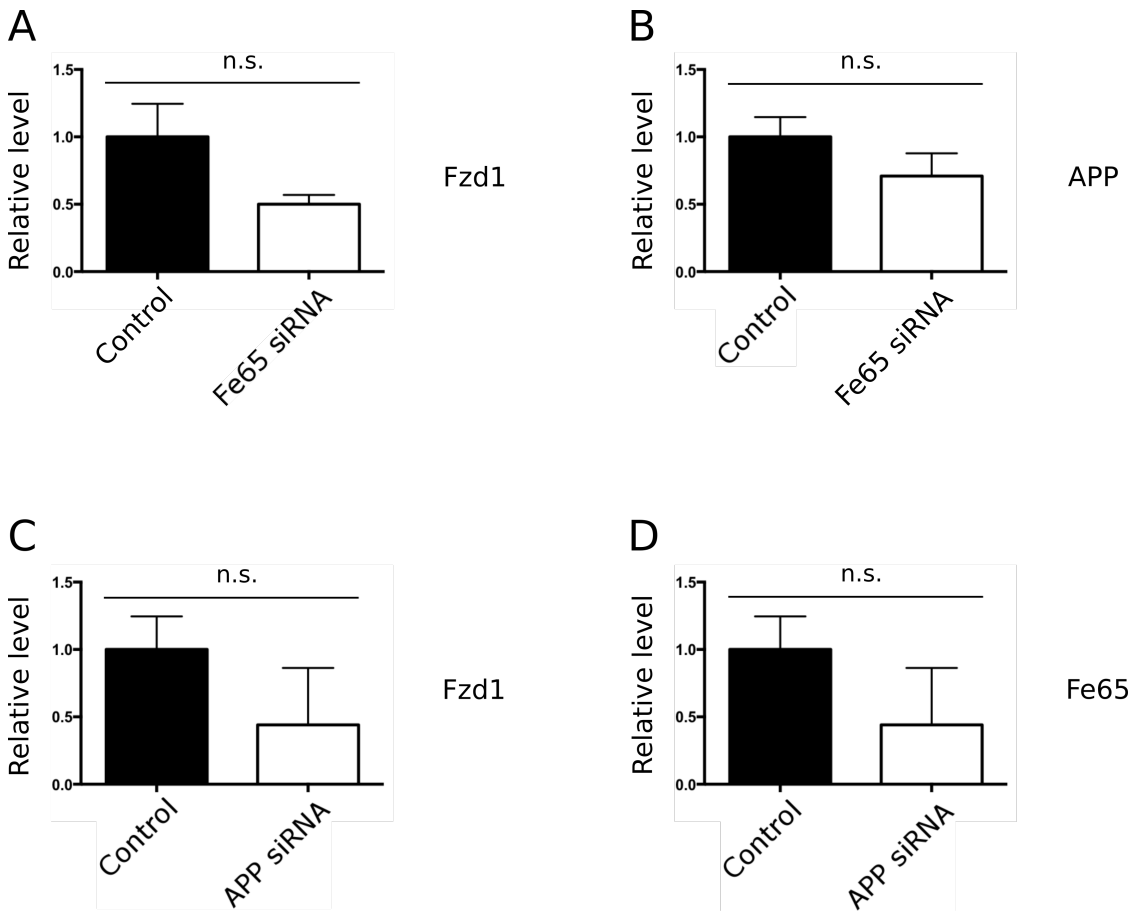

Figure 4.8: Loss of Fe65 does not alter Fzd1 or APP mRNA levels in Fe65 siRNA treated rat cortical neurons and loss of APP does not affect Fzd1 or Fe65 mRNA levels in APP siRNA treated rat cortical neurons

DIV3 rat cortical neurons were treated with control, A, B) Fe65 siRNA or C, D) APP siRNAs at a concentration of 1 μM for 4 days. Relative mRNA levels of Fzd1, APP and Fe65 were measured by RT-qPCR of cDNA samples reverse transcribed from mRNAs isolated from cell lysates. Relative quantification was calculated using the $2^{-\Delta\Delta Ct}$ method (Livak and Schmittgen, 2001) using *GAPDH/ATP5B* reference genes and samples were further normalised to the control siRNA sample mean. Statistical analysis was performed using Mann-Witney tests on $2^{-\Delta Ct}$ values (Livak and Schmittgen, 2001), bar charts were plotted using normalised $2^{-\Delta\Delta Ct}$ values (error bars show S.D., * = $p < 0.05$, n.s. = not significant, n = 3).

4.2.6 Loss of Fe65 has no significant effect on tau Ser^{202} phosphorylation or GSK3β Ser^{9} phosphorylation in Fe65KO brains

The studies undertaken in this chapter were based upon findings from Solexa NGS analysis of Fe65KO mice which suggested that loss of Fe65 might impact the wnt signalling pathway by mediating changes in expression of Fzd1, GSK3α and wnt3a. Verification experiments in Fe65KO mice and siRNA treated neurons confirmed that loss of Fe65 expression results in altered Fzd1 expression but did not confirm a change in GSK3α or wnt3a expression. Because the canonical wnt signalling pathway regulates the activity of tau kinases GSK3α and GSK3β (Hernandez et al., 2012; Hooper et al., 2008; Kaidanovich-Beilin and Woodgett, 2011; Noble et al., 2013), these findings might reveal a new link between APP (via Fe65) and tau phosphorylation.

To investigate this link, tau phosphorylation at an AD-relevant site and GSK3β activity were investigated in Fe65KO and WT mouse brains. Brain homogenates of 3 WT and 3 Fe65KO mice were analysed by SDS-PAGE and western blotting. Blots were probed for phosphorylated tau using CP13, a phospho-specific tau antibody. CP13 recognises tau that has been phosphorylated at Ser^{202}, a known GSK3β-responsive site (Goedert et al., 1995). Similarly, blots were probed for phosphorylated GSK3β using a phospho-specific antibody that detects GSK3β phosphorylation at Ser^{9}. Phosphorylation at this site inhibits GSK3β activity so a higher proportion of phosphorylated GSK3β indicates a decrease in GSK3β activity (Kaidanovich-Beilin and Woodgett, 2011; Sutherland et al., 1993).

As shown in Figure 4.6, levels of total tau expression were not significantly different in Fe65KO mice. However, the proportion of tau that was phosphorylated at Ser^{202} showed a non-significant trend towards a decrease of phosphorylation in Fe65KO mouse brains (Figure 4.9A, B) There was also no significant difference in GSK3β Ser^{9} phosphorylation between Fe65KO and WT mice (Figure 4.9C, D).

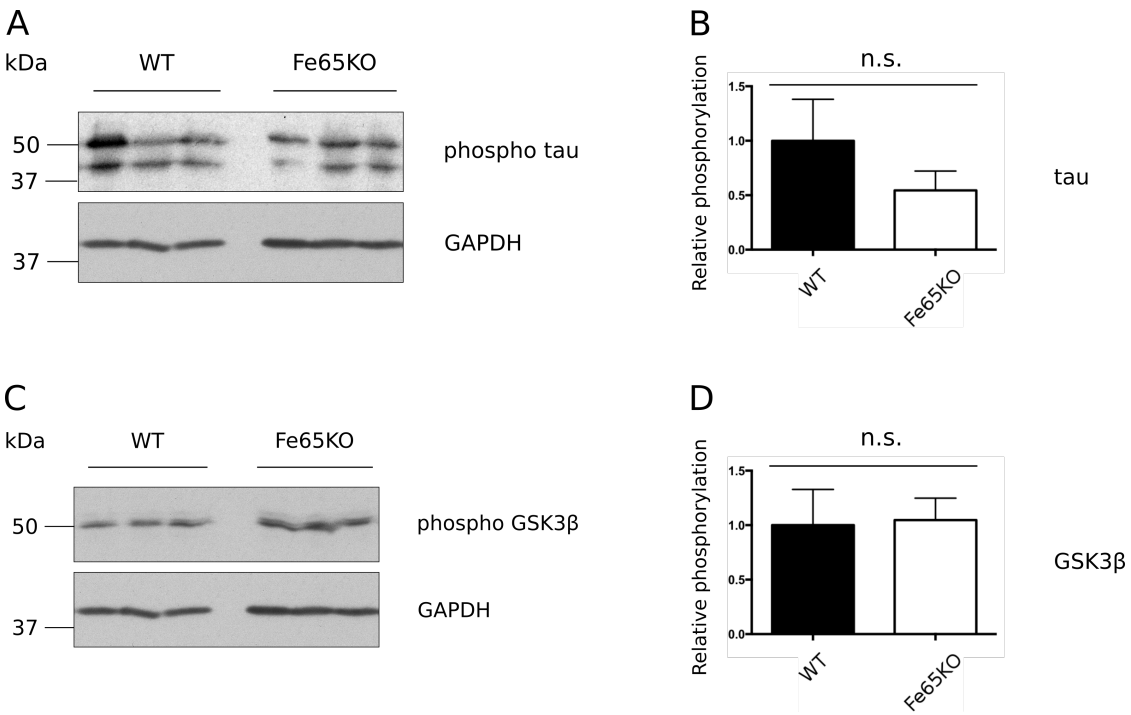

Figure 4.9: Loss of Fe65 has no significant effect on tau phosphorylation or GSK3β phosphorylation in Fe65KO brains

Brain homogenates from 3 WT and 3 Fe65KO mice were analysed by SDS-PAGE and western blotting. A) Blots were probed for tau phosphorylated at Ser^{202} with CP13. C) Blots were probed for GSK3β phosphorylated at Ser^{9} with 9336. GAPDH (loading control) was detected using 14C10. Molecular mass markers are shown. B, D) Bar charts show relative protein phosphorylation. Signals on western blots were quantified by densitometry and phosphorylated protein levels were normalised to total protein expression levels. Relative protein phosphorylation levels of Fe65KO samples were then normalised to WT controls and statistical analyses were carried out using Mann-Witney tests (error bars show S.D., n.s. = not significant, n = 3).

4.2.7 Loss of Fe65 reduces tau phosphorylation and GSK3β activity in rat cortical neurons

To complement the above studies, the effects of siRNA loss of Fe65 on tau phosphorylation and GSK3β activity (via Ser^{9} phosphorylation) using ELISAs were investigated. ELISAs provide quantitative data and compared to western blots, are more robust at detecting small changes. The tau ELISAs measured levels of total tau and tau phosphorylated on Ser^{199}, another GSK3β-responsive site (Hanger et al., 2009). The GSK3β ELISA measured both total GSK3β and GSK3β phosphorylated on Ser^{9} (inactive GSK3β).

For these experiments, DIV 3 rat cortical neurons were treated with control siRNAs or Fe65 siRNAs for 4 days before cell lysates were analysed by the ELISAs. siRNA-induced loss of Fe65 had no effect on total tau expression, which is in agreement with the findings from the Fe65KO mice. However, consistent with the non-significant trend seen in the mouse data, tau phosphorylation (relative to tau expression) was significantly reduced in siRNA treated neurons (Figure 4.10A). siRNA knockdown of Fe65 had no effect on total GSK3β levels but a small but significant increase in GSK3β Ser^{9} phosphorylation was detected (Figure 4.10B). Because the effect of loss of Fe65 on GSK3β phosphorylation was so small, these experiments need to be repeated to confirm these findings. These results indicate that loss of Fe65 decreases tau phosphorylation and decreases GSK3β activity by enhancing GSK3β Ser^{9} phosphorylation.

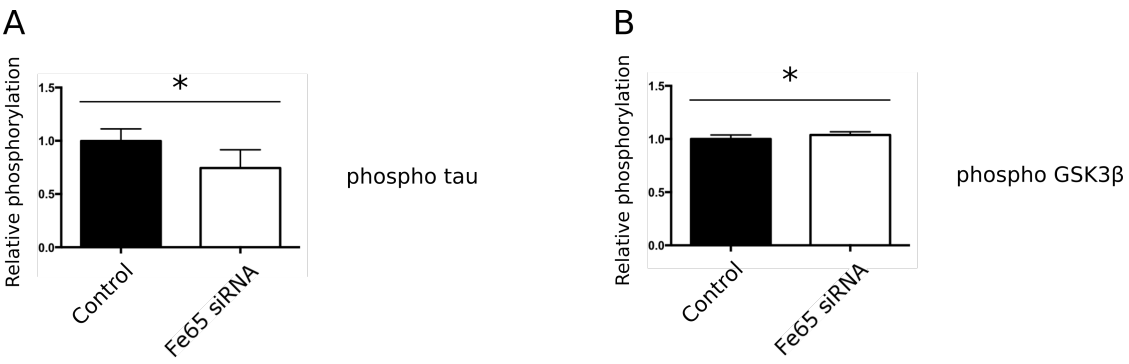

Figure 4.10: Loss of Fe65 reduces tau phosphorylation and GSK3β activity in Fe65 siRNA treated rat cortical neurons

DIV 3 rat cortical neurons were treated with either control siRNA or Fe65 siRNA at a concentration of 1 μM for 4 days. Cell lysates were analysed for tau phosphorylated on Ser^{199} and GSK3β phosphorylated on Ser^{9} using ELISAs. A) Bar chart showing tau Ser^{199} phosphorylation following normalisation of signals to total tau levels in the samples. B) Bar chart showing GSK3β Ser^{9} phosphorylation following normalisation of signals to total GSK3β levels in the samples. For both charts, samples were further normalised to the control siRNA sample mean and statistical analyses were carried out using Mann-Witney tests (error bars show S.D., * = $p < 0.05$, n = 6 for tau ELISA, n = 10 for GSK3β ELISA).

4.3 Discussion

In this chapter, the effect of loss of Fe65 on the expression of seven genes was investigated. This was achieved by monitoring mRNA and protein levels of genes of interest in WT and Fe65KO mice and siRNA-mediated Fe65 knockdown in rat cortical neurons. In addition, the effect of APP knockdown on the expression of two of these genes was also examined. Finally, the effect of loss of Fe65 on tau and GSK3β was studied.

Regulation of gene transcription is thought to be one of the key roles for APP-Fe65 nuclear signalling (see section 1.3.2). However, the exact target genes of this signalling complex are unknown and the relevance of this function has also been questioned (Hébert et al., 2006; Waldron et al., 2008). Due to the role of APP in AD, it is understandable that the majority of these studies have focussed on APP/AICD signalling with less attention on the role of Fe65. As discussed in section 1.3.2, APP was originally thought to act in a similar fashion to Notch, another type-1 membrane spanning protein that is cleaved by γ-secretase and involved in gene transcription. However, there are differences between AICD and the Notch intracellular domain, most notably the smaller size of AICD, which inhibits its ability to bind to multiple proteins that may be required for gene transcription. Fe65 on the other hand has several protein-protein interaction domains and has been shown to interact with a number of nuclear proteins including CP2/LSF/LBP1, Tip60 and SET (Cao and Südhof, 2001; Kim et al., 2003; Stante et al., 2009; Telese et al., 2005; Zambrano et al., 1998), so an alternative possibility is that the AICD-Fe65 complex recruits transcriptional proteins to perform a role similar to the Notch intracellular domain. The studies described in this chapter were aimed at exploring this possibility further.

Initial experiments followed up data generated by a Solexa NGS study aimed at identifying genes that are regulated by Fe65. Bioinformatic analyses identified the wnt signalling pathway as a pathway that is regulated by Fe65. In particular, the wnt receptor Fzd1, GSK3α and wnt3a, which are all components of the canonical wnt pathway, were identified as genes with altered expression in the Fe65KO mice. While NGS allows the monitoring of mRNA expression for a high number of genes simultaneously, it is a high-throughput method that should be verified and validated using low-throughput techniques with higher accuracy. For NGS, the most common methods of validating data are measuring mRNA expression by RT-qPCR and protein levels by western blotting. To validate the Solexa findings, the expression levels of these genes were monitored by RT-qPCR in Fe65KO and WT littermate mouse brains. In addition, the expression of GSK3β and LRP6, which are also components of the wnt

signalling pathway, along with APP and tau were analysed. Of these seven genes, only Fzd1 expression was shown to be different in the Fe65KO mice brains, where loss of Fe65 led to a decrease in Fzd1 mRNA expression. The reduction of Fzd1 expression displayed by the Fe65KO mice suggests that Fe65 normally acts to positively regulate the expression of this gene. Because wnt signalling has a negative impact on GSK3α/β activity, enhancing Fzd1 levels may lead to reduced GSK3α/β activity. It should be noted that due to the low sample size and high variability of the samples, these studies are likely to be underpowered and therefore may be susceptible to Type 2 statistical error (failing to reject a null hypothesis). Increasing the sample size could help to reduce the variation and increase the sensitivity of the study to detect changes in gene expression.

Changes in gene transcription do not always lead to changes in protein levels so it was important to determine whether loss of Fe65 also affects Fzd1 protein levels. However, despite using Fzd1 siRNAs to test several commercial antibodies, none were capable of detecting Fzd1. Since these studies were performed, my supervisor Professor Chris Miller has contacted Professor Patricia Salinas (University College London), who is an authority on the wnt signalling pathway and she has confirmed that currently there are no reliable antibodies that detect Fzd1 or other members of the Fzd family (personal communication). Because of this, measuring changes in Fzd1 protein levels after Fe65 loss was not possible during this investigation.

To complement these studies using an alternative approach, methods were established to knockdown Fe65 expression in cultured rat cortical neurons using siRNAs. Although siRNAs are a common route for reducing expression in cultured cells, achieving siRNA-mediated knockdown in neurons can be difficult (Gärtner et al., 2006; Nakajima et al., 2012). Despite this, Accell siRNAs produced reliable and efficient knockdown of both Fe65 and APP expression in neurons. The siRNA studies confirmed the Fe65KO mouse findings that loss of Fe65 reduces Fzd1 expression in neurons. Interestingly, loss of Fe65 had no effect on APP expression and indeed, APP knockdown did not alter the expression of Fe65 or Fzd1. These results demonstrate the specificity of the effect of Fe65 on Fzd1 expression. In particular, the finding that APP loss had no effect on Fzd1 or Fe65 expression means it is unlikely that AICD is involved in Fe65-mediated regulation of Fzd1 expression. In addition, the siRNA experiments were carried out in neuronal cultures, indicating that these changes occur in neurons. This is consistent with Fe65 being predominantly expressed in neurons (Kesavapany et al., 2002), but does not eliminate the possibility that Fzd1 expression is affected in other cell types in the brain.

The results of RT-qPCR experiments in both Fe65KO mouse brains and Fe65 siRNA treated neurons confirm the Solexa NGS data for changes in Fzd1 expression. However, they do not corroborate changes seen in other genes linked to the wnt signalling pathway, specifically GSK3α or wnt3a. The reasons for this are unclear but it is possible that the sample sizes used were too small and high variation within the samples may have masked the effect of loss of Fe65 on gene expression. For future experiments, a larger sample size might allow better detection of differences between Fe65KO and WT mice. It would also be interesting to measure the changes in expression of the other genes of interest in the siRNA treated neurons, which typically showed less variation within treatment groups compared to the Fe65KO brain samples.

To continue the investigation into the functional consequences of altered Fzd1 expression, the activity of the wnt signalling pathway could be monitored. Activation of the canonical wnt pathway reduces the degradation of the nuclear signalling molecule β-catenin. As β-catenin accumulates in the nucleus, it binds to TCF/LEF transcription factors to enhance the transcription of target genes (Kaidanovich-Beilin and Woodgett, 2011; Schuijers et al., 2014). Luciferase reporter assays using TCF/LEF reporter constructs have previously been generated to monitor wnt signalling (Smalley et al., 1999) and could be used in both neurons from Fe65KO mice and Fe65 siRNA treated neurons. In addition, it would be interesting to determine whether overexpression of Fe65 has the opposite effect to loss of Fe65 and enhances Fzd1 expression. Again these experiments could be extended into monitoring wnt signalling in response to Fe65 overexpression via luciferase reporter assays.

Loss of Fe65 causes a decrease in Fzd1 expression in both Fe65KO mouse brains and in Fe65 siRNA treated neurons. This reduction of Fzd1 expression suggests that Fe65 acts to positively regulate the expression of Fzd1, one of the receptors in the wnt signalling pathway. Since wnt signalling has a negative impact on GSK3α/β activity, reducing Fzd1 levels may lead to increased GSK3α/β activity. This is of particular interest in the field of AD because GSK3β is one of the key kinases involved in the hyperphosphorylation of tau (Killick et al., 2014; Scali et al., 2006; Stoothoff et al., 2002; Wagner et al., 1997; Zhang et al., 2008). Indeed, defective wnt signalling has recently been linked to AD (Purro et al., 2014). To assess whether loss of Fe65 affected tau phosphorylation, levels of total and phosphorylated tau protein were monitored. Both western blotting of Fe65KO mouse brains and ELISAs on siRNA treated neurons demonstrated that while loss of Fe65 had no effect on tau expression, it caused a decrease in tau phosphorylation at Ser^{202} and Ser^{199} respectively. These

residues are known to be hyperphosphorylated in AD and are targets of GSK3β (Hanger et al., 2009; Noble et al., 2013).

Although one route of GSK3β activity regulation is via the wnt signalling pathway, another mechanism involves inhibitory phosphorylation on Ser^{9} (Kaidanovich-Beilin and Woodgett, 2011). To determine whether the reduced $Ser^{199/202}$ tau phosphorylation induced by Fe65 loss coincided with a change in GSK3β activity via Ser^{9} phosphorylation, western blots and ELISAs were performed on Fe65KO brain samples and Fe65 siRNA treated neurons, respectively. Fe65KO mice showed no change in GSK3β phosphorylation while siRNA-induced loss of Fe65 in neurons showed a small increase in GSK3β phosphorylation. This is consistent with a reduction in tau phosphorylation as increased GSK3β phosphorylation represents a decrease in GSK3β kinase activity. Again, the discrepancy between western blots of Fe65KO samples and ELISAs on siRNA treated neurons could be due to the higher sensitivity of the ELISA. These experiments need to be repeated to confirm the findings but they indicate that loss of Fe65 reduces GSK3β activity via Ser^{9} phosphorylation to reduce tau phosphorylation. While the change in GSK3β phosphorylation is small (3 % decrease) and the change in tau phosphorylation is much larger (46 % decrease in western blots and 36 % decrease in ELISAs), GSK3β is an enzyme so small changes in its catalytic activity may translate into larger changes in substrate phosphorylation, in this case tau. However, the relatively small sample size means that this study could be susceptible to Type 1 statistical error (incorrectly rejecting a null hypothesis) and this result should not be overinterpreted. Increasing the sample size would reduce the chance of Type 1 error and enable a proper confirmation of this result.

The mechanisms behind this effect of loss of Fe65 on GSK3β are not clear but interestingly other studies have linked Fe65 with GSK3β. Overexpression of Fe65 and/or AICD has been shown to increase GSK3β expression and tau phosphorylation and there is also evidence that Fe65 may bind directly to tau (Barbato et al., 2005; Kim et al., 2003; Perkinton et al., 2004). Clearly, further work is required in this area and it would be interesting to investigate whether Fe65 loss affects other tau phosphorylation sites (particularly, those that are targeted by GSK3α/GSK3β) and the expression or activity of other kinases that phosphorylate tau. Further studies should also include the investigation into how overexpression of Fe65 impacts tau and GSK3β phosphorylation in neurons.

This investigation has shown that loss of Fe65 causes a reduction in the expression of Fzd1 and an increase in GSK3β and tau phosphorylation. More work needs to be done

to elucidate the exact mechanisms at play here and whether a single pathway or a more complex network of changes links these findings. Because Fzd1 is a receptor for wnt and activation of the wnt signalling pathway inhibits GSK3β, it was predicted that loss of Fe65-induced inhibition of Fzd1 expression would cause an increase in GSK3β activity and therefore an increase in tau phosphorylation. However, this is not the case and less Fzd1 expression occurs alongside decreased tau phosphorylation. There are two main models that could explain these results. The first is that while Fe65 loss reduces Fzd1, other Fzd isoforms compensate for the reduced receptor expression to rescue wnt signalling impairments. This is supported by the observation that there are 10 Fzd receptors that can act in wnt signalling pathways. The complex relationship between different wnt and Fzd isoforms has yet to be fully characterised, but it is thought that there is some functional redundancy between the Fzd receptors (Clevers and Nusse, 2012). The second model is that Fe65 loss may reduce wnt signalling but also regulate another protein that is involved in tau phosphorylation and this second pathway is a more potent mechanism for regulating tau phosphorylation than wnt signalling. The increase in GSK3β Ser^{9} phosphorylation seen in Fe65 siRNA treated neurons suggests that the second model may be a better fit for the data because wnt signalling-mediated control of GSK3β is Ser^{9} phosphorylation-independent and is thought to instead rely on changes to protein localisation (Metcalfe & Bienz 2011). However, these models are not mutually exclusive. Monitoring changes in wnt signalling via luciferase reporter assays and measuring changes in protein expression and activity of other tau kinases in response to loss of Fe65 should help to shed light on this.

Over the last 25 years, the amyloid cascade hypothesis has formed the major framework for studying pathogenic mechanisms in AD. Despite this, Aβ-targeting drugs have been unsuccessful and most APP animal models do not develop both neuritic plaques and neurofibrillary tangles (Elder et al., 2010; Herrup, 2015; Richardson and Burns, 2002). Definitively proving the link between APP and tau pathology has also proved elusive and a recent study involving human neurons generated from induced pluripotent stem cells from AD patients showed that familial AD-linked APP mutations cause increases in GSK3β and tau phosphorylation in an Aβ-independent manner (Israel et al., 2012). This finding suggests that tau hyperphosphorylation is linked to a different function of APP. AD-linked mutations that alter APP processing to increase Aβ production are likely to also alter APP function and may affect the amount of AICD generated by the amyloidogenic pathway, which has been shown to be the only transcriptionally active form (Belyaev et al., 2010; Goodger et al., 2009). The findings

reported in this chapter support this theory by providing evidence for an effect of Fe65, a known APP binding protein that is linked to APP function on tau phosphorylation.

4.3.1 Limitations

1. The mouse studies carried out in this chapter used small sample sizes and these carried high levels of variability. Because of this, some changes in protein expression may not have been detected, but could become apparent in larger study sizes.

2. When performing western blots, specific antibodies that detect Fzd1 and wnt3 were not available so although RT-qPCR data detected a change in Fzd1 mRNA expression, this could not be confirmed at the protein level.

CHAPTER 5: FE65 INTERACTS WITH ARF6 TO REGULATE NEURITE OUTGROWTH

5.1 Introduction

During the course of this PhD, my supervisors were contacted by Dr Kwok-Fai Lau from the Chinese University of Hong Kong, who also works on Fe65. Dr Lau had discovered that Fe65 binds to the GTPase protein ARF6 and enquired whether we would like to collaborate on investigating the interaction between Fe65 and ARF6. This was because his laboratory has little expertise on neuronal cell preparation and experimentation. I therefore became involved in this project, specifically in performing immunofluorescence and quantitative intensity correlation analysis to determine whether Fe65 and ARF6 colocalise in cultured rat cortical neurons.

Small GTPases are involved in a wide range of cellular functions and ARF6 in particular has been reported to play a role in regulating the actin cytoskeleton, cell adherence, neurite development and endocytosis/exocytosis (Gillingham and Munro, 2007). This is of particular interest since both Fe65 and APP are also believed to regulate cell motility and the actin cytoskeleton although the precise mechanisms by which they carry out these functions are unclear (Cheung et al., 2014; Ermekova et al., 1997; Ma et al., 2008; Sabo et al., 2001; Wang et al., 2011), Neurite outgrowth and actin cytoskeletal dynamics are vital tasks for neuronal growth, survival and normal function. Abnormalities in these processes could contribute to impaired synapse formation or maintenance and impaired migration of neurons and neurite development. ARF6 acts upstream of other small GTPases Rac1 and RhoA that influence the actin cytoskeleton, although the exact pathway by which ARF6 interacts with these proteins is unknown (Gillingham and Munro, 2007).

In this chapter, the interaction between Fe65 and ARF6 was investigated and the function of this interaction on axonal growth was studied. To achieve this, Fe65 deletion constructs were used to determine which of the three protein-protein interaction domains of Fe65 mediated binding to ARF6, while immunofluorescence techniques were utilised to elucidate the subcellular localisation and function of Fe65-ARF6 complexes.

5.2 Results

5.2.1 Fe65 interacts with ARF6 in CHO cells and rat brain lysate

To validate the results of a yeast 2-hybrid screen, which indicated that ARF6 interacts with Fe65 (Cheung et al., 2014), co-immunoprecipitation assays were carried out on CHO cells transfected with either control vector (CAT; EV), Fe65 or Fe65+ARF6-myc plasmid vectors (see Table 2.2). ARF6 was immunoprecipitated with myc antibody 9B11 and the presence of bound Fe65 was determined following SDS-PAGE and western blotting of the samples. Probing of total cell lysates for Fe65 and ARF6 demonstrated that the cells were appropriately transfected and analyses of the immunoprecipitates confirmed that ARF6 bound to Fe65 (see Figure 5.1A). This interaction was also demonstrated between endogenous proteins by performing co-immunoprecipitation assays from rat brain lysates (see Figure 5.1B).

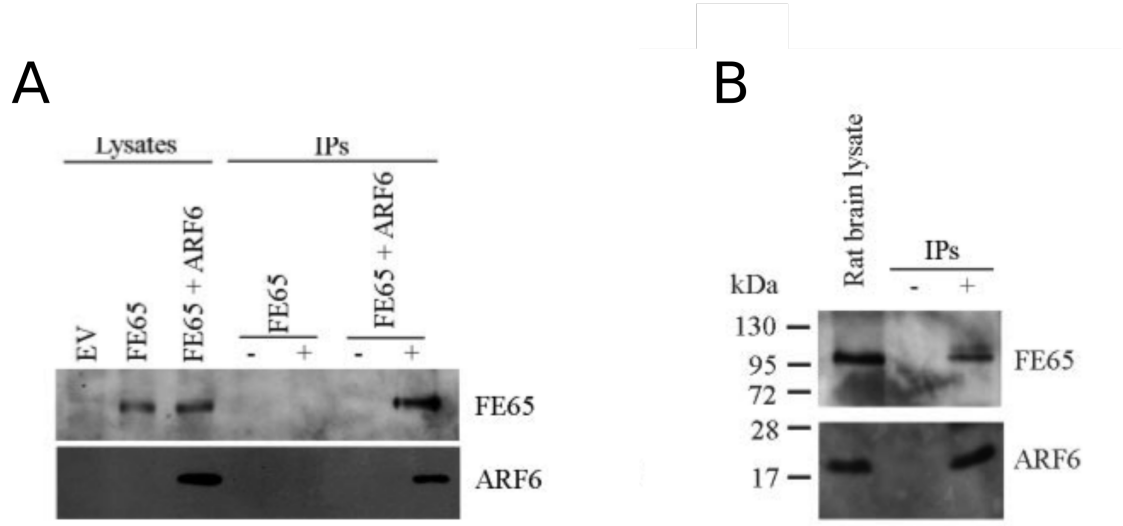

Figure 5.1: Fe65 interacts with ARF6 in CHO cells and rat brain lysates

A) CHO cells were transiently transfected with CAT (EV), Fe65 or Fe65+ARF6-myc plasmid vectors. ARF6 was immunoprecipitated using 9B11 anti-myc antibody and bound Fe65 was detected by western blotting. B) ARF6 was immunoprecipitated from rat brain lysates using an in house generated ARF6 rat antibody and the precipitates were analysed via SDS-PAGE and western blotting. Molecular mass markers are shown. For both figures, Fe65 was detected using sc-19751 and ARF6 using the rat antibody.

5.2.2 ARF6 binds to the PTB1 domain of Fe65

To identify which of the three Fe65 protein-protein interaction domains might mediate binding to ARF6, GST pull-down assays were carried out using a series of GST fusion proteins containing each of the three Fe65 interaction domains. CHO cells were transiently transfected with either CAT (EV), GST+ARF6-myc, GST-Fe65WW+ARF6-myc, GST-Fe65PTB1+ARF6-myc or GST-Fe65PTB2+ARF6-myc plasmid vectors (see Table 2.2). GST pull down assays were then performed and these were analysed by SDS-PAGE and western blotting. Such analyses revealed that while all of the GST fusion proteins were pulled down by glutathione-Sepharose 4B beads, only GST-Fe65PTB1 also pulled down ARF6. This indicates that ARF6 interacts with the PTB1 domain of Fe65 (see Figure 5.2A).

To complement these studies, co-immunoprecipitation assays were performed on CHO cells transiently transfected with either CAT (EV), Fe65+ARF6-myc or Fe65ΔPTB1+ARF6 plasmid vectors (see Table 2.2). Fe65ΔPTB1 is a deletion construct lacking the PTB1 domain of Fe65 (Cao and Südhof, 2001; Cheung et al., 2014). SDS-PAGE and western blotting was used to detect whether both Fe65 and Fe65ΔPTB1 interact with ARF6. Probing of total cell lysates for Fe65 and ARF6 indicated that the cells were appropriately transfected and that Fe65ΔPTB1 migrated at a lower molecular weight compared to Fe65. Analyses of the immunoprecipitated samples complemented the GST pull down assays and showed that Fe65 but not Fe65ΔPTB1 bound to ARF6 (see Figure 5.2B). Therefore, Fe65 binds to ARF6 and this interaction involves the Fe65 PTB1 domain.

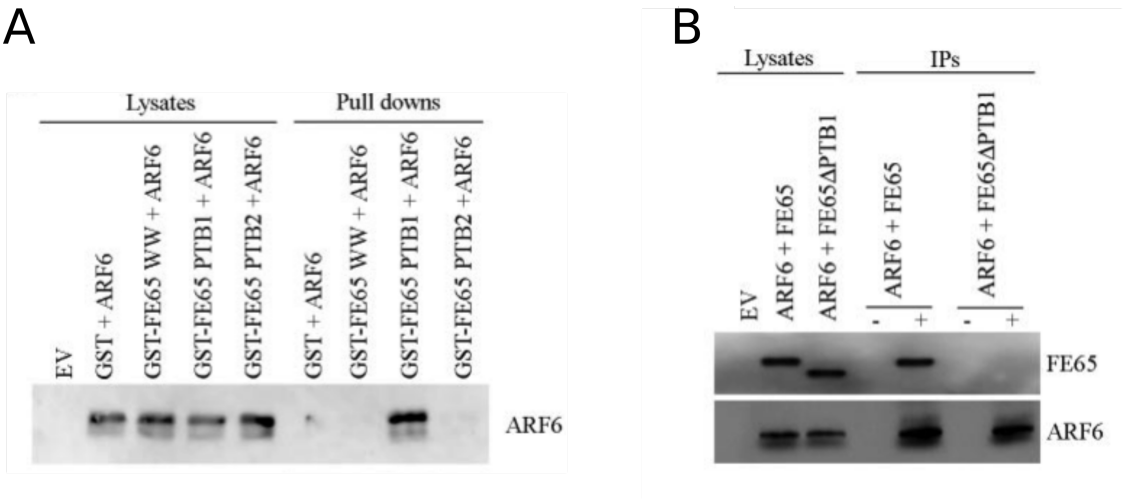

Figure 5.2: ARF6 binds to the PTB1 domain of Fe65

A) CHO cells were transiently transfected with either CAT (EV), GST+ARF6-myc, GST-Fe65WW+ARF6-myc, GST-Fe65PTB1+ARF6-myc or GST-Fe65PTB2+ARF6-myc plasmid vectors. The GST/GST-Fe65 constructs were pulled down with glutathione sepharose 4B beads and bound ARF6 was analysed by western blotting. ARF6 was detected using an in house ARF6 rat antibody. B) CHO cells were transiently transfected with CAT (EV), Fe65+ARF6-myc or Fe65ΔPTB1+ARF6-myc plasmid vectors. Fe65ΔPTB1 is a deletion mutant that does not contain the PTB1 domain of Fe65. ARF6 was immunoprecipitated using 9B11 anti-myc antibody and bound Fe65 was detected by western blotting. Fe65 was detected using sc-19751 and ARF6 using an in house rat antibody.

5.2.3 ARF6 is localised to perinuclear regions and colocalises with Fe65 in growth cones of rat cortical neurons

Studies described in sections 5.2.1-5.2.2 revealed that Fe65 binds to ARF6. Both Fe65 and ARF6 are reported to play a role in the dynamics of the actin cytoskeleton (Cheung et al., 2014; Ermekova et al., 1997; Ma et al., 2008; Sabo et al., 2001; Wang et al., 2011). The actin cytoskeleton plays a major role in neurite outgrowth in growth cones (Gomez and Letourneau, 2014; Kessels et al., 2011). Developing rat cortical neurons were therefore immunostained for Fe65 and ARF6 to determine the subcellular locations of these proteins and to study whether Fe65 and ARF6 displayed any colocalisation.

DIV 3 rat cortical neurons fixed and immunostained for ARF6 showed that ARF6 is predominantly a cytoplasmic protein concentrated in the perinuclear region. Staining for ARF6 was also detected along neurites and in growth cones (Figure 5.3). Co-staining for Fe65 revealed that Fe65 shows similar patterns of expression, including localisation to growth cones where Fe65-ARF6-mediated actin cytoskeletal rearrangement may occur (Figure 5.3). To quantify the level of colocalisation of these proteins, intensity correlation analyses (ICA) were performed. ICA determines not just whether pixels from the two labels colocalise but also whether the intensities of these pixel signals vary in synchrony. It therefore provides a more robust assay than simply comparing colocalisation of signals (Li et al., 2004). ICA generates an intensity correlation quotient (ICQ) value that can be statistically tested to identify the spatial relationship between the two proteins under investigation. ICQ = 0 describes random staining, $-0.5 \leq ICQ < 0$ describes segregated staining and $0 < ICQ \leq 0.5$ describes colocalisation of staining. ICA analysis of Fe65 and ARF6 staining showed that the proteins significantly colocalise in growth cones of developing neurons (mean ± SEM; ICQ = 0.225 ± 0.001; one-sample t-test; $p < 0.001$, n = 36 cells).

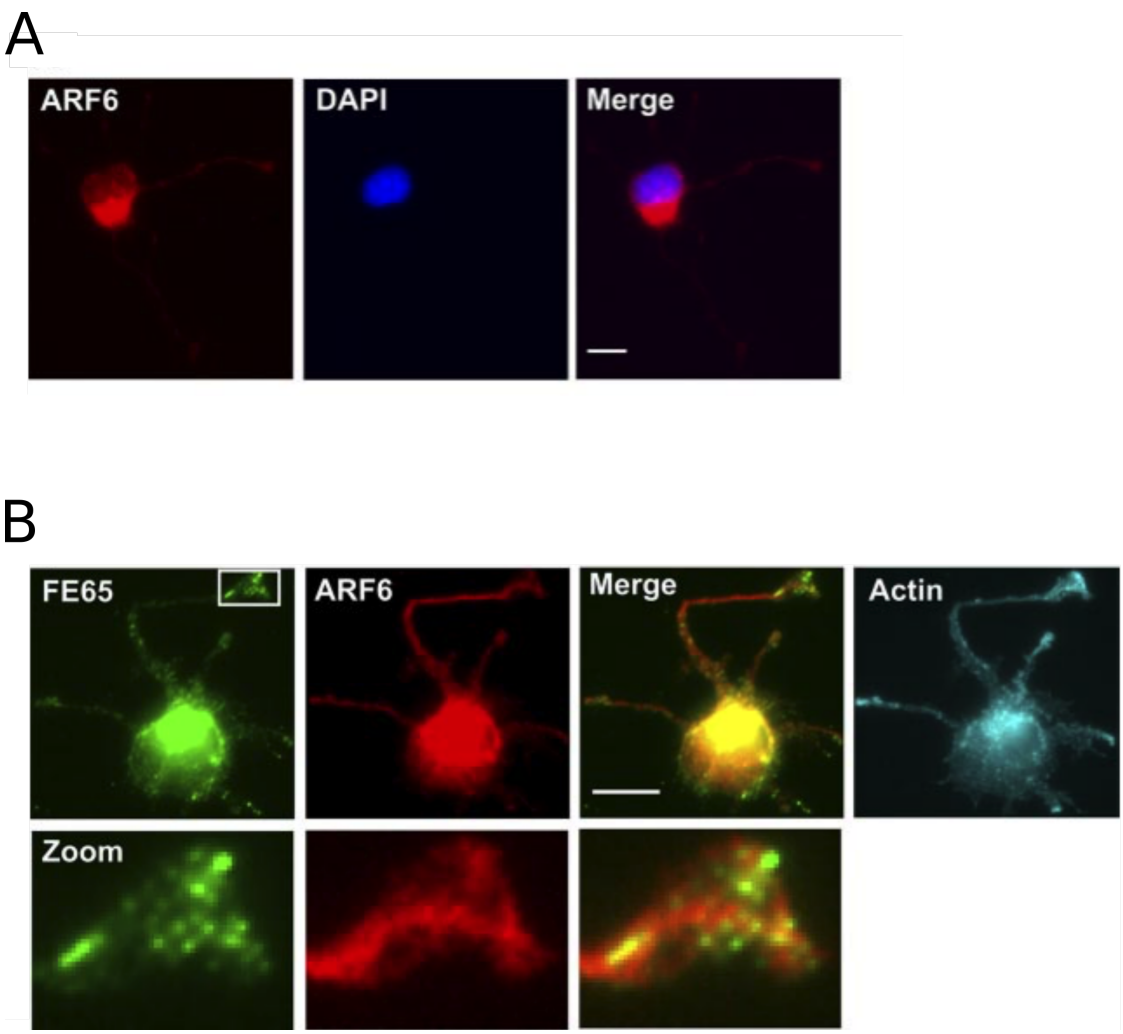

Figure 5.3: ARF6 is present in perinuclear regions and colocalises with Fe65 in the growth cones of developing neurites

DIV 3 rat cortical neurons were fixed, permeabilised and immunostained for endogenous ARF6 using an in house rat antibody, Fe65 using sc-19751 and actin using Alexa Fluor-546-labelled phalloidin. Nuclei were labelled using DAPI. A) ARF6 is present in perinuclear regions and neurites. B) Fe65 and ARF6 show similar patterns of staining and are enriched in growth cones. Zoom box shows growth cone from the region identified in the Fe65 image. Scale bars = 10 μM.

5.2.4 Fe65 and ARF6 enhance neurite outgrowth

Fe65 and ARF6 are both reported to play a role in regulating the actin cytoskeleton. In addition, these proteins colocalise in the growth cones of developing neurites (section 5.2.3). To determine whether Fe65 and ARF6 affected neurite outgrowth, DIV 2 rat cortical neurons were co-transfected with EGFP so as to facilitate measurements of neuron morphology and either CAT (EV), Fe65, Fe65ΔPTB1, Fe65ΔPTB2, ARF6, ARF6+Fe65, ARF6+Fe65ΔPTB1 or ARF6+Fe65ΔPTB2 plasmid vectors (see Table 2.2). 24 hours later, the length of the longest neurite was measured in neurons from each transfection group. Transfection of Fe65 or ARF6 enhanced neurite outgrowth and this outgrowth was further enhanced in neurons transfected with plasmids for both proteins (Figure 5.4). Moreover, the stimulatory affect of Fe65 on neurite outgrowth was lost in neurons transfected with Fe65ΔPTB1 and partially lost in neurons transfected with Fe65ΔPTB2 (Figure 5.4).

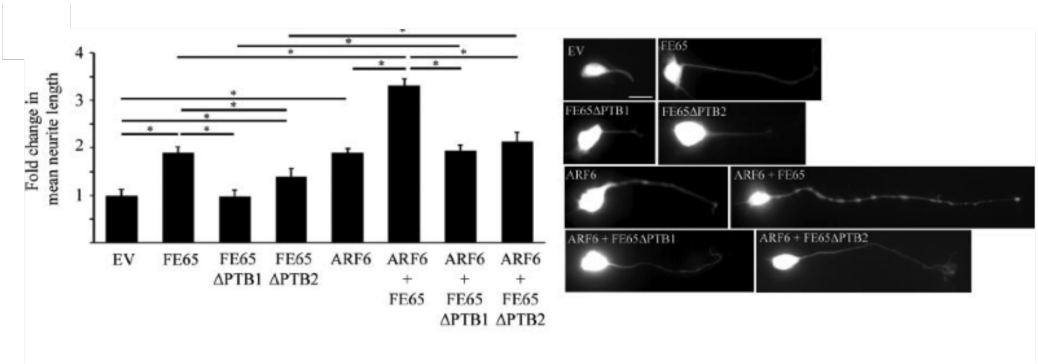

Figure 5.4: Fe65 and ARF6 enhance neurite outgrowth

DIV 3 rat cortical neurons were transiently co-transfected with EGFP along with CAT (EV), Fe65, Fe65ΔPTB1, Fe65ΔPTB2, ARF6, ARF6+Fe65, ARF6+Fe65ΔPTB1 or ARF6+Fe65ΔPTB2 plasmid vectors. The length of the longest neurite was measured 24 hr after transfection as the distance between growth cone tip and cell body. A minimum of 40 cells were analysed per treatment group and statistical analyses were carried out using one-way ANOVA with Bonferroni *post* hoc test (error bars show S.D., * p = 0.001, n = 3).

5.3 Discussion

In this chapter, the interaction between Fe65 and ARF6 was investigated. ARF6 was identified as a putative Fe65 binding protein via a yeast 2-hybrid screen in Kwok-Fai Lau's research group (Chinese University of Hong Kong). Confirmation of the interaction was then achieved via a number of experimental approaches. These involved using co-immunoprecipitation assays of transfected proteins and endogenous proteins in brain, GST pull down assays and finally colocalisation studies in cultured rat neurons. The GST pull down assays demonstrated that binding of ARF6 to Fe65 involved the PTB1 domain of Fe65; the Fe65 WW and PTB2 domains did not bind ARF6. Also co-immunoprecipitations using a deletion mutant of Fe65 lacking the PTB1 domain (Fe65ΔPTB1) revealed that this mutant did not bind ARF6.

To gain insight into the cellular localisation of both ARF6 and Fe65, immunofluorescence studies were carried out on fixed rat cortical neurons. These demonstrated that both ARF6 and Fe65 are present in cell bodies and neurites of developing neurons. Of particular interest was the observation that they were both also enriched in the growth cones of extending axons. Indeed, colocalisation assays of ARF6 and Fe65 in growth cones using ICA analyses revealed that they displayed significant colocalisation in growth cones.

Both Fe65 and ARF6 are involved in mediating actin dynamics and actin is required in the growth cones of developing neurons for neurite outgrowth (Akiyama and Kanaho, 2015; Cheung et al., 2014; Ermekova et al., 1997; Gillingham and Munro, 2007; Gomez and Letourneau, 2014; Kessels et al., 2011; Ma et al., 2008; Sabo et al., 2001; Wang et al., 2011). The affects of overexpression of Fe65 and ARF6 on neurite outgrowth in developing cultured rat neurons were therefore investigated. Both Fe65 and ARF6 stimulated neurite outgrowth and this stimulation was enhanced in neurons expressing both proteins. Moreover, the effect of Fe65 on neurite outgrowth was lost in Fe65ΔPTB1 expressing cells; Fe65ΔPTB1 does not bind to ARF6. This indicates that the stimulatory effect of Fe65 on neurite outgrowth involves its binding to ARF6.

Interestingly, expression of Fe65ΔPTB2 (Fe65 lacking the second PTB domain) was also less potent at promoting neurite outgrowth than wild-type Fe65. The Fe65 PTB2 domain binds APP (see Table 1.1) and so it is possible that APP may also be involved in Fe65 and possibly ARF6 mediated neurite outgrowth. This could be tested by monitoring the effects on neurite outgrowth on overexpression of APP and mutants of APP in which the YENPTY motif that mediates binding to Fe65 have been altered to preclude the interaction.

Finally, BDNF is a neurotrophin and axon guidance molecule (Markus et al., 2002). The results presented in Chapter 3 demonstrate that BDNF induces phosphorylation of Fe65 by ERK. It would therefore be interesting to determine whether BDNF-mediated phosphorylation of Fe65 also alters the interaction between ARF6 and Fe65, and whether the phosphorylation mutants of Fe65 described earlier in this thesis alter the capability of Fe65 to promote neurite outgrowth.

CHAPTER 6: SUMMARY AND FUTURE DIRECTIONS

6.1 Summary

The amyloid cascade hypothesis has provided the dominant framework for studying AD and therapeutic targets. However, effective drugs that target Aβ production or clearance have so far proved elusive and this has prompted a re-appraisal of the hypothesis (Herrup, 2015; Karran and De Strooper, 2016). Alterations to APP processing that impact Aβ production are also likely to affect APP function and one possibility is that changes to this function might also contribute to AD. Fe65 is major binding protein of APP and the work described in this thesis is focused on the role of Fe65. In particular, it aimed to begin to test two related hypotheses. Firstly, that BDNF signalling, which leads to activation of ERK1/2 in neurons, induces phosphorylation of Fe65 by ERK1/2 to regulate its binding to APP. Secondly, that Fe65 regulates genes that are linked to GSK3α/β activity and tau phosphorylation.

The studies in Chapter 3 were designed to further our understanding of the regulatory pathways that mediate the APP-Fe65 interaction. Firstly, BDNF was shown to induce Fe65 phosphorylation in an ERK1/2-dependent manner. Assays were then established to quantify APP-Fe65 binding. These were co-immunoprecipitation assays, GST pull-down assays using a GST-APP_C fusion protein bait and finally PLAs. BDNF treatment consistently reduced the interaction between APP and Fe65 in both CHO cells stably expressing the BDNF receptor TrkB and cultured rat cortical neurons. To gain insight into whether the effect of BDNF on APP-Fe65 binding involved phosphorylation of Fe65 by ERK1/2, phospho-mimicking Fe65 mutants containing substitutions of the four known ERK1/2 phosphorylation sites to either alanine or glutamic acid were used. Mutation to alanine precludes phosphorylation while mutation to glutamic acid mimics permanent phosphorylation. The phospho-mimicking Fe65 mutant showed less binding to APP in both co-immunoprecipitation and GST-APP_C pull-down assays, confirming that this effect was due to the phosphorylation of one or more of four ERK1/2-responsive residues. These results show that a BDNF-induced signalling pathway activates ERK1/2 to phosphorylate Fe65 and inhibit APP-Fe65 binding.

There is evidence that BDNF treatment may have therapeutic value for AD as it shows a neuroprotective effect in models of AD (Ando et al., 2002; Blurton-Jones et al., 2009; Nagahara et al., 2009). The precise mechanism that underlies this effect is unknown but one possibility raised by the findings reported in Chapter 3 is that it might involve changes to Fe65 phosphorylation and its interaction with APP.

In Chapter 4, experiments were carried out to confirm results from next generation sequencing studies performed by others that compared gene expression in the brains of Fe65KO mice to their non-transgenic littermates. These experiments had identified several components of the wnt signalling pathway including Fzd1, GSK3α and wnt3a as showing altered gene expression. The wnt signalling pathway has been implicated in AD because it regulates the activity of GSK3β, which is strongly linked to AD as a tau kinase. In this thesis, Fe65KO mice and neurons treated with Fe65 siRNA, were used to investigate the role of Fe65 in regulating the expression of these three genes along with two other wnt signalling components, GSK3α and LRP6, and APP and tau, which have strong links to AD. Of the seven genes tested however, these experiments revealed that loss of Fe65 only affected Fzd1 expression. To test whether APP also contributes to the regulation of Fzd1, expression levels were measured in neurons treated with APP siRNAs. In contrast to loss of Fe65, APP knockdown had no effect on Fzd1 expression, indicating that Fe65 regulates Fzd1 expression in an APP-independent pathway.

The studies discussed in Chapter 5 demonstrate an interaction between Fe65 and the small GTPase ARF6. They also show that Fe65-ARF6 complexes are present in the growth cones of developing neurons and play an important role in enhancing neurite outgrowth. The development and maintenance of synapses between neurons is a vital part of normal neuronal function. Disruption to neurite outgrowth may impair synaptic development and plasticity. The finding that loss of PTB1 (and therefore ARF6 binding) as well as loss of PTB2 domains of Fe65 can impair neurite outgrowth suggests that Fe65 might act as a bridge between ARF6 and a PTB2-interacting protein, such as APP, which has also been reported to regulate the actin cytoskeleton (Cheung et al., 2014; Ermekova et al., 1997; Ma et al., 2008; Sabo et al., 2001; Wang et al., 2011),.

To investigate other routes that might connect Fe65 to tau phosphorylation, the effect of loss of Fe65 in both Fe65KO mice and Fe65 siRNA-treated rat cortical neurons was studied. These revealed that loss of Fe65 decreased tau phosphorylation on Ser^{199} and Ser^{202}, which are both phosphorylated by GSK3β in AD brains (Hanger et al., 2009). As well as regulation by the wnt signalling pathway, GSK3β is also regulated by inhibitory phosphorylation on Ser^{9}, predominantly by the kinase Akt (Kaidanovich-Beilin and Woodgett, 2011). The effect of loss of Fe65 on GSK3β Ser^{9} phosphorylation was therefore investigated and was found to increase inhibitory GSK3β Ser^{9} phosphorylation. This demonstrated that loss of Fe65 inhibits GSK3β activity via phosphorylation of its regulatory site Ser^{9} and leads to reduced tau phosphorylation on at least two known AD-linked sites. These are exciting findings since they demonstrate

that Fe65 can regulate tau phosphorylation and so reveal a new potential pathway in which APP, via its interaction with Fe65, might also influence tau phosphorylation.

6.2 Future directions

The findings presented in this thesis demonstrate that Fe65 binding is modulated by the ERK1/2 MAP kinase cascade and reveal a new target for Fe65-mediated regulation of gene transcription. They also provide evidence that Fe65 can regulate tau phosphorylation, possibly by altering GSK3β activity and may demonstrate a novel link between APP and tau. Some suggestions for future research directions are listed below.

1. The use of Fe65 phosphorylation mutants revealed that four known phosphorylation sites targeted by ERK1/2 could mimic the impairment of APP-Fe65 binding displayed by BDNF treatment. It would be useful to identify whether all or just some of these four sites are responsible for the observed change in APP-Fe65 binding. This could be investigated using the biochemical assays employed in Chapter 3 on phosphorylation mutants that contain individual sites or combinations of sites mutated to mimic Fe65 phosphorylation or preclude phosphorylation. It would also be interesting to perform these experiments using phosphorylation mutants combined with BDNF treatment to verify that the phosphorylation precluding mutants rescue the inhibition of APP-Fe65 binding mediated by BDNF. This would confirm that no alternative, as yet unidentified, BDNF-responsive phosphorylation sites are involved.

2. The studies in Chapter 3 demonstrate that BDNF induces Fe65 phosphorylation by ERK1/2 and reduces APP-Fe65 binding. It would be interesting to investigate what effect this has on the function of Fe65, particularly its role in nuclear signalling and gene transactivation. Subcellular localisation studies using immunofluorescence and biochemical techniques could determine whether the nuclear translocation of Fe65, or indeed APP are altered by BDNF treatment. In addition, since Fzd1 mRNA expression was shown to be regulated by Fe65 expression, Fzd1 mRNA levels could be used as a measure of the transcriptional activity of Fe65 after BDNF treatment.

3. Fe65KO mice and Fe65 siRNA treated neurons showed reduced expression of Fzd1, a receptor of the wnt signalling pathway, which may be linked to AD because wnt signalling inhibits GSK3β activity. As there is suspected redundancy between the different Fzd receptor isoforms in the wnt signalling pathway (Clevers and Nusse, 2012; Niehrs, 2012), it is important to ascertain whether Fe65 loss leads to

physiologically relevant changes to wnt signalling. This could be achieved using TCF/LEF reporter gene assays or monitoring of β-catenin protein levels.

4. Loss of Fe65 also caused a decrease in GSK3β activity and a decrease in the level of tau phosphorylation at two AD-relevant sites. This demonstration of a relationship between Fe65 and tau phosphorylation may provide a link between APP and tau pathologies. This avenue of research could be explored further by monitoring levels how loss of Fe65 affects phosphorylation of other GSK3β-responsive phosphorylation sites in tau. It would also be interesting to determine whether overexpression of Fe65 produces the opposite effect on tau phosphorylation. Since neurons transfect at low efficiency, lenti- or adeno-viral vectors could be used to overexpress Fe65 in neurons.
5. Finally, it would be interesting to determine the role of APP in this pathway. This could be achieved by studying the effect of loss of APP and APP overexpression in combination with Fe65 on tau and GSK3β Ser^9 phosphorylation in neurons.

To summarise, the finding that loss of Fe65 alters GSK3β activity (via Ser^9 phosphorylation) and tau phosphorylation might be of particular relevance to AD. This area of research should therefore be prioritised for future studies.

CHAPTER 7: REFERENCES

Ackerley, S., Thornhill, P., Grierson, A.J., Brownlees, J., Anderton, B.H., Leigh, P.N., Shaw, C.E., Miller, C.C.J., 2003. Neurofilament Heavy Chain Side Arm Phosphorylation Regulates Axonal Transport of Neurofilaments. J. Cell Biol. 161, 489–495.

Adlard, P.A., Cotman, C.W., 2004. Voluntary Exercise Protects Against Stress-Induced Decreases in Brain-Derived Neurotrophic Factor Protein Expression. Neuroscience 124, 985–992.

Adlard, P.A., Perreau, V.M., Engesser-Cesar, C., Cotman, C.W., 2004. The Timecourse of Induction of Brain-Derived Neurotrophic Factor mRNA and Protein in the Rat Hippocampus Following Voluntary Exercise. Neurosci. Lett. 363, 43–48.

Adlard, P.A., Perreau, V.M., Pop, V., Cotman, C.W., 2005. Voluntary Exercise Decreases Amyloid Load in a Transgenic Model of Alzheimer's Disease. J. Neurosci. 25, 4217–4221.

Akiyama, M., Kanaho, Y., 2015. Physiological Functions of the Small GTPase Arf6 in the Nervous System. Small GTPases 6, 160–4. doi:10.1080/21541248.2015.1043041

Alderson, R.F., Alterman, A.L., Barde, Y.-A., Lindsay, R.M., 1990. Brain-Derived Neurotrophic Factor Increases Survival and Differentiated Functions of Rat Septal Cholinergic Neurons in Culture. Neuron 5, 297–306.

Allinquant, B., Hantraye, P., Mailleux, P., Moya, K., Bouillot, C., Prochiantz, A., 1995. Downregulation of Amyloid Precursor Protein Inhibits Neurite Outgrowth In Vitro. J. Cell Biol. 128, 919–927.

Almeida, R.D., Manadas, B.J., Melo, C. V, Gomes, J.R., Mendes, C.S., Grãos, M.M., Carvalho, R.F., Carvalho, a P., Duarte, C.B., 2005. Neuroprotection by BDNF Against Glutamate-Induced Apoptotic Cell Death is Mediated by ERK and PI3-Kinase Pathways. Cell Death Differ. 12, 1329–1343.

Alonso, M., Medina, J.H., Pozzo-miller, L., 2004. ERK1/2 Activation Is Necessary for BDNF to Increase Dendritic Spine Density in Hippocampal CA1 Pyramidal Neurons. Learn. Mem. 11, 172–178.

Alvarez, A.R., Godoy, J.A., Mullendorff, K., Olivares, G.H., Bronfman, M., Inestrosa, N.C., 2004. Wnt-3a Overcomes β-Amyloid Toxicity in Rat Hippocampal Neurons. Exp. Cell Res. 297, 186–196.

Alves da Costa, C., Sunyach, C., Pardossi-Piquard, R., Sevalle, J., Vincent, B., Boyer, N., Kawarai, T., Girardot, N., St George-Hyslop, P., Checler, F., 2006. Presenilin-Dependent γ-Secretase-Mediated Control of p53-Associated Cell Death in Alzheimer's Disease. J. Neurosci. 26, 6377–6385.

Alvira-Botero, X., Pérez-Gonzalez, R., Spuch, C., Vargas, T., Antequera, D., Garzón,

M., Bermejo-Pareja, F., Carro, E., 2010. Megalin Interacts with APP and the Intracellular Adapter Protein FE65 in Neurons. Mol. Cell. Neurosci. 45, 306–315.

Anderson, J.P., Esch, F.S., Keim, P.S., Sambamurti, K., Lieberburg, I., Robakis, N.K., 1991. Exact Cleavage Site of Alzheimer Amyloid Precursor in Neuronal PC-12 Cells. Neurosci. Lett. 128, 126–128.

Ando, K., Iijima, K.I., Elliott, J.I., Kirino, Y., Suzuki, T., 2001. Phosphorylation-Dependent Regulation of the Interaction of Amyloid Precursor Protein with Fe65 Affects the Production of β-Amyloid. J. Biol. Chem. 276, 40353–40361.

Ando, S., Kobayashi, S., Waki, H., Kon, K., Fukui, F., Tadenuma, T., Iwamoto, M., Takeda, Y., Izumiyama, N., Watanabe, K., Nakamura, H., 2002. Animal Model of Dementia Induced by Entorhinal Synaptic Damage and Partial Restoration of Cognitive Deficits by BDNF and Carnitine. J. Neurosci. Res. 70, 519–527.

Arai, H., Lee, V.M., Messinger, M.L., Greenberg, B.D., Lowery, D.E., Trojanowski, J.Q., 1991. Expression Patterns of β-Amyloid Precursor Protein (β-APP) in Neural and Nonneural Human Tissues From Alzheimer's Disease and Control Subjects. Ann. Neurol. 30, 686–693.

Araki, Y., Miyagi, N., Kato, N., Yoshida, T., Wada, S., Nishimura, M., Komano, H., Yamamoto, T., De Strooper, B., Yamamoto, K., Suzuki, T., 2004. Coordinated Metabolism of Alcadein and Amyloid β-Protein Precursor Regulates FE65-Dependent Gene Transactivation. J. Biol. Chem. 279, 24343–24354.

Araki, Y., Tomita, S., Yamaguchi, H., Miyagi, N., Sumioka, A., Kirino, Y., Suzuki, T., 2003. Novel Cadherin-Related Membrane Proteins, Alcadeins, Enhance the X11-Like Protein-Mediated Stabilization of Amyloid β-Protein Precursor Metabolism. J. Biol. Chem. 278, 49448–49458.

Arancibia, S., Silhol, M., Moulière, F., Meffre, J., Höllinger, I., Maurice, T., Tapia-Arancibia, L., 2008. Protective Effect of BDNF against Beta-Amyloid Induced Neurotoxicity In Vitro and In Vivo in Rats. Neurobiol. Dis. 31, 316–326.

Armstrong, R.A., Lantos, P.L., Cairns, N.J., 2008. What Determines the Molecular Composition of Abnormal Protein Aggregates in Neurodegenerative Disease? Neuropathology 28, 351–365.

Ayton, S., Lei, P., Bush, A.I., 2013. Metallostasis in Alzheimer's Disease. Free Radic. Biol. Med. 62, 76–89.

Baek, S.H., Ohgi, K.A., Rose, D.W., Koo, E.H., Glass, C.K., Rosenfeld, M.G., 2002. Exchange of N-CoR Corepressor and Tip60 Coactivator Complexes Links Gene Expression by NF-κB and β-Amyloid Precursor Protein. Cell 110, 55–67.

Bahmanyar, S., Higgins, G.., Goldgaber, D., Lewis, D.., Morrison, J.H., Wilson, M.C., Shankar, S.K., Gajdusek, D.C., 1987. Localization of Amyloid β Protein Messenger RNA in Brains from Patients with Alzheimer's Disease. Science (80-.).

237, 77–80.

Bao, J., Cao, C., Zhang, X., Jiang, F., Nicosia, S. V., Bai, W., 2007. Suppression of β-Amyloid Precursor Protein Signaling into the Nucleus by Estrogens Mediated through Complex Formation between the Estrogen Receptor and Fe65. Mol. Cell. Biol. 27, 1321–1333.

Barbagallo, A.P.M., Weldon, R., Tamayev, R., Zhou, D., Giliberto, L., Foreman, O., D'Adamio, L., 2010. Tyr682 in the Intracellular Domain of APP Regulates Amyloidogenic APP Processing In Vivo. PLoS One 5, 1–11.

Barbato, C., Canu, N., Zambrano, N., Serafino, A., Minopoli, G., Ciotti, M.T., Amadoro, G., Russo, T., Calissano, P., 2005. Interaction of Tau with Fe65 Links Tau to APP. Neurobiol. Dis. 18, 399–408.

Barco, A., Patterson, S.L., Patterson, S.L., Alarcon, J.M., Gromova, P., Mata-Roig, M., Morozov, A., Kandel, E.R., 2005. Gene Expression Profiling of Facilitated L-LTP in VP16-CREB Mice Reveals that BDNF is Critical for the Maintenance of LTP and its Synaptic Capture. Neuron 48, 123–137.

Basi, G., Frigon, N., Barbour, R., Doan, T., Gordon, G., McConlogue, L., Sinha, S., Zeller, M., 2003. Antagonistic Effects of β-Site Amyloid Precursor Protein-Cleaving Enzymes 1 and 2 β-Amyloid Peptide Production in Cells. J. Biol. Chem. 278, 31512–31520.

Behrens, J., von Kries, J.P., Kühl, M., Bruhn, L., Wedlich, D., Grosschedl, R., Birchmeier, W., 1996. Functional Interaction of β-Catenin with the Transcription Factor LEF-1. Nature.

Belyaev, N.D., Kellett, K.A.B., Beckett, C., Makova, N.Z., Revett, T.J., Nalivaeva, N.N., Hooper, N.M., Turner, A.J., 2010. The Transcriptionally Active Amyloid Precursor Protein (APP) Intracellular Domain is Preferentially Produced from the 695 Isoform of APP in a β-Secretase-Dependent Pathway. J. Biol. Chem. 285, 41443–41454.

Belyaev, N.D., Nalivaeva, N.N., Makova, N.Z., Turner, A.J., 2009. Neprilysin Gene Expression Requires Binding of the Amyloid Precursor Protein Intracellular Domain to its Promoter: Implications for Alzheimer Disease. EMBO Rep. 10, 94–100.

Benilova, I., Karran, E., De Strooper, B., 2012. The Toxic Aβ Oligomer and Alzheimer's Disease: an Emperor in Need of Clothes. Nat. Neurosci. 15, 349–357.

Bennett, B.D., Babu-Khan, S., Loeloff, R., Louis, J.C., Curran, E., Citron, M., Vassar, R., 2000. Expression Analysis of BACE2 in Brain and Peripheral Tissues. J. Biol. Chem. 275, 20647–20651.

Bertram, L., Lill, C.M., Tanzi, R.E., 2010. The Genetics of Alzheimer Disease: Back to the Future. Neuron 68, 270–281.

Blurton-Jones, M., Kitazawa, M., Martinez-Coria, H., Castello, N.A., Müller, F.-J., Loring, J.F., Yamasaki, T.R., Poon, W.W., Green, K.N., LaFerla, F.M., 2009. Neural Stem Cells Improve Cognition via BDNF in a Transgenic Model of Alzheimer Disease. Proc. Natl. Acad. Sci. 106, 13594–13599.

Bonni, A., Brunet, A., West, A.E., Datta, S.R., Takasu, M.A., Greenberg, M.E., 1999. Cell Survival Promoted by the Ras-MAPK Signaling Pathway by Transcription-Dependent and -Independent Mechanisms. Science (80-.). 286, 1358–1362.

Borg, J.P., Ooi, J., Levy, E., Margolis, B., 1996. The Phosphotyrosine Interaction Domains of X11 and FE65 Bind to Distinct Sites on the YENPTY Motif of Amyloid Precursor Protein. Mol. Cell. Biol. 16, 6229–6241.

Bork, P., Margolis, B., 1995. A Phosphotyrosine Interaction Domain. Cell 80, 693–694.

Bork, P., Sudol, M., 1994. The WW Domain: A Signalling Site in Dystrophin? Trends Biochem. Sci. 19, 531–533.

Braak, H., Braak, E., 1991. Neuropathological Stageing of Alzheimer-Related Changes. Acta Neuropathol. 82, 239–259.

Bradford, M.M., 1976. A Rapid and Sensitive Method for the Quantitation of Microgram Quantities of Protein Utilizing the Principle of Protein-Dye Binding. Anal. Biochem. 72, 248–254.

Bressler, S.L., Gray, M.D., Sopher, B.L., Hu, Q., Hearn, M.G., Pham, D.G., Dinulos, M.B., Fukuchi, K., Sisodia, S.S., Miller, M.A., Disteche, C.M., Martin, G.M., 1996. cDNA Cloning and Chromosome Mapping of the Human Fe65 Gene: Interaction of the Conserved Cytoplasmic Domains of the Human β-Amyloid Precursor Protein and its Homologues with the Mouse Fe65 Protein. Hum. Mol. Genet. 5, 1589–1598.

Brunholz, S., Sisodia, S., Lorenzo, A., Deyts, C., Kins, S., Morfini, G., 2012. Axonal Transport of APP and the Spatial Regulation of APP Cleavage and Function in Neuronal Cells. Exp. Brain Res. 217, 353–364.

Bruni, P., Minopoli, G., Brancaccio, T., Napolitano, M., Faraonio, R., Zambrano, N., Hansen, U., Russo, T., 2002. Fe65, a Ligand of the Alzheimer's β-Amyloid Precursor Protein, Blocks Cell Cycle Progression by Down-Regulating Thymidylate Synthase Expression. J. Biol. Chem. 277, 35481–35488.

Caccamo, A., Maldonado, M.A., Bokov, A.F., Majumder, S., Oddo, S., 2010. CBP Gene Transfer Increases BDNF Levels and Ameliorates Learning and Memory Deficits in a Mouse Model of Alzheimer's Disease. Proc. Natl. Acad. Sci. 107, 22687–22692.

Cao, X., Südhof, T.C., 2004. Dissection of Amyloid-β Precursor Protein-Dependent Transcriptional Transactivation. J. Biol. Chem. 279, 24601–24611.

Cao, X., Südhof, T.C., 2001. A Transcriptionally Active Complex of APP with Fe65 and

Histone Acetyltransferase Tip60. Science (80-.). 293, 115–120.

Caricasole, A., Copani, A., Caraci, F., Aronica, E., Rozemuller, A.J., Caruso, A., Storto, M., Gaviraghi, G., Terstappen, G.C., Nicoletti, F., 2004. Induction of Dickkopf-1, a Negative Modulator of the Wnt Pathway, Is Associated with Neuronal Degeneration in Alzheimer's Brain. J. Neurosci. 24, 6021–6027.

Carroll, R.C., Zukin, R.S., 2002. NMDA-Receptor Trafficking and Targeting: Implications for Synaptic Transmission and Plasticity. Trends Neurosci. 25, 571–577.

Castellano, J.M., Kim, J., Stewart, F.R., Jiang, H., Demattos, R.B., Patterson, B.W., Fagan, A.M., Morris, J.C., Mawuenyega, K.G., Cruchaga, C., 2011. Human APOE Isoforms Differentially Regulate Brain Amyloid-β Peptide Clearance. Sci Transl Med 3, 89ra57.

Chacón, M. a., Varela-Nallar, L., Inestrosa, N.C., 2008. Frizzled-1 is Involved in the Neuroprotective Effect of Wnt3a Against Aβ Oligomers. J. Cell. Physiol. 217, 215–227.

Chang, K.-A., Kim, H.-S., Ha, T.-Y., Ha, J.-W., Shin, K.Y., Jeong, Y.H., Lee, J.-P., Park, C.-H., Kim, S., Baik, T.-K., Suh, Y.-H., 2006. Phosphorylation of Amyloid Precursor Protein (APP) at Thr668 Regulates the Nuclear Translocation of the APP Intracellular Domain and Induces Neurodegeneration. Mol. Cell. Biol. 26, 4327–4338.

Cherfils, J., Zeghouf, M., 2013. Regulation of Small GTPases by GEFs, GAPs, and GDIs. Physiol. Rev. 93, 269–309. doi:10.1152/physrev.00003.2012

Cheung, H.N.M., Dunbar, C., Mórotz, G.M., Cheng, W.H., Chan, H.Y.E., Miller, C.C.J., Lau, K.-F., 2014. FE65 Interacts with ADP-Ribosylation Factor 6 to Promote Neurite Outgrowth. FASEB J. 28, 337–349.

Chow, V.W., Mattson, M.P., Wong, P.C., Gleichmann, M., 2010. An Overview of APP Processing Enzymes and Products. NeuroMolecular Med. 12, 1–12.

Chow, W.N.V., Cheung, H.N.M., Li, W., Lau, K.-F., 2015a. FE65: Roles Beyond Amyloid Precursor Protein Processing. Cell. Mol. Biol. Lett. 20, 66–87.

Chow, W.N.V., Luk, H.W., Chan, H.Y.E., Lau, K., 2012. Degradation of Mutant Huntingtin via the Ubiquitin/Proteasome System is Modulated by FE65. Biochem. J. 443, 681–689.

Chow, W.N.V., Ngo, J.C.K., Li, W., Chen, Y.W., Tam, K.M.V., Chan, H.Y.E., Miller, C.C.J., Lau, K., 2015b. Phosphorylation of FE65 Ser610 by Serum-and Glucocorticoid-Induced Kinase 1 Modulates Alzheimer's Disease Amyloid Precursor Protein Processing. Biochem. J. 470, 303–317.

Clevers, H., Nusse, R., 2012. Wnt/β-Catenin Signaling and Disease. Cell 149, 1192–1205.

Conner, J.M., Lauterborn, J.C., Yan, Q., Gall, C.M., Varon, S., 1997. Distribution of Brain-Derived Neurotrophic Factor (BDNF) Protein and mRNA in the Normal Adult Rat CNS: Evidence for Anterograde Axonal Transport. J. Neurosci. 17, 2295–2313.

Cool, B.H., Zitnik, G., Martin, G.M., Hu, Q., 2010. Structural and Functional Characterization of a Novel FE65 Protein Product Up-regulated in Cognitively Impaired FE65 Knockout Mice. J. Neurochem. 112, 410–419.

Corder, E.H., Saunders, A.M., Risch, N.J., Strittmatter, W.J., Schmechel, D.E., Gaskell, P.C., Rimmler, J.B., Locke, P.A., Conneally, P.M., Schmader, K.E., 1994. Protective Effect of Apolipoprotein E Type 2 Allele for Late Onset Alzheimer Disease. Nat. Genet. 7, 180–184.

Corder, E.H., Saunders, A.M., Strittmatter, W.J., Schmechel, D.E., Gaskell, P.C., Small, G.W., Roses, A.D., Haines, J.L., Pericak-Vance, M.A., 1993. Gene Dose of Apolipoprotein E Type 4 Allele and the Risk of Alzheimer's Disease in Late Onset Families. Science (80-.). 261, 921–923.

Corona, C., Masciopinto, F., Silvestri, E., Viscovo, A. Del, Lattanzio, R., Sorda, R. La, Ciavardelli, D., Goglia, F., Piantelli, M., Canzoniero, L.M.T., Sensi, S.L., 2010. Dietary Zinc Supplementation of 3xTg-AD Mice Increases BDNF Levels and Prevents Cognitive Deficits as well as Mitochondrial Dysfunction. Cell Death Dis. 1, e91.

Cousins, S.L., Hoey, S.E. a., Anne Stephenson, F., Perkinton, M.S., 2009. Amyloid Precursor Protein 695 Associates with Assembled NR2A- and NR2B-containing NMDA Receptors to Result in the Enhancement of their Cell Surface Delivery. J. Neurochem. 111, 1501–1513.

Dawkins, E., Small, D.H., 2014. Insights into the Physiological Function of the β-Amyloid Precursor Protein: Beyond Alzheimer's Disease. J. Neurochem. 129, 756–769.

De Ferrari, G.V., Chacón, M.A., Barría, M.I., Garrido, J.L., Godoy, J.A., Olivares, G., Reyes, A.E., Alvarez, A., Bronfman, M., Inestrosa, N.C., 2003. Activation of Wnt Signaling Rescues Neurodegeneration and Behavioral Impairments Induced by β-Amyloid Fibrils. Mol. Psychiatry 8, 195–208.

De Strooper, B., Annaert, W., 2010. Novel Research Horizons for Presenilins and γ-Secretases in Cell Biology and Disease. Annu. Rev. Cell Dev. Biol. 26, 235–260.

De Strooper, B., Iwatsubo, T., Wolfe, M.S., 2012. Presenilins and γ-Secretase: Structure, Function and Role in Alzheimer Disease. Cold Spring Harb. Perspect. Med. 2, a006304.

De Strooper, B., Vassar, R., Golde, T., 2010. The Secretases: Enzymes with Therapeutic Potential in Alzheimer Disease. Nat. Rev. Neurol. 6, 99–107.

Delatour, B., Mercken, L., El Hachimi, K., Colle, M.-A., Pradier, L., Duyckaerts, C., 2001. Fe65 in Alzheimer's Disease: Neuronal Distribution and Association with Neurofibrillary Tangles. Am. J. Pathol. 158, 1585–1591.

Deng, Y., Wang, Z., Wang, R., Zhang, X., Zhang, S., Wu, Y., Staufenbiel, M., Cai, F., Song, W., 2013. Amyloid-β Protein (Aβ) Glu11 is the Major β-Secretase Site of β-Site Amyloid-β Precursor Protein-Cleaving Enzyme 1(BACE1), and Shifting the Cleavage Site to Aβ Asp1 Contributes to Alzheimer Pathogenesis. Eur. J. Neurosci. 37, 1962–1969.

Devi, L., Ohno, M., 2012. 7,8-Dihydroxyflavone, a Small-Molecule TrkB Agonist, Reverses Memory Deficits and BACE1 Elevation in a Mouse Model of Alzheimer's Disease. Neuropsychopharmacology 37, 434–444.

Dickson, D.W., 1997. The Pathogenesis of Senile Plaques. J. Neuropathol. Exp. Neurol.

Ding, V.W., Chen, R.-H., McCormick, F., 2000. Differential Regulation of Glycogen Synthase Kinase 3 by Insulin and Wnt Signaling. J. Biol. Chem. 275, 32475–32481.

Domingues, S.C., Henriques, A.G., Fardilha, M., Da Cruz E Silva, E.F., Da Cruz E Silva, O.A.B., 2011. Identification and Characterization of a Neuronal Enriched Novel Transcript Encoding the Previously Described p60Fe65 Isoform. J. Neurochem. 119, 1086–1098.

Doody, R.S., Thomas, R.G., Farlow, M., Iwatsubo, T., Vellas, B., Joffe, S., Kieburtz, K., Raman, R., Sun, X., Aisen, P.S., Siemers, E., Liu-Seifert, H., Mohs, R., 2014. Phase 3 Trials of Solanezumab for Mild-to-Moderate Alzheimer's Disease. N. Engl. J. Med. 370, 311–321.

Duff, K., Eckman, C., Zehr, C., Yu, X., Prada, C.M., Perez-tur, J., Hutton, M., Buee, L., Harigaya, Y., Yager, D., Morgan, D., Gordon, M.N., Holcomb, L., Refolo, L., Zenk, B., Hardy, J., Younkin, S., 1996. Increased Amyloid-β42(43) in Brains of Mice Expressing Mutant Presenilin 1. Nature.

Duilio, A., Faraonio, R., Minopoli, G., Zambrano, N., Russo, T., 1998. Fe65L2: A New Member of the Fe65 Protein Family Interacting with the Intracellular Domain of the Alzheimer's β-Amyloid Precursor Protein. Biochem. J. 330, 513–519.

Duilio, A., Zambrano, N., Mogavero, A.R., Ammendola, R., Cimino, F., Russo, T., 1991. A Rat Brain mRNA Encoding a Transcriptional Activator Homologous to the DNA Binding Domain of Retroviral Integrases. Nucleic Acids Res. 19, 5269–5274.

Dumanis, S.B., Chamberlain, K.A., Sohn, Y.J., Lee, Y.J., Guenette, S.Y., Suzuki, T., Mathews, P.M., Pak, D.T.S., Rebeck, G.W., Suh, Y., Park, H.-S., Hoe, H.-S., 2012. FE65 as a Link Between VLDLR and APP to Regulate their Trafficking and Processing. Mol. Neurodegener. 7.

Durany, N., Michel, T., Kurt, J., Cruz-Sánchez, F.F., Cervás-Navarro, J., Riederer, P., 2000. Brain-Derived Neurotrophic Factor and Neurotrophin-3 Levels in Alzheimer's Disease Brains. Int. J. Dev. Neurosci. 18, 807–813.

Dyrks, T., Weidemann, A., Multhaup, G., Salbaum, J.M., Lemaire, H.G., Kang, J., Müller-Hill, B., Masters, C.L., Beyreuther, K., 1988. Identification, Transmembrane Orientation and Biogenesis of the Amyloid A4 Precursor of Alzheimer's Disease. EMBO J. 7, 949–957.

Eggert, S., Paliga, K., Soba, P., Evin, G., Masters, C.L., Weidemann, A., Beyreuther, K., 2004. The Proteolytic Processing of the Amyloid Precursor Protein Gene Family Members APLP-1 and APLP-2 Involves α-, β-, γ-, and ε-Like Cleavages. J. Biol. Chem. 279, 18146–18156.

Elder, G.A., Gama Sosa, M.A., De Gasperi, R., 2010. Transgenic Mouse Models of Alzheimer's Disease. Mt. Sinai J. Med. 77, 69–81.

Elie, A., Prezel, E., Guérin, C., Denarier, E., Ramirez-Rios, S., Serre, L., Andrieux, A., Fourest-Lieuvin, A., Blanchoin, L., Arnal, I., 2015. Tau Co-Organizes Dynamic Microtubule and Actin Networks. Sci. Rep. 5, 09964.

Ermekova, K.S., Zambrano, N., Linn, H., Minopoli, G., Gertler, F., Russo, T., Sudol, M., 1997. The WW Domain of Neural Protein FE65 Interacts with Proline-Rich Motifs in Mena, the Mammalian Homolog of Drosophila Enabled. J. Biol. Chem. 272, 32869–32877.

Esch, F.S., Keim, P.S., Beattie, E.C., Blacher, R.W., Culwell, A.R., Oltersdorf, T., McClure, D., Ward, P.J., 1990. Cleavage of Amyloid β Peptide During Constitutive Processing of its Precursor. Science (80-.). 248, 1122–1124.

Favata, M.F., Horiuchi, K.Y., Manos, E.J., Daulerio, A.J., Stradley, D.A., Feeser, W.S., Van Dyk, D.E., Pitts, W.J., Earl, R.A., Hobbs, F., Copeland, R.A., Magolda, R.L., Scherle, P.A., Trzaskos, J.M., 1998. Identification of a Novel Inhibitor of Mitogen-Activated Protein Kinase Kinase. J. Biol. Chem. 273, 18623–18632.

Fernandez, M.A., Klutkowski, J.A., Freret, T., Wolfe, M.S., 2014. Alzheimer Presenilin-1 Mutations Dramatically Reduce Trimming of Long Amyloid β-Peptides (Aβ) by γ-Secretase to Increase 42-to-40-Residue Aβ. J. Biol. Chem. 289, 31043–31052.

Ferreira, S.T., Clarke, J.R., Bomfim, T.R., De Felice, F.G., 2014. Inflammation, Defective Insulin Signaling, and Neuronal Dysfunction in Alzheimer's Disease. Alzheimer's Dement. 10, S76–S83.

Ferrer, I., Marin, C., Rey, M.J., Ribalta, T., Goutan, E., Blanco, R., Tolosa, E., Marti, E., 1999. BDNF and Full-Length and Truncated TrkB Expression in Alzheimer's Disease. Implications in Therapeutic Strategies. J. Neuropathol. Exp. Neurol. 58, 729–739.

Fiore, F., Zambrano, N., Minopoli, G., Donini, V., Duilio, A., Russo, T., 1995. The

Regions of the Fe65 Protein Homologous to the Phosphotyrosine Interaction/Phosphotyrosine Binding Domain of Shc Bind the Intracellular Domain of the Alzheimer's Amyloid Precursor Protein. J. Biol. Chem. 270, 30853–30856.

Forster, B., Van De Ville, D., Berent, J., Sage, D., Unser, M., 2004. Complex Wavelets for Extended Depth-of-Field: A New Method for the Fusion of Multichannel Microscopy Images. Microsc. Res. Tech. 65, 33–42.

Fragoso, M.A., Yi, H., Nakamura, R.E.I., Hackam, A.S., 2011. The Wnt Signaling Pathway Protects Retinal Ganglion Cell 5 (RGC-5) Cells from Elevated Pressure. Cell. Mol. Neurobiol. 31, 163–173.

Frank, L., Wiegand, S.J., Siuciak, J.A., Lindsay, R.M., Rudge, J.S., 1997. Effects of BDNF Infusion on the Regulation of TrkB Protein and Message in Adult Rat Brain. Exp. Neurol. 145, 62–70.

Franz-Wachtel, M., Eisler, S.A., Krug, K., Wahl, S., Carpy, A., Nordheim, A., Pfizenmaier, K., Hausser, A., Macek, B., 2012. Global Detection of Protein Kinase D-Dependent Phosphorylation Events in Nocodazole-Treated Human Cells. Mol. Cell. Proteomics 11, 160–170.

Fu, M.M., Holzbaur, E.L.F., 2013. JIP1 Regulates the Directionality of APP Axonal Transport by Coordinating Kinesin and Dynein Motors. J. Cell Biol. 202, 495–508.

Gabrielsson, B.G., Olofsson, L.E., Sjögren, A., Jernås, M., Elander, A., Lönn, M., Rudemo, M., Carlsson, L.M.S., 2005. Evaluation of Reference Genes for Studies of Gene Expression in Human Adipose Tissue. Obes. Res. 13, 649–652.

Gärtner, A., Collin, L., Lalli, G., 2006. Nucleofection of Primary Neurons. Methods Enzymol. 406, 374–388.

Gautam, V., D'Avanzo, C., Berezovska, O., Tanzi, R.E., Kovacs, D.M., 2015. Synaptotagmins Interact with APP and Promote Aβ Generation. Mol. Neurodegener. 10, 1–15.

Genin, E., Hannequin, D., Wallon, D., Sleegers, K., Hiltunen, M., Combarros, O., Bullido, M.J., Engelborghs, S., De Deyn, P., Berr, C., Pasquier, F., Dubois, B., Tognoni, G., Fiévet, N., Brouwers, N., Bettens, K., Arosio, B., Coto, E., Del Zompo, M., Mateo, I., Epelbaum, J., Frank-Garcia, A., Helisalmi, S., Porcellini, E., Pilotto, A., Forti, P., Ferri, R., Scarpini, E., Siciliano, G., Solfrizzi, V., Sorbi, S., Spalletta, G., Valdivieso, F., Vepsäläinen, S., Alvarez, V., Bosco, P., Mancuso, M., Panza, F., Nacmias, B., Bossù, P., Hanon, O., Piccardi, P., Annoni, G., Seripa, D., Galimberti, D., Licastro, F., Soininen, H., Dartigues, J.-F., Kamboh, M.I., Van Broeckhoven, C., Lambert, J.C., Amouyel, P., Campion, D., 2011. APOE and Alzheimer Disease: A Major Gene with Semi-dominant Inheritance. Mol. Psychiatry 16, 903–907.

Ghosal, K., Stathopoulos, A., Pimplikar, S.W., 2010. APP Intracellular Domain Dmpairs

Adult Neurogenesis in Transgenic Mice by Inducing Neuroinflammation. PLoS One 5, e11866.

Ghosal, K., Vogt, D.L., Liang, M., Shen, Y., Lamb, B.T., Pimplikar, S.W., 2009. Alzheimer's Disease-like Pathological Features in Transgenic Mice Expressing the APP Intracellular Domain. Proc. Natl. Acad. Sci. 106, 18367–18372.

Ghosh, A., Carnahan, J., Greenberg, M.E., 1994. Requirement for BDNF in Activity-Dependent Survival of Cortical Neurons. Science (80-.). 263, 1618–1623.

Giliberto, L., Zhou, D., Weldon, R., Tamagno, E., De Luca, P., Tabaton, M., D'Adamio, L., 2008. Evidence that the Amyloid Beta Precursor Protein-Intracellular Domain Lowers the Stress Threshold of Neurons and has a "Regulated" Transcriptional Role. Mol. Neurodegener. 3.

Gillingham, A.K., Munro, S., 2007. The Small G Proteins of the Arf Family and their Regulators. Annu. Rev. Cell Dev. Biol. 23, 579–611. doi:10.1146/annurev.cellbio.23.090506.123209

Goedert, M., Ghetti, B., Spillantini, M.G., Selkoe, D.J., Tanzi, R.E., Nixon, R., 2012. Frontotemporal Dementia: Implications for Understanding Alzheimer Disease. Cold Spring Harb. Perspect. Med. 4, a006254.

Goedert, M., Jakes, R., Vanmechelen, E., 1995. Monoclonal Antibody AT8 Recognises Tau Protein Phosphorylated at Both Serine 202 and Threonine 205. Neurosci. Lett. 189, 167–170.

Goldgaber, D., Lerman, M., McBride, O.W., Saffiotti, U., Gajdusek, D.C., 1987. Characterization and Chromosomal Localization of a cDNA Encoding Brain Amyloid of Alzheimer's Disease. Science (80-.). 235, 877–880.

Gomez, T.M., Letourneau, P.C., 2014. Actin Dynamics in Growth Cone Motility and Navigation. J. Neurochem. 129, 221–234. doi:10.1111/jnc.12506

Goodger, Z. V, Rajendran, L., Trutzel, A., Kohli, B.M., Nitsch, R.M., Konietzko, U., 2009. Nuclear Signaling by the APP Intracellular Domain Occurs Predominantly through the Amyloidogenic Processing Pathway. J. Cell Sci. 122, 3703–3714.

Gravina, S.A., Ho, L., Eckman, C.B., Long, K.E., Otvos, L., Younkin, L.H., Suzuki, N., Younkin, S.G., 1995. Amyloid β Protein (Aβ) in Alzheimer's Disease Brain Biochemical and Immunocytochemical Analysis with Antibodies Specific for Forms Ending at Aβ40 or Aβ42(43). J. Biol. Chem.

Grimm, M.O.W., Mett, J., Stahlmann, C.P., Grösgen, S., Haupenthal, V.J., Blümel, T., Hundsdörfer, B., Zimmer, V.C., Mylonas, N.T., Tanila, H., Müller, U., Grimm, H.S., Hartmann, T., 2015. APP Intracellular Domain Derived from Amyloidogenic β- and γ-Secretase Cleavage Regulates Neprilysin Expression. Front. Aging Neurosci. 7, 77.

Guénette, S., Chang, Y., Hiesberger, T., Richardson, J.A., Eckman, C.B., Eckman,

E.A., Hammer, R.E., Herz, J., 2006. Essential Roles for the FE65 Amyloid Precursor Protein-interacting Proteins in Brain Development. EMBO J. 25, 420–431.

Guénette, S.Y., Chen, J., Jondro, P.D., Tanzi, R.E., 1996. Association of a Novel Human FE65-like Protein with the Cytoplasmic Domain of the β-Amyloid Precursor Protein. Proc. Natl. Acad. Sci. 93, 10832–10837.

Haass, C., Kaether, C., Thinakaran, G., Sisodia, S., 2012. Trafficking and Proteolytic Processing of APP. Cold Spring Harb. Perspect. Med. 2, a006270.

Haass, C., Koo, E.H., Mellon, A., Hung, A.Y., Selkoe, D.J., 1992. Targeting of Cell-Surface β-Amyloid Precursor Protein to Lysosomes: Alternative Processing into Amyloid-Bearing Fragments. Nature 357, 500–503.

Han, B.H., Holtzman, D.M., 2000. BDNF Protects the Neonatal Brain from Hypoxic-Ischemic Injury In Vivo Via the ERK Pathway. J. Neurosci. 20, 5775–5781.

Hanger, D.P., Anderton, B.H., Noble, W., 2009. Tau Phosphorylation: The Therapeutic Challenge for Neurodegenerative Disease. Trends Mol. Med. 15, 112–119.

Hardy, J., 2009. The Amyloid Hypothesis for Alzheimer's Disease: A Critical Reappraisal. J. Neurochem. 110, 1129–1134.

Harold, D., Abraham, R., Hollingworth, P., Sims, R., Hamshere, M., Pahwa, J.S., Moskvina, V., Williams, A., Jones, N., Thomas, C., Stretton, A., Lovestone, S., Powell, J., Proitsi, P., Lupton, M.K., Rubinsztein, D.C., Gill, M., Lawlor, B., Lynch, A., Brown, K., Passmore, P., Craig, D., Mcguinness, B., Todd, S., Holmes, C., Mann, D., Smith, a D., Love, S., Patrick, G., Hardy, J., Mead, S., Fox, N., Rossor, M., Collinge, J., Wichmann, H., Carrasquillo, M.M., Pankratz, V.S., 2009. Genome-Wide Association Study Identifies Variants at CLU and PICALM Associated with Alzheimer's Disease, and Shows Evidence for Additional Susceptibility Genes. Nat. Genet. 41, 1088–1093.

Hartmann, T., Bieger, S.C., Brühl, B., Tienari, P.J., Ida, N., Allsop, D., Roberts, G.W., Masters, C.L., Dotti, C.G., Unsicker, K., Beyreuther, K., 1997. Distinct Sites of Intracellular Production for Alzheimer's Disease Aβ40/42 Amyloid Peptides. Nat. Med. 3, 1016–1020.

He, P., Shen, Y., 2009. Interruption of β-Catenin Signaling Reduces Neurogenesis in Alzheimer's Disease. J. Neurosci. 29, 6545–6557.

Heber, S., Herms, J., Gajic, V., Hainfellner, J., Aguzzi, A., Rülicke, T., von Kretzschmar, H., von Koch, C., Sisodia, S., Tremml, P., Lipp, H.P., Wolfer, D.P., Müller, U., 2000. Mice with Combined Gene Knock-outs Reveal Essential and Partially Redundant Functions of Amyloid Precursor Protein Family Members. J. Neurosci. 20, 7951–7963.

Hébert, S.S., Serneels, L., Tolia, A., Craessaerts, K., Derks, C., Filippov, M.A., Müller,

U., De Strooper, B., 2006. Regulated Intramembrane Proteolysis of Amyloid Precursor Protein and Regulation of Expression of Putative Target Genes. EMBO Rep. 7, 739–745.

Herms, J., Anliker, B., Heber, S., Ring, S., Fuhrmann, M., Kretzschmar, H., Sisodia, S., Müller, U., 2004. Cortical Dysplasia Resembling Human Type 2 Lissencephaly in Mice Lacking All Three APP Family Members. EMBO J. 23, 4106–4115.

Hernández, F., Gómez de Barreda, E., Fuster-Matanzo, A., Lucas, J.J., Avila, J., 2010. GSK3: A Possible Link between Beta Amyloid Peptide and Tau Protein. Exp. Neurol. 223, 322–325.

Hernandez, F., Lucas, J.J., Avila, J., 2012. GSK3 and Tau: Two Convergence Points in Alzheimer's Disease. Adv. Alzheimer's Dis. 33, 141–144.

Herrup, K., 2015. The Case for Rejecting the Amyloid Cascade Hypothesis. Nat. Neurosci. 18, 794–799.

Hewitson, T.D., Wigg, B., Becker, G.J., 2010. Tissue Preparation for Histochemistry: Fixation, Embedding, and Antigen Retrieval for Light Microscopy, Histology Protocols, Methods in Molecular Biology. Humana Press, Totowa, NJ.

Ho, A., Südhof, T.C., 2004. Binding of F-Spondin to Amyloid-β Precursor Protein: A Candidate Amyloid-β Precursor Protein Ligand that Modulates Amyloid-β Precursor Protein Cleavage. Proc. Natl. Acad. Sci. 101, 2548–2553.

Hoe, H.S., Magill, L.A., Guenette, S., Fu, Z., Vicini, S., Rebeck, G.W., 2006. FE65 Interaction with the APOE Receptor ApoEr2. J. Biol. Chem. 281, 24521–24530.

Hoe, H.S., Rebeck, G.W., 2008. Functional Interactions of APP with the apoE Receptor Family. J. Neurochem. 106, 2263–2271.

Hofer, M., Pagliusi, S.R., Hohn, A., Leibrock, J., Barde, Y.A., 1990. Regional Distribution of Brain-Derived Neurotrophic Factor mRNA in the Adult Mouse Brain. EMBO J. 9, 2459–2464.

Hollingworth, P., Harold, D., Sims, R., Gerrish, A., Lambert, J.-C., Carrasquillo, M.M., Abraham, R., Hamshere, M.L., Pahwa, J.S., Moskvina, V., Dowzell, K., Jones, N., Stretton, A., Thomas, C., Richards, A., Ivanov, D., Widdowson, C., Chapman, J., Lovestone, S., Powell, J., Proitsi, P., Lupton, M.K., Brayne, C., Rubinsztein, D.C., Gill, M., Lawlor, B., Lynch, A., Brown, K.S., Passmore, P.A., Craig, D., McGuinness, B., Todd, S., Holmes, C., Mann, D., Smith, A.D., Beaumont, H., Warden, D., Wilcock, G., Love, S., Kehoe, P.G., Hooper, N.M., Vardy, E.R.L.C., Hardy, J., Mead, S., Fox, N.C., Rossor, M., Collinge, J., Maier, W., Jessen, F., Rüther, E., Schürmann, B., Heun, R., Kölsch, H., van den Bussche, H., Heuser, I., Kornhuber, J., Wiltfang, J., Dichgans, M., Frölich, L., Hampel, H., Gallacher, J., Hüll, M., Rujescu, D., Giegling, I., Goate, A.M., Kauwe, J.S.K., Cruchaga, C., Nowotny, P., Morris, J.C., Mayo, K., Sleegers, K., Bettens, K., Engelborghs, S.,

De Deyn, P.P., Van Broeckhoven, C., Livingston, G., Bass, N.J., Gurling, H., McQuillin, A., Gwilliam, R., Deloukas, P., Al-Chalabi, A., Shaw, C.E., Tsolaki, M., Singleton, A.B., Guerreiro, R., Mühleisen, T.W., Nöthen, M.M., Moebus, S., Jöckel, K.-H., Klopp, N., Wichmann, H.-E., Pankratz, V.S., Sando, S.B., Aasly, J.O., Barcikowska, M., Wszolek, Z.K., Dickson, D.W., Graff-Radford, N.R., Petersen, R.C., van Duijn, C.M., Breteler, M.M.B., Ikram, M.A., DeStefano, A.L., Fitzpatrick, A.L., Lopez, O., Launer, L.J., Seshadri, S., Berr, C., Campion, D., Epelbaum, J., Dartigues, J.-F., Tzourio, C., Alpérovitch, A., Lathrop, M., Feulner, T.M., Friedrich, P., Riehle, C., Krawczak, M., Schreiber, S., Mayhaus, M., Nicolhaus, S., Wagenpfeil, S., Steinberg, S., Stefansson, H., Stefansson, K., Snædal, J., Björnsson, S., Jonsson, P. V., Chouraki, V., Genier-Boley, B., Hiltunen, M., Soininen, H., Combarros, O., Zelenika, D., Delepine, M., Bullido, M.J., Pasquier, F., Mateo, I., Frank-Garcia, A., Porcellini, E., Hanon, O., Coto, E., Alvarez, V., Bosco, P., Siciliano, G., Mancuso, M., Panza, F., Solfrizzi, V., Nacmias, B., Sorbi, S., Bossù, P., Piccardi, P., Arosio, B., Annoni, G., Seripa, D., Pilotto, A., Scarpini, E., Galimberti, D., Brice, A., Hannequin, D., Licastro, F., Jones, L., Holmans, P.A., Jonsson, T., Riemenschneider, M., Morgan, K., Younkin, S.G., Owen, M.J., O'Donovan, M., Amouyel, P., Williams, J., 2011. Common Variants at ABCA7, MS4A6A/MS4A4E, EPHA1, CD33 and CD2AP are Associated with Alzheimer's Disease. Nat. Genet. 43, 429–435.

Holmes, C., Boche, D., Wilkinson, D., Yadegarfar, G., Hopkins, V., Bayer, A., Jones, R.W., Bullock, R., Love, S., Neal, J.W., Zotova, E., Nicoll, J.A.R., 2008. Long-Term Effects of Aβ42 Immunisation in Alzheimer's Disease: Follow-up of A Randomised, Placebo-Controlled Phase I Trial. Lancet 372, 216–223.

Homayouni, R., Rice, D.S., Sheldon, M., Curran, T., 1999. Disabled-1 Binds to the Cytoplasmic Domain of Amyloid Precursor-Like Protein 1. J. Neurosci. 19, 7507–7515.

Hooper, C., Killick, R., Lovestone, S., 2008. The GSK3 Hypothesis of Alzheimer's Disease. J. Neurochem. 104, 1433–1439.

Howell, B.W., Lanier, L.M., Frank, R., Gertler, F.B., Cooper, J.A., 1999. The Disabled 1 Phosphotyrosine-Binding Domain Binds to the Internalization Signals of Transmembrane Glycoproteins and to Phospholipids. Mol. Cell. Biol. 19, 5179–5188.

Hsiao, Y., Hung, H., Chen, S., Gean, X.P., 2014. Social Interaction Rescues Memory Deficit in an Animal Model of Alzheimer's Disease by Increasing BDNF-Dependent Hippocampal Neurogenesis. J. Neurosci. 34, 16207–16219.

http://web.stanford.edu/group/nusselab/cgi-bin/wnt/target_genes, n.d. The Wnt Homepage: Wnt Target Genes [WWW Document]. URL

http://web.stanford.edu/group/nusselab/cgi-bin/wnt/target_genes

Hu, J., Liu, C.-C., Chen, X.-F., Zhang, Y., Xu, H., Bu, G., 2015. Opposing Effects of Viral Mediated Brain Expression of Apolipoprotein E2 (apoE2) and apoE4 on apoE Lipidation and Aβ Metabolism in apoE4-Targeted Replacement Mice. Mol. Neurodegener. 10, 6.

Hu, Q., Kukull, W.A., Bressler, S.L., Gray, M.D., Cam, J.A., Larson, E.B., Martin, G.M., Deeb, S.S., 1998. The Human FE65 Gene: Genomic Structure and an Intronic Biallelic Polymorphism Associated with Sporadic Dementia of the Alzheimer Type. Hum. Genet. 103, 295–303.

Hu, Q., Wang, L., Yang, Z., Cool, B.H., Zitnik, G., Martin, G.M., 2005. Endoproteolytic Cleavage of FE65 Converts the Adaptor Protein to a Potent Suppressor of the sAPPα Pathway in Primates. J. Biol. Chem. 280, 12548–12558.

Hu, Q.A., Hearn, M.G., Jin, L.W., Bressler, S.L., Martin, G.M., 1999. Alternatively Spliced Isoforms of FE65 Serve as Neuron-Specific and Non-Neuronal Markers. J. Neurosci. Res. 58, 632–640.

Huang, E.J., Reichardt, L.F., 2001. Neurotrophins: Roles in Neuronal Development and Function. Annu. Rev. Neurosci. 24, 677–736.

Huysseune, S., Kienlen-Campard, P., Octave, J.N., 2007. Fe65 Does Not Stabilize AICD During Activation of Transcription in a Luciferase Assay. Biochem. Biophys. Res. Commun. 361, 317–322.

Inestrosa, N.C., Varela-Nallar, L., 2014. Wnt Signaling in the Nervous System and in Alzheimer's Disease. J. Mol. Cell Biol. 6, 64–74.

Inomata, H., Nakamura, Y., Hayakawa, A., Takata, H., Suzuki, T., Miyazawa, K., Kitamura, N., 2003. A Scaffold Protein JIP-1b Enhances Amyloid Precursor Protein Phosphorylation by JNK and Its Association with Kinesin Light Chain 1. J. Biol. Chem. 278, 22946–22955.

Israel, M.A., Yuan, S.H., Bardy, C., Reyna, S.M., Mu, Y., Herrera, C., Hefferan, M.P., Van Gorp, S., Nazor, K.L., Boscolo, F.S., Carson, C.T., Laurent, L.C., Marsala, M., Gage, F.H., Remes, A.M., Koo, E.H., Goldstein, L.S.B., 2012. Probing Sporadic and Familial Alzheimer's Disease using Induced Pluripotent Stem Cells. Nature 482, 216–220.

Ittner, L.M., Götz, J., 2011. Amyloid-β and Tau - A Toxic Pas de Deux in Alzheimer's Disease. Nat. Rev. Neurosci. 12, 67–72.

Jarrett, J.T., Berger, E.P., Lansbury, P.T., 1993. The Carboxy Terminus of the β Amyloid Protein is Critical for the Seeding of Amyloid Formation: Implications for the Pathogenesis of Alzheimer's Disease. Biochemistry 32, 4693–4697.

Jellinger, K., Attems, J., 2010. Prevalence of Dementia Disorders in the Oldest-Old: An Autopsy Study. Acta Neuropathol. 119, 421–433.

Jonsson, T., Atwal, J.K., Steinberg, S., Snaedal, J., Jonsson, P. V., Bjornsson, S., Stefansson, H., Sulem, P., Gudbjartsson, D., Maloney, J., Hoyte, K., Gustafson, A., Liu, Y., Lu, Y., Bhangale, T., Graham, R.R., Huttenlocher, J., Bjornsdottir, G., Andreassen, O.A., Jönsson, E.G., Palotie, A., Behrens, T.W., Magnusson, O.T., Kong, A., Thorsteinsdottir, U., Watts, R.J., Stefansson, K., 2012. A Mutation in APP Protects Against Alzheimer's Disease and Age-Related Cognitive Decline. Nature 488, 96–99.

Jowsey, P.A., Blain, P.G., 2015. Fe65 Ser228 is Phosphorylated by ATM/ATR and Inhibits Fe65-APP-Mediated Gene Transcription. Biochem. J. 465, 413–421.

Kaidanovich-Beilin, O., Woodgett, J.R., 2011. GSK-3: Functional Insights from Cell Biology and Animal Models. Front. Mol. Neurosci. 4, 1–25.

Kajiwara, Y., Akram, A., Katsel, P., Haroutunian, V., Schmeidler, J., Beecham, G., Haines, J.L., Pericak-Vance, M.A., Buxbaum, J.D., 2009. FE65 Binds Teashirt, Inhibiting Expression of the Primate-Specific Caspase-4. PLoS One 4, e5071.

Kang, H.J., Schuman, E.M., 1995. Neurotrophin-Induced Modulation of Synaptic Transmission in the Adult Hippocampus. J. Physiol. Paris 89, 11–22.

Kang, J., Lemaire, H.G., Unterbeck, A., Salbaum, J.M., Masters, C.L., Grzeschik, K.H., Multhaup, G., Beyreuther, K., Müller-Hill, B., 1987. The Precursor of Alzheimer's Disease Amyloid A4 Protein Resembles a Cell-Surface Receptor. Nature.

Kaplan, D.R., Miller, F.D., 2000. Neurotrophin Signal Transduction in the Nervous System. Curr. Opin. Neurobiol. 10, 381–391.

Karch, C.M., Cruchaga, C., Goate, A.M., 2014. Alzheimer's Disease Genetics: From the Bench to the Clinic. Neuron 83, 11–26.

Karch, C.M., Goate, A.M., 2015. Alzheimer's Disease Risk Genes and Mechanisms of Disease Pathogenesis. Biol. Psychiatry 77, 43–51.

Karran, E., De Strooper, B., 2016. The Amyloid Cascade Hypothesis: Are We Poised for Success or Failure? J. Neurochem. 10.1111/jnc.13632.

Kells, A.P., Fong, D.M., Dragunow, M., During, M.J., Young, D., Connor, B., 2004. AAV-Mediated Gene Delivery of BDNF or GDNF is Neuroprotective in a Model of Huntington Disease. Mol. Ther. 9, 682–688.

Kesavapany, S., Banner, S.J., Lau, K.-F., Shaw, C.E., Miller, C.C.J., Cooper, J.D., McLoughlin, D.M., 2002. Expression of the Fe65 Adapter Protein in Adult and Developing Mouse Brain. Neuroscience 115, 951–960.

Kessels, M.M., Schwintzer, L., Schlobinski, D., Qualmann, B., 2011. Controlling Actin Cytoskeletal Organization and Dynamics During Neuronal Morphogenesis. Eur. J. Cell Biol. 90, 926–933. doi:10.1016/j.ejcb.2010.08.011

Killick, R., Ribe, E.M., Al-Shawi, R., Malik, B., Hooper, C., Fernandes, C., Dobson, R., Nolan, P.M., Lourdusamy, A., Furney, S., Lin, K., Breen, G., Wroe, R., To,

A.W.M., Leroy, K., Causevic, M., Usardi, A., Robinson, M., Noble, W., Williamson, R., Lunnon, K., Kellie, S., Reynolds, C.H., Bazenet, C., Hodges, A., Brion, J.-P., Stephenson, J., Simons, J.P., Lovestone, S., 2014. Clusterin Regulates β-Amyloid Toxicity via Dickkopf-1-Driven Induction of the Wnt-PCP-JNK Pathway. Mol. Psychiatry 19, 88–98.

Kim, H., Kim, E., Lee, J., Park, C.H., Kim, S., 2003. C-Terminal Fragments of Amyloid Precursor Protein Exert Neurotoxicity by Inducing Glycogen Synthase Kinase-3β Expression. FASEB J. 17, 1951–1953.

Kim, J., Basak, J.M., Holtzman, D.M., 2009. The Role of Lipoprotein E in Alzheimer's Disease. Neuron 63, 287–303.

Kim, M.Y., Mo, J.S., Ann, E.J., Yoon, J.H., Park, H.S., 2012. Dual Regulation of Notch1 Signaling Pathway by Adaptor Protein Fe65. J. Biol. Chem. 287, 4690–4701.

Kimberly, W.T., Zheng, J.B., Guénette, S.Y., Selkoe, D.J., 2001. The Intracellular Domain of the β-Amyloid Precursor Protein is Stabilized by Fe65 and Translocates to the Nucleus in a Notch-Like Manner. J. Biol. Chem. 276, 40288–40292.

Kimberly, W.T., Zheng, J.B., Town, T., Flavell, R.A., Selkoe, D.J., 2005. Physiological Regulation of the β-Amyloid Precursor Protein Signaling Domain by c-Jun N-Terminal Kinase JNK3 during Neuronal Differentiation. J. Neurosci. 25, 5533–5543.

Kimelman, D., Xu, W., 2006. β-Catenin Destruction Complex: Insights and Questions From a Structural Perspective. Oncogene 25, 7482–7491.

Kinoshita, A., Shah, T., Tangredi, M.M., Strickland, D.K., Hyman, B.T., 2003. The Intracellular Domain of the Low Density Lipoprotein Receptor-Related Protein Modulates Transactivation Mediated by Amyloid Precursor Protein and Fe65. J. Biol. Chem. 278, 41182–41188.

Kinoshita, A., Whelan, C.M., Smith, C.J., Berezovska, O., Hyman, B.T., 2002. Direct Visualization of the Gamma Secretase-Generated Carboxyl-Terminal Domain of the Amyloid Precursor Protein: Association with Fe65 and Translocation to the Nucleus. J. Neurochem. 82, 839–847.

Kinoshita, A., Whelan, C.M., Smith, C.J., Mikhailenko, I., Rebeck, G.W., Strickland, D.K., Hyman, B.T., 2001. Demonstration by Fluorescence Resonance Energy Transfer of Two Sites of Interaction Between the Low-Density Lipoprotein Receptor-Related Protein and the Amyloid Precursor Protein: Role of the Intracellular Adapter Protein Fe65. J. Neurosci. 21, 8354–8361.

Kitaguchi, N., Takahashi, Y., Tokushima, Y., Shiojiri, S., Ito, H., 1988. Novel Precursor of Alzheimer's Disease Amyloid Protein Shows Protease Inhibitory Activity. Nature 331, 530–532.

Knüsel, B., Beck, K.D., Winslow, J.W., Rosenthal, A., Burton, L.E., Widmer, H.R., Nikolics, K., Hefti, F., 1992. Brain-Derived Neurotrophic Factor Administration Protects Basal Forebrain Cholinergic but not Nigral Dopaminergic Neurons from Degenerative Changes after Axotomy in the Adult Rat Brain. J. Neurosci. 12, 4391–4402.

Knüsel, B., Hefti, F., 1992. K-252 Compounds: Modulators of Neurotrophin Signal Transduction. J. Neurochem. 59, 1987–96.

Koike, M.A., Lin, A.J., Pham, J., Nguyen, E., Yeh, J.J., Rahimian, R., Tromberg, B.J., Choi, B., Green, K.N., LaFerla, F.M., 2012. APP Knockout Mice Experience Acute Mortality as the Result of Ischemia. PLoS One 7, e42665.

Koo, E.H., Park, L., Selkoe, D.J., 1993. Amyloid β-Protein as a Substrate Interacts with Extracellular Matrix to Promote Neurite Outgrowth. Proc. Natl. Acad. Sci. 90, 4748–4752.

Koo, E.H., Sisodia, S.S., Archer, D.R., Martin, L.., Weidemann, A., Beyreuther, K., Fischer, P., Masters, C.L., Price, D.L., 1990. Precursor of Amyloid Protein in Alzheimer Disease Undergoes Fast Anterograde Axonal Transport. Proc. Natl. Acad. Sci. 87, 1561–1565.

Kopan, R., Ilagan, M.X.G., 2009. The Canonical Notch Signaling Pathway: Unfolding the Activation Mechanism. Cell 137, 216–233.

Korte, M., Carroll, P., Wolf, E., Brem, G., Thoenen, H., Bonhoeffer, T., 1995. Hippocampal Long-Term Potentiation is Impaired in Mice Lacking Brain-Derived Neurotrophic Factor. Proc. Natl. Acad. Sci. 92, 8856–8860.

Kuhn, P.-H., Wang, H., Dislich, B., Colombo, A., Zeitschel, U., Ellwart, J.W., Kremmer, E., Rossner, S., Lichtenthaler, S.F., 2010. ADAM10 is the Physiologically Relevant, Constitutive α-Secretase of the Amyloid Precursor Protein in Primary Neurons. EMBO J. 29, 3020–3032.

Kwon, O.Y., Hwang, K., Kim, J.A., Kim, K., Kwon, I.C., Song, H.K., Jeon, H., 2010. Dab1 Binds to Fe65 and Diminishes the Effect of Fe65 or LRP1 on APP Processing. J. Cell. Biochem. 111, 508–519.

Lambert, J.-C., 2013. Meta-Analysis of 74,046 Individuals Identifies 11 New Susceptibility Loci for Alzheimer's Disease. Nat. Genet. 45, 1452–1458.

Lau, C.G., Zukin, R.S., 2007. NMDA Receptor Trafficking in Synaptic Plasticity and Neuropsychiatric Disorders. Nat. Rev. Neurosci. 8, 413–426.

Lau, K.-F., Chan, W.M., Perkinton, M.S., Tudor, E.L., Chang, R.C.C., Chan, H.Y.E., McLoughlin, D.M., Miller, C.C.J., 2008. Dexras1 Interacts with FE65 to Regulate FE65-Amyloid Precursor Protein-Dependent Transcription. J. Biol. Chem. 283, 34728–34737.

Lau, K.-F., Howlett, D.R., Kesavapany, S., Standen, C.L., Dingwall, C., McLoughlin,

D.M., Miller, C.C.J., 2002. Cyclin-Dependent Kinase-5/p35 Phosphorylates Presenilin 1 to Regulate Carboxy-Terminal Fragment Stability. Mol. Cell. Neurosci. 20, 13–20.

Lau, K.-F., McLoughlin, D.M., Standen, C., Miller, C.C., 2000a. X11α and x11β Interact with Presenilin-1 via their PDZ Domains. Mol. Cell. Neurosci. 16, 557–565.

Lau, K.-F., McLoughlin, D.M., Standen, C.L., Irving, N.G., Miller, C.C.J., 2000b. Fe65 and X11β Co-localize with and Compete for Binding to the Amyloid Precursor Protein. Neuroreport 11, 3607–3610.

Lee, E.J., Chun, J., Hyun, S., Ahn, H.R., Jeong, J.M., Hong, S.-K., Hong, J.T., Chang, I.K., Jeon, H.Y., Han, Y.S., Auh, C.-K., Park, J.I., Kang, S.S., 2008a. Regulation Fe65 Localization to the Nucleus by SGK1 Phosphorylation of its Ser566 Residue. BMB Rep. 41, 41–47.

Lee, E.J., Hyun, S., Chun, J., Shin, S.H., Lee, K.E., Yeon, K.H., Park, T.Y., Kang, S.S., 2008b. The PPLA Motif of Glycogen Synthase Kinase 3β is Required for Interaction with Fe65. Mol. Cells 26, 100–105.

Lee, K.J., Moussa, C.E.H., Lee, Y., Sung, Y., Howell, B.W., Turner, R.S., Pak, D.T.S., Hoe, H.S., 2010. Beta Amyloid-Independent Role of Amyloid Precursor Protein in Generation and Maintenance of Dendritic Spines. Neuroscience 169, 344–356.

Lee, M.S., Kao, S.C., Lemere, C.A., Xia, W., Tseng, H.C., Zhou, Y., Neve, R., Ahlijanian, M.K., Tsai, L.H., 2003. APP Processing is Regulated by Cytoplasmic Phosphorylation. J. Cell Biol. 163, 83–95.

Lee, V.M.-Y., Goedert, M., Trojanowski, J.Q., 2001. Neurodegenerative Tauopathies. Annu. Rev. Neurosci. 24, 1121–1159.

Leissring, M.A., Murphy, M.P., Mead, T.R., Akbari, Y., Sugarman, M.C., Jannatipour, M., Anliker, B., Müller, U., Saftig, P., De Strooper, B., Wolfe, M.S., Golde, T.E., LaFerla, F.M., 2002. A Physiologic Signaling Role for the γ-Secretase-Derived Intracellular Fragment of APP. Proc. Natl. Acad. Sci. 99, 4697–4702.

Leyhe, T., Stransky, E., Eschweiler, G.W., Buchkremer, G., Laske, C., 2008. Increase of BDNF Serum Concentration During Donepezil Treatment of Patients with Early Alzheimer's Disease. Eur. Arch. Psychiatry Clin. Neurosci. 258, 124–128.

Li, H., Koshiba, S., Hayashi, F., Tochio, N., Tomizawa, T., Kasai, T., Yabuki, T., Motoda, Y., Harada, T., Watanabe, S., Inoue, M., Hayashizaki, Y., Tanaka, A., Kigawa, T., Yokoyama, S., 2008. Structure of the C-Terminal Phosphotyrosine Interaction Domain of FE65L1 Complexed with the Cytoplasmic Tail of Amyloid Precursor Protein Reveals a Novel Peptide Binding Mode. J. Biol. Chem. 283, 27165–27178.

Li, H., Wang, B., Wang, Z., Guo, Q., Tabuchi, K., Hammer, R.E., Südhof, T.C., Zheng, H., 2010. Soluble Amyloid Precursor Protein (APP) Regulates Transthyretin and

Klotho Gene Expression Without Rescuing the Essential Function of APP. Proc. Natl. Acad. Sci. 107, 17362–17367.

Li, Q., Lau, A., Morris, T.J., Guo, L., Fordyce, C.B., Stanley, E.F., 2004. A Syntaxin 1, Gαo, and N-Type Calcium Channel Complex at a Presynaptic Nerve Terminal: Analysis by Quantitative Immunocolocalization. J. Neurosci. 24, 4070–4081. doi:10.1523/JNEUROSCI.0346-04.2004

Lindholm, D., Carroll, P., Tzimagiogis, G., Thoenen, H., 1996. Autocrine-Paracrine Regulation of Hippocampal Neuron Survival by IGF-1 and the Neurotrophins BDNF, NT-3 and NT-4. Eur. J. Neurosci. 8, 1452–1460.

Liu, F., Su, Y., Li, B., Zhou, Y., Ryder, J., Gonzalez-dewhitt, P., May, P.C., Ni, B., 2003. Regulation of Amyloid Precursor Protein (APP) Phosphorylation and Processing by p35/Cdk5 and p25/Cdk5. FEBS Lett. 547, 193–196.

Liu, Y., Liu, F., Grundke-iqbal, I., Iqbal, K., Gong, C., 2011. Deficient Brain Insulin Signalling Pathway in Alzheimer's Disease and Diabetes. J. Pathol. 225, 54–62.

Livak, K.J., Schmittgen, T.D., 2001. Analysis of Relative Gene Expression Data Using Real-Time Quantitative PCR and the 2-ΔΔCT Method. Methods 25, 402–408.

Logan, C., Nusse, R., 2004. The Wnt Signaling Pathway in Development and Disease. Annu. Rev. Cell Dev. Biol. 20, 781–810.

Ma, Q.-H., Futagawa, T., Yang, W.-L., Jiang, X.-D., Zeng, L., Takeda, Y., Xu, R.-X., Bagnard, D., Schachner, M., Furley, A.J., Karagogeos, D., Watanabe, K., Dawe, G.S., Xiao, Z.-C., 2008. A TAG1-APP Signalling Pathway Through Fe65 Negatively Modulates Neurogenesis. Nat. Cell Biol. 10, 283–294.

MacDonald, B.T., Tamai, K., He, X., 2009. Wnt/β-Catenin Signaling: Components, Mechanisms, and Diseases. Dev. Cell 17, 9–26.

Marquez-Sterling, N.R., Lo, A.C., Sisodia, S.S., Koo, E.H., 1997. Trafficking of Cell-Surface β-Amyloid Precursor Protein: Evidence that A Sorting Intermediate Participates in Synaptic Vesicle Recycling. J. Neurosci. 17, 140–151.

Masin, M., Kerschensteiner, D., Dümke, K., Rubio, M.E., Soto, F., 2006. Fe65 Interacts with P2X2 Subunits at Excitatory Synapses and Modulates Receptor Function. J. Biol. Chem. 281, 4100–4108.

Matrone, C., Barbagallo, A.P.M., La Rosa, L.R., Florenzano, F., Ciotti, M.T., Mercanti, D., Chao, M.V., Calissano, P., D'Adamio, L., 2011. APP is Phosphorylated by TrkA and Regulates NGF/TrkA Signaling. J. Neurosci. 31, 11756–11761.

Matrone, C., Ciotti, M.T., Mercanti, D., Marolda, R., Calissano, P., 2008. NGF and BDNF Signaling Control Amyloidogenic Route and Aβ Production in Hippocampal Neurons. Proc. Natl. Acad. Sci. 105, 13139–13144.

Matsuda, S., Yasukawa, T., Homma, Y., Ito, Y., Niikura, T., Hiraki, T., Hirai, S., Ohno, S., Kita, Y., Kawasumi, M., Kouyama, K., Yamamoto, T., Kyriakis, J.M.,

Nishimoto, I., 2001. c-Jun N-terminal (JNK)-Interacting Protein-1b/Islet-Bran-1 Scaffolds Alzheimer's Amyloid Precursor Protein with JNK. J. Neurosci. 21, 6597–6607.

McCaulley, M.E., Grush, K.A., 2015. Alzheimer's Disease: Exploring the Role of Inflammation and Implications for Treatment. Int. J. Alzheimers. Dis. 2015.

Mcloughlin, D.M., Irving, N.G., Brownlees, J., Brion, J., Leroy, K., Miller, C.C.J., 1999. Mint2/X11-Like Colocalizes with the Alzheimer's Disease Amyloid Precursor Protein and is Associated with Neuritic Plaques in Alzheimer's Disease. Eur. J. Neurosci. 11, 1988–1994.

McLoughlin, D.M., Miller, C.C.J., 2008. The FE65 Proteins and Alzheimer's Disease. J. Neurosci. Res. 86, 744–754.

McLoughlin, D.M., Miller, C.C.J., 1996. The Intracellular Cytoplasmic Domain of the Alzheimer's Disease Amyloid Precursor Protein Interacts with Phosphotyrosine-Binding Domain Proteins in the Yeast Two-Hybrid System. FEBS Lett. 397, 197–200.

Meng, C., He, Z., Xing, D., 2013. Low-Level Laser Therapy Rescues Dendrite Atrophy via Upregulating BDNF Expression: Implications for Alzheimer's Disease. J. Neurosci. 33, 13505–13517.

Metcalfe, C., Bienz, M., 2011. Inhibition of GSK3 by Wnt Signalling - Two Contrasting Models. J. Cell Sci. 124, 3537–3544.

Meyer-Luehmann, M., Spires-Jones, T.L., Prada, C., Garcia-Alloza, M., de Calignon, A., Rozkalne, A., Koenigsknecht-Talboo, J., Holtzman, D.M., Bacskai, B.J., Hyman, B.T., 2008. Rapid Appearance and Local Toxicity of Amyloid-β Plaques in a Mouse Model of Alzheimer's Disease. Nature 451, 720–724.

Mi, H., Poudel, S., Muruganujan, A., Casagrande, J.T., Thomas, P.D., 2016. PANTHER Version 10: Expanded Protein Families and Functions, and Analysis Tools. Nucleic Acids Res. 44, D336–D342.

Milward, E.A., Papadopoulos, R., Fuller, S.J., Moir, R.D., Small, D., Beyreuther, K., Masters, C.L., 1992. The Amyloid Protein Precursor of Alzheimer's Disease is a Mediator of the Effects of Nerve Growth Factor on Neurite Outgrowth. Neuron 9, 129–137.

Minopoli, G., De Candia, P., Bonetti, A., Faraonio, R., Zambrano, N., Russo, T., 2001. The β-Amyloid Precursor Protein Functions as a Cytosolic Anchoring Site That Prevents Fe65 Nuclear Translocation. J. Biol. Chem. 276, 6545–6550.

Minopoli, G., Gargiulo, A., Parisi, S., Russo, T., 2012. Fe65 Matters: New Light on an Old Molecule. IUBMB Life 64, 936–942.

Minopoli, G., Stante, M., Napolitano, F., Telese, F., Aloia, L., De Felice, M., Di Lauro, R., Pacelli, R., Brunetti, A., Zambrano, N., Russo, T., 2007. Essential Roles for

Fe65, Alzheimer Amyloid Precursor-Binding Protein, in the Cellular Response to DNA Damage. J. Biol. Chem. 282, 831–835.

Moghbelinejad, S., Nassiri-Asl, M., Naserpour Farivar, T., Abbasi, E., Sheikhi, M., Taghiloo, M., Farsad, F., Samimi, A., Hajiali, F., 2014. Rutin Activates the MAPK Pathway and BDNF Gene Expression on Beta-Amyloid Induced Neurotoxicity in Rats. Toxicol. Lett. 224, 108–113.

Morris, J.C., Storandt, M., McKeel, D.W., Rubin, E.H., Price, J.L., Grant, E.A., Berg, L., 1996. Cerebral Amyloid Deposition and Diffuse Plaques in "Normal'' Aging: Evidence for Presymptomatic and Very Mild Alzheimer's Disease. Neurology 46, 707–719.

Moya, K.L., Benowitz, L.I., Schneider, G.E., Allinquant, B., 1994. The Amyloid Precursor Protein is Developmentally Regulated and Correlated with Synaptogenesis. Dev. Biol.

Mueller, H.T., Borg, J.P., Margolis, B., Turner, R.S., 2000. Modulation of Amyloid Precursor Protein Metabolism by X11α/Mint-1. J. Biol. Chem. 275, 39302–39306.

Müller, T., Concannon, C.G., Ward, M.W., Walsh, C.M., Tirniceriu, A.L., Tribl, F., Kögel, D., Prehn, J.H.M., Egensperger, R., 2007. Modulation of Gene Expression and Cytoskeletal Dynamics by the Amyloid Precursor Protein Intracellular Domain (AICD). Mol. Biol. Cell 18, 201–210.

Müller, T., Schrötter, A., Loosse, C., Pfeiffer, K., Theiss, C., Kauth, M., Meyer, H.E., Marcus, K., 2013. A Ternary Complex Consisting of AICD, FE65, and TIP60 Down-Regulates Stathmin1. Biochim. Biophys. Acta 1834, 387–394.

Müller, U.C., Zheng, H., 2012. Physiological Functions of APP Family Proteins. Cold Spring Harb. Perspect. Med. 4, a006288.

Mulvihill, M.M., Guttman, M., Komives, E.A., 2011. Protein Interactions Among Fe65, the Low-Density Lipoprotein Receptor-Related Protein, and the Amyloid Precursor Protein. Biochemistry 50, 6208–6216.

Murer, M.G., Boissiere, F., Yan, Q., Hunot, S., Villares, J., Faucheux, B., Agid, Y., Hirsch, E., Raisman-Vozari, R., 1999. An Immunohistochemical Study of the Distribution of Brain-Derived Neurotrophic Factor in the Adult Human Brain, with Particular Reference to Alzheimer’s Disease. Neuroscience 88, 1015–1032.

Muresan, Z., Muresan, V., 2005. Coordinated Transport of Phosphorylated Amyloid-β Precursor Protein and c-Jun NH2-Terminal Kinase-Interacting Protein-1. J. Cell Biol. 171, 615–625.

Murray, K.D., Gall, C.M., Jones, E.G., Isackson, P.J., 1994. Differential Regulation of Brain-Derived Neurotrophic Factor and Type II Calcium/Calmodulin-Dependent Protein Kinase Messenger RNA Expression in Alzheimer’s Disease. Neuroscience 60, 37–48.

Nagahara, A.H., Mateling, M., Kovacs, I., Wang, L., Eggert, S., Rockenstein, E., Koo, E.H., Masliah, E., Tuszynski, M.H., 2013. Early BDNF Treatment Ameliorates Cell Loss in the Entorhinal Cortex of APP Transgenic Mice. J Neurosci 33, 15596–15602.

Nagahara, A.H., Merrill, D. a, Coppola, G., Tsukada, S., Brock, E., Shaked, G.M., Wang, L., Blesch, A., Kim, A., James, M., Rockenstein, E., Chao, M. V, Koo, E.H., Geschwind, D., Masliah, E., Chiba, A. a, Tuszynski, M.H., 2009. Neuroprotective Effects of Brain-Derived Neurotrophic Factor in Rodent and Primate Models of Alzheimer's Disease. Nat. Med. 15, 331–337.

Naj, A.C., Jun, G., Beecham, G.W., Wang, L., Narayan, B., Buros, J., Gallins, P.J., Buxbaum, J.D., Jarvik, G.P., Crane, P.K., Larson, E.B., Bird, T.D., Boeve, B.F., Graff-, N.R., 2011. Common Variants in MS4A4/MS4A6E, CD2uAP, CD33, and EPHA1 are Associated with Late-Onset Alzheimer's Disease. Nat. Genet. 43, 436–441.

Nakajima, H., Kubo, T., Semi, Y., Itakura, M., Kuwamura, M., Izawa, T., Azuma, Y.T., Takeuchi, T., 2012. A Rapid, Targeted, Neuron-Selective, In Vivo Knockdown Following a Single Intracerebroventricular Injection of a Novel Chemically Modified siRNA in the Adult Rat Brain. J. Biotechnol. 157, 326–333.

Nakaya, T., Kawai, T., Suzuki, T., 2008. Regulation of FE65 Nuclear Translocation and Function by Amyloid β-Protein Precursor in Osmotically Stressed Cells. J. Biol. Chem. 283, 19119–19131.

Nakaya, T., Suzuki, T., 2006. Role of APP Phosphorylation in FE65-Dependent Gene Transactivation Mediated by AICD. Genes to Cells 11, 633–645.

Narisawa-Saito, M., Wakabayashi, K., Tsuji, S., Takahashi, H., Nawa, H., 1996. Regional Specificity of Alterations in NGF, BDNF and NT-3 Levels in Alzheimer's Disease. Clin. Neurosci. Neuropathol. 7, 2925–2928.

Nensa, F.M., Neumann, M.H.D., Schrötter, A., Przyborski, A., Mastalski, T., Susdalzew, S., Looβe, C., Helling, S., El Magraoui, F., Erdmann, R., Meyer, H.E., Uszkoreit, J., Eisenacher, M., Suh, J., Guénette, S.Y., Röhner, N., Kögel, D., Theiss, C., Marcus, K., Müller, T., 2014. Amyloid Beta A4 Precursor Protein-Binding Family B Member 1 (FE65) Interactomics Revealed Synaptic Vesicle Glycoprotein 2A (SV2A) and Sarcoplasmic/Endoplasmic Reticulum Calcium ATPase 2 (SERCA2) as New Binding Proteins in the Human Brain. Mol. Cell. Proteomics 13, 475–488.

Nguyen, N., Lee, S.B., Lee, Y.S., Lee, K.H., Ahn, J.Y., 2009. Neuroprotection by NGF and BDNF Against Neurotoxin-Exerted Apoptotic Death in Neural Stem Cells are Mediated Through TRK Receptors, Activating PI3-Kinase and MAPK Pathways. Neurochem. Res. 34, 942–951.

Niehrs, C., 2012. The Complex World of WNT Receptor Signalling. Nat. Rev. Mol. Cell Biol. 13, 767–779.

Nishimura, M., Yu, G., Levesque, G., Zhang, D.M., Ruel, L., Chen, F., Milman, P., Holmes, E., Liang, Y., Kawarai, T., Jo, E., Supala, A., Rogaeva, E., Xu, D.M., Janus, C., Levesque, L., Bi, Q., Duthie, M., Rozmahel, R., Mattila, K., Lannfelt, L., Westaway, D., Mount, H.T., Woodgett, J., Fraser, P.E., St George-Hyslop, P., 1999. Presenilin Mutations Associated with Alzheimer Disease Cause Defective Intracellular Trafficking of β-Catenin, a Component of the Presenilin Protein Complex. Nat. Med. 5, 164–169.

Nizzari, M., Venezia, V., Repetto, E., Caorsi, V., Magrassi, R., Gagliani, M.C., Carlo, P., Florio, T., Schettini, G., Tacchetti, C., Russo, T., Diaspro, A., Russo, C., 2007. Amyloid Precursor Protein and Presenilin1 Interact with the Adaptor GRB2 and Modulate ERK1,2 Signaling. J. Biol. Chem. 282, 13833–13844.

Noble, W., Hanger, D.P., Miller, C.C.J., Lovestone, S., 2013. The Importance of Tau Phosphorylation for Neurodegenerative Diseases. Front. Neurol. 4, 1–11.

Numakawa, T., Suzuki, S., Kumamaru, E., Adachi, N., Richards, M., Kunugi, H., 2010. BDNF Function and Intracellular Signaling in Neurons. Histol. Histopathol. 25, 237–258.

Ohmichi, M., Decker, S.J., Pang, L., Saltiel, A.R., 1992. Inhibition of the Cellular Actions of Nerve Growth Factor by Staurosporine and K252A Results from the Attenuation of the Activity of the Trk Tyrosine Kinase. Biochemistry 31, 4034–4039.

Ohsawa, I., Takamura, C., Morimoto, T., Ishiguro, M., Kohsaka, S., 1999. Amino-Terminal Region of Secreted Form of Amyloid Precursor Protein Stimulates Proliferation of Neural Stem Cells. Eur. J. Neurosci. 11, 1907–1913.

Oltersdorf, T., Fritz, L.C., Schenk, D.B., Lieberburg, I., Johnson-Wood, K.L., Beattie, E.C., Ward, P.J., Blacher, R.W., Dovey, H.F., Sinha, S., 1989. The Secreted Form of the Alzheimer's Amyloid Precursor Protein with the Kunitz Domain is Protease Nexin-II. Nature 341, 144–147.

Pardossi-Piquard, R., Petit, A., Kawarai, T., Sunyach, C., Da Costa, C.A., Vincent, B., Ring, S., D'Adamio, L., Shen, J., Müller, U., Hyslop, P.S.G., Checler, F., 2005. Presenilin-Dependent Transcriptional Control of the Aβ-Degrading Enzyme Neprilysin by Intracellular Domains of βAPP and APLP. Neuron 46, 541–554.

Patapoutian, A., Reichardt, L.F., 2001. Trk Receptors: Mediators of Neurotrophin Action. Curr. Opin. Neurobiol. 11, 272–280.

Patterson, S.L., Abel, T., Deuel, T.A.S., Martin, K.C., Rose, J.C., Kandel, E.R., 1996. Recombinant BDNF Rescues Deficits in Basal Synaptic Transmission and Hippocampal LTP in BDNF Knockout Mice. Neuron 16, 1137–1145.

Perkinton, M.S., Standen, C.L., Lau, K.-F., Kesavapany, S., Byers, H.L., Ward, M., McLoughlin, D.M., Miller, C.C.J., 2004. The c-Abl Tyrosine Kinase Phosphorylates the Fe65 Adaptor Protein to Stimulate Fe65/Amyloid Precursor Protein Nuclear Signaling. J. Biol. Chem. 279, 22084–22091.

Petersen, L.C., Bjorn, S.E., Norris, F., Norris, K., Sprecher, C., Foster, D.C., 1994. Expression, Purification and Characterization of a Kunitz-Type Protease Inhibitor Domain from Human Amyloid Precursor Protein Homolog. FEBS Lett 338, 53–57. doi:0014-5793(94)80115-0 [pii]

Phillips, H.S., Hains, J.M., Armanini, M., Laramee, G.R., Johnson, S.A., Winslow, J.W., 1991. BDNF mRNA is Decreased in the Hippocampus of Individuals with Alzheimer's Disease. Neuron 7, 695–702.

Phillips, H.S., Hains, J.M., Laramee, G.R., Rosenthal, A., Winslow, J.W., 1990. Widespread Expression of BDNF but not NT3 by Target Areas of Basal Forebrain Cholinergic Neurons. Science (80-.). 250, 290–294.

Pietrzik, C.U., Yoon, I.-S., Jaeger, S., Busse, T., Weggen, S., Koo, E.H., 2004. FE65 Constitutes the Functional Link between the Low-Density Lipoprotein Receptor-Related Protein and the Amyloid Precursor Protein. J. Neurosci. 24, 4259–4265.

Pike, C.J., Cummings, B.J., Cotman, C.W., 1995. Early Association of Reactive Astrocytes with Senile Plaques in Alzheimer's Disease. Exp. Neurol. 132, 172–179.

Pláteník, J., Fišar, Z., Buchal, R., Jirák, R., Kitzlerová, E., Zvěřová, M., Raboch, J., 2014. GSK3β, CREB, and BDNF in Peripheral Blood of Patients with Alzheimer's Disease and Depression. Prog. Neuropsychopharmacol. Biol. Psychiatry 50, 83–93.

Ponte, P., Gonzalez-DeWhitt, P., Schilling, J., Miller, J., Hsu, D., Greenberg, B., Davis, K., Wallace, W., Lieberburg, I., Fuller, F., 1988. A New A4 Amyloid mRNA Contains a Domain Homologous to Serine Proteinase Inhibitors. Nature 331, 525–527.

Priller, C., Bauer, T., Mitteregger, G., Krebs, B., Kretzschmar, H.A., Herms, J., 2006. Synapse Formation and Function Is Modulated by the Amyloid Precursor Protein. J. Neurosci. 26, 7212–7221.

Purro, S.A., Dickins, E.M., Salinas, P.C., 2012. The Secreted Wnt Antagonist Dickkopf-1 Is Required for Amyloid β-Mediated Synaptic Loss. J. Neurosci. 32, 3492–3498.

Purro, S.A., Galli, S., Salinas, P.C., 2014. Dysfunction of Wnt Signaling and Synaptic Disassembly in Neurodegenerative Diseases. J. Mol. Cell Biol. 6, 75–80.

Qiu, W.Q., Ferreira, A., Miller, C., Koo, E.H., Selkoe, D.J., 1995. Cell-Surface β-Amyloid Precursor Protein Stimulates Neurite Outgrowth of Hippocampal Neurons in an Isoform-Dependent Manner. J. Neurosci. 15, 2157–2167.

Rebelo, S., Domingues, S.C., Santos, M., Fardilha, M., Esteves, S.L.C., Vieira, S.I., Vintém, A.P.B., Wu, W., Da Cruz E Silva, E.F., Da Cruz E Silva, O.A.B., 2013. Identification of a Novel Complex AβPP:Fe65:PP1 that Regulates AβPP Thr668 Phosphorylation Levels. J. Alzheimer's Dis. 35, 761–775.

Rebelo, S., Vieira, S.I., Esselmann, H., Wiltfang, J., da Cruz E Silva, E.F., Da Cruz E Silva, O.A.B., 2007. Tyr687 Dependent APP Endocytosis and Abeta Production. J. Mol. Neurosci. 31, 1–8. doi:10.1007/s

Richardson, J.A., Burns, D.K., 2002. Mouse Models of Alzheimer's Disease: A Quest for Plaques. ILAR J. 43, 89–99.

Robakis, N.K., Ramakrishna, N., Wolfe, G., Wisniewski, H.M., 1987. Molecular Cloning and Characterization of a cDNA Encoding the Cerebrovascular and the Neuritic Plaque Amyloid Peptides. Proc. Natl. Acad. Sci. 84, 4190–4194.

Robinson, A., Grösgen, S., Mett, J., Zimmer, V.C., Haupenthal, V.J., Hundsdörfer, B., Stahlmann, C.P., Slobodskoy, Y., Müller, U.C., Hartmann, T., Stein, R., Grimm, M.O.W., 2014. Upregulation of PGC-1α Expression by Alzheimer's Disease-Associated Pathway: Presenilin 1/Amyloid Precursor Protein (APP)/Intracellular Domain of APP. Aging Cell 13, 263–272.

Rogelj, B., Mitchell, J.C., Miller, C.C.J., McLoughlin, D.M., 2006. The X11/Mint Family of Adaptor Proteins. Brain Res. Rev. 52, 305–315.

Roher, a E., Lowenson, J.D., Clarke, S., Woods, a S., Cotter, R.J., Gowing, E., Ball, M.J., 1993. β-Amyloid-(1-42) is a Major Component of Cerebrovascular Amyloid Deposits: Implications for the Pathology of Alzheimer Disease. Proc. Natl. Acad. Sci. 90, 10836–10840.

Rovelet-Lecrux, A., Hannequin, D., Raux, G., Le Meur, N., Laquerrière, A., Vital, A., Dumanchin, C., Feuillette, S., Brice, A., Vercelletto, M., Dubas, F., Frebourg, T., Campion, D., 2006. APP Locus Duplication Causes Autosomal Dominant Early-Onset Alzheimer Disease with Cerebral Amyloid Angiopathy. Nat. Genet. 38, 24–26.

Russo, C., Dolcini, V., Salis, S., Venezia, V., Zambrano, N., Russo, T., Schettini, G., 2002. Signal Transduction Through Tyrosine-Phosphorylated C-Terminal Fragments of Pmyloid Precursor Protein via an Enhanced Interaction with Shc/Grb2 Adaptor Proteins in Reactive Astrocytes of Alzheimer's Disease Brain. J. Biol. Chem. 277, 35282–35288.

Russo, C., Venezia, V., Repetto, E., Nizzari, M., Violani, E., Carlo, P., Schettini, G., 2005. The Amyloid Precursor Protein and its Network of Interacting Proteins: Physiological and Pathological Implications. Brain Res. Rev. 48, 257–264.

Ryan, K.A., Pimplikar, S.W., 2005. Activation of GSK-3 and Phosphorylation of CRMP2 in Transgenic Mice Expressing APP Intracellular Domain. J. Cell Biol. 171, 327–

335.

Sabo, S.L., Ikin, A.F., Buxbaum, J.D., Greengard, P., 2003. The Amyloid Precursor Protein and its Regulatory Protein, FE65, in Growth Cones and Synapses In Vitro and In Vivo. J. Neurosci. 23, 5407–5415.

Sabo, S.L., Ikin, A.F., Buxbaum, J.D., Greengard, P., 2001. The Alzheimer Amyloid Precursor Protein (APP) and FE65, an APP-Binding Protein, Regulate Cell Movement. J. Cell Biol. 153, 1403–1414.

Sabo, S.L., Lanier, L.M., Ikin, A.F., Khorkova, O., Sahasrabudhe, S., Greengard, P., Buxbaum, J.D., 1999. Regulation of β-Amyloid Secretion by FE65, an Amyloid Protein Precursor-Binding Protein. J. Biol. Chem. 274, 7952–7957.

Saido, T., Leissring, M.A., 2012. Proteolytic Degradation of Amyloid β-Protein. Cold Spring Harb. Perspect. Med. 2, a006379.

Sakono, M., Zako, T., 2010. Amyloid Oligomers: Formation and Toxicity of Aβ Oligomers. FEBS J. 277, 1348–1358.

Salah, Z., Alian, A., Aqeilan, R.I., 2012. WW Domain-Containing Proteins: Retrospectives and the Future. Front. Biosci. 17, 331–348.

Salloway, S., Sperling, R., Fox, N.C., Blennow, K., Klunk, W., Raskind, M., Sabbagh, M., Honig, L.S., Porsteinsson, A.P., Ferris, S., Reichert, M., Ketter, N., Nejadnik, B., Guenzler, V., Miloslavsky, M., Wang, D., Lu, Y., Lull, J., Tudor, I.C., Liu, E., Grundman, M., Yuen, E., Black, R., Brashear, H.R., 2014. Two Phase 3 Trials of Bapineuzumab in Mild-to-Moderate Alzheimer's Disease. N. Engl. J. Med. 370, 322–333.

Santiard-Baron, D., Langui, D., Delehedde, M., Delatour, B., Schombert, B., Touchet, N., Tremp, G., Paul, M.-F., Blanchard, V., Sergeant, N., Delacourte, A., Duyckaerts, C., Pradier, L., Mercken, L., 2005. Expression of Human FE65 in Amyloid Precursor Protein Transgenic Mice is Associated with a Reduction in β-Amyloid Load. J. Neurochem. 93, 330–338.

Scali, C., Caraci, F., Gianfriddo, M., Diodato, E., Roncarati, R., Pollio, G., Gaviraghi, G., Copani, A., Nicoletti, F., Terstappen, G.C., Caricasole, A., 2006. Inhibition of Wnt Signaling, Modulation of Tau Phosphorylation and Induction of Neuronal Cell Death by DKK1. Neurobiol. Dis. 24, 254–265.

Scheinfeld, M.H., Roncarati, R., Vito, P., Lopez, P.A., Abdallah, M., D'Adamio, L., 2002. Jun NH2-terminal Kinase (JNK) Interacting Protein 1 (JIP1) Binds the Cytoplasmic Domain of the Alzheimer's β Amyloid Precursor Protein (APP). J. Biol. Chem. 277, 3767–3775.

Schellenberg, G.D., Montine, T.J., 2012. The Genetics and Neuropathology of Alzheimer's Disease. Acta Neuropathol. 124, 305–323.

Scheuner, D., Eckman, C., Jensen, M., Song, X., Citron, M., Suzuki, N., Bird, T.D.,

Hardy, J., Hutton, M., Kukull, W., Larson, E., Levy-Lahad, E., Viitanen, M., Peskind, E., Poorkaj, P., Schellenberg, G., Tanzi, R., Wasco, W., Lannfelt, L., Selkoe, D., Younkin, S., 1996. Secreted Amyloid β-Protein Similar to that in the Senile Plaques of Alzheimer's Disease is Increased In Vivo by the Presenilin 1 and 2 and APP Mutations Linked to Familial Alzheimer's Disease. Nat. Med. 2, 864–870.

Schmaier, a H., Dahl, L.D., Rozemuller, a J., Roos, R. a, Wagner, S.L., Chung, R., Van Nostrand, W.E., 1993. Protease Nexin-2/Amyloid Beta Protein Precursor. A Tight-Binding Inhibitor of Coagulation Factor IXa. J. Clin. Invest. 92, 2540–2545. doi:10.1172/JCI116863

Schrötter, A., Mastalski, T., Nensa, F.M., Neumann, M., Loosse, C., Pfeiffer, K., Magraoui, F. El, Platta, H.W., Erdmann, R., Theiss, C., Uszkoreit, J., Eisenacher, M., Meyer, H.E., Marcus, K., Müller, T., 2013. FE65 Regulates and Interacts with the Bloom Syndrome Protein in Dynamic Nuclear Spheres - Potential Relevance to Alzheimer's Disease. J. Cell Sci. 126, 2480–2492.

Schubert, W., Prior, R., Weidemann, A., Dircksen, H., Multhaup, G., Masters, C.L., Beyreuther, K., 1991. Localization of Alzheimer βA4 Amyloid Precursor Protein at Central and Peripheral Synaptic Sites. Brain Res. 563, 184–194.

Schuijers, J., Mokry, M., Hatzis, P., Cuppen, E., Clevers, H., 2014. Wnt-Induced Transcriptional Activation is Exclusively Mediated by TCF/LEF. EMBO J. 33, 146–156.

Seger, R., Krebs, E.G., 1995. The MAPK Signaling Cascade. FASEB J. 9, 726–735.

Seitz, R., Hackl, S., Seibuchner, T., Tamm, E.R., Ohlmann, A., 2010. Norrin Mediates Neuroprotective Effects on Retinal Ganglion Cells via Activation of the Wnt/β-Catenin Signaling Pathway and the Induction of Neuroprotective Growth Factors in Muller Cells. J. Neurosci. 30, 5998–6010.

Selvey, S., Thompson, E.W., Matthaei, K., Lea, R. a, Irving, M.G., Griffiths, L.R., 2001. Beta-Actin - An Unsuitable Internal Control for RT-PCR. Mol. Cell. Probes 15, 307–311.

Serrano-Pozo, A., Frosch, M.P., Masliah, E., Hyman, B.T., 2011. Neuropathological Alterations in Alzheimer Disease. Cold Spring Harb. Perspect. Med. 1, a006189.

Seshadri, S., Fitzpatrick, A.L., Ikram, M.A., DeStefano, A.L., Gudnason, V., Boada, M., Bis, J.C., Smith, A. V., Carrasquillo, M.M., Lambert, J.C., Harold, D., Schrijvers, E.M.C., Ramirez-Lorca, R., Debette, S., Longstreth Jr., W.T., Janssens, A.C.J.W., Pankratz, V.S., Dartigues, J.F., Hollingworth, P., Aspelund, T., Hernandez, I., Beiser, A., Kuller, L.H., Koudstaal, P.J., Dickson, D.W., Tzourio, C., 2010. Genome-wide Analysis of Genetic Loci. JAMA 303, 1832–1840.

Seubert, P., Oltersdorf, T., Lee, M.G., Barbour, R., Blomquist, C., Davis, D.L., Bryant,

K., Fritz, L.C., Galasko, D., Thal, L.J., 1993. Secretion of β-Amyloid Precursor Protein Cleaved at the Amino Terminus of the β-Amyloid Peptide. Nature 361, 260–263.

Shariati, S.A.M., De Strooper, B., 2013. Redundancy and Divergence in the Amyloid Precursor Protein Family. FEBS Lett. 587, 2036–2045.

Shoji, M., Golde, T.E., Ghiso, J., Cheung, T.T., Estus, S., Shaffer, L.M., Cai, X., Mckay, D.M., Tintner, R., Frangione, B., Younkin, S.G., 1992. Production of the Alzheimer Amyloid β Protein by Normal Proteolytic Processing. Science (80-.). 258, 126–129.

Simeone, A., Duilio, A., Fiore, F., Acampora, D., De Felice, C., Farraonio, R., Paolocci, F., Cimino, F., Russo, T., 1994. Expression of the Neuron-Specific Fe65 Gene Marks the Development of Embryo Ganglionic Derivatives. Dev. Neurosci. 16, 53–60.

Šimić, G., Babić Leko, M., Wray, S., Harrington, C., Delalle, I., Jovanov-Milošević, N., Bažadona, D., Buée, L., de Silva, R., Di Giovanni, G., Wischik, C., Hof, P., 2016. Tau Protein Hyperphosphorylation and Aggregation in Alzheimer's Disease and Other Tauopathies, and Possible Neuroprotective Strategies. Biomolecules 6, 6.

Sinha, S., Anderson, J.P., Barbour, R., Basi, G.S., Caccavello, R., Davis, D., Doan, M., Dovey, H.F., Frigon, N., Hong, J., Jacobson-Croak, K., Jewett, N., Keim, P., Knops, J., Lieberburg, I., Power, M., Tan, H., Tatsuno, G., Tung, J., Schenk, D., Seubert, P., Suomensaari, S.M., Wang, S., Walker, D., Zhao, J., McConlogue, L., John, V., 1999. Purification and Cloning of Amyloid Precursor Protein β-Secretase from Human Brain. Nature 402, 537–540.

Sisodia, S.S., 1992. β-Amyloid Precursor Protein Cleavage by a Membrane-Bound Protease. Proc. Natl. Acad. Sci. 89, 6075–6079.

Sisodia, S.S., Koo, E.H., Beyreuther, K., Unterbeck, A., Price, D.L., 1990. Evidence that β-Amyloid Protein in Alzheimer's Disease is not Derived by Normal Processing. Science (80-.). 248, 492–495.

Sleegers, K., Brouwers, N., Gijselinck, I., Theuns, J., Goossens, D., Wauters, J., Del-Favero, J., Cruts, M., van Duijn, C.M., Broeckhoven, C.V., 2006. APP Duplication is Sufficient to Cause Early Onset Alzheimer's Dementia with Cerebral Amyloid Angiopathy. Brain 129, 2977–2983.

Slunt, H.H., Thinakaran, G., Von Koch, C., Lo, A.C., Tanzi, R.E., Sisodia, S.S., 1994. Expression of a Ubiquitous, Cross-Reactive Homologue of the Mouse β-Amyloid Precursor Protein (APP). J. Biol. Chem. 269, 2637–2644.

Smalley, M.J., Sara, E., Paterson, H., Naylor, S., Cook, D., Jayatilake, H., Fryer, L.G., Hutchinson, L., Fry, M.J., Dale, T.C., 1999. Interaction of Axin and Dvl-2 Proteins Regulates Dvl-2-Stimulated TCF-Dependent Transcription. EMBO J. 18, 2823–

2835.

Smith, R.P., Higuchi, D. a, Broze, G.J., 1990. Platelet Coagulation Factor XIa-Inhibitor, A Form of Alzheimer Amyloid Precursor Protein. Science (80-.). 248, 1126–1128. doi:10.1126/science.2111585

Snowdon, D., Greiner, L., Mortimer, J., Riley, K., Greiner, P., Markesbery, W., 1997. Brain Infarction and the Clinical Expression of Alzheimer Disease: The Nun Study. J. Am. Med. Assoc. 277, 813–817.

Snyder, E.M., Nong, Y., Almeida, C.G., Paul, S., Moran, T., Choi, E.Y., Nairn, A.C., Salter, M.W., Lombroso, P.J., Gouras, G.K., Greengard, P., 2005. Regulation of NMDA Receptor Trafficking by Amyloid-β. Nat. Neurosci. 8, 1051–1058.

Söderberg, O., Gullberg, M., Jarvius, M., Ridderstråle, K., Leuchowius, K.-J., Jarvius, J., Wester, K., Hydbring, P., Bahram, F., Larsson, L.-G., Landegren, U., 2006. Direct Observation of Individual Endogenous Protein Complexes In Situ by Proximity Ligation. Nat. Methods 3, 995–1000.

Spillantini, M.G., Goedert, M., 2013. Tau Pathology and Neurodegeneration. Lancet Neurol. 12, 609–622.

Sprecher, C.A., Grant, F.J., Grimm, G., O'Hara, P.J., Norris, F., Norris, K., Foster, D.C., 1993. Molecular Cloning of the cDNA for a Human Amyloid Precursor Protein Homolog: Evidence for a Multigene Family. Biochemistry 32, 4481–4486.

St George-Hyslop, P.H., Tanzi, R.E., Polinsky, R.J., Haines, J.L., Nee, L., Watkins, P.C., Myers, R.H., Feldman, R.G., Pollen, D., Drachman, D., Growdon, J., Bruni, A., Foncin, J.-F., Salmon, D., Frommelt, P., Amaducci, L., Sorbi, S., Piacentini, S., Stewart, G.D., Hobbs, W.J., Conneally, P.M., Gusella, J.F., Jonathan, L., Nee, L., Watkins, P.C., Myers, R.H., Feldman, R.G., Pollen, D., Drachman, D., Growdon, J., Bruni, A., Foncin, J.-F., Salmon, D., Amaducci, L., Sorbi, S., Piacentini, S., Stewart, G.D., Wendy, J., Conneally, P.M., Gusella, J.F., 1987. The Genetic Defect Causing Familial Alzheimer's Disease Maps on Chromosome 21. Science (80-.). 235, 885–890.

Standen, C.L., Brownlees, J., Grierson, A.J., Kesavapany, S., Lau, K.-F., McLoughlin, D.M., Miller, C.C.J., 2001. Phosphorylation of Thr(668) in the Cytoplasmic Domain of the Alzheimer's Disease Amyloid Precursor Protein by Stress-Activated ProteinKkinase 1b (Jun N-Terminal Kinase-3). J. Neurochem. 76, 316–320.

Standen, C.L., Perkinton, M.S., Byers, H.L., Kesavapany, S., Lau, K.-F., Ward, M., McLoughlin, D., Miller, C.C.J., 2003. The Neuronal Adaptor Protein Fe65 is Phosphorylated by Mitogen-Activated Protein Kinase (ERK1/2). Mol. Cell. Neurosci. 24, 851–857.

Stante, M., Minopoli, G., Passaro, F., Raia, M., Vecchio, L. Del, Russo, T., 2009. Fe65 is Required for Tip60-Directed Histone H4 Acetylation at DNA Strand Breaks.

Proc. Natl. Acad. Sci. 106, 5093–5098.

Stelzmann, R.A., Schnitzlein, H.N., Murtagh, F.R., 1995. An English Translation of Alzheimer's 1907 Paper, "Über eine eigenartige Erkankung der Hirnrinde." Clin. Anat. 8, 429–431.

Stokin, G.B., Lillo, C., Falzone, T.L., Brusch, R.G., Rockenstein, E., Mount, S.L., Raman, R., Davies, P., Masliah, E., Williams, D.S., Goldstein, L.S.B., 2005. Axonopathy and Transport Deficits Early in the Pathogenesis of Alzheimer's Disease. Science (80-.). 307, 1282–1288.

Stoothoff, W.H., Bailey, C.D.C., Mi, K., Lin, S.-C., Johnson, G.V.W., 2002. Axin Negatively Affects Tau Phosphorylation by Glycogen Synthase Kinase 3β. J. Neurochem. 83, 904–913.

Su, S.C., Tsai, L.-H., 2011. Cyclin-Dependent Kinases in Brain Development and Disease. Annu. Rev. Cell Dev. Biol. 27, 465–491.

Suh, J., Lyckman, A., Wang, L., Eckman, E. a., Guénette, S.Y., 2011. FE65 Proteins Regulate NMDA Receptor Activation-Induced Amyloid Precursor Protein Processing. J. Neurochem. 119, 377–388.

Sun, X., Zhou, H., Luo, X., Li, S., Yu, D., Hua, J., Mu, D., Mao, M., 2008. Neuroprotection of Brain-Derived Neurotrophic Factor Against Hypoxic Injury In Vitro Requires Activation of Extracellular Signal-Regulated Kinase and Phosphatidylinositol 3-Kinase. Int. J. Dev. Neurosci. 26, 363–370.

Sun, Y., Kasiappan, R., Tang, J., Webb, P.L., Quarni, W., Zhang, X., Bai, W., 2014. A Novel Function of the Fe65 Neuronal Adaptor in Estrogen Receptor Action in Breast Cancer Cells. J. Biol. Chem. 289, 12217–12231.

Sutherland, C., Leighton, I. a, Cohen, P., 1993. Inactivation of Glycogen Synthase Kinase-3 Beta by Phosphorylation: New Kinase Connections in Insulin and Growth-Factor Signalling. Biochem. J. 296, 15–19.

Takahashi, K., Niidome, T., Akaike, A., Kihara, T., Sugimoto, H., 2008. Phosphorylation of Amyloid Precursor Protein (APP) at Tyr687 Regulates APP Processing by α- and γ-Secretase. Biochem. Biophys. Res. Commun. 377, 544–549. doi:10.1016/j.bbrc.2008.10.013

Tamayev, R., Zhou, D., D'Adamio, L., 2009. The Interactome of the Amyloid β Precursor Protein Family Members is Shaped by Phosphorylation of their Intracellular Domains. Mol. Neurodegener. 4, 28.

Tanzi, R.E., 2012. The Genetics of Alzheimer Disease. Cold Spring Harb. Perspect. Med. 2, a006296.

Tanzi, R.E., McClatchey, A.I., Lamperti, E.D., Villa-Komaroff, L., Gusella, J.F., Neve, R.L., 1988. Protease Inhibitor Domain Encoded by an Amyloid Protein Precursor mRNA Associated with Alzheimer's Disease. Nature 331, 528–530.

Tanzi, R.E., St George-Hyslop, P.H., Haines, J.L., Polinsky, R.J., Nee, L., Foncin, J.F., Neve, R.L., McClatchey, A.I., Conneally, P.M., Gusella, J.F., 1987. The Genetic Defect in Familial Alzheimer's Disease is not Tightly Linked to the Amyloid β-Protein Gene. Nature 329, 156–157.

Tarr, P.E., Contursi, C., Roncarati, R., Noviello, C., Ghersi, E., Scheinfeld, M.H., Zambrano, N., Russo, T., Adamio, L.D., 2002a. Evidence for a Role of the Nerve Growth Factor Receptor TrkA in Tyrosine Phosphorylation and Processing of β-APP. Biochem. Biophys. Res. Commun. 295, 324–329.

Tarr, P.E., Roncarati, R., Pelicci, G., Pelicci, P.G., Adamio, L.D., 2002b. Tyrosine Phosphorylation of the β-Amyloid Precursor Protein Cytoplasmic Tail Promotes Interaction with Shc. J. Biol. Chem. 277, 16798–16804.

Telese, F., Bruni, P., Donizetti, A., Gianni, D., D'Ambrosio, C., Scaloni, A., Zambrano, N., Rosenfeld, M.G., Russo, T., 2005. Transcription Regulation by the Adaptor Protein Fe65 and the Nucleosome Assembly Factor SET. EMBO Rep. 6, 77–82.

Trommsdorff, M., Borg, J.P., Margolis, B., Herz, J., 1998. Interaction of Cytosolic Adaptor Proteins with Neuronal Apolipoprotein E Receptors and the Amyloid Precursor Protein. J. Biol. Chem. 273, 33556–33560.

Tyan, S.-H., Shih, A.Y.-J., Walsh, J.J., Maruyama, H., Sarsoza, F., Ku, L., Eggert, S., Hof, P.R., Koo, E.H., Dickstein, D.L., 2012. Amyloid Precursor Protein (APP) Regulates Synaptic Structure and Function. Mol. Cell. Neurosci. 51, 43–52.

Vagnoni, A., Glennon, E.B.C., Perkinton, M.S., Gray, E.H., Noble, W., Miller, C.C.J., 2013. Loss of c-Jun N-terminal Kinase-Interacting Protein-1 does not Affect Axonal Transport of the Amyloid Precursor Protein or Aβ Production. Hum. Mol. Genet. 22, 4646–4652.

Vagnoni, A., Perkinton, M.S., Gray, E.H., Francis, P.T., Noble, W., Miller, C.C.J., 2012. Calsyntenin-1 Mediates Axonal Transport of the Amyloid Precursor Protein and Regulates Aβ Production. Hum. Mol. Genet. 21, 2845–2854.

Vagnoni, A., Rodriguez, L., Manser, C., De Vos, K.J., Miller, C.C.J., 2011. Phosphorylation of Kinesin Light Chain 1 at Serine 460 Modulates Binding and Trafficking of Calsyntenin-1. J. Cell Sci. 124, 1032–1042.

van der Kant, R., Goldstein, L.S.B., 2015. Cellular Functions of the Amyloid Precursor Protein from Development to Dementia. Dev. Cell 32, 502–515.

Van Gassen, G., Annaert, W., Van Broeckhoven, C., 2000. Binding Partners of Alzheimer's Disease Proteins: Are They Physiologically Relevant? Neurobiol. Dis. 7, 135–151.

Vandesompele, J., De Preter, K., Pattyn, F., Poppe, B., Van Roy, N., De Paepe, A., Speleman, F., 2002. Accurate Normalization of Real-Time Quantitative RT-PCR Data by Geometric Averaging of Multiple Internal Control Genes. Genome Biol. 3,

Research0034.1–0034.11.

Vassar, R., Bennett, B.D., Babu-Khan, S., Kahn, S., Mendiaz, E.A., Denis, P., Teplow, D.B., Ross, S., Amarante, P., Loeloff, R., Luo, Y., Fisher, S., Fuller, J., Edenson, S., Lile, J., Jarosinski, M.A., Biere, A.L., Curran, E., Burgess, T., Louis, J.C., Collins, F., Treanor, J., Rogers, G., Citron, M., 1999. β-Secretase Cleavage of Alzheimer's Amyloid Precursor Protein by the Transmembrane Aspartic Protease BACE. Science (80-.). 286, 735–741.

Vázquez, M.C., Vargas, L.M., Inestrosa, N.C., Alvarez, A.R., 2009. c-Abl Modulates AICD Dependent Cellular Responses: Transcriptional Induction and Apoptosis. J. Cell. Physiol. 220, 136–143.

Venezia, V., Nizzari, M., Repetto, E., Violani, E., Corsaro, A., Thellung, S., Villa, V., Carlo, P., Schettini, G., Florio, T., Russo, C., 2006. Amyloid Precursor Protein Modulates ERK-1 and -2 Signaling. Ann. N. Y. Acad. Sci. 1090, 455–465.

Verghese, P.B., Castellano, J.M., Holtzman, D.M., 2011. Roles of Apolipoprotein E in Alzheimer's Disease and Other Neurological Disorders. Lancet Neurol. 10, 241–252.

Vingtdeux, V., Marambaud, P., 2012. Identification and Biology of α-Secretase. J. Neurochem. 120, 34–45.

Vogt, D.L., Thomas, D., Galvan, V., Bredesen, D.E., Lamb, B.T., Pimplikar, S.W., 2011. Abnormal Neuronal Networks and Seizure Susceptibility in Mice Overexpressing the APP Intracellular Domain. Neurobiol. Aging 32, 1725–1729.

von Rotz, R.C., Kohli, B.M., Bosset, J., Meier, M., Suzuki, T., Nitsch, R.M., Konietzko, U., 2004. The APP Intracellular Domain Forms Nuclear Multiprotein Complexes and Regulates the Transcription of its Own Precursor. J. Cell Sci. 117, 4435–4448.

Wagner, U., Brownlees, J., Irving, N.G., Lucas, F.R., Salinas, P.C., Miller, C.C.J., 1997. Overexpression of the Mouse Dishevelled-1 Protein Inhibits GSK-3β-Mediated Phosphorylation of Tau in Transfected Mammalian Cells. FEBS Lett. 411, 369–372.

Waldron, E., Isbert, S., Kern, A., Jaeger, S., Martin, A.M., Hébert, S.S., Behl, C., Weggen, S., De Strooper, B., Pietrzik, C.U., 2008. Increased AICD Generation does not Result in Increased Nuclear Translocation or Activation of Target Gene Transcription. Exp. Cell Res. 314, 2419–2433.

Wallace, W.C., Akar, C.A., Lyons, W.E., 1997. Amyloid Precursor Protein Potentiates the Neurotrophic Activity of NGF. Behav. Brain Res. 52, 201–212.

Walsh, D.M., Fadeeva, J. V., LaVoie, M.J., Paliga, K., Eggert, S., Kimberly, W.T., Wasco, W., Selkoe, D.J., 2003. γ-Secretase Cleavage and Binding to FE65 Regulate the Nuclear Translocation of the Intracellular C-Terminal Domain (ICD)

of the APP Family of Proteins. Biochemistry 42, 6664–6673.

Wang, B., Hu, Q., Hearn, M.G., Shimizu, K., Ware, C.B., Liggitt, D.H., Jin, L.W., Cool, B.H., Storm, D.R., Martin, G.M., 2004. Isoform-Specific Knockout of FE65 Leads to Impaired Learning and Memory. J. Neurosci. Res. 75, 12–24.

Wang, P., 2005. Defective Neuromuscular Synapses in Mice Lacking Amyloid Precursor Protein (APP) and APP-Like Protein 2. J. Neurosci. 25, 1219–1225.

Wang, P., Niidome, T., Kume, T., Akaike, A., 2011. Functional and Molecular Interactions between Rac1 and FE65. Cell. Mol. Dev. Neurosci. 22, 716–720.

Wang, R., Meschia, J.F., Cotter, R.J., Sisodia, S.S., 1991. Secretion of the β/A4 Amyloid Precursor Protein. J. Biol. Chem. 266, 16960–16964.

Wang, Y., Mandelkow, E., 2015. Tau in Physiology and Pathology. Nat. Rev. Neurosci. 17, 5–21.

Wang, Y., Zhang, M., Moon, C., Hu, Q., Wang, B., Martin, G., Sun, Z., Wang, H., 2009. The APP-Interacting Protein FE65 is Required for Hippocampus-Dependent Learning and Long-Term Potentiation. Learn. Mem. 16, 537–544.

Wasco, W., Bupp, K., Magendantz, M., Gusella, J.F., Tanzi, R.E., Solomon, F., 1992. Identification of a Mouse Brain cDNA that Encodes a Protein Related to the Alzheimer Disease-Associated Amyloid β Protein Precursor. Proc. Natl. Acad. Sci. 89, 10758–10762.

Wasco, W., Gurubhagavatula, S., Paradis, M.D., Romano, D., Sisodiajtil, S.S., Hyman, B.T., Neve, R.L., Tanzi, R.E., 1993. Isolation and Characterization of APLP2 Encoding a Homologue of the Alzheimer's Associated Amyloid β Protein Precursor. Nat. Genet. 5, 95–100.

Weibrecht, I., Leuchowius, K.-J., Clausson, C.-M., Conze, T., Jarvius, M., Howell, W.M., Kamali-Moghaddam, M., Söderberg, O., 2010. Proximity Ligation Assays: A Recent Addition to the Proteomics Toolbox. Expert Rev. Proteomics 7, 401–409.

Weyer, S.W., Klevanski, M., Delekate, A., Voikar, V., Aydin, D., Hick, M., Filippov, M., Drost, N., Schaller, K.L., Saar, M., Vogt, M.A., Gass, P., Samanta, A., Jäschke, A., Korte, M., Wolfer, D.P., Caldwell, J.H., Müller, U.C., 2011. APP and APLP2 are Essential at PNS and CNS Synapses for Transmission, Spatial Learning and LTP. EMBO J. 30, 2266–2280.

Wilcock, G.K., Esiri, M.M., 1982. Plaques, Tangles and Dementia. A Quantitative Study. J. Neurol. Sci. 56, 343–356.

Wiley, J.C., Smith, E.A., Hudson, M.P., Ladiges, W.C., Bothwell, M., 2007. Fe65 Stimulates Proteolytic Liberation of the β-Amyloid Precursor Protein Intracellular Domain. J. Biol. Chem. 282, 33313–33325.

Willem, M., Tahirovic, S., Busche, M.A., Ovsepian, S. V, Chafai, M., Kootar, S., Hornburg, D., Evans, L.D.B., Moore, S., Daria, A., Hampel, H., Müller, V., Giudici,

C., Nuscher, B., Wenninger-Weinzierl, A., Kremmer, E., Heneka, M.T., Thal, D.R., Giedraitis, V., Lannfelt, L., Müller, U., Livesey, F.J., Meissner, F., Herms, J., Konnerth, A., Marie, H., Haass, C., 2015. η-Secretase Processing of APP Inhibits Neuronal Activity in the Hippocampus. Nature 526, 443–447.

Wisniewski, K.E., Wisniewski, H.M., Wen, G.Y., 1985. Occurrence of Neuropathological Changes and Dementia of Alzheimer's Disease in Down's Syndrome. Ann. Neurol. 17, 278–282.

World Health Organization, 2012. Dementia: A Public Health Priority. Dementia.

Xie, Z., Dong, Y., Maeda, U., Xia, W., Tanzi, R.E., 2007. RNA Interference Silencing of the Adaptor Molecules ShcC and Fe65 Differentially Affect Amyloid Precursor Protein Processing and Aβ Generation. J. Biol. Chem. 282, 4318–4325.

Xu, X., Zhou, H., Boyer, T.G., 2011. Mediator is a Transducer of Amyloid-Precursor-Protein-Dependent Nuclear Signalling. EMBO Rep. 12, 216–222.

Yan, R., Bienkowski, M.J., Shuck, M.E., Miao, H., Tory, M.C., Pauley, a M., Brashier, J.R., Stratman, N.C., Mathews, W.R., Buhl, a E., Carter, D.B., Tomasselli, a G., Parodi, L. a, Heinrikson, R.L., Gurney, M.E., 1999. Membrane-Anchored Aspartyl Protease with Alzheimer's Disease β-Secretase Activity. Nature 402, 533–537.

Yan, R., Munzner, J.B., Shuck, M.E., Bienkowski, M.J., 2001. BACE2 Functions as an Alternative α-Secretase in Cells. J. Biol. Chem. 276, 34019–34027.

Yang, S.H., Sharrocks, A.D., Whitmarsh, A.J., 2013. MAP Kinase Signalling Cascades and Transcriptional Regulation. Gene 513, 1–13.

Yang, Z., Cool, B.H., Martin, G.M., Hu, Q., 2006. A Dominant Role for FE65 (APBB1) in Nuclear Signaling. J. Biol. Chem. 281, 4207–4214.

Yarza, R., Vela, S., Solas, M., Ramirez, M.J., 2016. c-Jun N-terminal Kinase (JNK) Signaling as a Therapeutic Target for Alzheimer's Disease. Front. Pharmacol. 6, 321.

Yi, H., Hu, J., Qian, J., Hackam, A.S., 2012. Expression of Brain-Derived Neurotrophic Factor (BDNF) is Regulated by the Wnt Signaling Pathway. Neuroreport 23, 189–194.

Young-Pearse, T.L., Bai, J., Chang, R., Zheng, J.B., LoTurco, J.J., Selkoe, D.J., 2007. A Critical Function for β-Amyloid Precursor Protein in Neuronal Migration Revealed by In Utero RNA Interference. J. Neurosci. 27, 14459–14469.

Young-Pearse, T.L., Chen, A.C., Chang, R., Marquez, C., Selkoe, D.J., 2008. Secreted APP Regulates the Function of Full-Length APP in Neurite Outgrowth through Interaction with Integrin Beta1. Neural Dev. 3.

Zambrano, N., Bruni, P., Minopoli, G., Mosca, R., Molino, D., Russo, C., Schettini, G., Sudol, M., Russo, T., 2001. The β-Amyloid Precursor Protein APP is Tyrosine-Phosphorylated in Cells Expressing a Constitutively Active Form of the Abl

Protoncogene. J. Biol. Chem. 276, 19787–19792.

Zambrano, N., Buxbaum, J.D., Minopoli, G., Fiore, F., Candia, P. De, Renzis, S. De, Faraonio, R., Sabo, S., Cheetham, J., Sudol, M., Russo, T., 1997. Interaction of the Phosphotyrosine Interaction/Phosphotyrosine Binding-related Domains of Fe65 with Wild-type and Mutant Alzheimer's β-Amyloid Precursor Proteins. J. Biol. Chem. 272, 6399–6405.

Zambrano, N., Minopoli, G., Candia, P. De, Russo, T., 1998. The Fe65 Adaptor Protein Interacts through its PID1 Domain with the Transcription Factor CP2/LSF/LBP1. J. Biol. Chem. 273, 20128–20133.

Zhang, Q., Wang, R., Khan, M., Mahesh, V., Brann, D.W., 2008. Role of Dickkopf-1, an Antagonist of the Wnt/β-Catenin Signaling Pathway, in Estrogen-Induced Neuroprotection and Attenuation of Tau Phosphorylation. J. Neurosci. 28, 8430–8441.

Zhang, Y., Thompson, R., Zhang, H., Xu, H., 2011. APP Processing in Alzheimer's Disease. Mol. Brain 4, 3.

Zhang, Z., Hartmann, H., Do, V.M., Abramowski, D., Sturchler-Pierrat, C., Staufenbiel, M., Sommer, B., van de Wetering, M., Clevers, H., Saftig, P., De Strooper, B., He, X., Yankner, B.A., 1998. Destabilization of β-Catenin by Mutations in Presenilin-1 Potentiates Neuronal Apoptosis. Nature 395, 698–702.

Zhou, D., Noviello, C., D'Ambrosio, C., Scaloni, A., D'Adamio, L., 2004. Growth Factor Receptor-Bound Protein 2 Interaction with the Tyrosine-Phosphorylated Tail of Amyloid β Precursor Protein is Mediated by its Src Homology 2 Domain. J. Biol. Chem. 279, 25374–25380.

Zhou, D., Zambrano, N., Russo, T., D'Adamio, L., 2009. Phosphorylation of a Tyrosine in the Amyloid-β Protein Precursor Intracellular Domain Inhibits Fe65 Binding and Signaling. J. Alzheimer's Dis. 16, 301–307.

Zhou, F., Gong, K., Song, B., Ma, T., van Laar, T., Gong, Y., Zhang, L., 2012. The APP Intracellular Domain (AICD) Inhibits Wnt Signalling and Promotes Neurite Outgrowth. Biochim. Biophys. Acta 1823, 1233–1241.

FE65 interacts with ADP-ribosylation factor 6 to promote neurite outgrowth

Hei Nga Maggie Cheung,* Charlotte Dunbar,† Gábor M. Mórotz,† Wai Hang Cheng,* Ho Yin Edwin Chan,* Christopher C. J. Miller,† and Kwok-Fai Lau*,[1]

*School of Life Sciences, Chinese University of Hong Kong, Shatin, Hong Kong, China; and †King's College London Centre for Neurodegeneration Research, Department of Neuroscience, King's College London Institute of Psychiatry, London, UK

ABSTRACT **FE65 is an adaptor protein that binds to the amyloid precursor protein (APP). As such, FE65 has been implicated in the pathogenesis of Alzheimer's disease. In addition, evidence suggests that FE65 is involved in brain development. It is generally believed that FE65 participates in these processes by recruiting various interacting partners to form functional complexes. Here, we show that *via* its first phosphotyrosine binding (PTB) domain, FE65 binds to the small GTPase ADP-ribosylation factor 6 (ARF6). FE65 preferentially binds to ARF6-GDP, and they colocalize in neuronal growth cones. Interestingly, FE65 stimulates the activation of both ARF6 and its downstream GTPase Rac1, a regulator of actin dynamics, and functions in growth cones to stimulate neurite outgrowth. We show that transfection of FE65 and/or ARF6 promotes whereas small interfering RNA knockdown of FE65 or ARF6 inhibits neurite outgrowth in cultured neurons as compared to the mock-transfected control cells. Moreover, knockdown of ARF6 attenuates FE65 stimulation of neurite outgrowth and defective neurite outgrowth seen in FE65-deficient neurons is partially corrected by ARF6 overexpression. Notably, the stimulatory effect of FE65 and ARF6 on neurite outgrowth is abrogated either by dominant-negative Rac1 or knockdown of Rac1. Thus, we identify FE65 as a novel regulator of neurite outgrowth *via* controlling ARF6-Rac1 signaling.—Cheung, H. N., Dunbar, C., Mórotz, G. M., Cheng, W. H., Chan, H. Y., Miller, C. C., Lau, K.-F. FE65 interacts with ADP-ribosylation factor 6 to promote neurite outgrowth. *FASEB J.* 28, 337–349 (2014). www.fasebj.org**

Key Words: ARF6 · amyloid-β · A4 precursor protein-binding family B member 1 · neurons · Rac1

FE65 IS AN ADAPTOR PROTEIN that interacts with the intracellular C terminus of the Alzheimer's disease amyloid precursor protein (APP; ref. 1–3). The interaction between FE65 and APP can influence APP processing and production of amyloid-β (Aβ) peptide that is deposited in the brains of Alzheimer's disease patients (4–8). In addition, FE65 and APP participate in nuclear signaling (9, 10) and DNA repair after damage (11, 12) and these functions have also been linked to Alzheimer's disease (for reviews, see refs. 13–15).

However, along with these nuclear functions, FE65 is also believed to have cytoplasmic roles in neurons and in particular in neurodevelopmental processes and synaptic function. Evidence to support this notion comes from a number of findings. First, FE65 is developmentally regulated in the brain and has been linked to neurogenesis (16, 17). Also, FE65-knockout mice display defective brain development (5). Second, FE65 regulates actin-based membrane motility and localizes in actin-rich mobile structures within the growth cones (18, 19). Finally, learning and memory deficits have been reported in FE65-knockout mice, and these are linked to synaptic changes (8, 20). However, the precise mechanisms by which FE65 regulates neuronal development and synaptic function are not properly understood.

Here, we show that FE65 binds to ADP-ribosylation factor 6 (ARF6). ARF6 is a ubiquitously expressed Ras superfamily GTPase that is involved in both endocytic membrane trafficking and actin cytoskeletal rearrangements. These functions are regulated by cycling of ARF6 between GTP (active) and GDP (inactive) states that are modulated *via* the actions of guanine nucleotide exchange factors (GEFs) and GTPase-activating proteins (GAPs) (for review, see ref. 21). In the nervous system, ARF6 has been shown to regulate early neuronal morphogenesis (for review, see ref. 22) and axon

Abbreviations: Aβ, amyloid-β; APP, amyloid precursor protein; ARF6, ADP-ribosylation factor 6; CHO, Chinese hamster ovary; DAPI, 4′,6-diamidino-2-phenylindole; DIV, days *in vitro*; EGFP, enhanced green fluorescent protein; EV, empty vector; GAP, GTPase-activating protein; GEF, guanine nucleotide exchange factor; GFP, green fluorescent protein; GST, glutathione *S* transferase; ICA, intensity correlation analysis; ICQ, intensity correlation quotient; PBD, protein-binding domain; PTB, phosphotyrosine binding

[1] Correspondence: School of Life Sciences, Chinese University of Hong Kong, Shatin, NT, Hong Kong SAR, China. E-mail: kflau@cuhk.edu.hk

doi: 10.1096/fj.13-232694

This article includes supplemental data. Please visit *http://www.fasebj.org* to obtain this information.

development (23, 24). The effect of ARF6 on neural development involves, at least in part, Rac1, which is a regulator of actin dynamics (for reviews, see refs. 25, 26). In this report, we characterize FE65-ARF6 interaction and demonstrate that FE65 and ARF6 promote neurite outgrowth and regulate the activation of Rac1.

MATERIALS AND METHODS

Yeast 2-hybrid system

Yeast 2-hybrid screens were performed essentially as described previously (27). Briefly, sequence encoding the human FE65 phosphotyrosine binding (PTB) 1 + 2 domains (aa 361–676 of FE65) was subcloned into the yeast "bait" pGBKT7 vector and then transformed into yeast Y2H Gold. To perform the library screen, the bait-containing yeast Y2H Gold was mated with yeast Y187 pretransformed with a human brain cDNA library (Clontech, Mountain View, CA, USA). After selection, vigorously growing clones were subjected to freeze-fracture β-galactosidase assays. Candidate library pACT2 plasmids were rescued by transforming into *Escherichia coli* DH5α, and the brain library cDNA inserts were then sequenced.

Cell culture and transfection

Chinese hamster ovary (CHO) and SH-SY5Y cells were cultured as described previously (27, 28). Primary rat cortical neurons were dissected from E18 embryos and grown on glass coverslips coated with poly-D-lysine in Neurobasal medium with B27 supplement (Life Technologies, Grand Island, NY, USA).

For plasmid transfection, CHO cells were transfected with FuGene 6 (Roche, Perzberg, Germany), and SH-SY5Y and rat cortical neurons were transfected with Lipofectamine 2000 (Life Technologies) according to the manufacturers' instructions and as described previously (29). All siRNAs were obtained from Dharmacon ThermoScientific (Rockford, IL, USA). For CHO and SHSY5Y cells, siRNAs were transfected using Lipofectamine RNAiMAX (Life Technologies). For cultured neurons, cells were incubated with Accell siRNAs previously described (27, 29). For cytochalasin D (CytoD; Life Technologies) treatment, neurons were incubated with 0.25 μg/ml CytoD (in DMSO) for 24 h.

Plasmids

A mammalian expression vector of glutathione *S* transferase (GST) was prepared by cloning GST cDNA into pCI-neo (Promega, Madison, WI, USA) to form pCIneo-GST. The GST fusion protein constructs of pCIneo-GST-FE65 WW, pCIneo-GST-FE65 PTB1, and pCIneo-GST-FE65 PTB2 were made by subcloning of the FE65 corresponding cDNAs (WW domain, aa 248–290; PTB1 domain, aa 361–514; and PTB2 domain, aa 531–676) into pCIneo-GST, respectively. The GST fusion protein constructs of pCIneo-GST-ARF6, pCIneo-GST-ARF6 1–80, pCIneo-GST-ARF6 28–175, pCIneo-GST-ARF6 48–175, and pCIneo-GST-ARF6 73–175 were made by subcloning of the ARF6 corresponding cDNAs into pCIneo-GST, respectively. Mammalian expression constructs for wild-type FE65, myc-tagged FE65, myc-tagged FE65 ΔPTB1, and APP were as described previously (9, 10, 30). Wild-type Rac1 and N17Rac1 were as described previously (31). V12Rac1 mutant was generated by using QuikChange II site-directed mutagenesis kit (Agilent Technologies, Santa Clara, CA, USA). Myc/His- and GST-tagged wild-type ARF6 constructs were generated by subcloning the full-length ARF6 cDNA into pcDNA3.1/myc-His vectors (Life Technologies) and pGEX-6P-1 (GE Healthcare Biosciences, Pittsburgh, PA, USA), respectively. Myc/His-tagged mutant ARF6 T27N and Q67L were generated by site-directed mutagenesis.

Antibodies

Mouse (9B11) and rabbit (71D10) anti-myc antibodies were purchased from Cell Signaling Technology (Boston, MA, USA). Rabbit anti-α-tubulin and mouse anti-α-tubulin (DM1A) were from Abcam (Cambridge, MA, USA) and Sigma (St. Louis, MO, USA), respectively. Anti-polyHistidine (HIS-1) and anti-GST were purchased from Sigma. Rabbit anti-α-tubulin was from Abcam. Anti-Rac1 (23A8) was obtained from Millipore (Billerica, MA, USA). Rat polyclonal antibody against ARF6 (AR3) was created by immunization of a rat with GST-ARF6 fusion protein. Anti-ARF6 antibodies 3A-1 and 6ARF01 were purchased from Santa Cruz Biotechnology (Dallas, TX, USA) and Millipore, respectively). Rabbit anti-FE65 was as described previously (32); goat anti-FE65 (E20) was obtained from Santa Cruz Biotechnology, and mouse anti-FE65 (4H324) was from Abcam. FE65 is reported to be phosphorylated by several kinases at various residues, which can lead to reduction in electrophoretic mobility of FE65 (10, 33, 34). Therefore, multiple FE65 bands would be seen in Western blot analysis. Since the phosphorylation status of FE65 might vary from different samples, different banding patterns might be observed.

GST fusion protein binding assays

The GST-ARF6 and GST-FE65 PTB1 were expressed in *E. coli* BL21 and captured by glutathione-Sepharose 4B (GE Healthcare Biosciences) according to the manufacturer's instructions. GST pulldown assays were performed essentially as described previously (32). In ARF6 pulldown assays, GST and GST-ARF6 baits were used to pull down FE65 from transfected cell lysates. Cells were harvested in ice-cold lysis buffer (50 mM Tris/HCl, pH 7.5; 150 mM NaCl; 1 mM EDTA; 1% Triton X-100; and Complete protease inhibitor; Roche). Following lysis, cells were cleared by centrifugation at 14,000 *g* at 4°C. The lysates were incubated with the baits at 4°C for 1 h. The captured proteins were boiled in SDS-PAGE sample buffer and then analyzed by SDS-PAGE and Western blotting.

For mammalian GST fusion protein binding assays, CHO cells were transfected with GST + ARF6, GST-FE65 WW + ARF6, GST-FE65 PTB1 + ARF6, or GST-FE65 PTB2 + ARF6. Cells were harvested in ice-cold lysis buffer as described above. Lysates were incubated with glutathione-Sepharose at 4°C for 1 h. The captured proteins were then analyzed by SDS-PAGE and immunoblotting. Similar assays were also performed for cells transfected with GST-FE65 PTB1 + ARF6, GST-FE65 PTB1 + ARF6 T27N, or GST-FE65 PTB1 + ARF6 Q67L. Mammalian GST-ARF6 fusion protein pulldown of FE65 were also performed by the method as described above. To perform direct protein-binding assay, His_6-ARF6 was expressed in *E. coli* BL21, purified by Ni-NTA agarose (Qiagen, Hilden, Germany), and incubated with purified GST or GST-FE65 PTB1 baits in ice-cold lysis buffer. The protein complexes were captured by glutathione-Sepharose 4B and analyzed by SDS-PAGE.

To determine the state of ARF6 (*i.e.*, ARF6-GDP or ARF6-GTP) that interacts with FE65, bacterial GST-FE65 PTB1 was used to pull down dominant negative ARF6 T27N and constituently active ARF6 Q67L mutants from transfected CHO

cell lysates. In brief, ARF6-transfected cells were harvested in ice-cold lysis/binding/wash buffer (25 mM Tris-HCl, pH 7.2; 150 mM NaCl; 5 mM $MgCl_2$; 1% Nonidet P-40; 5% glycerol; and protease inhibitor cocktail) and then cleared by centrifugation. The lysates were incubated with the bacterial GST-FE65 PTB1 baits at 4°C for 1 h. The captured proteins were boiled in SDS-PAGE sample buffer and then analyzed by SDS-PAGE and Western blotting.

To further confirm the state of ARF6 that interacts with FE65, wild-type ARF6-transfected cell lysates were loaded with either GDP or GTP by incubating with 1 mM GDP or 10 mM nonhydrolyzable GTPγS, respectively, at 30°C for 15 min and then followed by bacterial GST-FE65 PTB1 pulldown assays as described above.

Coimmunoprecipitation assays

CHO cells transfected with either FE65, FE65 + myc-tagged ARF6, or FE65ΔPTB1 + myc-tagged ARF6 were harvested in ice-cold lysis buffer. Myc-tagged ARF6 was immunoprecipitated from cell lysates by 9B11 anti-myc antibody at 4°C for 16 h. The antibody was captured by protein A-agarose (Sigma) at 4°C for 2 h. The immunoprecipitates were washed 3 times with ice-cold lysis buffer and then boiled in SDS/PAGE sample buffer for 10 min. Proteins in the immunoprecipitates were analyzed by SDS-PAGE and Western blotting. For endogenous interaction between FE65 and ARF6, the rat brain was homogenized in ice-cold lysis buffer and cleared by centrifugation as described above. ARF6 was immunoprecipitated from the lysate and was detected by 3A-1 anti-ARF6 antibody, whereas FE65 was detected by E20 anti-FE65 antibody.

ARF6 activation assays

ARF6 activation was determined using an active Arf6 pulldown kit (Cell Biolabs, San Diego, CA, USA). The principle of the kit is based on the fact that active ARF6 (*i.e.*, ARF6-GTP) binds specifically to the protein-binding domain (PBD) of GGA3 (33). To determine the ARF6-GTP level, cells were harvested in ice-cold lysis/binding/wash buffer and then cleared by centrifugation. The cleared lysates were incubated with GST-GGA3-PBD bait (*i.e.*, GST-GGA3-PBD fusion protein coupled on glutathione-Sepharose that is supplied with the kit) at 4°C for 3 h. The amounts of ARF6-GTP pulled down by the bait and total ARF6 in the lysates were analyzed by immunoblotting using 6ARF01 mouse monoclonal antibody.

Rac 1 activation assays

Rac1-GTP levels in cells were determined by using a Rac1 activation assay (ThermoScientific). In this assay, only Rac1-GTP interacts with GST-PAK1-PBD bait (34, 35). In brief, cells were harvested in assay/lysis buffer (25 mM HEPES. pH 7.5, 150 mM NaCl; 1% Nonidet P-40; 10 mM $MgCl_2$; 1 mM EDTA; 2% glycerol; and protease inhibitor cocktail) and followed by centrifugation. The cleared lysates were incubated with GST-PAK1-PBD bait (*i.e.*, GST-PAK1-PBD fusion protein coupled on glutathione-Sepharose that is supplied with the kit) to pull down Rac1-GTP. The levels of Rac1-GTP pulled down by the bait and total Rac1in the cell lysates were detected by Western blotting using 23A8 mouse monoclonal antibody.

Immunofluorescence studies and neurite length measurements

Neurons grown on coverslips were fixed in 4% (w/v) paraformaldehyde in PBS for 10 min, permeabilized in 0.1% Triton X-100 in PBS, blocked with 5% fetal bovine serum (FBS) in PBS for 30 min, and then probed with primary antibodies in 5% FBS/PBS. For FE65 and ARF6 colocalization studies, FE65 was detected using goat anti-FE65 (E20) and rat anti-ARF6. Primary antibodies were detected using AlexaFluor-coupled secondary Igs and nuclei labeled with 4′,6-diamidino-2-phenylindole (DAPI) (all from Invitrogen). Coverslips were mounted in Fluorescence Mounting Medium (Dako, Carpinteria, CA, USA). For intensity correlation analysis, images were captured using a Zeiss LSM510Meta confocal microscope equipped with a ×63, Plan-Apochromat 1.4 NA objective (Zeiss, Oberkochen, Germany), and analyzed using ImageJ (U.S. National Institutes of Health, Bethesda, MD, USA) with the intensity correlation analysis plug-in essentially as described by us and others (29, 36, 37). Further calculations and statistical analyses were performed using Excel (Microsoft Corp., Redmond, WA, USA) and SPSS 15 (IBM, Chicago, IL, USA). Light-microscopy was performed using a Leica DM5000B microscope with ×63 HCX PL Fluotar phase objective.

For neurite length measurements, we employed a widely used approach that involves cotransfecting enhanced green fluorescent protein (EGFP)-expressing plasmid [pEGFP-C1 (Clontech) in this study] into neurons (31, 38, 39). Since GFP has a uniform distribution throughout neurons, it therefore was used to determine cell shape and also act as a marker for transfected neurons. In brief, pEGFP-C1 was cotransfected with different constructs and/or with different siRNAs into 2-day *in vitro* (DIV) primary rat cortical neurons. All GFP-expressing neurons were immunostained for cotransfected protein to confirm expression. Healthy neurons were distinguished based on their morphologically normal nuclei stained by DAPI. The longest neurite of the transfected neurons was analyzed after 24 h for each treatment. Three independent experiments, with ≥40 neurons each, were performed in a blind manner. The lengths were determined as the distance from the growth cone tip to the periphery of the cell body and quantified using ImageJ with NeuronJ plug-in (40). Statistical analyses were performed using 1-way ANOVA test with Bonferroni *post hoc* test. Differences were considered significant at $P < 0.05$.

RESULTS

FE65 interacts directly with ARF6 through the PTB1 domain

From a yeast 2-hybrid screen of a human brain cDNA library using FE65 PTB1 + 2 domain as bait, we isolated a cDNA clone encoding the small GTPase ARF6. The FE65-ARF6 interaction in yeast was confirmed using LacZ liquid assays (data not shown).

To further analyze the FE65-ARF6 interaction, bacterially expressed GST and GST-ARF6 fusion proteins were used as baits to pull down FE65 from transfected cells. In this assay, GST-ARF6, but not GST, interacted with FE65 (**Fig. 1*A***). We next tested the FE65-ARF6 interaction using immunoprecipitation assays from transfected cells. FE65 was transfected either alone or cotransfected with myc-tagged ARF6 and ARF6 then immunoprecipitated *via* the myc tag. FE65 was present in immunoprecipitates from the FE65 + ARF6 but not FE65 singly transfected control cells (Fig. 1*B*). To demonstrate that endogenous FE65 interacts with en-

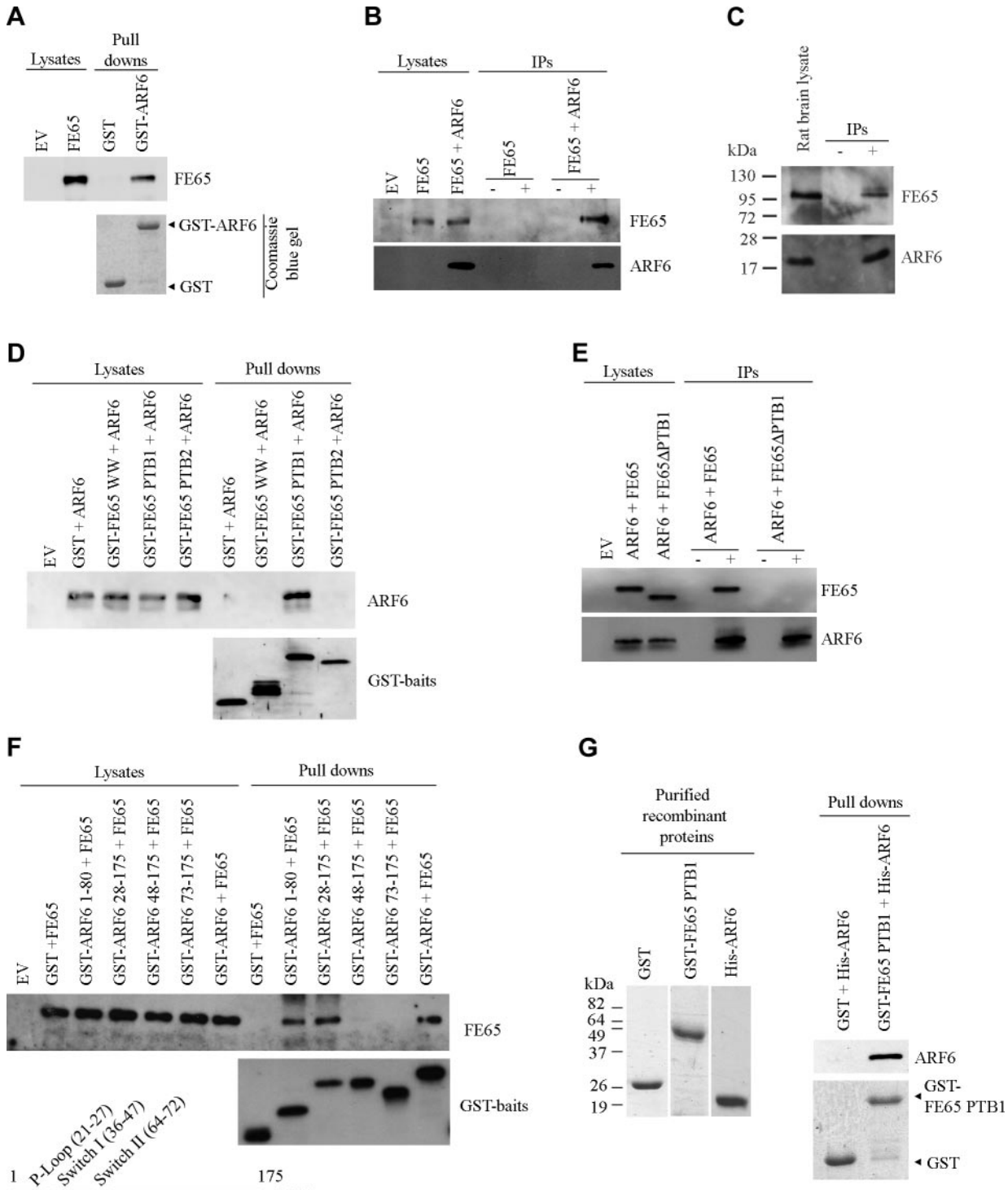

Figure 1. FE65 interacts with ARF6 *via* its PTB1 domain. *A*) ARF6 binds to FE65 in GST pulldown assays. *E. coli*-expressed GST and GST-ARF6 were used as baits in pulldown assays from FE65-transfected cells. FE65 in the cell lysates and pulldowns were detected using a goat anti-FE65. Coomassie blue gel showed the GST and GST-ARF6 baits. *B*) FE65 and ARF6 interact in immunoprecipitation assays from transfected cells. Immunoprecipitations were performed from CHO cells transfected with FE65 or FE65 + myc-tagged ARF6. ARF6 was immunoprecipitated using anti-myc antibody 9B11. Immunoprecipitated FE65 and ARF6 were detected by a goat anti-FE65 and a rat anti-ARF6, respectively. Symbols − and + indicate the absence or presence of myc antibody 9B11 in the immunoprecipitations. *C*) FE65 interacts endogenously with ARF6. ARF6 was immunoprecipitated from rat brain lysate using anti-ARF6 (3A-1). ARF6 was detected using rat anti-ARF6 antibody and FE65 using goat anti FE65 antibody. Immunoprecipitated FE65 and ARF6 were detected by a goat anti-FE65 and a rat anti-ARF6, respectively. Symbols − and + indicate the absence or presence of anti-ARF6 (3A-1) in the immunoprecipitations. *D*) ARF6

(*continued on next page*)

dogenous ARF6, we immunoprecipitated ARF6 from rat brain and probed these immunoprecipiates for FE65. FE65 was present in the ARF6 immunoprecipitates (Fig. 1*C*). Thus, FE65 and ARF6 interact in yeast 2-hybrid, GST pulldown, and immunoprecipitation assays, and endogenous FE65 interacts with endogenous ARF6 in immunoprecipitation assays from rat brain.

We next determined which domain of FE65 interacts with ARF6. To do so, we cotransfected CHO cells with full-length ARF6 and mammalian expression constructs encoding GST or GST fused to different domains of FE65. The domains were the WW domain, the first PTB domain (PTB1), and the second PTB domain (PTB2). GST pulldowns from the cell lysates were performed, and these were then probed on immunoblots for ARF6. These assays revealed that only GST-FE65 PTB1 interacted with ARF6 (Fig. 1*D*). Furthermore, FE65ΔPTB1 mutant could not interact with ARF6 in coimmunoprecipitation assay (Fig. 1*E*). To determine the region in ARF6 that mediates FE65-ARF6 interaction, we pulled down FE65 from transfected cell lysate using various GST-ARF6 deletion mutants. FE65 could be pulled down by GST-ARF6 28–175 (also ARF6 1–80 and full-length ARF6) but not ARF6 48–175 (Fig. 1*F*). This result suggests that aa 28–47 of AFR6 (a region that contains the guanine nucleotide binding switch I, residues 36–47, of ARF6) are critical for the interaction with FE65. To examine whether this interaction is direct (and not mediated by some other intermediary protein), we incubated *E. coli* purified His-ARF6 with *E. coli* purified GST or GST-FE65 PTB1 baits. Similar to the assays above, His-ARF6 was pulled down by GST-FE65 PTB1 but not GST (Fig. 1*G*). Taken together, these results demonstrate that ARF6 interacts directly with the FE65 PTB1 domain.

FE65 preferentially binds to the inactive ARF6-GDP form

Similar to other small GTPases, ARF6 exists in a GTP-bound active and a GDP-bound inactive state. These two states have distinct structures that alter the interactions between ARF6 and its binding proteins (for reviews, see refs. 21, 22). Therefore, it is possible that FE65 binds differentially to these two states of ARF6. To test this possibility, ARF6 Q67L and T27N mutants, which mimic the GTP- and GDP-bound states, respectively (for reviews, see refs. 21, 22), were utilized in both mammalian and bacterial GST-FE65 PTB1 pulldown assays (**Fig. 2*A*, *B***). In the mammalian GST pulldown assay, GST-FE65 PTB1 was cotransfected with either wild-type ARF6 or the ARF6 mutants. GST-FE65 PTB1 was pulled down from the transfected cell lysates, and the amounts of bound ARF6 were detected by immunoblotting. FE65 PTB1 domain interacted more strongly with ARF6 T27N than wild-type ARF6 but did not interact with ARF6 Q67L (Fig. 2*A*). Likewise, similar pulldown assays using bacterial expressed GST-FE65 PTB1 as bait revealed that FE65 PTB1 domain bound strongly to ARF6 T27N but not ARF6 Q67L (Fig. 2*B*). The specificities of the ARF6 mutants were confirmed by GST-GGA3 pulldown assay in which the bait preferably binds to ARF6 Q67L mutant (Fig. 2*B*), which is similar to those published elsewhere (41, 42). To further preclude the possibility that this differential binding is an artifact of using the artificial mutants, we treated the wild-type ARF6 transfected cell lysates with either GDP or nonhydrolyzable GTPγS to load either GDP or GTP nucleoside triphosphates onto ARF6 and then tested binding of GDP- and GTP-bound ARF6 to FE65 in pulldown assays. The GDP-bound and GTP-bound states of ARF6 were confirmed by performing ARF6 GTPase activation assays; GTP bound ARF6 interacts more strongly with GGA3 in these assays (Fig. 2*C*, bottom panel). In line with the assays involving mutants of ARF6, GDP-ARF6 interacted stronger than GTP-ARF6 with FE65 PTB1 domain (Fig. 2*C*, top panel). Thus, FE65 preferentially interacts with GDP- but not GTP-bound ARF6.

FE65 activates both endogenous ARF6 and Rac1

Typically, ARF effectors bind to ARF-GTP, and this suggests that FE65 does not function downstream of ARF6 as an effector protein. We therefore speculated that FE65 functions upstream to regulate ARF6 activation in some fashion. To test this possibility, we monitored the effect of modulating FE65 expression on the ARF6 activation. Overexpression of FE65 increased endogenous ARF6 activation (as detected using GGA3 pulldown ARF6 assays), whereas FE65 siRNA knockdown reduced ARF6 activation (**Fig. 3*A*, *B***). These findings implicate that although it preferentially binds to ARF6-GDP form, FE65 promotes the activation of ARF6.

A large body of evidence indicates that the small

interacts with FE65 *via* FE65 PTB1 domain. Myc-tagged ARF6 was cotransfected with GST, GST-FE65 WW, PTB1, or PTB2 domains into CHO cells. GST-FE65 fusion proteins were then pulled down, and the samples were probed on immunoblots for ARF6 and the GST baits as indicated. Approximately 12% of ARF6 in the input lysate was pulled down by GST-FE65 PTB1. *E*) FE65 PTB1 domain is essential for the interaction. Myc-tagged ARF6 was cotransfected with FE65 or FE65ΔPTB1 into CHO cells. ARF6 was immunoprecipitated from the lysates using myc antibody 9B11. ARF6 and FE65 in the precipitates were detected using rat anti-ARF6 antibody and FE65 using goat anti FE65 antibody, respectively. Symbols − and + indicate the absence or presence of myc antibody 9B11 in the immunoprecipitations. *F*) Residues 28 to 47 of ARF6 is important for FE65-ARF6 interaction. Myc-tagged FE65 was cotransfected with GST, GST-ARF6, ARF6 1–80, ARF6 28–175, ARF6 48–175, or ARF6 73–175 into CHO cells. GST-ARF6 fusion proteins were then pulled down and the samples probed on immunoblots for FE65 and the GST baits as indicated. Schematic diagram shows the ARF6 mutants. *G*) FE65 PTB1 domain interacts directly with ARF6. *E. coli*-expressed GST and GST-FE65 PTB1 were used to pull down purified His-tagged ARF6. Left panel: Coomassie-stained gel of the recombinant proteins. Right panel: pulldown assays.

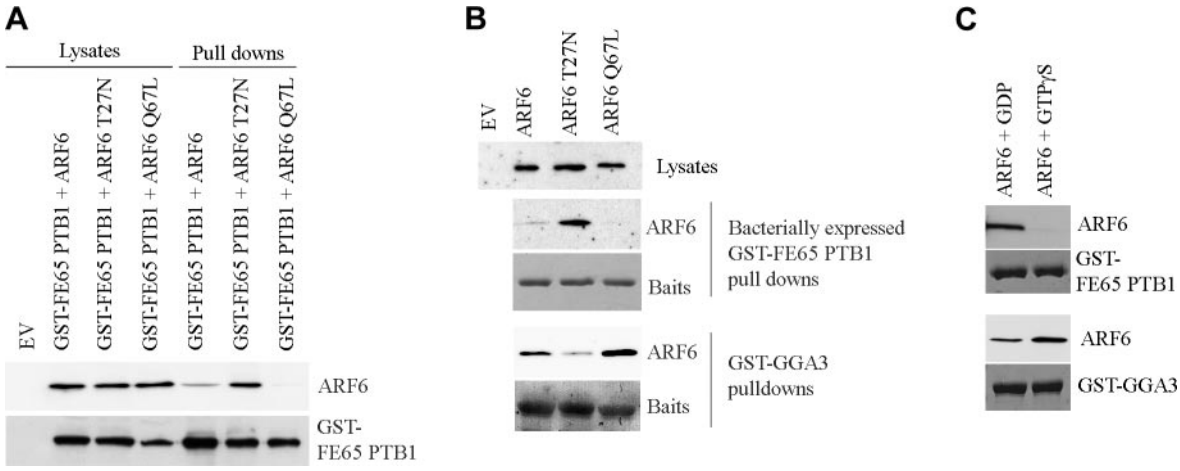

Figure 2. FE65 preferentially binds to GDP bound ARF6. *A*) Mammalian expression construct of GST-FE65 PTB1 was cotransfected with ARF6, ARF6 T72N (mimicking ARF6-GDP), or ARF6 Q67L (mimicking ARF6-GTP). FE65 was pulled down using the GST tag, and the amounts of bound ARF6 were detected by immunoblotting. Samples of both the input lysates and pulldowns are shown. GST-FE65 PTB1 bait pulled down 10, 23, and 2% of ARF6, ARF6 T27N, and ARF6 Q67L from the corresponding input lysates, respectively. *B*) *E. coli*-expressed GST-FE65 PTB1 domain was used as bait in pulldown assays from CHO cells transfected with myc-tagged ARF6, ARF6 T27N, or ARF6 Q67L. ARF6 in the input lysates and pulldowns was detected by anti-myc 9B11. Coomassie blue gel (third panel) showed GST-FE65 PTB1 baits used in the pulldowns. GST-FE65 PTB1 bait pulled down 12, 27, and 0.7% of ARF6, ARF6 T27N, and ARF6 Q67L from the corresponding input lysates, respectively. Control pulldowns using GST-GGA3 as bait were performed in which the bait preferably binds to ARF6 Q67L mutant. EV-transfected cell lysates are included in panels *A* and *B* to demonstrate overexpression of ARF6. *C*) *E. coli*-expressed GST-FE65 PTB1was used as baits in pulldown assays from myc-tagged ARF6-transfected lysates incubated with either GDP or GTPγS (to load either GDP or GTP onto ARF6). ARF6 was detected by anti-myc 9B11. Also shown is an ARF6 activation assay (bottom panels) to demonstrate activation of ARF6 (increased binding to GST-GGA3 bait) in GTPγS-treated lysates.

GTPase Rac1 is a downstream effector of ARF6 activation (refs. 43–47; for review, see ref. 48). The above observations prompted us to investigate whether FE65 also activates endogenous Rac1. We therefore performed Rac1 activation assays (which involved assaying binding of Rac1 to its effector PAK1 in pulldown assays) in cells in which FE65 expression was modulated. Overexpression of FE65 by transfection increased Rac1 activation, whereas siRNA knockdown of FE65 reduced Rac1 activation in these assays (Figs. 3*C*, *D*). To determine whether this stimulatory effect of FE65 on Rac1 activation involved ARF6, we performed similar Rac1 activation assays in cells in which ARF6 levels were depleted using siRNAs. In control siRNA-transfected cells, overexpression of FE65 again increased Rac1 activation but this stimulatory effect was abolished in ARF6 knockdown cells (Fig. 3*E*). Thus, FE65 acts upstream of ARF6 to regulate Rac1 activation.

FE65 and ARF6 colocalize in neuronal growth cones

Rac1 regulates actin dynamics within neurons, and during development, Rac1 controls neurite outgrowth *via* effects on the actin cytoskeleton within growth cones (for reviews, see refs. 49–51). Since FE65 regulates Rac1 activity, we therefore enquired whether FE65 and ARF6 colocalize in developing neurons and in particular, whether they colocalized in growth cones. Immunostaining for ARF6 revealed that it was principally a cytoplasmic protein in neurons that was enriched in perinuclear regions but also present in processes and growth cones (**Fig. 4*A*, *B***). To determine whether FE65 and ARF6 colocalize in growth cones, we immunostained neurons and utilized intensity correlation analyses (ICAs; ref. 37) to determine whether there was significant overlap in the distribution of the two proteins in growth cones. ICA compares the scatter plots of 2 stains against the product of the difference of the pixel intensities of each of the two stains from their respective means. Thus, ICA determines whether the pixel intensities from 2 signals vary in synchrony and as such is superior to many other methods for determining the extent of colocalization of proteins in cells and tissues. The values obtained from the analyses can be reported as an intensity correlation quotient (ICQ), which is a statistically testable, single value assessment of the relationship between 2 stained protein pairs: for random staining, ICQ = 0; for dependent staining (colocalization), $0 < \text{ICQ} \leq +0.5$; and for segregated staining, $-0.5 \leq \text{ICQ} < 0$. Both ARF6 and FE65 were enriched in growth cones of developing rat cortical neurons (Fig. 4*B*), and ICA revealed that they colocalized to a highly significant level within this subcellular compartment (mean$\pm$SEM ICQ=0.225$\pm$0.01, $P<0.001$; $n=36$ cells).

FE65 and ARF6 stimulate neurite outgrowth

Since Rac1 regulates neurite outgrowth and we demonstrated that FE65 and ARF6 regulate Rac1 activity, we determined the effects of modulating FE65 and ARF6 expression on neurite outgrowth in rat cortical neu-

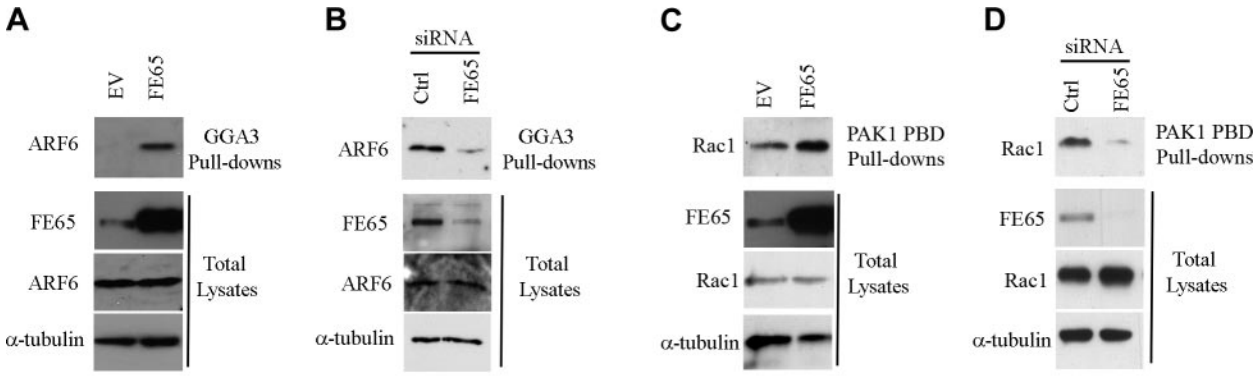

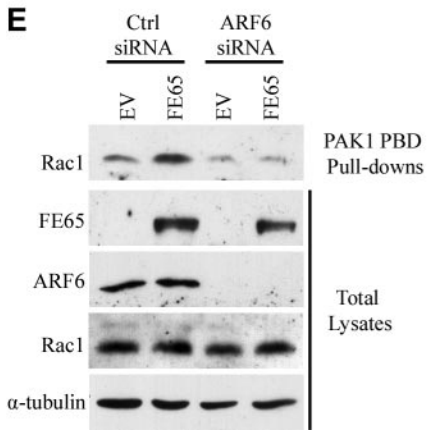

Figure 3. FE65 stimulates both endogenous ARF6 and Rac1 activation. *A, B*) FE65 stimulates ARF6 activation. CHO cells were either transfected with EV or FE65 (*A*), or treated with either control (Ctrl) or FE65 siRNAs (*B*). Endogenous active ARF6 was pulled down from the transfected cell lysates using GST-GGA3-PBD bait (supplied in the active ARF6 pulldown kit; Cell Biolabs) that interacts specifically with ARF6-GTP. ARF6-GTP bound to the bait was analyzed on immunoblots. Immunoblots showing FE65, ARF6, and α-tubulin levels as a loading control in the cell lysates are also shown. FE65 was detected using anti-FE65 E20, ARF6 using anti-ARF6 6ARF01 and anti-α-tubulin DM1A. Overexpression of FE65 stimulates (*A*, top panel) while siRNA knockdown of FE65 inhibits (*B*, top panel) ARF6 activation. Longer exposures revealed the presence of ARF6 in the GGA3 pulldowns in control transfected cells in panel *A*. *C, D*) FE65 stimulates Rac1 activation. CHO cells were either EV transfected or transfected with FE65 (*C*) or treated with either control or FE65 siRNAs (*D*). Endogenous active Rac1 was pulled down from the transfected cell lysates using GST-PAK1 PBD bait [supplied in the Rac1 activation assay (ThermoScientific), which binds Rac1-GTP]. Rac1-GTP bound to the bait was analyzed on immunoblots using anti-Rac1 23A8. Immunobots showing FE65, Rac1, and α-tubulin levels as a loading control in the cell lysates are also shown. Overexpression of FE65 stimulates (*C*, top panel) while knockdown of FE65 inhibits (*D*, top panel) Rac1 activation. *E*) Rac1 activation by FE65 requires ARF6. CHO cells were treated with control or ARF6 siRNAs and transfected with either EV or FE65. Rac1 activation assays were then performed. Top panel: immunoblot of the amounts of Rac1 in the PAK1 PBD pulldown assays. Also shown are immunoblots for FE65, ARF6, Rac1, and α-tubulin levels as a loading control in the cell lysates. Overexpression of FE65 did not trigger Rac1 activation in ARF6 knockdown cells (top panel, lane 2 *vs.* lane 4).

rons. We first tested the effect of overexpressing FE65 and/or ARF6 on neurite outgrowth. To do so, we transfected DIV2 rat cortical neurons with either FE65; FE65 lacking PTB1 (FE65ΔPTB1, which does not bind ARF6); or FE65 lacking PTB2 (FE65ΔPTB2) together with ARF6 and monitored neurite outgrowth, as de-

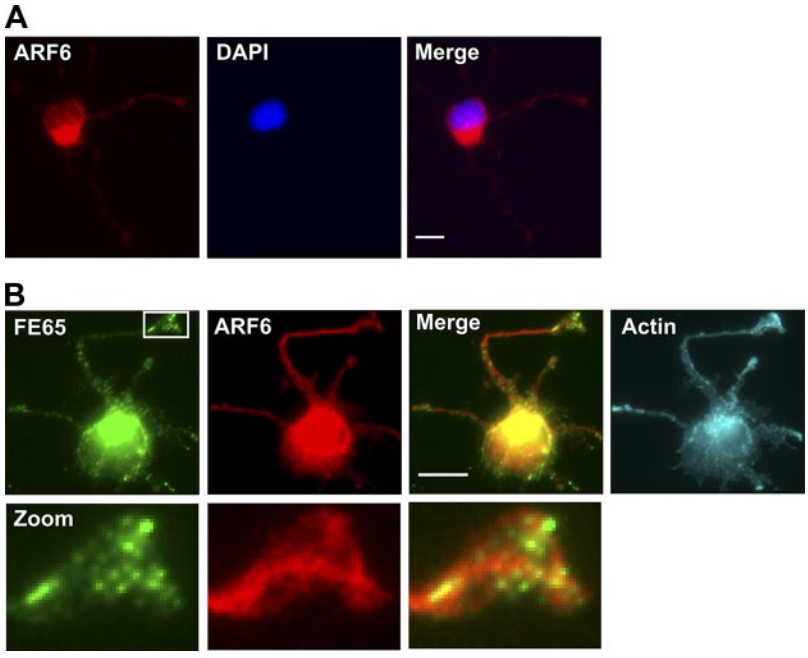

Figure 4. ARF6 is present in perinuclear regions and processes in developing neurons and colocalizes with FE65 in growth cones. Rat cortical neurons were immunostained at DIV2 for endogenous ARF6, FE65, and actin (*via* AlexaFluor-546 labeled phalloidin) and nuclei labeled using DAPI. *A*) Perinuclear and neurite labeling of ARF6. *B*) FE65 and ARF6 are present in both the cell bodies and processes but show a high level of colocalization in growth cones. Zoomed area of box with growth cone is shown. Scale bars = 10 μm.

scribed previously (31). Expression of FE65 or ARF6 both stimulated neurite outgrowth, and this effect was more pronounced in FE65 + ARF6 cotransfected neurons. However, the effect of FE65 was lost in neurons expressing FE65ΔPTB1 that does not bind ARF6 (**Fig. 5*A***). Intriguingly, the stimulatory effect of FE65 was also markedly decreased when the PTB2 domain was deleted (Fig. 5*A*). This suggests that FE65 PTB2 domain also plays a role in mediating neurite extension.

We next tested how loss of ARF6 or FE65 influenced neurite outgrowth. Analyses of these neurons revealed that siRNA knockdown of either ARF6 or FE65 both reduced neurite outgrowth (Fig. 5*B*, *C*). However, overexpression of FE65 did not rescue the effect of ARF6 knockdown (Fig. 5*B*) and FE65 knockdown did not influence the stimulatory effect of ARF6 on neurite outgrowth (Fig. 5*C*). Immunoblots revealed that both the FE65 and ARF6 siRNAs induced efficient knockdown in the neurons (Fig. 5*D*). These results support the notion that FE65 acts upstream of ARF6 to promote neurite outgrowth and are thus complementary to the biochemical studies (Figs. 2 and 3), which place FE65 as an upstream regulator of ARF6 and Rac1.

Rac1 is indispensible for FE65 and ARF6 stimulation of neurite outgrowth

As shown in the biochemical assays, FE65 stimulates ARF6-Rac1 signaling (Fig. 3*C*, *D*). It is therefore possible that the effect of FE65 on neurite outgrowth involves Rac1. To test this possibility, we monitored the stimulatory effect of FE65 + ARF6 expression on neurite outgrowth in cells expressing a dominant-negative Rac1 (N17Rac1; ref. 31). Overexpression of wild-type Rac1 enhanced neurite outgrowth in FE65 + ARF6 cotransfected neurons. However, N17Rac1 blocked

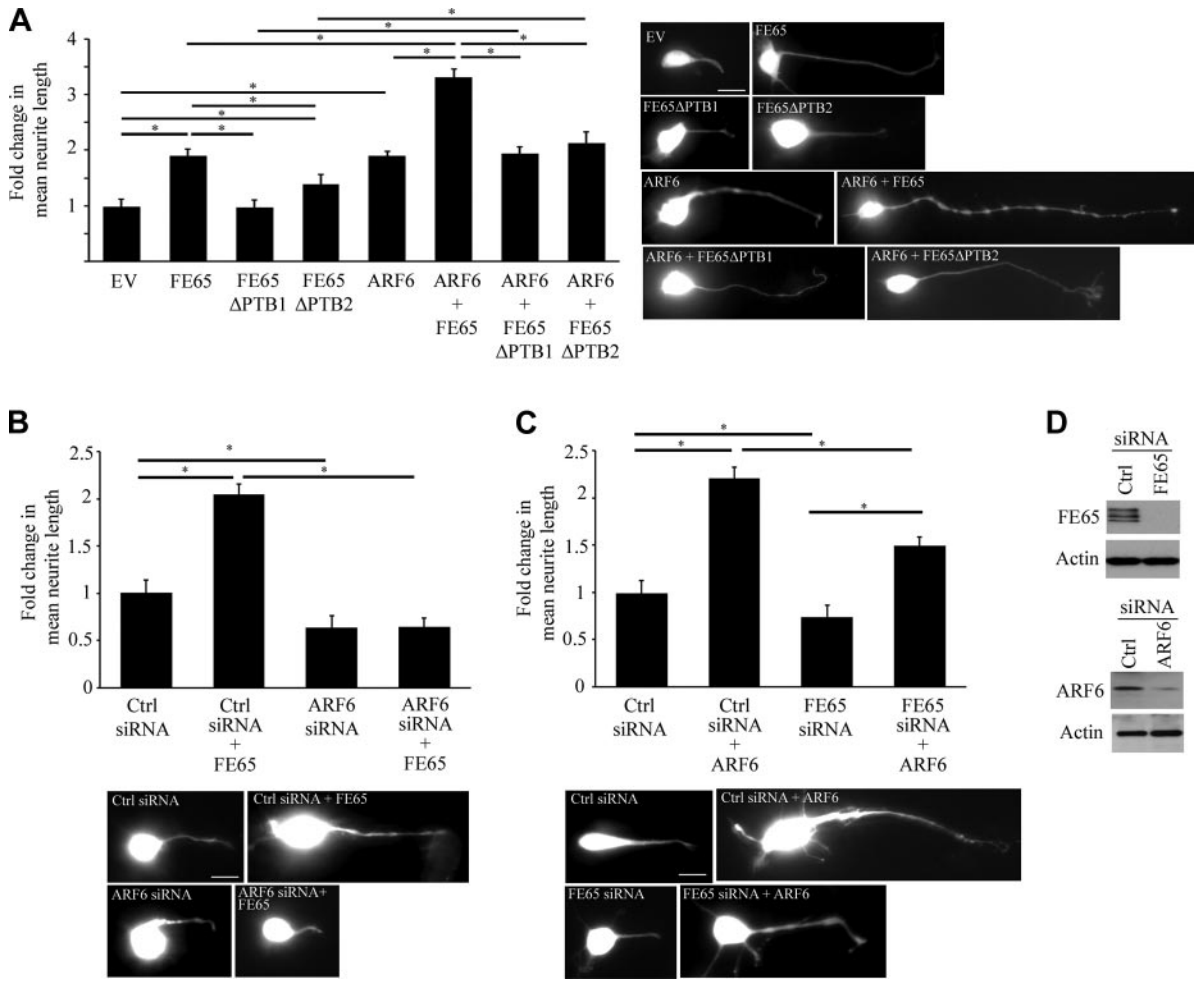

Figure 5. FE65 and ARF6 both stimulate neurite outgrowth, but the effect of FE65 is lost in the absence of ARF6. *A–C*) Rat cortical neurons were transfected with EGFP as a cell morphology marker and different combinations of EV control plasmid, FE65, FE65ΔPTB1, FE65ΔPTB2, ARF6, and either control, FE65, or ARF6 siRNAs as indicated. All transfections received the same amounts of DNA. The length of the longest neurite was then determined 24 h later. Bar charts show fold changes in mean neurite length for the longest neurite. Also shown are representative images of the different transfected cells. *A*) FE65 and ARF6 but not FE65ΔPTB1 stimulate neurite outgrowth. On the other hand, FE65ΔPTB2 induces a small increase in neurite extension. *B*) Knockdown of ARF6 inhibits neurite outgrowth, and this affect is not influenced by overexpression of FE65. *C*) Knockdown of FE65 inhibits neurite outgrowth, but this effect is rescued by overexpression of ARF6. Data were obtained from ≥40 cells/transfection, and the experiments were repeated 3 times. Error bars = SD. Scale bars = 10 μm. $*P < 0.001$. *D*) Immunoblot demonstrating siRNA knockdown of FE65 and ARF6; also shown is an immunoblot for actin as a loading control.

this effect of FE65 + ARF6 (**Fig. 6*A***). In agreement with this, the stimulatory effect of FE65 and ARF6 on neurite extension was markedly reduced in Rac1-knockdown neurons (Fig. 6*B*). On the other hand, expression of constitutively active Rac1 (V12Rac1) alone was sufficient to stimulate neurite outgrowth (Fig. 6*A*, *C*). Knockdown of either FE65 or ARF6 induced small decrease in neurite extension of the V12Rac1 transfected neurons (Fig. 6*C*). Such a reduction in neurite outgrowth might due to the inactivation of endogenous Rac1 in the FE65 and ARF6 knockdown cells. Nevertheless, Rac1 appears to be essential for the effect of FE65 and ARF6 on neurite outgrowth.

To test if the effect of Rac1 on neurite outgrowth is *via* actin-modeling, rat cortical neurons were treated with actin-destabilizing agent CytoD. Decrease of neurite outgrowth was observed in the empty vector (EV)-transfected neurons treated with CytoD (Fig. 6*D*). The stimulatory effect of V12Rac1 on neurite extension was suppressed in the presence of CytoD (Fig. 6*D*). This suggests that Rac1 stimulates neurite outgrowth in rat cortical neurons, at least in part, *via* actin modeling.

DISCUSSION

In this study, we identify the small GTPase ARF6 as a binding partner for the neuronal adaptor protein FE65. FE65 contains a number of protein-protein interaction domains, including an N-terminal WW domain and 2 C-terminal PTB domains, and we show that binding of ARF6 is mediated *via* the first (N-terminal) PTB1 domain. FE65 also binds to 2 nuclear proteins, the histone acetyl transferase Tip60, and the transcription factor CP2/LSF/LBP1 *via* PTB1 (9, 52, 53). Since ARF6 is a cytoplasmic protein (Fig. 4*A*), it is unlikely to compete CP2/LSF/LBP1 for binding to FE65. However, it is not known whether Tip60 competes with ARF6 for FE65 PTB1, as a splice variant of Tip60, PLA2 interacting protein, localizes to both cytoplasm and nucleus (54). In addition, several low-density lipoprotein receptor family members, including LRP1, ApoER2, and VLDLR, have been shown to interact with FE65 PTB1 (55–60). Of note, LRP1 has been recently shown to act as a myelin-associated glycoprotein receptor to inhibit neurite outgrowth (61), ApoER2 functions as a Reelin receptor to regulate neurite motility (62), and VLDLR has also been implicated in neurite development (63). Since we show here that binding of ARF6 to FE65 PTB1 promotes neurite outgrowth, it is possible that changes in binding of these different FE65 PTB1 ligands is a mechanism for regulating and fine-tuning neurite outgrowth in different neuronal populations during development. Indeed, such mechanisms may also be conserved in the adult to regulate plasticity.

The mechanisms for binding of PTB domains with their ligands has now been characterized in a number of studies (for review, see ref. 64). Many PTB domain ligands interact *via* canonical C-terminal NPXY or NXXY sequences in which the tyrosine can be either phosphorylated or nonphosphorylated (64). Although ARF6 does not contain such sequences, the PTB domains are now known to interact with ligands that do not contain NPXY/NXXY sequences. For example, binding of Deleted in liver cancer-1 to the tensin2 PTB domain has recently been shown to involve a novel interface and not the classical NPXY/NXXY sequence (65). Association of ARF6 with the FE65 PTB1 domain thus appears to resemble this less well-characterized mode of interaction.

Since FE65 interacts with the guanine nucleotide binding switch I of ARF6, this may provide an explanation for the fact that FE65 preferably binds to the ARF6-GDP as switch I undergoes conformational reorganization during GDP/GTP cycle of ARF6 (66, 67). Notably, such FE65-ARF6-GDP interaction stimulates ARF6 activation. The mechanism that underlies this stimulatory effect is unclear; certainly FE65 does not structurally resemble any known GEF. Of note, several ARF-interacting adaptor proteins that lack of intrinsic GEF and GAP activities have been shown to alter ARF activity. For example, Arfaptin1 was found to inhibit ARF even though it binds to constitutively active mutant of ARF (68, 69). As an adaptor protein, it seems likely that FE65 may somehow mediate the recruitment of other proteins (perhaps ARF6 GEFs) to modulate ARF6 activity. Indeed, there are precedents for such a model. For example, GULP1 binds to ARF6 and the ARF6-GAP ACAP1 to stimulate ARF6 activation (70).

ARF6 regulates a number of physiological processes, including endocytosis, secretion, phagocytosis, cell adhesion, and cell migration; in neurons, ARF6 also regulates axon and neurite outgrowth (refs. 21, 22, 71–73; and results described here). This role in neurite outgrowth is mediated, at least in part, *via* Rac1 dependent actin remodeling in the growth cone; ARF6 localizes to the plasma membrane and recruits Rac1 to the cell surface (for reviews, see refs. 21, 22). Interestingly, APP is also present within growth cones and functions in axonal outgrowth (19, 74–76), but the mechanisms that underlie this function are not properly understood. Both APP and FE65 have been implicated in various cytoplasmic and nuclear processes (14). Of note, APP has been shown to function as a cytosolic docking site to retain FE65 in the cytoplasm through the interaction between FE65 PTB2 and APP intracellular domain (77). Therefore, it is possible that the role of APP in axonal outgrowth may be to recruit FE65 to growth cone membranes where it can then interact with ARF6 *via* PTB1. In support of this notion, the stimulatory effect of FE65 on neurite outgrowth was significantly reduced when the PTB2 domain was deleted (*i.e.*, FE65ΔPTB2). Since FE65ΔPTB2 remains concentrated at the growth cone (Supplemental Fig. S1), such recruitment of FE65 by APP may occur after FE65 entry to growth cones. Once recruited, the FE65-ARF6 interaction might then stimulate the activation of ARF6 and downstream Rac1 so as to modulate actin dynamics. Interestingly, FE65 also binds *via* its WW domain to mammalian enabled (Mena), a member of

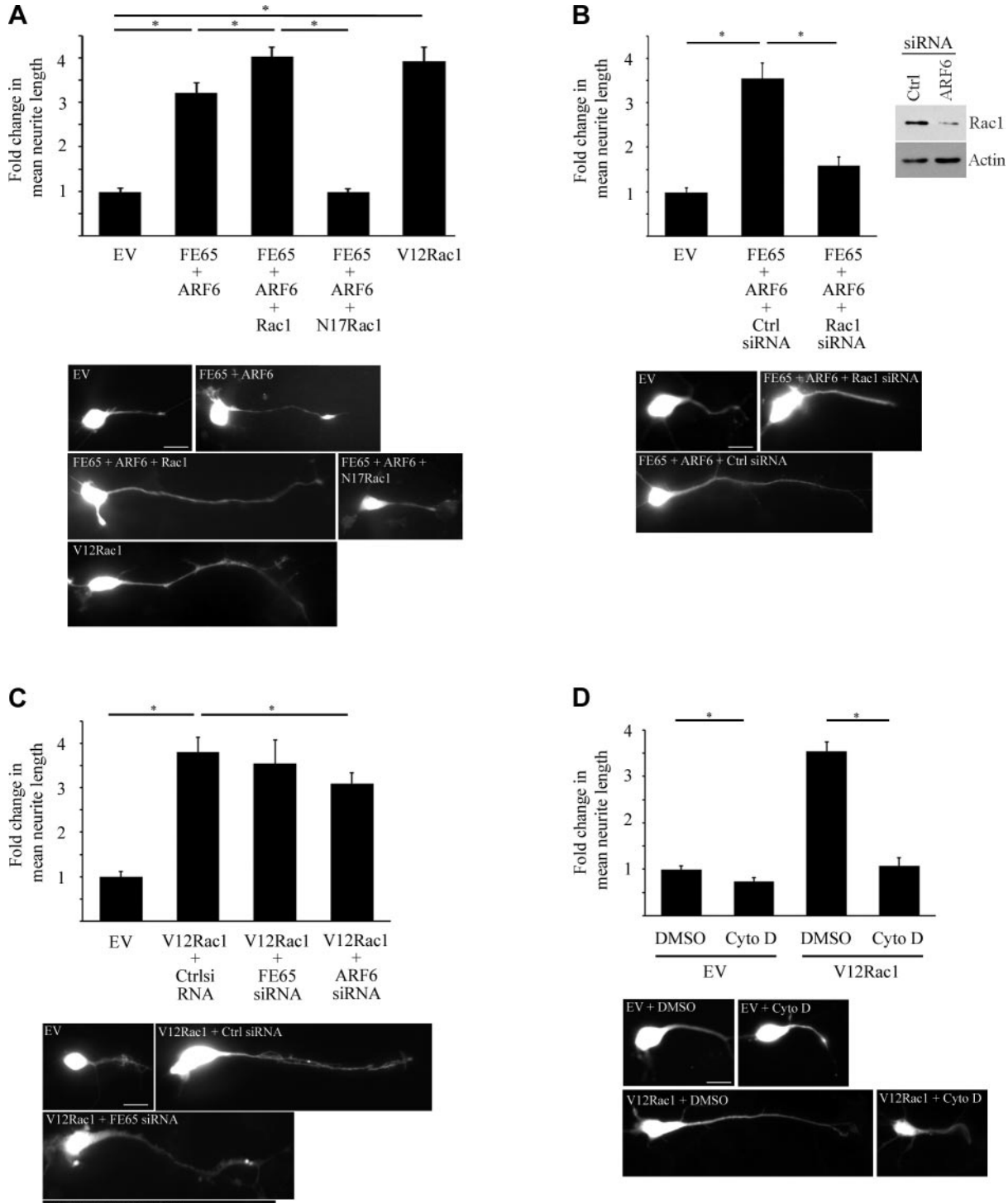

Figure 6. Rac1 is indispensable for FE65 and ARF6 stimulation of neurite outgrowth. *A*, *B*) Stimulation of neurite outgrowth by FE65 and ARF6 is abrogated in cells coexpressing a dominant-negative Rac1 (*A*) or transfected with Rac1 siRNA (*B*). *A*) Rat cortical neurons were transfected with EGFP and either EV, FE65 + ARF6, FE65 + ARF6 + Rac1, FE65 + ARF6 + N17Rac1 (dominant-negative Rac1), or V12Rac1 (constitutively active Rac1). *B*) Rat cortical neurons were transfected with EGFP and either EV, FE65 + ARF6 + control siRNA, and FE65 + ARF6 + Rac1 siRNA. *C*) Immunoblot shows siRNA knockdown of Rac1. Constitutively active Rac1 stimulates neurite outgrowth. Rat cortical neurons were transfected with EGFP and either EV, V12Rac1 + control siRNA, V12Rac1 + FE65 siRNA, or V12Rac1 + ARF6 siRNA. In panels *A–C*, the length of the longest neurite was determined 24 h later. *D*) Effect of constitutively active Rac1 on neurite outgrowth is suppressed in the presence of CytoD. Rat cortical neurons were transfected with EGFP and either EV or V12Rac1. Neurons were treated with either DMSO or 0.25 μg/ml CytoD for 24 h. Length of the longest neurite was then measured. Bar charts show fold changes in mean neurite length for the longest neurite. Also shown are representative images of the different transfected cells. Data were obtained from ≥40 cells/transfection, and the experiments were repeated 3 times. Error bars = SD. Scale bars = 10 μm. $^*P < 0.001$.

the Ena/Vasp family of actin regulatory proteins (78). Furthermore, FE65 and Rac1 have been shown to interact in a coimmunoprecipitation assay (79). Thus, FE65 may perform critical functions within growth cones to recruit various molecules and integrate a variety of signaling cascades that control axon outgrowth.

In our study, actin-destabilizing agent CytoD abolished the stimulatory effect of V12Rac1 on neurite extension (Fig. 6). It may suggest that destabilization of actin has an inhibitory effect on the process. However, the role of actin depolymerization in neurite development remains controversial (80–90). The causes for such contradictory data are not fully understood; however, they may due to the differences of neuron types, ages, animal strains, culture conditions, and experimental approaches employed. Further studies are required to find out the reasons for such conflicting observations.

Many of the cellular mechanisms that regulate axon and dendritic outgrowth during development are conserved in the adult and function at the synapse to control plasticity. As such, the FE65-ARF6-Rac1 interaction we describe here may also function in synapses. Synaptic dysfunction and loss are key features of Alzheimer's disease. Disruption to ARF6 function has recently been implicated in the pathogenesis of Alzheimer's disease *via* ARF6 control of BACE1 trafficking; BACE1 processing of APP is required for production of Aβ (91). Our findings suggest that perturbation of FE65/ARF6 function might also disrupt synaptic function *via* alterations in Rac1 dependent actin remodeling. FJ

This work was supported by funds from the Research Grant Council Hong Kong (CUHK467712); the CUHK Direct Grant Scheme (2030443); United College Endowment Fund (CA11156 and CA11188); Wellcome Trust; Medical Research Council (UK); and Alzheimer's Research UK. The authors thank Ka Ming Vincent Tam for technical assistance.

REFERENCES

1. Borg, J. P., Ooi, J., Levy, E., and Margolis, B. (1996) The phosphotyrosine interaction domains of X11 and FE65 bind to distinct sites on the YENPTY motif of amyloid precursor protein. *Mol. Cell. Biol.* **16,** 6229–6241
2. Fiore, F., Zambrano, N., Minopoli, G., Donini, V., Duilio, A., and Russo, T. (1995) The regions of the Fe65 protein homologous to the phosphotyrosine interaction/phosphotyrosine binding domain of Shc bind the intracellular domain of the Alzheimer's amyloid precursor protein. *J. Biol. Chem.* **270,** 30853–30856
3. McLoughlin, D. M., and Miller, C. C. (1996) The intracellular cytoplasmic domain of the Alzheimer's disease amyloid precursor protein interacts with phosphotyrosine-binding domain proteins in the yeast two-hybrid system. *FEBS Lett.* **397,** 197–200
4. Ando, K., Iijima, K. I., Elliott, J. I., Kirino, Y., and Suzuki, T. (2001) Phosphorylation-dependent regulation of the interaction of amyloid precursor protein with Fe65 affects the production of b-amyloid. *J. Biol. Chem.* **276,** 40353–40361
5. Guenette, S., Chang, Y., Hiesberger, T., Richardson, J. A., Eckman, C. B., Eckman, E. A., Hammer, R. E., and Herz, J. (2006) Essential roles for the FE65 amyloid precursor protein-interacting proteins in brain development. *EMBO J.* **25,** 420–431
6. King, G. D., and Scott Turner, R. (2004) Adaptor protein interactions: modulators of amyloid precursor protein metabolism and Alzheimer's disease risk? *Exp. Neurol.* **185,** 208–219
7. Sabo, S. L., Lanier, L. M., Ikin, A. F., Khorkova, O., Sahasrabudhe, S., Greengard, P., and Buxbaum, J. D. (1999) Regulation of b-amyloid secretion by FE65, an amyloid protein precursor-binding protein. *J. Biol. Chem.* **274,** 7952–7957
8. Wang, B., Hu, Q., Hearn, M. G., Shimizu, K., Ware, C. B., Liggitt, D. H., Jin, L. W., Cool, B. H., Storm, D. R., and Martin, G. M. (2004) Isoform-specific knockout of FE65 leads to impaired learning and memory. *J. Neurosci. Res.* **75,** 12–24
9. Cao, X., and Sudhof, T. C. (2001) A transcriptionally [correction of transcriptively] active complex of APP with Fe65 and histone acetyltransferase Tip60. *Science* **293,** 115–120
10. Perkinton, M. S., Standen, C. L., Lau, K. F., Kesavapany, S., Byers, H. L., Ward, M., McLoughlin, D. M., and Miller, C. C. (2004) The c-Abl tyrosine kinase phosphorylates the Fe65 adaptor protein to stimulate Fe65/amyloid precursor protein nuclear signaling. *J. Biol. Chem.* **279,** 22084–22091
11. Nakaya, T., Kawai, T., and Suzuki, T. (2008) Regulation of FE65 nuclear translocation and function by amyloid beta-protein precursor in osmotically stressed cells. *J. Biol. Chem.* **283,** 19119–19131
12. Stante, M., Minopoli, G., Passaro, F., Raia, M., Vecchio, L. D., and Russo, T. (2009) Fe65 is required for Tip60-directed histone H4 acetylation at DNA strand breaks. *Proc. Natl. Acad. Sci. U. S. A.* **106,** 5093–5098
13. McLoughlin, D. M., Irving, N. G., and Miller, C. C. (1998) The Fe65 and X11 families of proteins: proteins that interact with the Alzheimer's disease amyloid precursor protein. *Biochem. Soc. Trans.* **26,** 497–500
14. Minopoli, G., Gargiulo, A., Parisi, S., and Russo, T. (2012) Fe65 matters: New light on an old molecule. *IUBMB Life* **64,** 936–942
15. Turner, A. J., Belyaev, N. D., and Nalivaeva, N. N. (2011) Mediator: the missing link in amyloid precursor protein nuclear signalling. *EMBO Rep.* **12,** 180–181
16. Kesavapany, S., Banner, S. J., Lau, K. F., Shaw, C. E., Miller, C. C., Cooper, J. D., and McLoughlin, D. M. (2002) Expression of the Fe65 adapter protein in adult and developing mouse brain. *Neuroscience* **115,** 951–960
17. Ma, Q. H., Futagawa, T., Yang, W. L., Jiang, X. D., Zeng, L., Takeda, Y., Xu, R. X., Bagnard, D., Schachner, M., Furley, A. J., Karagogeos, D., Watanabe, K., Dawe, G. S., and Xiao, Z. C. (2008) A TAG1-APP signalling pathway through Fe65 negatively modulates neurogenesis. *Nat. Cell Biol.* **10,** 283–294
18. Sabo, S. L., Ikin, A. F., Buxbaum, J. D., and Greengard, P. (2001) The Alzheimer amyloid precursor protein (APP) and FE65, an APP-binding protein, regulate cell movement. *J. Cell Biol.* **153,** 1403–1414
19. Sabo, S. L., Ikin, A. F., Buxbaum, J. D., and Greengard, P. (2003) The amyloid precursor protein and its regulatory protein, FE65, in growth cones and synapses in vitro and in vivo. *J. Neurosci.* **23,** 5407–5415
20. Wang, Y., Zhang, M., Moon, C., Hu, Q., Wang, B., Martin, G., Sun, Z., and Wang, H. (2009) The APP-interacting protein FE65 is required for hippocampus-dependent learning and long-term potentiation. *Learn. Mem.* **16,** 537–544
21. D'Souza-Schorey, C., and Chavrier, P. (2006) ARF proteins: roles in membrane traffic and beyond. *Nat. Rev. Mol. Cell. Biol.* **7,** 347–358
22. Jaworski, J. (2007) ARF6 in the nervous system. *Eur. J. Cell Biol.* **86,** 513–524
23. Hernandez-Deviez, D. J., Roth, M. G., Casanova, J. E., and Wilson, J. M. (2004) ARNO and ARF6 regulate axonal elongation and branching through downstream activation of phosphatidylinositol 4-phosphate 5-kinase alpha. *Mol. Biol. Cell* **15,** 111–120
24. Eva, R., Crisp, S., Marland, J. R., Norman, J. C., Kanamarlapudi, V., Ffrench-Constant, C., and Fawcett, J. W. (2012) ARF6 directs axon transport and traffic of integrins and regulates axon growth in adult DRG neurons. *J. Neurosci.* **32,** 10352–10364
25. Schweitzer, J. K., Sedgwick, A. E., and D'Souza-Schorey, C. (2011) ARF6-mediated endocytic recycling impacts cell movement, cell division and lipid homeostasis. *Semin. Cell Dev. Biol.* **22,** 39–47
26. De Curtis, I. (2008) Functions of Rac GTPases during neuronal development. *Dev. Neurosci.* **30,** 47–58

27. Hao, C. Y., Perkinton, M. S., Chan, W. W., Chan, H. Y., Miller, C. C., and Lau, K. F. (2011) GULP1 is a novel APP-interacting protein that alters APP processing. *Biochem. J.* **436,** 631–639
28. Chow, W. N., Luk, H. W., Chan, H. Y., and Lau, K. F. (2012) Degradation of mutant huntingtin via the ubiquitin/proteasome system is modulated by FE65. *Biochem. J.* **443,** 681–689
29. Vagnoni, A., Perkinton, M. S., Gray, E. H., Francis, P. T., Noble, W., and Miller, C. C. (2012) Calsyntenin-1 mediates axonal transport of the amyloid precursor protein and regulates Abeta production. *Hum. Mol. Genet.* **21,** 2845–2854
30. Lau, K. F., McLoughlin, D. M., Standen, C. L., Irving, N. G., and Miller, C. C. (2000) Fe65 and X11b co-localize with and compete for binding to the amyloid precursor protein. *Neuroreport* **11,** 3607–3610
31. Tudor, E. L., Perkinton, M. S., Schmidt, A., Ackerley, S., Brownlees, J., Jacobsen, N. J., Byers, H. L., Ward, M., Hall, A., Leigh, P. N., Shaw, C. E., McLoughlin, D. M., and Miller, C. C. (2005) ALS2/Alsin regulates Rac-PAK signaling and neurite outgrowth. *J. Biol. Chem.* **280,** 34735–34740
32. Lau, K. F., Chan, W. M., Perkinton, M. S., Tudor, E. L., Chang, R. C., Chan, H. Y., McLoughlin, D. M., and Miller, C. C. (2008) Dexras1 interacts with FE65 to regulate FE65-amyloid precursor protein-dependent transcription. *J. Biol. Chem.* **283,** 34728–34737
33. Santy, L. C., and Casanova, J. E. (2001) Activation of ARF6 by ARNO stimulates epithelial cell migration through downstream activation of both Rac1 and phospholipase D. *J. Cell Biol.* **154,** 599–610
34. Taylor, S. J., and Shalloway, D. (1996) Cell cycle-dependent activation of Ras. *Curr. Biol.* **6,** 1621–1627
35. Benard, V., Bohl, B. P., and Bokoch, G. M. (1999) Characterization of rac and cdc42 activation in chemoattractant-stimulated human neutrophils using a novel assay for active GTPases. *J. Biol. Chem.* **274,** 13198–13204
36. Tudor, E. L., Galtrey, C. M., Perkinton, M. S., Lau, K. F., De Vos, K. J., Mitchell, J. C., Ackerley, S., Hortobagyi, T., Vamos, E., Leigh, P. N., Klasen, C., McLoughlin, D. M., Shaw, C. E., and Miller, C. C. (2010) Amyotrophic lateral sclerosis mutant vesicle-associated membrane protein-associated protein-B transgenic mice develop TAR-DNA-binding protein-43 pathology. *Neuroscience* **167,** 774–785
37. Li, Q., Lau, A., Morris, T. J., Guo, L., Fordyce, C. B., and Stanley, E. F. (2004) A syntaxin 1, Galpha(o), and N-type calcium channel complex at a presynaptic nerve terminal: analysis by quantitative immunocolocalization. *J. Neurosci.* **24,** 4070–4081
38. Bryan, B., Kumar, V., Stafford, L. J., Cai, Y., Wu, G., and Liu, M. (2004) GEFT, a Rho family guanine nucleotide exchange factor, regulates neurite outgrowth and dendritic spine formation. *J. Biol. Chem.* **279,** 45824–45832
39. May, V., Schiller, M. R., Eipper, B. A., and Mains, R. E. (2002) Kalirin Dbl-homology guanine nucleotide exchange factor 1 domain initiates new axon outgrowths via RhoG-mediated mechanisms. *J. Neurosci.* **22,** 6980–6990
40. Meijering, E., Jacob, M., Sarria, J. C., Steiner, P., Hirling, H., and Unser, M. (2004) Design and validation of a tool for neurite tracing and analysis in fluorescence microscopy images. *Cytometry A* **58,** 167–176
41. Macia, E., Luton, F., Partisani, M., Cherfils, J., Chardin, P., and Franco, M. (2004) The GDP-bound form of Arf6 is located at the plasma membrane. *J. Cell Sci.* **117,** 2389–2398
42. Nekhoroshkova, E., Albert, S., Becker, M., and Rapp, U. R. (2009) A-RAF kinase functions in ARF6 regulated endocytic membrane traffic. *PLoS One* **4,** e4647
43. Boshans, R. L., Szanto, S., van Aelst, L., and D'Souza-Schorey, C. (2000) ADP-ribosylation factor 6 regulates actin cytoskeleton remodeling in coordination with Rac1 and RhoA. *Mol. Cell. Biol.* **20,** 3685–3694
44. Radhakrishna, H., Al-Awar, O., Khachikian, Z., and Donaldson, J. G. (1999) ARF6 requirement for Rac ruffling suggests a role for membrane trafficking in cortical actin rearrangements. *J. Cell Sci.* **112,** 855–866
45. Balasubramanian, N., Scott, D. W., Castle, J. D., Casanova, J. E., and Schwartz, M. A. (2007) Arf6 and microtubules in adhesion-dependent trafficking of lipid rafts. *Nat. Cell Biol.* **9,** 1381–1391
46. Monteleon, C. L., Sedgwick, A., Hartsell, A., Dai, M., Whittington, C., Voytik-Harbin, S., and D'Souza-Schorey, C. (2012) Establishing epithelial glandular polarity: interlinked roles for ARF6, Rac1, and the matrix microenvironment. *Mol. Biol. Cell* **23,** 4495–4505
47. Chen, P. W., Jian, X., Yoon, H. Y., and Randazzo, P. A. (2013) ARAP2 signals through Arf6 and Rac1 to control focal adhesion morphology. *J. Biol. Chem.* **288,** 5849–5860
48. Myers, K. R., and Casanova, J. E. (2008) Regulation of actin cytoskeleton dynamics by Arf-family GTPases. *Trends Cell Biol.* **18,** 184–192
49. Nikolic, M. (2002) The role of Rho GTPases and associated kinases in regulating neurite outgrowth. *Int. J. Biochem. Cell Biol.* **34,** 731–745
50. Lundquist, E. A. (2003) Rac proteins and the control of axon development. *Curr. Opin. Neurobiol.* **13,** 384–390
51. Etienne-Manneville, S., and Hall, A. (2002) Rho GTPases in cell biology. *Nature* **420,** 629–635
52. Kim, H. S., Kim, E. M., Lee, J. P., Park, C. H., Kim, S., Seo, J. H., Chang, K. A., Yu, E., Jeong, S. J., Chong, Y. H., and Suh, Y. H. (2003) C-terminal fragments of amyloid precursor protein exert neurotoxicity by inducing glycogen synthase kinase-3b expression. *FASEB J.* **17,** 1951–1953
53. Zambrano, N., Minopoli, G., de Candia, P., and Russo, T. (1998) The Fe65 adaptor protein interacts through its PID1 domain with the transcription factor CP2/LSF/LBP1. *J. Biol. Chem.* **273,** 20128–20133
54. Sheridan, A. M., Force, T., Yoon, H. J., O'Leary, E., Choukroun, G., Taheri, M. R., and Bonventre, J. V. (2001) PLIP, a novel splice variant of Tip60, interacts with group IV cytosolic phospholipase A(2), induces apoptosis, and potentiates prostaglandin production. *Mol. Cell. Biol.* **21,** 4470–4481
55. Dumanis, S. B., Chamberlain, K. A., Jin Sohn, Y., Jin Lee, Y., Guenette, S. Y., Suzuki, T., Mathews, P. M., Pak, D., Rebeck, G. W., Suh, Y. H., Park, H. S., and Hoe, H. S. (2012) FE65 as a link between VLDLR and APP to regulate their trafficking and processing. *Mol. Neurodegener.* **7,** 9
56. Hoe, H. S., Magill, L. A., Guenette, S., Fu, Z., Vicini, S., and Rebeck, G. W. (2006) FE65 interaction with the ApoE receptor ApoEr2. *J. Biol. Chem.* **281,** 24521–24530
57. Trommsdorff, M., Borg, J. P., Margolis, B., and Herz, J. (1998) Interaction of cytosolic adaptor proteins with neuronal apolipoprotein E receptors and the amyloid precursor protein. *J. Biol. Chem.* **273,** 33556–33560
58. Pietrzik, C. U., Yoon, I. S., Jaeger, S., Busse, T., Weggen, S., and Koo, E. H. (2004) FE65 constitutes the functional link between the low-density lipoprotein receptor-related protein and the amyloid precursor protein. *J. Neurosci.* **24,** 4259–4265
59. Mulvihill, M. M., Guttman, M., and Komives, E. A. (2011) Protein interactions between Fe65, the LDL receptor-related protein and the amyloid precursor protein. *Biochemistry* **50,** 6208–6216
60. Kounnas, M. Z., Moir, R. D., Rebeck, G. W., Bush, A. I., Argraves, W. S., Tanzi, R. E., Hyman, B. T., and Strickland, D. K. (1995) LDL receptor-related protein, a multifunctional ApoE receptor, binds secreted beta-amyloid precursor protein and mediates its degradation. *Cell* **82,** 331–340
61. Stiles, T. L., Dickendesher, T. L., Gaultier, A., Fernandez-Castaneda, A., Mantuano, E., Giger, R. J., and Gonias, S. L. (2013) LDL receptor-related protein-1 is a sialic-acid-independent receptor for myelin-associated glycoprotein that functions in neurite outgrowth inhibition by MAG and CNS myelin. *J. Cell Sci.* **126,** 209–220
62. Leemhuis, J., Bouche, E., Frotscher, M., Henle, F., Hein, L., Herz, J., Meyer, D. K., Pichler, M., Roth, G., Schwan, C., and Bock, H. H. (2010) Reelin signals through apolipoprotein E receptor 2 and Cdc42 to increase growth cone motility and filopodia formation. *J. Neurosci.* **30,** 14759–14772
63. Sepp, K. J., Hong, P., Lizarraga, S. B., Liu, J. S., Mejia, L. A., Walsh, C. A., and Perrimon, N. (2008) Identification of neural outgrowth genes using genome-wide RNAi. *PLoS Genet.* **4,** e1000111
64. Uhlik, M. T., Temple, B., Bencharit, S., Kimple, A. J., Siderovski, D. P., and Johnson, G. L. (2005) Structural and evolutionary division of phosphotyrosine binding (PTB) domains. *J. Mol. Biol.* **345,** 1–20
65. Chen, L., Liu, C., Ko, F. C., Xu, N., Ng, I. O., Yam, J. W., and Zhu, G. (2012) Solution structure of the phosphotyrosine binding (PTB) domain of human tensin2 protein in complex

with deleted in liver cancer 1 (DLC1) peptide reveals a novel peptide binding mode. *J. Biol. Chem.* **287,** 26104–26114
66. Pasqualato, S., Menetrey, J., Franco, M., and Cherfils, J. (2001) The structural GDP/GTP cycle of human Arf6. *EMBO Rep.* **2,** 234–238
67. Menetrey, J., Macia, E., Pasqualato, S., Franco, M., and Cherfils, J. (2000) Structure of Arf6-GDP suggests a basis for guanine nucleotide exchange factors specificity. *Nat. Struct. Biol.* **7,** 466–469
68. Kanoh, H., Williger, B. T., and Exton, J. H. (1997) Arfaptin 1, a putative cytosolic target protein of ADP-ribosylation factor, is recruited to Golgi membranes. *J. Biol. Chem.* **272,** 5421–5429
69. Tsai, S. C., Adamik, R., Hong, J. X., Moss, J., Vaughan, M., Kanoh, H., and Exton, J. H. (1998) Effects of arfaptin 1 on guanine nucleotide-dependent activation of phospholipase D and cholera toxin by ADP-ribosylation factor. *J. Biol. Chem.* **273,** 20697–20701
70. Ma, Z., Nie, Z., Luo, R., Casanova, J. E., and Ravichandran, K. S. (2007) Regulation of Arf6 and ACAP1 signaling by the PTB-domain-containing adaptor protein GULP. *Curr. Biol.* **17,** 722–727
71. Albertinazzi, C., Za, L., Paris, S., and de Curtis, I. (2003) ADP-ribosylation factor 6 and a functional PIX/p95-APP1 complex are required for Rac1B-mediated neurite outgrowth. *Mol. Biol. Cell* **14,** 1295–1307
72. Mo, J., Choi, S., Ahn, P. G., Sun, W., Lee, H. W., and Kim, H. (2012) PDZ-scaffold protein, Tamalin promotes dendritic outgrowth and arborization in rat hippocampal neuron. *Biochem. Biophys. Res. Commun.* **422,** 250–255
73. Yamazaki, T., Koo, E. H., and Selkoe, D. J. (1997) Cell surface amyloid beta-protein precursor colocalizes with beta 1 integrins at substrate contact sites in neural cells. *J. Neurosci.* **17,** 1004–1010
74. Hoe, H. S., Lee, K. J., Carney, R. S., Lee, J., Markova, A., Lee, J. Y., Howell, B. W., Hyman, B. T., Pak, D. T., Bu, G., and Rebeck, G. W. (2009) Interaction of reelin with amyloid precursor protein promotes neurite outgrowth. *J. Neurosci.* **29,** 7459–7473
75. Perez, R. G., Zheng, H., Van der Ploeg, L. H., and Koo, E. H. (1997) The beta-amyloid precursor protein of Alzheimer's disease enhances neuron viability and modulates neuronal polarity. *J. Neurosci.* **17,** 9407–9414
76. Rama, N., Goldschneider, D., Corset, V., Lambert, J., Pays, L., and Mehlen, P. (2012) Amyloid precursor protein regulates netrin-1-mediated commissural axon outgrowth. *J. Biol. Chem.* **287,** 30014–30023
77. Minopoli, G., de Candia, P., Bonetti, A., Faraonio, R., Zambrano, N., and Russo, T. (2001) The b-amyloid precursor protein functions as a cytosolic anchoring site that prevents Fe65 nuclear translocation. *J. Biol. Chem.* **276,** 6545–6550
78. Ermekova, K. S., Zambrano, N., Linn, H., Minopoli, G., Gertler, F., Russo, T., and Sudol, M. (1997) The WW domain of neural protein FE65 interacts with proline-rich motifs in Mena, the mammalian homolog of *Drosophila* enabled. *J. Biol. Chem.* **272,** 32869–32877
79. Wang, P. L., Niidome, T., Kume, T., Akaike, A., Kihara, T., and Sugimoto, H. (2011) Functional and molecular interactions between Rac1 and FE65. *Neuroreport* **22,** 716–720
80. Yamada, K. M., Spooner, B. S., and Wessells, N. K. (1970) Axon growth: roles of microfilaments and microtubules. *Proc. Natl. Acad. Sci. U. S. A.* **66,** 1206–1212
81. Bentley, D., and Toroian-Raymond, A. (1986) Disoriented pathfinding by pioneer neurone growth cones deprived of filopodia by cytochalasin treatment. *Nature* **323,** 712–715
82. Marsh, L., and Letourneau, P. C. (1984) Growth of neurites without filopodial or lamellipodial activity in the presence of cytochalasin B. *J. Cell Biol.* **99,** 2041–2047
83. Luo, L. (2002) Actin cytoskeleton regulation in neuronal morphogenesis and structural plasticity. *Annu. Rev. Cell Dev. Biol.* **18,** 601–635
84. Flynn, K. C., Hellal, F., Neukirchen, D., Jacob, S., Tahirovic, S., Dupraz, S., Stern, S., Garvalov, B. K., Gurniak, C., Shaw, A. E., Meyn, L., Wedlich-Soldner, R., Bamburg, J. R., Small, J. V., Witke, W., and Bradke, F. (2012) ADF/cofilin-mediated actin retrograde flow directs neurite formation in the developing brain. *Neuron* **76,** 1091–1107
85. Lu, W., Fox, P., Lakonishok, M., Davidson, M. W., and Gelfand, V. I. (2013) Initial neurite outgrowth in *Drosophila* neurons is driven by kinesin-powered microtubule sliding. *Curr. Biol.* **23,** 1018–1023
86. Dent, E. W., Kwiatkowski, A. V., Mebane, L. M., Philippar, U., Barzik, M., Rubinson, D. A., Gupton, S., Van Veen, J. E., Furman, C., Zhang, J., Alberts, A. S., Mori, S., and Gertler, F. B. (2007) Filopodia are required for cortical neurite initiation. *Nat. Cell Biol.* **9,** 1347–1359
87. Williams, K. L., Rahimtula, M., and Mearow, K. M. (2005) Hsp27 and axonal growth in adult sensory neurons in vitro. *BMC Neurosci.* **6,** 24
88. Frey, D., Laux, T., Xu, L., Schneider, C., and Caroni, P. (2000) Shared and unique roles of CAP23 and GAP43 in actin regulation, neurite outgrowth, and anatomical plasticity. *J. Cell Biol.* **149,** 1443–1454
89. Montenegro-Venegas, C., Tortosa, E., Rosso, S., Peretti, D., Bollati, F., Bisbal, M., Jausoro, I., Avila, J., Caceres, A., and Gonzalez-Billault, C. (2010) MAP1B regulates axonal development by modulating Rho-GTPase Rac1 activity. *Mol. Biol. Cell* **21,** 3518–3528
90. Tahirovic, S., Hellal, F., Neukirchen, D., Hindges, R., Garvalov, B. K., Flynn, K. C., Stradal, T. E., Chrostek-Grashoff, A., Brakebusch, C., and Bradke, F. (2010) Rac1 regulates neuronal polarization through the WAVE complex. *J. Neurosci.* **30,** 6930–6943
91. Sannerud, R., Declerck, I., Peric, A., Raemaekers, T., Menendez, G., Zhou, L., Veerle, B., Coen, K., Munck, S., De Strooper, B., Schiavo, G., and Annaert, W. (2011) ADP ribosylation factor 6 (ARF6) controls amyloid precursor protein (APP) processing by mediating the endosomal sorting of BACE1. *Proc. Natl. Acad. Sci. U. S. A.* **108,** E559–568

Received for publication April 18, 2013.
Accepted for publication September 12, 2013.